Deciphering the impact of perturbations in developmental hematopoiesis

Alina Sommer

Deciphering the impact of perturbations in developmental hematopoiesis

Doctoral thesis in cell biology and development
École doctorale Complexité du Vivant, Sorbonne Université

Presented by

Alina Sommer

Macrophages and Endothelial Cells
Department of Stem Cell and Developmental Biology
Institut Pasteur

Directed by

Elisa Gomez Perdiguero

Publicly presented and defended on November 19th, 2024
In front of a jury composed of

Dr Charles Durand	President of the Jury
Dr Anna Bigas	Reviewer
Dr Philipp Henneke	Reviewer
Dr Elisa Laurenti	Examiner
Dr Claus Nerlov	Examiner
Dr Ana Cumano	Examiner
Dr Elisa Gomez Perdiguero	PhD Supervisor

Cover:
6 um thick maximum projection
of an E9.5 yolk sac from a *Csf1r*^{iCre} *R26*^{YFP} embryo.
white: CD31, green: YFP

To Felix

Acknowledgment

At the end of an incredible journey, I would like to thank all the people who have accompanied me over the past four years. This PhD study was conducted from 2020-2024 in the "Macrophages and Endothelial Cells" unit in the Department of Stem Cell and Developmental Biology and the Department of Immunology at Institut Pasteur in Paris.

First of all, I would like to express my deep gratitude to my PhD supervisor, Elisa Gomez Perdiguero, for trusting me and giving me the opportunity to conduct my PhD in her lab. Thank you for showing me how to be a good scientist, not only on a scientific but also on a personal level. Thank you for giving me the freedom to explore projects, make mistakes, and test my limits. In particular, I would like to thank you for giving me the possibility to attend several scientific conferences abroad, which have been truly life-changing experiences for me.

My special thanks also go to the members of my PhD jury, Charles Durand (president), Anna Bigas (rapporteur), Philipp Henneke (rapporteur), Elisa Laurenti (examiner), Claus Nerlov (examiner) and Ana Cumano (examiner), who agreed to review my doctoral manuscript, travel to Paris and discuss with me at the defense.

Many thanks also to Marella De Bruijn, Mélanie Hamon, and Thierry Jaffredo for their participation in my thesis committee (comité de suivi de thèse) in 2022 and 2023, their suggestions and advice. I would also like to thank my Pasteur-tutor Mariana Alonso for checking in on me annually.

I would like to thank the numerous scientific collaborators and platforms for supporting my experimental work. A big thanks goes to Stephan Fischer from the Bioinformatics Hub for analyzing my multiome dataset. Thanks to the flow cytometry platform, the single-cell and biomarker platform, and the biomics platform. My special thanks to the animal facility for taking care of my mice, without which this work would not have been possible.

I would also like to thank Francisca Soares-da-Silva and Marcia Peixoto from Ana Cumano's lab for providing reagents and protocols and for scientific exchange. Many thanks also to Benjamin Montagne, Tara Fournier, and all other members of Miria Ricchetti's lab for letting me use their cell culture room and for their technical support.

I would like to thank all former and current members of the lab for their friendship, support, and the fun we had together over the years. You have made even very long experiments not only bearable but enjoyable.

Thanks to Laina Freyer, who took me under her wing during my Erasmus internship before my PhD. Without her, I would never have had the opportunity to move to Paris and do

some super cool live imaging experiments. It was this internship that sparked my initial passion for developmental hematopoiesis and working with embryos. Thank you for being an important friend to me, even long after you left the lab. Thank you also to Lorea Iturri for teaching me how to perform single-cell liquid cultures and for laying the foundation for my project through your work. I would also like to thank Kémy Adé, Rebecca Ponce Landete, and Tobias Weinberger for their friendship and the great time we spent together in the lab. Thanks to Ramy Elsaid for many scientific discussions, constructive feedback, and lots of laughter even in difficult times. Thanks to Alessia Arifi, Laurie Choux, and Krista Barone for some unforgettable experiences in and outside the lab ;) . Thanks to Isabelle Sou, Claire Lagu, and Natalie Chan for your administrative help.

I would also like to thank Dorian Obino for always being available for mental support. You have been a very important mentor for me and I will always be grateful for that. Un grand merci à Pascal, pour les nombreuses conversations agréables et pour l'assistance technique avec les souris. Many thanks to Yvan Lallemand, for your constant technical and moral support and many humorous moments in the lab during the last four years. We were a great weekend-plug-check-team! I especially appreciate the friendship with Clarisabel Garcia that we have built up over the last years. Thank you for being "all in this together" and for supporting each other in through the highs and lows of the PhD. I am very proud of both of us!

During my doctoral thesis, I also had the opportunity to supervise three students. Corentin Guichen, Julia Sanchez Viladevall, and Abigail Jolteus. Thank you for being great students and for your patience with me! I would especially like to thank Julia for becoming an good friend to me.

Thanks to my fellow PhD fighters Tara Fournier and Mathilde Chouly – we finally all made it to the finish line!

I would like to thank my friends and family outside Pasteur. Special thanks to my parents for supporting me in my decision to move to Paris.

A doctoral thesis is an exciting but also challenging experience in many aspects. In particular, performing lineage tracing experiments in embryos requires a lot of flexibility. My deepest gratitude and love goes to my husband Felix Sommer. Thank you for moving to Paris with me and leaving your family and friends behind for me. Thank you for never complaining, even when I had to check plugs, inject mice, or even run experiments on weekends. When the experiments took longer than expected, I got nothing but support. The experiences I had during my PhD have led us to some significant life changes for both of us that have made us better and stronger people. My love for you has nothing but grown for you throughout the PhD and I look forward to all the new and exciting adventures that lie ahead. - Alina

Table of Contents

1 Introduction

1.1 Hematopoiesis: production of blood and immune cells

"Blood is a very special juice"

– Mephistopheles to Faust, Goethe

Blood has fascinated humankind for thousands of years and has served as a symbol of life and death in literature, art, and religion. While the ancient understanding of blood was based on the four humors theory postulated by the Greek physician and scientist Claudius Galen, our modern view of the blood system began with groundbreaking discoveries in the 17th century. Harvey first described the closed circuit of blood circulation (1628) and van Leeuwenhoek (1648) and Hewson (1770) discovered red and white blood cells, respectively (reviewed by Coller, 2015).

According to our modern definition, blood is a liquid tissue that circulates through our body and consists of two main components: (1) plasma containing water, sugars, proteins, and salts, and (2) blood cells including mainly erythrocytes, platelets, monocytes, granulocytes (neutrophils, eosinophils, basophils), B cells, T cells, and innate lymphoid cells (ILCs). One microliter of blood contains around 5 million erythrocytes that fulfill the vital task of supplying the human body with oxygen. 150,000-300,000 platelets, also called thrombocytes, control bleeding and blood coagulation. 4,000-9,000 leukocytes, players of the immune system, protect the organism from pathogens and cancerous cells ("Haematology reference ranges," 2024). Leukocytes, or white blood cells comprise innate (monocytes, granulocytes, and dendritic cells, innate lymphoid cells (ILCs)) and adaptive immune cells (B, and T cells). Additionally, the bloodstream also replenishes tissue immune cells such as monocyte-derived macrophages, dendritic cells, and mast cells.

Blood and immune cells are constantly produced in the bone marrow (Bizzozero, 1868, 1869; Neumann, 1868, 1869) by a process called hematopoiesis, meaning 'production of blood' from the Greek terms αἷμα [haîma] (blood) and ποιεῖν [poieîn] (to make). The freshly formed blood and immune cells exit the bone marrow and enter the bloodstream, allowing them to reach all parts of the body. While some cells, such as patrolling monocytes circulate most of their lifetime, other cells migrate to lymphatic organs such as the spleen, thymus, tonsils, lymph nodes, and Peyer patches where they further mature and exert specific (immunological) functions. These organs collectively compose the

lymphatic system, which is intimately connected with the hematopoietic system, comprising the bone marrow and all blood and immune cells.

Due to the convenience of the mouse model, most of the research (literature and original work) discussed in this thesis was performed in mice.

1.1.1 Hematopoietic stem cells at the apex of the hematopoietic tree

Hematopoiesis is a hierarchical process that was deciphered using transplantation and spleen colony-forming unit assays in mice (Till & McCulloch, 1961; Becker, McCULLOCH & Till, 1963), and especially thanks to the advent of flow cytometry and cell sorting. Classically, the hematopoietic system is depicted as a tree with hematopoietic stem cells sitting at the top (Spangrude, Heimfeld & Weissman, 1988; Okada et al., 1991; Uchida & Weissman, 1992; Seita & Weissman, 2010) (**Figure 1**). Recently, the availability of single-cell sequencing techniques, including barcoding, has shed light on the heterogeneity among populations and the continuum between them (Naik et al., 2013; Sun et al., 2014; Perié et al., 2015; Paul et al., 2015; Nestorowa et al., 2016; Pei et al., 2017; Weinreb et al., 2020; Bowling et al., 2020; Li et al., 2023a). Therefore, cloud or Waddington-like representations have been introduced trying to better reflect the complexity of hematopoiesis than rigid tree models (reviewed in Laurenti & Göttgens, 2018).

Importantly, each method has its benefits and caveats. For example, single-cell RNA sequencing is useful to identify different cell states which however cannot be directly translated to their potential or function. Transplantation assays and colony-forming assays elucidate the potential of a single cell or population but this can differ from its potential *in situ*. *In vivo* barcoding on the other hand allows to trace the fate of a single cell *in situ* which however also comes with technical challenges such as the diversity of barcodes.

Bona fide Hematopoietic stem cells (HSCs) are defined by their self-renewal capacity (serial transplantations) and their potential to produce all blood cell types. They give rise to multipotent progenitors (MPPs) that compared to HSCs have lost their self-renewal capacity (Morrison & Weissman, 1994; Christensen & Weissman, 2001).

Among HSCs, long-term (LT-HSCs) and short-term HSCs (ST-HSCs) can be distinguished (Morrison & Weissman, 1994; Christensen & Weissman, 2001; Kiel et al., 2005). Both LT- and ST-HSCs are multipotent, meaning that they can contribute to erythroid, myeloid, and lymphoid potential for more than 3 months. However, only LT-HSCs and not ST-HSCs are capable of serial transplantation, indicating potent self-renewal activity (reviewed by Wilkinson et al., 2020). Furthermore, ST-HSCs exhaust before 4 months in contrast to LT-HSCs. Thus, only LT-HSCs are *bona fide* HSCs and it has been recently proposed to call ST-HSCs MPPs (Sommerkamp et al., 2021; Challen et al., 2021)

Figure 1

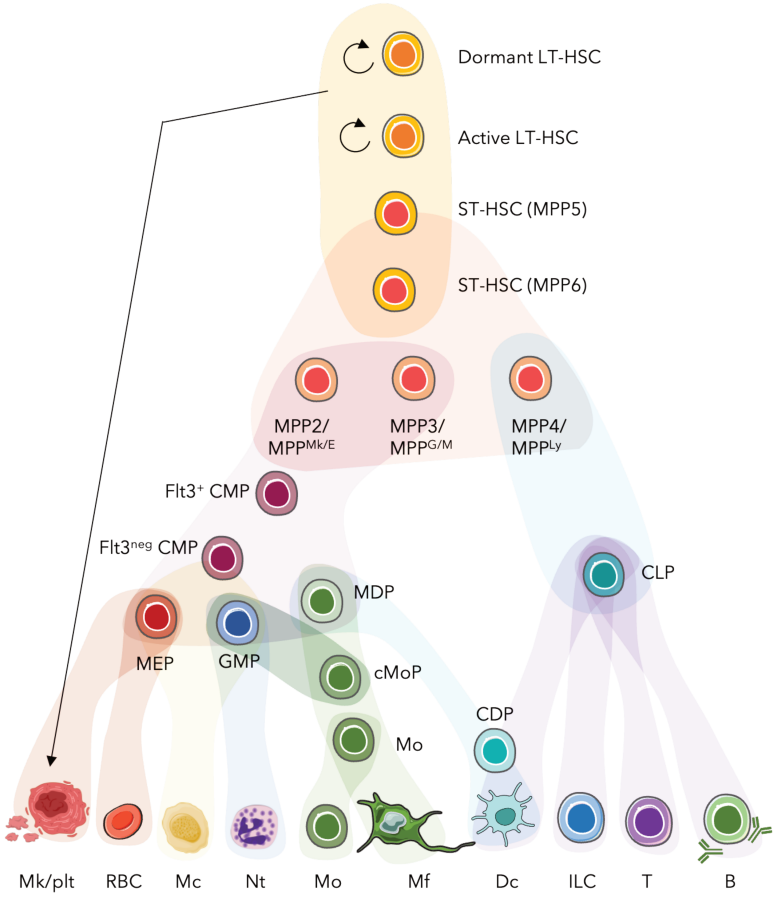

Figure 1. Model of the hematopoietic tree. LT-HSC, long-term hematopoietic stem cells; ST-HSC, short-term HSC; MPP, multipotent progenitor; CLP, common lymphoid progenitor; CMP, common myeloid progenitor; MEP, megakaryocyte-erythrocyte progenitor; GMP, granulocyte-monocyte progenitor; MDP, monocyte-dendritic cell progenitor; CDP, common dendritic cell progenitor, cMoP, common monocyte progenitor; Mk, megakaryocyte; plt, platelet, RBC, red blood cell; Mc, mast cell; Nt, neutrophil; Mo, monocyte; Mf, macrophage; Dc, dendritic cell; ILC, innate lymphoid cell; T, T cell; B, B cell. Partially created with biorender.com.

The definition of LT- and ST-HSCs has been even further refined (Wilson et al., 2008; Cabezas-Wallscheid et al., 2014; Pietras et al., 2015; Challen et al., 2021; Purton, 2022) (**Table 1**). Among LT-HSCs (Lin^{neg} Kit^{+} $Sca\text{-}1^{+}$ $CD48^{neg}$ $CD150^{+}$), dormant $CD34^{neg}$ LT-HSCs and active $CD34^{+}$ LT-HSCs (MPP1) can be distinguished (Wilson et al., 2008; Cabezas-Wallscheid et al., 2014; Pietras et al., 2015). ST-HSCs (Lin^{neg} Kit^{+} $Sca\text{-}1^{+}$ $CD48^{neg}$ $CD150^{neg}$) can also be either $CD34^{neg}$ or $CD34^{+}$ (Sommerkamp et al., 2021). Both $CD34^{neg}$ and $CD34^{+}$ ST-HSC populations have multi-lineage potential in transplantation, but $CD34^{neg}$ cells (MPP 6) were reported to be slower and contribute more long-term in contrast to $CD34^{+}$ ST-HSCs (MPP5) (Sommerkamp et al., 2021).

Additionally, it was discovered that LT-HSCs contain a subpopulation of platelet-biased HSCs that can be identified based on the expression (promoter activity) of a *van*

Willebrand factor-reporter (*vWf* ^{GFP} or *vWf* ^{Tom}) (Sanjuan-Pla et al., 2013; Carrelha et al., 2018). Both *vWf* $^{+}$ and *vWf* ^{neg} LT-HSCs are capable of long-term secondary reconstitution. However, *vWf* $^{+}$ LT-HSCs show a platelet bias and have little potential for lymphoid cells in contrast to their *vWf* ^{neg} counterpart which have a more balanced output (Sanjuan-Pla et al., 2013; Carrelha et al., 2018, 2024). *vWf* $^{+}$ and *vWf* ^{neg} LT-HSCs give rise to CD48^{low} or CD48$^{low/+}$ MkPs, respectively. In contrast to the *vWf* ^{neg}-CD48$^{low/+}$ pathway, the *vWf* $^{+}$-CD48^{low} path is a fast-track pathway skipping the MPP stage (identified by *Flt3* expression) which probably gives rise to functionally distinct platelets (Boyer et al., 2011; Buza-Vidas et al., 2011; Rodriguez-Fraticelli et al., 2018; Morcos et al., 2022; Carrelha et al., 2024; Poscablo et al., 2024). While several studies suggest that the platelet-biased *vWf* $^{+}$ path is mainly active in perturbed conditions such as aging, depletion, or inflammation (Boyer et al., 2011; Buza-Vidas et al., 2011; Carrelha et al., 2024; Poscablo et al., 2024), further research is required to understand the role of *vWf*$^{+}$ LT-HSCs in homeostatic conditions (Rodriguez-Fraticelli et al., 2018).

1.1.2 Lineage commitment downstream of multipotent progenitors

MPPs are a heterogeneous population (Arinobu et al., 2007) and can be categorized into three different subpopulations. Each of them is primed but not terminally committed towards a distinct lineage. MPP2s are biased towards megakaryocyte/platelet and erythrocyte fate (Wilson et al., 2008; Cabezas-Wallscheid et al., 2014; Pietras et al., 2015; Rodriguez-Fraticelli et al., 2018; Purton, 2022). MPP3s preferentially give rise to myeloid cells, whereas MPP4s (also called LMPP, lymphoid-primed multipotent progenitor) are primed towards the lymphoid lineage (Adolfsson et al., 2005; Wilson et al., 2008; Cabezas-Wallscheid et al., 2014; Pietras et al., 2015; Rodriguez-Fraticelli et al., 2018; Purton, 2022).

Downstream of MPPs, progenitor populations with progressively restricted potential have been identified that eventually differentiate into various types of mature blood and immune cells. It should be noted that these populations have mainly been defined based on their potential in colony-forming assays or transplantation experiments. However, these populations are often heterogeneous, containing a mix of both bi-potent and mono-potent cells.

In the first instance downstream of MPPs, lie the common lymphoid progenitors (CLPs, Lin^{neg} Kit^{+} Sca-1^{low} Flt3^{+} IL7ra^{+}) (Kondo, Weissman & Akashi, 1997; Adolfsson et al., 2005; Karsunky et al., 2008) and common myeloid progenitors (CMPs) (Akashi et al., 2000; Yáñez et al., 2017) (**Table 1, Figure 1**).

Table 1 Phenotype of hematopoietic stem and progenitor cells in the murine bone marrow

Cell type	Cell surface markers	References
dormant LT-HSC	Lin^{neg} Kit^{+} $Sca\text{-}1^{+}$ $CD48^{neg}$ $CD150^{+}$ $CD34^{neg}$ $Flt3^{neg}$	(Wilson et al., 2008; Cabezas-Wallscheid et al., 2014)
active LT-HSC/ MPP1	Lin^{neg} Kit^{+} $Sca\text{-}1^{+}$ $CD48^{neg}$ $CD150^{+}$ $CD34^{+}$ $Flt3^{neg}$	(Wilson et al., 2008; Cabezas-Wallscheid et al., 2014)
ST-HSC/MMP6	Lin^{neg} Kit^{+} $Sca\text{-}1^{+}$ $CD48^{neg}$ $CD150^{neg}$ $CD34^{neg}$ $Flt3^{neg}$	(Pietras et al., 2015; Sommerkamp et al., 2021)
ST-HSC/MMP5	Lin^{neg} Kit^{+} $Sca\text{-}1^{+}$ $CD48^{neg}$ $CD150^{neg}$ $CD34^{+}$ $Flt3^{neg}$	(Sommerkamp et al., 2021)
MPP2/$MPP^{Mk/E}$	Lin^{neg} Kit^{+} $Sca\text{-}1^{+}$ $CD48^{+}$ $CD150^{+}$ $Flt3^{neg}$	(Cabezas-Wallscheid et al., 2014; Pietras et al., 2015)
MPP3/$MPP^{G/M}$	Lin^{neg} Kit^{+} $Sca\text{-}1^{+}$ $CD48^{+}$ $CD150^{neg}$ $Flt3^{neg}$	(Cabezas-Wallscheid et al., 2014; Pietras et al., 2015)
MPP4/MPP^{Ly}/LMPP	Lin^{neg} Kit^{+} $Sca\text{-}1^{+}$ $CD48^{+}$ $CD150^{neg}$ $CD34^{+}$ $Flt3^{+}$	(Adolfsson et al., 2005; Cabezas-Wallscheid et al., 2014; Pietras et al., 2015)
CLP	Lin^{neg} Kit^{+} $Sca\text{-}1^{low}$ $Flt3^{+}$ $IL7ra^{+}$	(Kondo, Weissman & Akashi, 1997; Adolfsson et al., 2005; Karsunky et al., 2008)
$Flt3^{+}$ CMP	Lin^{neg} Kit^{+} $Sca\text{-}1^{neg}$ $CD34^{+}$ $CD16/32^{low}$ $Flt3^{+}$	(Akashi et al., 2000; Yáñez et al., 2017)
$Flt3^{neg}$ CMP	Lin^{neg} Kit^{+} $Sca\text{-}1^{neg}$ $CD34^{+}$ $CD16/32^{low}$ $Flt3^{neg}$	(Yáñez et al., 2017)
MEP	Lin^{neg} Kit^{+} $Sca\text{-}1^{neg}$ $CD34^{neg}$ $CD16/32^{neg}$	(Akashi et al., 2000)
GMP	Lin^{neg} Kit^{+} $Sca\text{-}1^{neg}$ $CD34^{+}$ $CD16/32^{high}$ $Flt3^{neg}$ $CD115^{neg}$ $Ly6C^{neg}$ $Cx3CR1^{low}$	(Akashi et al., 2000; Yáñez et al., 2017)
MDP	Lin^{neg} Kit^{+} $Sca\text{-}1^{neg}$ $CD34^{+}$ $CD16/32^{low}$ $Flt3^{+}$ $CD115^{+}$ $Ly6C^{neg}$ $Cx3CR1^{+}$	(Hettinger et al., 2013; Yáñez et al., 2017)
cMoP	Lin^{neg} Kit^{+} $Sca\text{-}1^{neg}$ $CD34^{+}$ $CD16/32^{high}$ $Flt3^{neg}$ $CD115^{+}$ $Ly6C^{+}$ $CD11b^{neg}$	(Hettinger et al., 2013; Yáñez et al., 2017)
CDP	Lin^{neg} Kit^{low} $Sca\text{-}1^{neg}$ $CD34^{+}$ $CD16/32^{low}$ $Flt3^{+}$ $CD115^{+}$ $Ly6C^{neg}$ $CD11b^{neg}$	(Schlitzer et al., 2015; Liu et al., 2019)

CLPs give rise to B, T, ILCs, and dendritic cells (Kondo, Weissman & Akashi, 1997; Manz et al., 2001). CMPs further commit to megakaryocyte-erythrocyte progenitors (MEPs, Lin^{neg} Kit^{+} $Sca\text{-}1^{neg}$ $CD34^{neg}$ $CD16/32^{neg}$), granulocyte-monocyte progenitors (GMPs, Lin^{neg} Kit^{+} $Sca\text{-}1^{neg}$ $CD34^{+}$ $CD16/32^{high}$ $Flt3^{neg}$ $CD115^{neg}$ $Ly6C^{neg}$ $Cx3CR1^{low}$), and monocyte-dendritic cell progenitors (MDPs, Lin^{neg} Kit^{+} $Sca\text{-}1^{neg}$ $CD34^{+}$ $CD16/32^{low}$ $Flt3^{+}$ $CD115^{+}$ $Ly6C^{neg}$ $Cx3CR1^{+}$) (Akashi et al., 2000; D'Amico & Wu, 2003; Auffray et al., 2009; Geissmann et al., 2010; Hettinger et al., 2013; Yáñez et al., 2017).

MEPs have the potential for megakaryocytes and erythrocytes (Pronk et al., 2007). GMPs give rise to granulocyte progenitors (GPs Lin^{neg} Kit^{+} $Sca\text{-}1^{neg}$ $CD34^{+}$ $CD16/32^{high}$ $Flt3^{neg}$ $CD115^{low}$ $Ly6C^{+}$) and common monocyte progenitors (cMoPs) (Yáñez et al., 2015). GPs differentiate into granulocytes, while cMoPs produce monocytes. MDPs give rise to common dendritic cell progenitors (CDPs, Lin^{neg} Kit^{low} $Sca\text{-}1^{neg}$ $CD34^{+}$ $CD16/32^{low}$ $Flt3^{+}$ $CD115^{+}$ $Ly6C^{neg}$ $CD11b^{neg}$) and common monocyte progenitors (cMoPs, Lin^{neg} Kit^{+} $Sca\text{-}1^{neg}$ $CD34^{+}$ $CD16/32^{high}$ $Flt3^{neg}$ $CD115^{+}$ $Ly6C^{+}$ $CD11b^{neg}$) (Hettinger et al., 2013; Schlitzer et al., 2015; Yáñez et al., 2017; Liu et al., 2019; Lösslein et al., 2021). The fact that dendritic cells (Traver et al., 2000; Manz et al., 2001), and cMoPs (Yáñez et al., 2017) can potentially both derive from two progenitor populations highlights the complexity of hematopoiesis. Whether the mature cells derived from different progenitor origins however are functionally identical or distinct remains unclear.

Similarly, the origin of mast cell progenitors (McPs, Lin^{neg} Kit^{+} $Sca\text{-}1^{neg}$ $Itgb7^{+}$) is complex and remains under discussion. Historically they have been described to develop from GMPs (Arinobu et al., 2005; Qi et al., 2013; Wanet et al., 2021). Recent transcriptional

analysis however positions mast cells closer to the erythro-megakaryocyte lineage (Drissen et al., 2016; Dahlin et al., 2018; Drissen et al., 2019; Vanuytsel et al., 2022).

Future studies will further refine the current view on the progenitor stages of hematopoietic commitment and differentiation.

1.1.3 Transcriptional regulation of lineage commitment

Complex regulations at several molecular levels govern the gradual restriction of a multipotent progenitor or stem cell into a unipotent precursor, and ultimately, the differentiation of a fully mature cell.

Not only the complexity but also the potentially low expression levels of lineage-determining transcription factors make it challenging to fully grasp the exact events governing the lineage-decision-making processes. Nevertheless, main regulators of lineage commitment and differentiation in hematopoiesis have been identified and extensively studied.

Transcriptional regulation of HSCs

Hematopoietic stem cells and multipotent progenitors express a heptad of transcription factors that all control each other and themselves in a tightly regulated circuit. The heptad transcription factors ensure the maintenance of the stem cell pool but are also involved in downstream commitment and differentiation both in mice and humans. This heptad consists of 7 transcription factors *Scl* (*Tal-1*), *Lyl1*, *Lmo2*, *Gata2*, *Runx1*, *Erg*, and *Fli-1* (Sun & Downing, 2004; Growney et al., 2005; Kruse et al., 2009; Wilson et al., 2010; Lacombe et al., 2010; Taoudi et al., 2011; Knudsen et al., 2015).

Next to heptad transcription factors HSCs and MPPs also express *Meis1*, *Gfi1b*, *Gfi1*, and *Pu.1* (Nutt et al., 2005; Arinobu et al., 2007; Wilson et al., 2010; Hoppe et al., 2016). which restrain the excessive proliferation and exhaustion of HSCs (Hock et al., 2004; Zeng et al., 2004; Khandanpour et al., 2010; Unnisa et al., 2012; Kocabas et al., 2012; Staber et al., 2013).

During the transition from HSC to MPP only very few genes change their expression levels both in mice (protein level) and humans (mRNA level) (Laurenti et al., 2013; Cabezas-Wallscheid et al., 2014). Most genes that are upregulated in MPPs compared to HSCs are cell cycle and DNA repair genes (Cabezas-Wallscheid et al., 2014). This is not surprising as one of the main features of the transition from HSC to MPP is increased proliferation (Cheshier et al., 1999; Wilson et al., 2008).

Erythro-myeloid lineage commitment

At the MPP stage, not only proliferation but also lineage commitment begins (Arinobu et al., 2007). An imbalance of heptad transcription factors skews progenitors towards distinct

fates. For example, upregulation *Lyl1*, *Tal1*, *Lmo2*, *Gata2,* and downregulation or *Erg* primes progenitors to the erythroid fate (Thoms et al., 2021). This is accompanied by the heterogenous expression of *Pu.1* and *Gata1* at the MPP level (Arinobu et al., 2007). *Pu.1* is an ETS-family transcription factor that instructs lymphoid or myeloid fate (Scott et al., 1994; Nerlov & Graf, 1998; see Cumano et al., 2019 for further information on lymphoid commitment). *Gata1* is the first member of the GATA family, a transcription factor family that binds (A/T)GATA(A/G) sequences with a C-zinc finger domain (Martin & Orkin, 1990). *Gata1* It is encoded on the X-chromosome and consists of two DNA-binding zinc fingers and a C- and N-terminal activation domain (Zon et al., 1990). Gata1 is essential for erythrocyte, megakaryocyte, and mast cell commitment and differentiation (Fujiwara et al., 1996; Shivdasani et al., 1997; Migliaccio et al., 2003; Drissen et al., 2016).

PU.1 and GATA1 positively autoregulate themselves and cross-inhibit each other (Tsai, Strauss & Orkin, 1991; Chen et al., 1995). The N-terminal finger domain of PU.1 blocks the binding of GATA1 to DNA (Zhang et al., 2000), whereas the C-terminal finger domain of Gata1 inhibits the ETS domain of Pu.1 (Nerlov et al., 2000). Due to this antagonistic but self-enhancing regulation it has been proposed that PU.1 and GATA1 regulate the lineage decision-making process between erythroid (erythrocytes, megakaryocytes, mast cells) and myeloid fate through a so-called "PU.1-GATA1-switch". However, it still remains unclear whether the PU.1-GATA1-switch regulates the bifurcation of erythroid and myeloid fate or whether these transcription factors rather further enforce or execute a lineage decision that was already made upstream (Hoppe et al., 2016; Wheat et al., 2020).

Gata1 and Gata2 regulate lineage commitment at the megakaryocyte-erythrocyte bifurcation

Once committed to the erythroid fate, GATA1 and GATA2 regulate the decision between erythrocyte and megakaryocyte fate, respectively (Doré & Crispino, 2011). GATA1 and GATA2 both bind similar GATA boxes. Some binding sites are selectively bound by only GATA1 or GATA2 but there are also regions that are bound by both GATA1 and GATA2 (Fujiwara et al., 2009; Suzuki et al., 2013). GATA1 and GATA2 both interact with FOG-1 through their N-terminal zinc finger domain. FOG-1 is necessary for erythrocyte and megakaryocyte but not mast cell development (Tsang et al., 1998; Chang et al., 2002; Gregory et al., 2010) and recruits other binding partners such as the deacetylase NuRD which remodels the chromatin state via histone acetylation (Hong et al., 2005).

Prior to Gata1 expression, Gata2 binds GATA switch sites that are found for example in the *Gata2* (Grass et al., 2003), *Kit* (Jing et al., 2008), *Klf1* (Tripic et al., 2009), or *Sfpi1* (Chou et al., 2009) genes. Upon *Gata1* expression, GATA1 then replaces GATA2 in a FOG-1-dependent manner (Pal et al., 2004). This is facilitated by the lower stability of the GATA2 protein compared to GATA1 (Lurie et al., 2008) and the concomitant repression

of *Gata2* transcription due to a decrease in histone acetylation at the *Gata2* domain which hampers the accessibility and recruitment of polymerases (Grass et al., 2003). This GATA switch induces erythrocyte gene expression while repressing megakaryocyte and mast cell genes (Welch et al., 2004; Gregory et al., 2010). In contrast, high GATA2 levels inhibit erythrocyte fate and instead drive megakaryocyte fate (Ikonomi et al., 2000). Nevertheless, GATA1 remains expressed in megakaryocytes and is essential to regulate polyploidization in late maturation (Muntean et al., 2007).

Transcriptional regulation of megakaryocyte commitment and differentiation

Interestingly, even though the GATA1-GATA2 switch is important in the decision between megakaryocyte and erythrocyte fate, GATA2 is not required for megakaryocyte production (Tsai & Orkin, 1997; Chang et al., 2002). Other transcription factors also regulate the decision between erythrocyte and megakaryocyte fate. KLF-1 and FLI-1 drive erythrocyte or megakaryocyte fate, respectively while inhibiting the other lineage (Miller & Bieker, 1993; Kawada et al., 2001; Wang et al., 2002; Frontelo et al., 2007; Kruse et al., 2009; Tallack & Perkins, 2010). Together with GATA1 and FOG-1, FLI-1 activates the expression of *Itga2b* (CD41), *Gp5* (CD42), *Mpl* (TPOR), *Pf4* (Cxcl4). Furthermore, miR150 induces the megakaryocyte fate while repressing erythrocyte programs, such as the expression of *Myb* (Lu et al., 2008).

Downstream of commitment, megakaryocyte differentiation is regulated by NF-E2. NF-E2 is essential for the proliferation and endomitosis of megakaryocytes (Shivdasani et al., 1995). It also regulates genes involved in platelet biogenesis such as *Rab27* and *Tubb* (β-tubulin) (Lecine et al., 2000; Tiwari et al., 2003).

1.1.4 Conclusion

Collectively, hematopoiesis in the bone marrow is a tightly regulated process that ensures the lifelong and continuous production of all major blood and immune cell types found in the mammalian organism.

Interestingly however, it has been discovered that there are hematopoietic cells, such as **tissue-resident macrophages** (van Furth & Diesselhoff-den Dulk, 1984; Ajami et al., 2007; Ginhoux et al., 2010; Schulz et al., 2012; Yona et al., 2013; Hashimoto et al., 2013; Gomez Perdiguero et al., 2015) or **γδ-T cells** (Havran & Allison, 1990; Haas et al., 2012; reviewed in Soares-da-Silva et al., 2023) that maintain themselves independently from the bone marrow. To elucidate the origins of these cells it is essential to understand the emergence of hematopoietic cells in the embryonic and fetal period.

1.2 Genesis of a layered hematopoietic system

1.2.1 Historical and current views on developmental hematopoiesis[1]

The first hematopoietic cells arise in the extra-embryonic yolk sac. This was initially discovered through direct observation of avian embryo development which showed that the first red blood cells of the embryo develop in the yolk sac, within vascular structures termed blood islands (Wolff, 1764; Pander, 1817), before the onset of circulation (His, 1868). Subsequent advances in histology at the beginning of the 20th century enabled pioneering scientists to observe the development of hematopoietic in the mammalian yolk sac in cats, rabbits, mice, and rats (Maximow, 1909) as well as in chicken (Dantschakoff, 1908; Sabin, 1920) and human (Bloom & Bartelmez, 1940). I would like to highlight the illuminating work performed by embryologists Vera Dantschakoff and Florence Sabin who noticed the close relationship between hematopoietic cells and endothelial cells (Dantschakoff, 1908; Sabin, 1920). It was hypothesized that hematopoietic stem cells might emerge during this developmental period.

Work in the chicken embryo demonstrated that hematopoietic stem cells arise intra-embryonically and not from the yolk sac, contrary to what was initially proposed (Moore & Metcalf, 1970; Dieterlen-Lievre, 1975). This was later confirmed in the mouse model by several research groups. They identified the para-aortic splanchnopleura (P-Sp), the precursor of the aorta-gonad mesonephros (AGM), in the embryo proper as the site of hematopoietic stem cell emergence (Medvinsky et al., 1993; Müller et al., 1994; Medvinsky & Dzierzak, 1996; Cumano et al., 2001). Within the AGM region, hematopoietic cells emerge from the endothelium through a *Runx1*-dependent endothelial-to-hematopoietic transition (EHT) and form intra-aortic hematopoietic clusters (IAHC) confirming the initial notion of a close relationship between hematopoietic and endothelial cells (North et al., 1999; de Bruijn et al., 2000; Kissa & Herbomel, 2010; Boisset et al., 2010; Bertrand et al., 2010). The EHT process has been extensively reviewed (Jaffredo et al., 2005; Ottersbach, 2019).

Thanks to morphological and histological observations, transplantation and colony-forming assays, lineage tracing, bar-coding, and single-cell omics, it is now widely accepted that the blood and immune system develops in several consecutive waves. These progenitor waves are not only spatio-temporally distinct but analysis of mutant

[1] This section of the introduction is based on the review "Extra-embryonic hematopoietic lineages – to macrophages and beyond" published in the special issue "Making blood: Mechanisms of early hematopoietic development" of the journal of Experimental Hematology in August 2024 (Sommer & Gomez Perdiguero, 2024).

embryos for key transcription factors (such as *Runx1*, *Myb*, etc.) also revealed that they are controlled by different molecular mechanisms (discussed below).

In mice, the extraembryonic yolk sac first gives rise to (1) a primitive wave of blood cells, followed by (2) a transient definitive wave consisting mainly of erythro-myeloid progenitors (EMPs) (Maximow, 1909; Moore & Metcalf, 1970; Palis et al., 1999; McGrath et al., 2015; Gomez Perdiguero et al., 2015; Goh et al., 2023). Hematopoiesis then switches to the embryo proper, where (3) embryonic multipotent progenitors (eMPPs) and (4) hematopoietic stem cells (HSCs) emerge from the major arteries, such as the vitelline artery, umbilical artery and the dorsal aorta in the AGM. Intra- but not extraembryonic hematopoiesis can sustain life-long hematopoiesis (A. L. Medvinsky et al., 1993; Müller et al., 1994; Cumano et al., 2001; Patel et al., 2022; Yokomizo et al., 2022) (**Figure 2**).

Figure 2

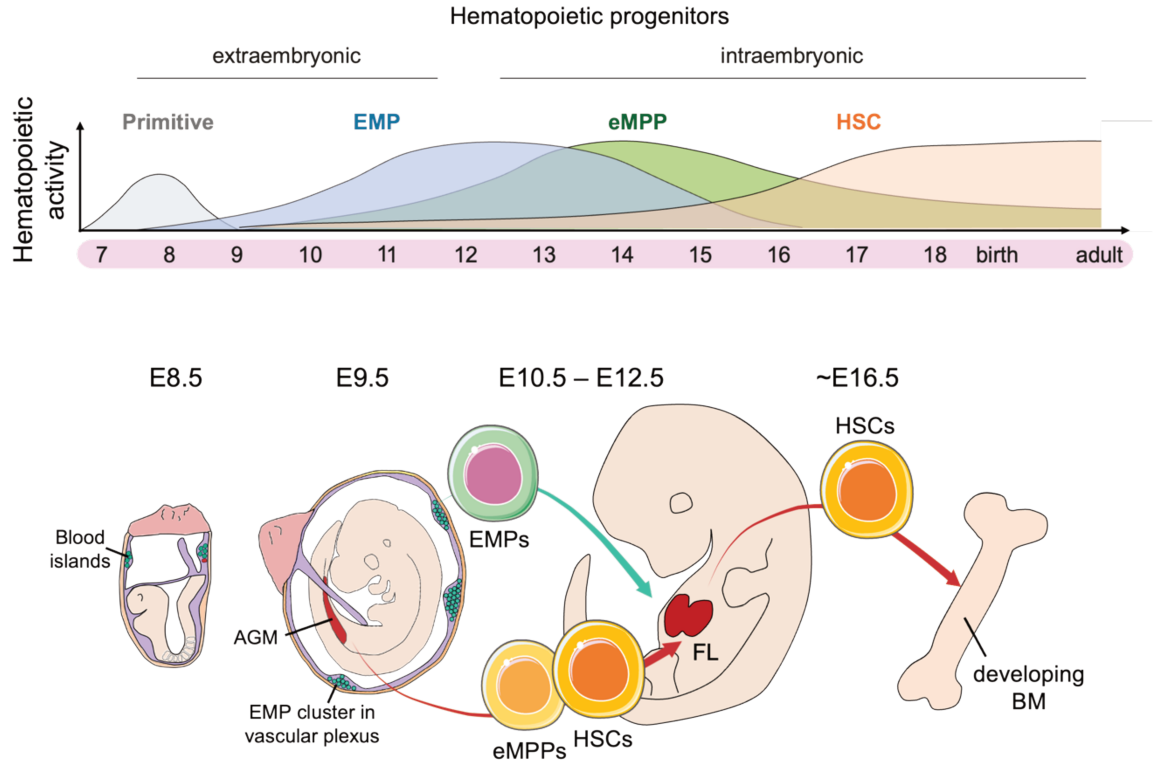

Figure 2. The hematopoietic system develops in sequential and overlapping waves. Primitive cells, mainly erythroblasts, emerge from the mesoderm in the yolk sac before embryonic day (E)8.5. Erythro-myeloid progenitors (EMPs) emerge from endothelial cells in the blood islands and vascular plexus in the yolk sac around E8.5 and are the main source of hematopoiesis until late gestation. Embryonic multipotent progenitors (eMPPs) emerge around E9.5 and give rise to committed progenitors around E14.5. Hematopoietic stem cells (HSCs) emerge around E10.5 in the aorta gonad mesonephro (AGM) region and produce mature cells only shortly before birth. EMPs, eMPPs, and HSCs seed the fetal liver, starting around E10.5, E11.5, and E12.5, respectively. Around E16.5, HSCs seed the developing bone marrow (BM), while hematopoietic activity persists in the fetal liver until after birth.

While it was long thought that yolk sac-derived hematopoiesis is simply a transient wave important for the survival of the embryo until hematopoietic stem cells are mature enough to supersede blood and immune cell production, research of the last decades has provided ample evidence that yolk sac-derived cells remain in the organism long after the end of yolk sac hematopoiesis and even into adulthood (Ginhoux et al., 2010; Schulz et al., 2012; Gomez Perdiguero et al., 2015; Gentek et al., 2018a; Soares-da-Silva et al., 2021).

1.2.2 Extraembryonic hematopoiesis

Extra-embryonic membranes, such as the amnion, chorion, yolk sac, and allantois, are essential for the survival of developing amniotic embryos (Sheng & Foley, 2012). These membranes take over functions such as absorption of macro- and micronutrients, gas exchange, excretion of metabolic waste as well as hematopoiesis, the production of blood cells (Cindrova-Davies et al., 2017).

Phylogenetically, the yolk sac is the oldest of these four extra-embryonic membranes and evolved in fish over 500 million years ago (Ross & Boroviak, 2020). It consists of an outer endodermal and an inner mesodermal lining (**Figure 3**). The endodermal layer of the yolk sac develops from the extra-embryonic visceral endoderm (originating from the primitive endoderm). The mesodermal layer on the other hand emerges from the posterior epiblast after epithelial-mesenchymal migration at the primitive streak during gastrulation (at Embryonic day (E)6.5) (reviewed by Arnold & Robertson, 2009). Around 24 hours later, the emergence of the first blood cells from this mesoderm layer will mark the start of hematopoiesis.

Primitive hematopoiesis

The first hematopoietic cells that emerge in the yolk sac are primitive cells. Here, we define primitive hematopoiesis as the production of mature blood cells from progenitors that arise directly from the mesoderm in the blood islands between E7.5 and E8.5, without undergoing an endothelial-to-hematopoietic process (Maximow, 1909; Palis et al., 1999; Ueno & Weissman, 2006) (**Figure 2, 3**). Primitive cells are independent of *c-Myb* (Tober, McGrath & Palis, 2008; Schulz et al., 2012) and *Runx1* (Lacaud et al., 2002; Potts et al., 2014), which means that they can develop in the absence of these factors whether they express them or not. Importantly, the term primitive can refer to different features and is further discussed below.

a. Primitive erythroblasts

Primitive erythroblasts are the first hematopoietic cells that develop in the vertebrate yolk sac and are essential for embryonic survival in mammals (Fujiwara et al., 1996). The development of primitive erythroblasts within the yolk sac blood islands is the best studied. Blood islands are mesodermal cell masses proliferating between the visceral

endoderm and mesothelial cell layer. While the outer cells differentiate into endothelial cells, mesodermal cells in the center of the cluster differentiate into primitive erythroblasts (Haar & Ackerman, 1971; reviewed by Ferkowicz & Yoder, 2005). These are larger than their definitive counterpart and contain both embryonic ζ -hemoglobin (εy- and βH1-globin) and adult α and β-hemoglobin (α1-, α2-, β1- and β2-globin) (Barker, 1968) and mature in circulation while retaining their nucleus until E12.5 (Kingsley et al., 2004). The primitive wave is the only source of red blood cells until E12.5 and can sustain the embryo until E15.5 (Mucenski et al., 1991; Kingsley et al., 2004). By E17.5 most primitive erythroblasts are gone but few are still detectable as late as 5 days after birth (Kingsley et al., 2004). Both in mice and humans, primitive erythroblasts contain more hemoglobin per cell than adult erythrocytes. In addition, they contain embryonic or fetal globins which have higher oxygen affinity than their adult counterpart which allows the transfer of oxygen from maternal to embryonic/fetal circulation (Kitchen & Brett, 1974; Palis, 2024; Kaufman, Khattar & Lappin, 2024).

b. Megakaryocytes

Concomitantly with primitive erythroblasts, megakaryocyte potential emerges in the yolk sac around E7.5, peaks around E8.5, and is no longer detectable after E13.5 (Maximow, 1909; Xu et al., 2001; Tober et al., 2007). Primitive megakaryocytes are more proliferative and require fewer cytokines than their adult counterparts (Xu et al., 2001). Compared to primitive erythroblast progenitors, primitive megakaryocytes are however low in number. Furthermore, these first megakaryocytes are smaller and have lower polyploidy when compared to their fetal liver or adult counterparts (Potts et al., 2014). Platelet formation from primitive megakaryocytes is also faster (Xu et al., 2001) and does not require thrombopoietin (Potts et al., 2015). Additionally, primitive-derived platelets are larger, contain more RNA, and show reduced clot-forming capacity than their adult counterparts (Margraf et al., 2017). They express CLEC-2 which is essential for lymph-angiogenesis, the establishment of the blood, and lymphatic vasculature. This is important to prevent hemorrhaging and to ensure that the blood and immune cells reach their targeted tissues. Dysfunctional or overactive platelets also perturb the correct development of the brain vasculature (Finney et al., 2012; Hoover et al., 2021).

c. Macrophages

Macrophage potential is first detected at E7.5 (on average 4 progenitors/yolk sac compared to 42 erythroid progenitors/yolk sac at the same stage) (Palis et al., 1999), while the first zygotic macrophages (defined as F4/80^{+}) only emerge in the yolk sac around E9.5 (Morris, Graham & Gordon, 1991). It is generally assumed that the first macrophages detected in the yolk sac are primitive, in accordance with findings in the zebrafish model (Herbomel, Thisse & Thisse, 2001). They were initially described as primitive based on their ultrastructural organization and detection prior to monocyte emergence (Takahashi, Yamamurma & Naito, 1989; Naito et al., 1989). Further, macrophage potential is more

abundant than erythro-myeloid potential at E8 in limiting dilution assays (Bertrand et al., 2005). Nevertheless, several findings are in support of a definitive (EMP) origin for yolk sac macrophages. First, macrophage potential in the yolk sac coincides with definitive erythroid potential and not with primitive erythroid potential (Palis et al., 1999; Lazarov et al., 2024). Second, macrophage numbers peak at E10, after definitive EMP progenitors emerge in the yolk sac (Gomez Perdiguero et al., 2015) . And last, yolk sac macrophages and microglia, the brain macrophage considered the prototype of primitive macrophages, are efficiently labeled with an endothelial inducible Cre driver (Gentek et al., 2018a) while primitive erythrocytes are not labeled (unpublished data from our laboratory), in line with an origin from a progenitor that underwent an endothelial-to-hematopoietic transition. Recently, a new mouse strain was proposed to specifically label the primitive wave but it also led to very efficient labeling (80%) of definitive EMPs at E10.5 (Zhao et al., 2023), limiting the scope of the conclusions. The lack of a robust primitive macrophage population in the mammalian embryo when compared to the zebrafish could be in part explained by the difference in "lifestyle" (*in utero* versus external development) and the presence of maternally derived macrophages in the early stages of mammalian development. Maternally derived macrophages are predominant in the yolk sac until E9, with their numbers peaking at E7.5/E8 (40 cells/yolk sac) (Bertrand et al., 2005). Indeed, to this day, a faithful tool to trace the primitive wave is not available and is most necessary to clarify in the mouse the quantitative contribution of primitive hematopoiesis to macrophage pools, and microglia in particular.

Yolk sac-derived definitive hematopoiesis – Erythro-myeloid progenitors (EMPs)

Erythro-myeloid progenitors (EMPs) are transient definitive multipotent progenitors that give rise to definitive erythrocytes, megakaryocytes, macrophages, mast cells, and granulocytes (Palis et al., 1999, 2001). They emerge in the yolk sac between E8.5 and E10.5 (Palis et al., 1999; Bertrand et al., 2005) from endothelial cells in the blood islands and vascular plexus through a *Runx1*-dependent endothelial-to-hematopoietic transition (EHT) (Chen et al., 2009; Frame et al., 2016; Kasaai et al., 2017). Unlike intra-embryonic hematopoiesis (North et al., 2009; Azzoni et al., 2021), EMP emergence is independent of blood flow and does not require an arterial origin (McGrath et al., 2015; Frame et al., 2016).

EMPs are defined by the expression of Kit, CD41, CD16/32, and AA4.1 (CD93) (McGrath et al., 2015; Gomez Perdiguero et al., 2015; Iturri et al., 2021). Kit is a marker for proliferation and survival. CD41 distinguishes hematopoietic from endothelial cells (Mikkola et al., 2003; Ferkowicz et al., 2003). CD16/32 (FcγRII/III) is a scavenger receptor for the Fc domain of IgG and labels early hematopoietic progenitors (de Andres et al., 1998). AA4.1 is an endothelial cell marker and labels nascent progenitors (Petrenko et al., 1999). Interestingly, EMP commitment and differentiation into mature cells is niche-dependent. While all EMPs express *Myb* – a transcription factor important for the

maintenance of proliferating hematopoietic stem and progenitor cells (reviewed by Ramsay & Gonda, 2008) – EMPs in the yolk sac differentiate *in situ* directly into macrophages and megakaryocytes without requiring *Myb* (Schulz et al., 2012; Gomez Perdiguero et al., 2015; Iturri et al., 2021). Additionally, they commit to more restricted erythroid and myeloid progenitors (Iturri et al., 2021). *Bona fide* multipotent EMPs, as well as downstream committed progenitors, seed the fetal liver around E9.0-E11.0 (Kieusseian et al., 2012; McGrath et al., 2015). Here, they unfold their full potential and differentiate in a *Myb*-dependent manner into definitive red blood cells, megakaryocytes, mast cells, granulocytes, and monocyte-like cells (McGrath et al., 2015; Li et al., 2018; Freyer et al., 2020; Iturri et al., 2021) (**Figure 3**). For some lineages, such as mast cells and macrophages, final maturation and/or tissue specialization will continue after seeding peripheral organs (Mass et al., 2016; Tauber et al., 2023).

a. Primitive versus definitive hematopoiesis

In the context of hematopoiesis, the terms "primitive" and "definitive have been used inconsistently in the literature.

Originally, the term "primitive" was introduced at the beginning of the 20th century to distinguish transient nucleated erythroblasts from the enucleated erythroblasts that replace the first (Saxer, 1896; Jolly, 1905; Dantschakoff, 1908; Maximow, 1909). "Primitive" in this case refers to the resemblance to red blood cells of lower vertebrates in which only large, nucleated red blood cells are found (Gulliver, 1875). The term also reflects the presence of embryonic hemoglobin. In this school of thought, blood cells emerging from the same ancestor as nucleated red blood cells will also be called primitive cells. Cells related to enucleated red blood cells without embryonic hemoglobin would be termed "definitive". Accordingly, EMPs should be termed "definitive".

However, the term "primitive" can also refer to the absence of full reconstitution potential in transplantation assays. By this definition, only *bona fide* stem cells and multipotent progenitors are "definitive" (Orkin & Zon, 2008; Ginhoux et al., 2010).

A third use of the term "primitive" is to describe cells not following the adult differentiation pathway. A well-known example of this is the differentiation of EMP-derived macrophages that develop without passing through a GMP or monocyte intermediate (Hoeffel et al., 2015; Gomez Perdiguero et al., 2015; Goh et al., 2023).

Lastly, "primitive" can also refer to differences in immature morphology or distinct functions in comparison to adult cells, which would be the case for most embryonic mature immune cells. This is the case in regards to primitive macrophages as termed by Naito and colleagues. Yolk sac macrophages at E10.5 lacked the classical ultrastructural features of fetal liver and adult macrophages (hence "primitive" morphology) and they

were observed before any monocytes were detected ("primitive" development that did not follow the classical adult differentiation cascade from monocytes) (Naito et al., 1989).

We propose that progenitors arising from an endothelial-to-hematopoietic transition should be termed as definitive, irrespective of the "primitive" or immature features of the mature cells they give rise to. In addition, the potential of primitive progenitors is restricted to a single lineage (either erythroid or myeloid). Recently, some papers have distinguished between primitive EMP and definitive EMP. EMP are defined as having erythroid and myeloid potential at the single-cell level (and they arise from an EHT), therefore they should not be referred to as primitive. To distinguish EMPs from *bona fide* HSCs and MPPs the terms "pro-definitive" (Canu & Ruhrberg, 2021) or "transient-definitive" (Calvanese & Mikkola, 2023) have been introduced.

b. Erythrocytes

EMPs are the main source of circulating erythrocytes (or red blood cells) from E12.5 onwards (Palis et al., 1999; Kingsley et al., 2004; Gomez Perdiguero et al., 2015), sustaining the embryo until late gestation (Mucenski et al., 1991; Chen et al., 2011; Soares-da-Silva et al., 2021). Accordingly, EMPs are skewed towards red blood cell production in the fetal liver (McGrath et al., 2015; Freyer et al., 2020). During differentiation, EMP-derived red blood cells pass through a megakaryocyte-erythrocyte progenitor (MEP) stage that is dependent on *Myb* (Mucenski et al., 1991; Iturri et al., 2021) (Figure 3). In contrast to primitive erythroblasts, EMP-derived red blood cells enucleate in the fetal liver before entering circulation (Kingsley et al., 2004). Further, they only express adult and not embryonic hemoglobin (Barker, 1968; Palis et al., 1999; Kingsley et al., 2004). Due to these differences compared to primitive erythroblasts, EMP-derived red blood cells are defined as "definitive".

c. Megakaryocytes

EMPs give rise to megakaryocytes through two distinct development trajectories in a time- and niche-specific manner: (1) through a direct *Myb*-independent differentiation path in the yolk sac, and (2) through a *Myb*-dependent MEP-intermediate in the fetal liver (Iturri et al., 2021) (Figure 3). The earlier differentiation pathway is reminiscent of the novel subset of Mk-primed HSCs that directly produce Mk in the adult bone marrow (Sanjuan-Pla et al., 2013; Carrelha et al., 2018; Rodriguez-Fraticelli et al., 2018; Morcos et al., 2022; Carrelha et al., 2024). EMP-derived *Myb*-independent megakaryocytes supersede primitive megakaryocytes in the yolk sac at E10.5. EMP-derived megakaryocytes then enter circulation, where they peak around E11.5, and are detectable until at least E14.5 (Iturri et al., 2021). Whether primitive megakaryocytes and *Myb*-independent EMP-derived megakaryocytes in the yolk sac are functionally different needs to be further investigated. However, the two waves of EMP-derived megakaryocytes likely have distinct traits since it has been shown that megakaryocytes in the yolk sac and the fetal liver reach

different polyploidy and have a distinct dependency on thrombopoietin (Potts et al., 2015).

Figure 3

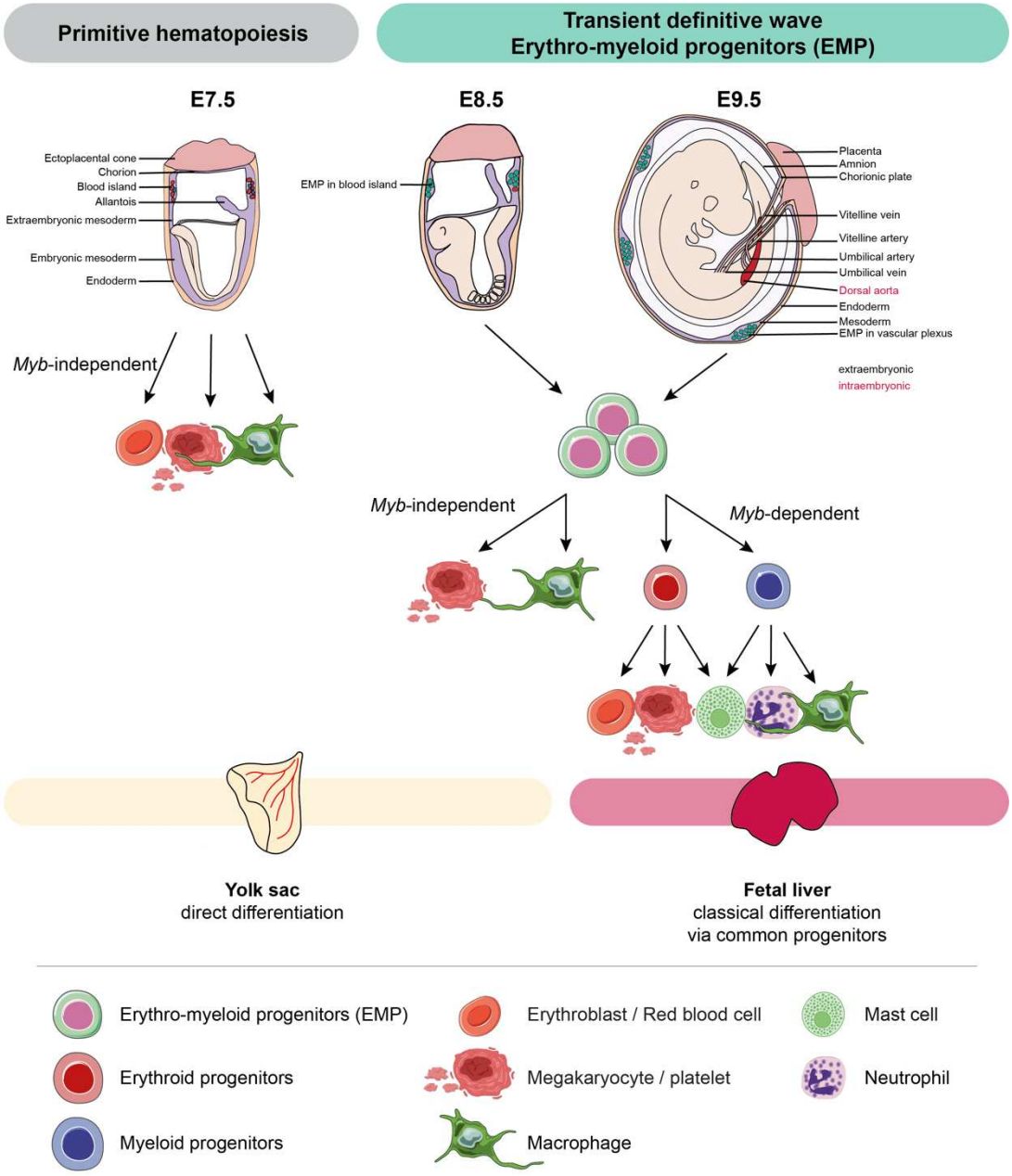

Figure 3. Yolk sac hematopoiesis. Primitive potential for erythroblasts, megakaryocytes and few macrophages is first detected around embryonic day (E)7.5 in the yolk sac. These primitive cells directly emerge from the mesoderm in the blood islands of the yolk sac. Around E8.5 transient definitive erythro-myeloid progenitors (EMPs) arise from the hemogenic endothelium in the yolk sac. *In situ* EMPs differentiate into megakaryocytes and macrophages in a *Myb*-independent manner. *Bona fide* EMPs and EMP-derived committed progenitors migrate to the fetal liver where they differentiate into definitive red blood cells, megakaryocytes, mast cells, neutrophils and macrophages in a *Myb*-dependent manner.

d. Mast cells

The first mast cells in the embryo derive from EMPs. Mast cell commitment from EMPs can be detected *in vitro* (Palis et al., 1999) and at the transcriptomic level (Iturri et al., 2021) in the yolk sac. However, mast cell progenitors, characterized by the expression of *Itgb7*, only start developing in the liver from E11 onwards, at the same time when the number of mast cell progenitors peaks in the yolk sac (Sonoda, Hayashi & Kitamura, 1983; Li et al., 2018). It is thus not clear whether the mast cell differentiation requires that fetal liver niche or not. Through the circulation mast cell progenitors seed tissues, such as the skin, spleen, lung, brain, heart, and peritoneal cavity where they complete their maturation (Li et al., 2018; Gentek et al., 2018a). EMP-derived tissue mast cells persist beyond birth and it was shown that ontogeny was linked to transcriptomic and immunophenotypic differences (Gentek et al., 2018a; Tauber et al., 2023).

e. Macrophages

The most famous EMP-derived cells are tissue-resident macrophages (Ginhoux et al., 2010; Hashimoto et al., 2013; Yona et al., 2013; Schulz et al., 2012; Gomez Perdiguero et al., 2015; Stremmel et al., 2018). In the yolk sac, EMPs directly differentiate into macrophages via a macrophage precursor, without passing through a monocyte-intermediate stage independently of *c-Myb* (Takahashi, Yamamurma & Naito, 1989; Schulz et al., 2012; Gomez Perdiguero et al., 2015; Hoeffel et al., 2015). Once the heart starts beating, EMP-derived macrophages seed the entire embryo proper via the circulation (Ginhoux et al., 2010; Stremmel et al., 2018). There, they adapt tissue-specific signatures over time (Mass et al., 2016). EMP-derived macrophages are often termed tissue-resident macrophages, as they self-maintain throughout life independently of bone marrow hematopoiesis (Ginhoux et al., 2010; Schulz et al., 2012; Hashimoto et al., 2013; Yona et al., 2013; Gomez Perdiguero et al., 2015). This is evident for microglia in the brain (Ginhoux et al., 2010), red-pulp macrophages in the spleen, alveolar macrophages in the lung, Langerhans cells in the epidermis, and Kupffer cells in the liver (Yona et al., 2013; Gomez Perdiguero et al., 2015), macrophages in the heart (Epelman et al., 2014) and testis (Lokka et al., 2020). We think that enhanced capability to give rise to tissue-resident macrophages is a distinct feature of EMPs and not a matter of window of opportunity (Monticelli et al., 2024).

It was proposed that EMPs can be distinguished as early and late EMPs, the latter presumably giving rise to monocyte-like cells in the fetal liver and proposed to contribute to tissue-resident macrophage pools (Hoeffel et al., 2015). The distinction of "early" and "late" is largely based on genetic labeling by tamoxifen (or 4-hydroxytamoxifen, its active metabolite)-induced Cre recombination at two time points that are 24 hours apart from each other (Hoeffel et al., 2015; Li et al., 2018; Iturri et al., 2021). More experimental evidence is required to support the existence of two biologically distinct EMP populations (and not just time- and niche-dependent effects) and to provide a quantitative assessment

of the contribution of EMP-derived monocytes to adult macrophages. Importantly, a recent study shows that Ly6C$^+$ monocyte labeling does not correlate with EMP-derived cells but rather with the eMPP progeny (Lazarov et al., 2024). The different macrophage differentiation pathways of early and late pulsed progenitors could thus rather reflect the contribution of different waves where the early pulse labels exclusively EMPs and the late wave a mix of EMPs and eMPPs.

f. Neutrophils

EMP-derived production of neutrophils begins around E11.5 in the fetal liver. These first neutrophils enter the blood around E12.5 where they circulate until at least E14.5 (McGrath et al., 2015; Freyer et al., 2020). Ontogenetic differences in neutrophils have been studied in zebrafish (García-López et al., 2023) and mouse (Sperandio et al., 2013). In the latter, there was a dramatic change in the ability of neutrophils to roll and adhere to inflamed yolk sac vessels, correlating with the change in neutrophil ontogeny. Before E15, when most blood neutrophils are EMP-derived (Freyer et al., 2020), rolling and adhesion were essentially absent. Later on (at E17), fetal neutrophils acquire the ability to roll and adhere as surface expression of CXCR2 begins to increase late in fetal life. Similarly, the rolling and adhesive capacities of fetal human neutrophils *in vitro* correlate with gestational age (Nussbaum et al., 2013). Thus, functional differences between EMP- and intra-embryonic-derived neutrophils exist and remain to be further investigated in the mouse model.

g. Lymphoid cells

Lymphoid cells are immune cells comprising innate (ILC1-3) or adaptive lymphoid cells (B and T cells). However, the first lymphoid cells emerge before *bona fide* HSCs appear (Yoshimoto et al., 2012). Most studies have not found lymphoid potential among EMPs. For instance, when McGrath et al. cultured EMPs (Kit$^+$ CD41$^+$ CD16/32$^+$) from E9.5 yolk sacs they did not detect any B cell output (McGrath et al., 2015). Furthermore, fate-mapping experiments using *Csf1r*^{MeriCreMer} pulsed at E8.5 came to the same conclusion that EMPs do not have B or T cell potential in the mouse (Gentek et al., 2018b; Elsaid et al., 2021). Intriguingly, a recent study based on fate mapping (*Csf1r*^{MeriCreMer} *Rosa26*^{YFP} pulsed at E9.5) claimed that EMPs produce the first NK cells (ILCs) in the fetal liver around E14.5, even though at low numbers (Dege et al., 2020). However, pulse labeling at E9.5 in this fate-mapping model also leads to low labeling of intra-embryonic HSPCs (Elsaid et al., 2021). Importantly, in a recent study, the labeling of lymphoid cells (T, B, and NK cells) in time-course fate-mapping experiments did not align with the labeling of EMP-derived erythrocytes, macrophages, or neutrophils (Lazarov et al., 2024). Lymphoid cells thus do not derive from EMPs.

1.2.3 Intraembryonic hematopoiesis

Transient intraembryonic-derived progenitors

The observation that the first lymphoid cells are neither EMP- nor HSC-dependent has led to the hypothesis of a distinct progenitor wave endowed with lymphoid potential (Böiers et al., 2013; Yoshimoto et al., 2012; Beaudin et al., 2016). Indeed, recent lineage tracing and barcoding experiments revealed a novel population of intraembryonic-derived hematopoietic progenitors labeled by *Hlf*^{CreERT2}, *Flt3*^{Cre}, or *Flt3*^{CreERT2} but not by HSC-specific lineage tracing such as *Evi1*^{CreERT2} (Beaudin et al., 2016; Yokomizo et al., 2022; Patel et al., 2022). In the *Cdh5*^{CreERT2} model, lymphoid cells are first labeled when pulsing with 4-OHT at E8.5 but not before (Barone et al., 2024).

Depending on the study, this progenitor wave has been given different names: developmentally restricted (drHSCs) (Beaudin et al., 2016), Lympho-myeloid biased progenitors (LMPs) (Zhu et al., 2020), embryonic multipotent progenitors (eMPPs) (Patel et al., 2022), or pre-HSPC/HSC-independent progenitors (Yokomizo et al., 2022). These transient progenitors emerge around E9.5 (**Figure 3**) and are multipotent (contribute to monocytes, granulocytes, erythrocytes, platelets, B and T cells) in the fetus and adult with a long-term bias for lymphoid cells (Beaudin et al., 2016; Patel et al., 2022).

In contrast to the 24 hours later emerging HSCs, they do not require a fully arterialized endothelium (Dignum et al., 2021). Interestingly, several studies observed that these transient progenitors may emerge preferentially in the vitelline and umbilical arteries (Yokomizo et al., 2022; Barone et al., 2024). The vitelline artery connects the AGM with the yolk sac and the borders between the tissues are obscure. This might explain the previously contradicting studies on whether the yolk sac is endowed with lymphoid potential (Cumano, Dieterlen-Lievre & Godin, 1996; Cumano et al., 2001; Yoshimoto et al., 2012).

Collectively, there is now a substantial body of research indicating that the initial lymphoid progenitors emerge in a distinct hematopoietic wave, characterized by unique spatial, temporal, and functional features in contrast to EMPs and HSCs.

Hematopoietic stem cells

HSCs emerge as the last hematopoietic wave around E10.5 in the AGM. Nascent HSCs are termed pre-HSCs as they first have to migrate to the fetal liver and mature before they acquire long-term reconstitution potential (Kieusseian et al., 2012; Rybtsov et al., 2016). The number of HSCs that emerge in the embryo is still under investigation (Kumaravelu et al., 2002; Ganuza et al., 2017). Similar to the adult bone marrow, the fetal liver contains long-term repopulation potential (secondary transplantation potential) in the Kit^{+} Sca-1^{+} CD150^{+} CD48^{neg} cells (immunophenotypic LT-HSCs) (Morrison et al., 1995; Sánchez et al., 1996; De Bruijn et al., 2002; Kim et al., 2006; Pietras et al., 2015). However,

there also might be long-term reconstitution potential in immunophenotypic ST-HSCs in contrast to the adult bone marrow since fetal and adult populations functionally differ despite expressing the same cell surface markers (Pietras et al., 2015; Stonehouse et al., 2024).

Attracted by CXCL12 (stem cell-derived factor 1, SDF-1) and stem cell factor (SCF) HSCs eventually leave the fetal liver niche and seed the spleen and the developing bone marrow around E15.5 and E16.5, respectively, via the bloodstream (Nagasawa et al., 1996; Ara et al., 2003; Christensen et al., 2004; Gekas et al., 2005; Coşkun et al., 2014; Hall et al., 2022). Hematopoietic potential is still detected in the liver until around two days, and in the spleen until around 14 days, after birth (Wolber et al., 2002; Collins et al., 2024; Monticelli et al., 2024). While HSCs are proliferative in the fetus, HSCs switch to a quiescent state between 3 and 4 weeks after birth (Bowie et al., 2007).

1.2.4 Developmental hematopoiesis from flies to humans

Drosophila melanogaster

Similar to vertebrates, the hematopoietic system of *Drosophila melanogaster* develops in consecutive waves (Holz et al., 2003; Crozatier & Meister, 2007; Banerjee et al., 2019) (Figure 4). Even though the hematopoietic system of drosophila consists of different cell types and hematopoietic organs than the mammalian model, some aspects of the fly blood system are highly conserved (Hoffmann et al., 1999; Traver & Zon, 2002; Gold & Brückner, 2014).

Drosophila does not have an adaptive immune system. Its blood and immune cell types are reduced to plasmatocytes, crystal cells, and lamellocytes which collectively are called hemocytes (Rizki, 1957; Lanot et al., 2001). Plasmatocytes (macrophage analog) have phagocytic and antimicrobial functions and secrete ECM proteins in all stages of development (Abrams et al., 1993; Tepass et al., 1994; Franc et al., 1996). Crystal cells are involved in oxygen transportation, wound healing, and the immune response through their phenoloxidase activity (Lebestky et al., 2000; Shin et al., 2024). Phenoloxidase is involved in the synthesis of melanin which clotts the hemolymph and encapsulates the pathogens (Söderhäll & Cerenius, 1998). Lamellocytes only appear upon wasp parasitization in the larval stage, upon which they destroy the parasitic wasp eggs by melanization (Rizki & Rizki, 1992, 1994).

Interestingly, the specification of hematopoietic potential and cell fate decisions are highly conserved between vertebrates and the fly (Lebestky et al., 2000). Serpent (Srp), Gata ortholog, is essential for hematopoietic development (Rehorn et al., 1996). U-shaped (Ush), a member of the Friend-of-GATA (FOG) family as well as Lozenge (Lz), a Runx1 homolog, are required for the development of crystal cells (Daga et al., 1996;

Lebestky et al., 2000; Fossett et al., 2001). Notch signaling is also required for crystal cell differentiation and lamellocyte proliferation during parasitization (Duvic et al., 2002).

a. Embryonic wave

The hematopoietic system of *Drosophila* is built through a first "embryonic wave" followed by a second "larval wave" (Holz et al., 2003). During the embryonic wave, hemocyte precursors emerge from procephalic mesoderm, also called head mesoderm in the early embryo (Tepass et al., 1994; Holz et al., 2003). This early wave gives rise to plasmatocytes (~90-95%, analog to tissue-resident macrophages) and crystal cells (~2-5%) (Tepass et al., 1994; Lanot et al., 2001). Plasmatocytes circulate through the hemolymph (analog to the blood) or attach to the body wall in sessile pools. Their migration is facilitated by autocrine secretion of the ECM-glycoprotein laminin (Sánchez-Sánchez et al., 2017). Importantly, embryonic hemocytes are the main active immune cell population during the larval stage and persist into adulthood (Lanot et al., 2001; Holz et al., 2003), reminiscent of EMP-derived macrophages (Ginhoux et al., 2010; Gomez Perdiguero et al., 2015).

b. Larval wave

During the larval stage, the dorsal or cardiogenic mesoderm gives rise to the dorsal vessels and lymph glands (Rugendorff, Younossi-Hartenstein & Hartenstein, 1994; Holz et al., 2003). The lymph gland is the hematopoietic organ of the larva and is comprised of one pair of large primary lobes and several smaller secondary lobes. The main lobe has an outer cortical and an inner medullary zone (Jung et al., 2005). Differentiated cells are only located in the cortical zone, whereas proliferating prohemocytes (progenitors) are found in both zones. The secondary lobes usually only contain immature hemocytes which do not differentiate in steady-state conditions (Jung et al., 2005).

As in the embryonic stage, prohemocytes in the larval stage differentiate into plasmatocytes, crystal cells, and lamellocytes (late-wave hemocytes) (Lanot et al., 2001). At the beginning of the pupal stage (after the third instar larva) the lymph glands disintegrate and release late-wave hemocytes, leaving behind empty lobes of ECM lamellae (Lanot et al., 2001; Holz et al., 2003; Grigorian, Mandal & Hartenstein, 2011).

c. Adult

Embryonic and larval hemocytes persist through metamorphosis and co-exist in the adult fly in a 60:40 ratio (Holz et al., 2003; Honti et al., 2014; Ghosh et al., 2015; Sanchez Bosch et al., 2019). Whether prohemocytes or hemocytes undergo proliferation and *de novo* differentiation in the adult fly remains under discussion (Ghosh et al., 2015; Sanchez Bosch et al., 2019).

Figure 4

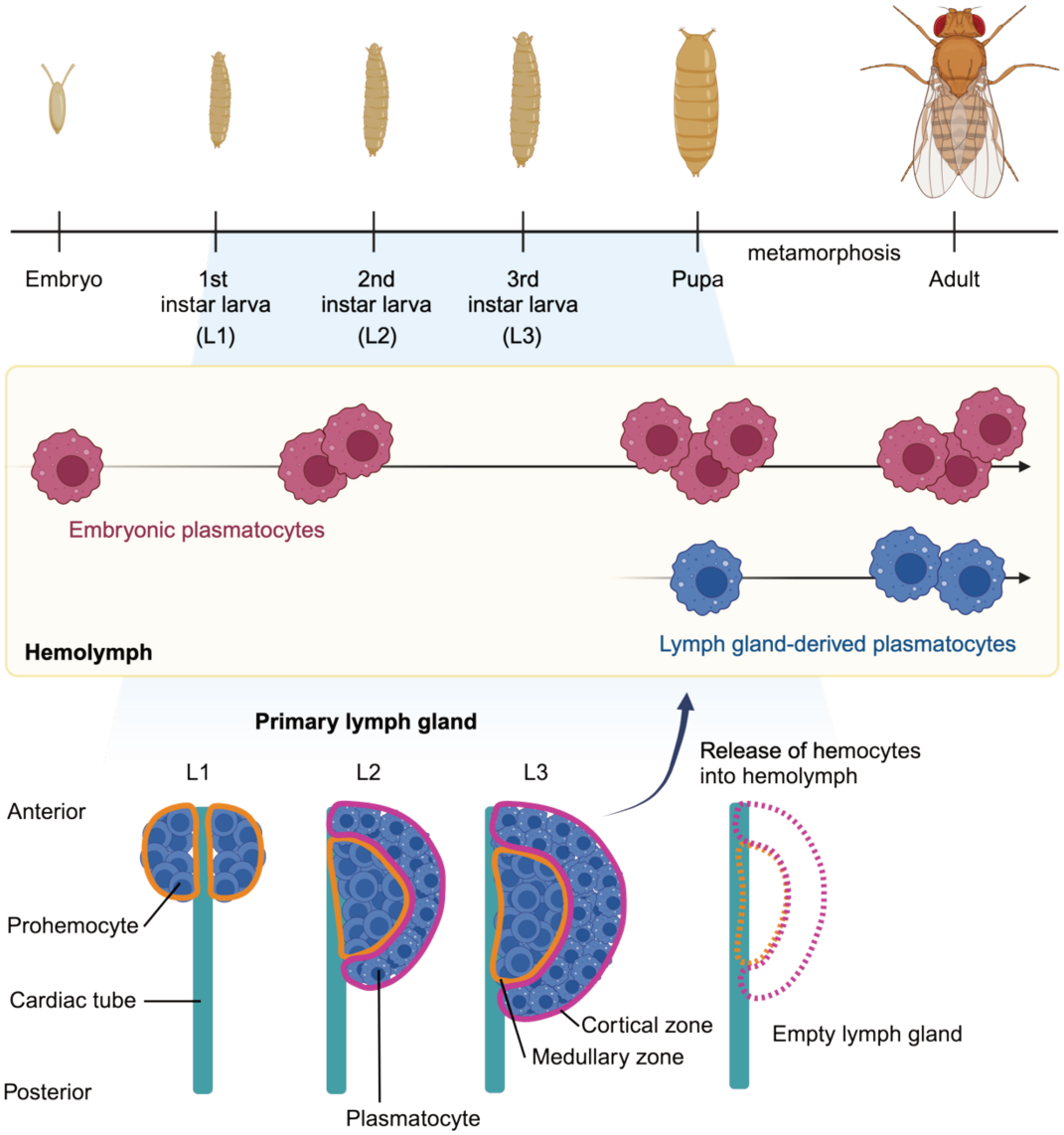

Figure 4. Developmental hematopoiesis in *Drosophila*. Early-wave plasmatocytes (macrophages, red) emerge in the embryo and are the main population of active immune cells in the larval stage. Late-wave plasmatocytes (blue) arise in the larval stage in the primary lymph gland where they expand and mature. At the end of the 3rd instar larva (L3), the lymph gland disintegrates and late-wave plasmatocytes are released into the hemolymph. In adulthood, embryonic and larval plasmatocytes co-exist in a ratio of 60:40. Created with biorender.com.

Zebrafish (*Danio rerio*)

Zebrafish have been instrumental in studying developmental hematopoiesis due to their high number of offspring, simple genetic manipulation, embryonic development outside of a womb, and optical transparency which enables visualization of blood and immune cells from emergence onwards. The hematopoietic system of zebrafish develops in sequential waves, a conserved feature in mammals and fish (**Figure 5**). Additionally, gene regulation in hematopoiesis as well as the close relationship between endothelial and hematopoietic cells are conserved.

a. Primitive hematopoiesis

Primitive hematopoiesis starts around the 2-9 somite stage (~11-14 hpf) in two different anatomical locations: The intermediate cell mass (ICM) derived from posterior lateral mesoderm (PLM) mainly gives rise to primitive erythrocytes characterized by expression of *gata*1 (Al-Adhami & Kunz, 1977; Detrich et al., 1995) (**Figure 5**). Similar to mice and humans, zebrafish primitive erythroblasts express embryonic hemoglobin which distinguishes them from definitive erythrocytes (Brownlie et al., 2003). Immature primitive erythroblasts migrate to the midtrunk region and exit onto the yolk sac, where they mature (Detrich et al., 1995; Herbomel, Thisse & Thisse, 1999). With the onset of the heartbeat around 24 hpf, primitive erythroid progenitors enter circulation (Willett et al., 1999).

The second site of primitive hematopoiesis are the rostral blood islands (RBIs) which lie on top of the yolk sac surface and originate from anterior lateral-plate mesoderm (ALPM) (Herbomel, Thisse & Thisse, 1999). Around 9 somites, the RBIs give rise to macrophage and neutrophil precursors expressing amongst others *l-plastin*, *pu.1, scl* and *flk1* (Herbomel, Thisse & Thisse, 1999; Willett et al., 1999; Le Guyader et al., 2008). They migrate to the yolk sac between the 14-30 somite stage before the arrival of primitive erythroblasts and before the onset of circulation (Herbomel, Thisse & Thisse, 1999). Compared to mammals, the zebrafish yolk sac mainly functions as a nutrient supply and does not show generative hematopoietic potential. Instead, the yolk sac is the site where neutrophils and macrophages proliferate and mature before they seed other tissues (Herbomel, Thisse & Thisse, 2001; Le Guyader et al., 2008).

By 16-18 hpf (17 to 18-somites) primitive macrophages seed the mesenchyme throughout the embryo (Herbomel, Thisse & Thisse, 2001). Reminiscent of mice, these first macrophages seed the brain and differentiate into microglia (Herbomel, Thisse & Thisse, 1999; Ginhoux et al., 2010). However, in contrast to mice, they are later progressively replaced by microglia from the definitive hematopoietic wave in adulthood (Xu et al., 2015; Ferrero et al., 2018).

The first neutrophils seed the mesenchyme and epidermis (Lieschke et al., 2001; Le Guyader et al., 2008). Primitive macrophages and neutrophils are important for immunity

and tissue repair in the embryo and larva and are regulated differently on the transcriptional level than their definitive counterparts (Le Guyader et al., 2008; Herbomel, Thisse & Thisse, 1999; Xu et al., 2015; García-López et al., 2023; Elsaid et al., 2024).

Figure 5

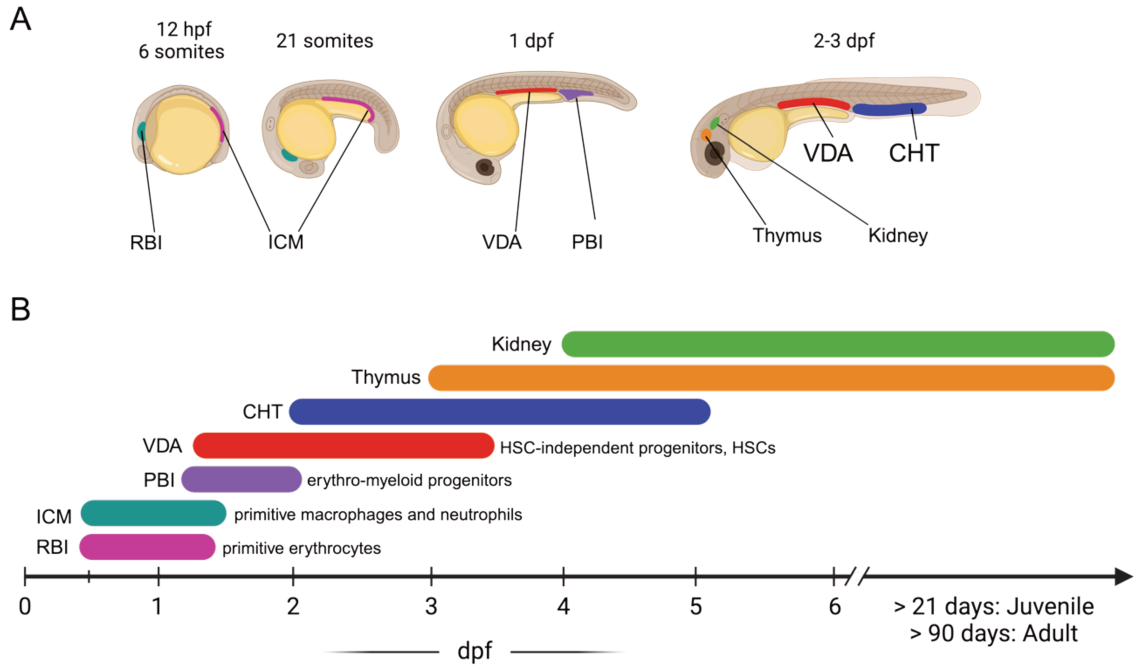

Figure 5. Developmental hematopoiesis in zebrafish. The hematopoietic system in zebrafish develops in several sequential and overlapping hematopoietic waves similar to mice. The first primitive erythrocytes emerge in the rostral blood islands (RBI). Primitive macrophages and neutrophils develop in the intermediate cell mass (ICM). Erythro-myeloid progenitors (Emp) arise in the posterior blood islands (PBI) and finally, hematopoietic stem and progenitor cells emerge from the ventral wall of the dorsal aorta (VDA). Adult hematopoiesis takes place in the kidney and thymus. (**A**) Scheme illustrating the hematopoietic organs in the zebrafish embryo between 12 hours post fertilization (hpf) and 3 days post fertilization (dpf). CHT, caudal hematopoietic tissue. (**B**) Scheme illustrating the period and organ in which the overlapping hematopoietic waves are active including their progenitor output. Created with biorender.com.

b. Definitive hematopoiesis

Around 30 hpf, hematopoiesis shifts from the yolk sac to the ventral side of the tail just behind the end of the yolk extension (posterior blood islands, PBI) (Bertrand et al., 2007). Around 30-36 hpf erythro-myeloid progenitors (EMPs) appear in the PBI that co-express *lmo2* (endothelial marker) and *gata1* and give rise to erythrocytes, thrombocytes macrophages, and neutrophils (Lin et al., 2005; Bertrand et al., 2007; Le Guyader et al., 2008). EMPs are independent of Notch-signaling and do not seed the thymus or kidney in contrast to lymphoid progenitors or HSCs that emerge later (Murayama et al., 2006; Bertrand et al., 2010b).

Lastly, HSC-independent progenitors with lymphoid potential and *bona fide* HSCs (*cd41*$^{+}$ *kdr*$^{+}$ *cmyb*$^{+}$ *cd45*$^{+}$) emerge via a *Runx1*-dependent endothelial-to-hematopoietic

transition (EHT) in the sub-aortic space in the ventral wall of the dorsal aorta (VDA, analog to the murine AGM region) in the zebrafish trunk 2 dpf or 3 dpf, respectively (Murayama et al., 2006; Jin, Xu & Wen, 2007; Bertrand et al., 2010a; Kissa & Herbomel, 2010; Tian et al., 2017; Ulloa Bianca A et al., 2021). Pro-inflammatory signals from primitive neutrophils induce hematopoietic specification of endothelial cells and matrix metalloproteinases (MMPs) facilitate the egress from the endothelium (Espín-Palazón et al., 2014; Theodore et al., 2017). The nascent progenitors seed the caudal hematopoietic tissue (CHT, developed from the PBI and analog to the murine fetal liver) through the blood circulation where they expand and differentiate until 7 dpf (Murayama et al., 2006). From there, HSC-independent lymphoid progenitors start seeding the developing thymus around 3 dpf whereas HSCs seed the kidney at 4 dpf (Willett et al., 1999; Murayama et al., 2006; Jin, Xu & Wen, 2007). HSC-independent progenitors produce mature blood and immune cells starting around 5 dpf. HSCs, by contrast, do not differentiate before 7 dpf (Ulloa Bianca A et al., 2021). This dynamic is reminiscent of the switch from eMPPs to HSCs in mice (Zhu et al., 2020; Yokomizo et al., 2022).

Finally, the mature kidney (bone marrow analog) starts producing mature erythroid, myeloid, and lymphoid cells around 2-3 weeks of development (Willett et al., 1999).

Human

Human pregnancies last on average 266 days or 38 weeks post conception (280 days/40 weeks post gestation) instead of 19 days (post gestation) in mice. Human embryos first develop a primary yolk sac (Carnegie stage (CS) 4, 1 post-conception week (pcw)). A secondary yolk sac replaces the primary yolk sac around 2.5 pcw (CS6) and persists until ~8 weeks (CS23) (Luckett, 1978). The secondary yolk sac, a balloon-like appendage inside the amnion, is the site where hematopoiesis begins in humans (Calvanese & Mikkola, 2023).

As in mice, the first blood cells in the human embryo are primitive erythroblasts that emerge in blood islands in the yolk sac between 16-18.5 days after fertilization (CS7-8) (Bloom & Bartelmez, 1940; Tavian, Hallais & Peault, 1999; Tyser et al., 2021). These primitive erythroblasts, contain embryonic hemoglobin (ζ/ε globins) and enter the circulation as nucleated cells around 3 pcw (~4 ssp) (Peschle et al., 1984). Human primitive erythroblasts enucleate starting around 5 pcw in the placenta through interaction with macrophages (Hofbauer cells) (Van Handel et al., 2010).

Next to primitive red blood cells, the human yolk sac gives rise to transient EMPs that emerge from endothelial cells (Tavian, Hallais & Peault, 1999). EMPs (also called early HSPCs in the literature) appear around 2-3 pcw and are detectable until 8 pcw at the most (Goh et al., 2023). They commit to myeloid progenitors and megakaryocyte-erythrocyte progenitors and eventually differentiate into mainly red blood cells, megakaryocytes, and macrophages in the yolk sac and fetal liver (Tavian, Hallais & Peault, 1999; Tyser et al.,

2021; Popescu et al., 2019; Goh et al., 2023). One study also attributed mast cell potential to human EMPs (Popescu et al., 2019). Unlike mice, EMPs in humans do not produce neutrophils. Granulopoiesis only takes place in the bone marrow at 14 pcw (Ohls et al., 1995; Popescu et al., 2019). Similar to findings in the mouse model (Schulz et al., 2012; Gomez Perdiguero et al., 2015; Hoeffel et al., 2015), human macrophages most likely differentiate in the yolk sac without passing through a monocyte stage (Goh et al., 2023).

Early experiments on human embryoid bodies led to the conclusion that yolk sac-derived EMPs have *de novo* T cell potential (Atkins et al., 2021). By contrast, previous culture experiments and recent findings from single-cell RNA sequencing of human hematopoietic tissues support the notion that the EMPs in the yolk sac have no lymphoid potential, as lymphoid cells in the yolk sac were detected only after the onset of AGM-hematopoiesis (Tavian et al., 1996; Tavian, Hallais & Peault, 1999; Goh et al., 2023). Nevertheless, this highlights that AGM-derived cells colonize the yolk sac before reaching the fetal liver (Calvanese et al., 2022).

As in mice, the human placenta is a site of hematopoiesis. Whether only maturation or also *de novo* generation occurs in the placenta is still under investigation (Ivanovs et al., 2011; Calvanese et al., 2022; Thomas et al., 2023).

One of the biggest differences between murine and human developmental hematopoiesis is the onset of bone marrow colonization by hematopoietic progenitors. Whereas in the mouse bone marrow hematopoiesis only starts around birth, in human fetuses, HSCs seed the bone marrow already around 12 pcw (Charbord et al., 1996; Gekas et al., 2005; Hall et al., 2022). Thus, while in mice EMPs are the main source of mature blood cells until birth, yolk sac-derived cells most likely have different kinetics in human development.

1.2.5 Conclusion

Altogether, this demonstrates that the sequential establishment of the hematopoietic system is highly conserved throughout the animal kingdom, suggesting its essential role in fetal development. In the following, I will discuss the molecular mechanisms that regulate each individual hematopoietic wave, the functional differences between them, and elaborate on some of the reasons why this complex process is beneficial for fetal development.

1.3 Commonalities, differences, and interplay between EMPs and HSCs

1.3.1 Molecular regulation of hematopoietic specification and emergence

The emergence of each hematopoietic wave is tightly regulated. As we will see below, there are minimum requirements to generate primitive hematopoietic cells, while definitive EMPs, eMPPs, and HSCs depend on increasingly complex signaling pathways and transcription factor networks (**Table 2, Figure 6**). As relatively little is known so far about eMPPs, I will mainly focus on EMPs and HSCs. Both emerge from hemogenic endothelium (endothelial cells with hematopoietic potential) through a hematopoietic-to-endothelial transition (EHT). The EHT process was concurrently described in mice and zebrafish by three independent laboratories (Kissa & Herbomel, 2010; Bertrand et al., 2010a; Boisset et al., 2010). The close relationship between endothelial cells and hematopoietic cells as well as the key molecular mechanisms of hematopoietic specification were however known long before the discovery of EHT (Dantschakoff, 1908; Sabin, 1920; Tsai et al., 1994; North et al., 1999; Kumano et al., 2003). During EHT, endothelial cells take on a hematopoietic fate. They bud into the lumen of the blood vessel in mice and into the subaortic space in zebrafish.

Even though EMPs and HSCs both emerge via an EHT, they derive from distinct populations of hemogenic endothelium (Chen et al., 2011). EMPs can emerge from endothelial cells in the yolk sac blood islands and vascular plexus before venous and arterial specification whereas HSC emergence is restricted to an arterial origin (Gordon-Keylock et al., 2013; Frame et al., 2016; Kasaai et al., 2017).

Table 2 Requirement of molecular regulators for the emergence of hematopoietic waves

Requirement of molecular regulator	Primitive cells	EMPs	HSCs
Wnt/β-catenin	?	yes	yes
Sox7	no	yes	yes
Sox17	no	no	yes
Notch1	no	no	yes
Gata2	no	yes	yes
Gata2 bookmarking during emergence	no	no	yes
Runx1	no	yes	yes
Zfat	yes	?	?

The specification and emergence of the hematopoietic fate in the endothelium are finely tuned by different transcription factors and signaling pathways.

Zfat

Zfat, a transcriptional regulator containing a zinc finger domain, is expressed in the yolk sac from E6.5 onwards (Tsunoda et al., 2010). *Zfat*-deficient embryos die around E9.5. The vascular system in the yolk sac is normal but the blood islands are devoid of hematopoietic cells. Zfat binds the promoters of *Scl*, *Lmo2*, and *Gata1*, key transcription factors in erythropoiesis (Robb et al., 1995; Shivdasani, Mayer & Orkin, 1995; Fujiwara et al., 1996; Tsunoda et al., 2010). Their expression is abolished in *Zfat*-deficient yolk sacs at E7.5. This indicates that ZFAT most likely is one of the key regulators of the emergence of primitive cells and is important for the initiation of the erythroid program. Interestingly, the lack of *Zfat* does not impair *Gata2* expression, indicating that *Zfat* and *Gata2* are regulated independently (Tsunoda et al., 2010).

Zfat expression is also detected in the early progenitor stages of erythropoiesis in the fetal liver indicating that it participates in definitive hematopoiesis (Tsunoda et al., 2018).

Wnt/β-catenin signaling

Wnt signaling is involved in countless processes in the organism. It is important for the maintenance and integrity of the vasculature and also for the emergence of EMPs and HSCs (Cattelino et al., 2003; Yamamizu et al., 2010; Ruiz-Herguido et al., 2012; Frame et al., 2016). The binding of Wnt ligands to Frizzled receptors initiates a phosphorylation cascade preventing the degradation of β-catenin. β-catenin thus accumulates and migrates from the cytoplasm to the nucleus where it regulates transcription by interacting with T-cell-specific factor/lymphoid enhancer-binding factor (TCF/LEF).

Conditional deletion of *β-catenin* in endothelial cells perturbs EMP emergence in the yolk sac (Frame et al., 2016). Similarly, inhibition of β-catenin in the AGM at E10.5 impairs HSC function in colony-forming assays as well as in reconstitution experiments. The same inhibition however did not affect the AGM at E11.5, indicating that HSCs become independent of *Wnt* signaling with progressive maturation (Ruiz-Herguido et al., 2012).

The hematopoietic specification in the AGM does not only rely on Wnt signaling but also requires other factors that act synergistically. Interestingly, in the regulation of endothelial cells Wnt signaling was placed upstream of *Sox17* and *Notch* signaling (Corada et al., 2013).

Figure 6

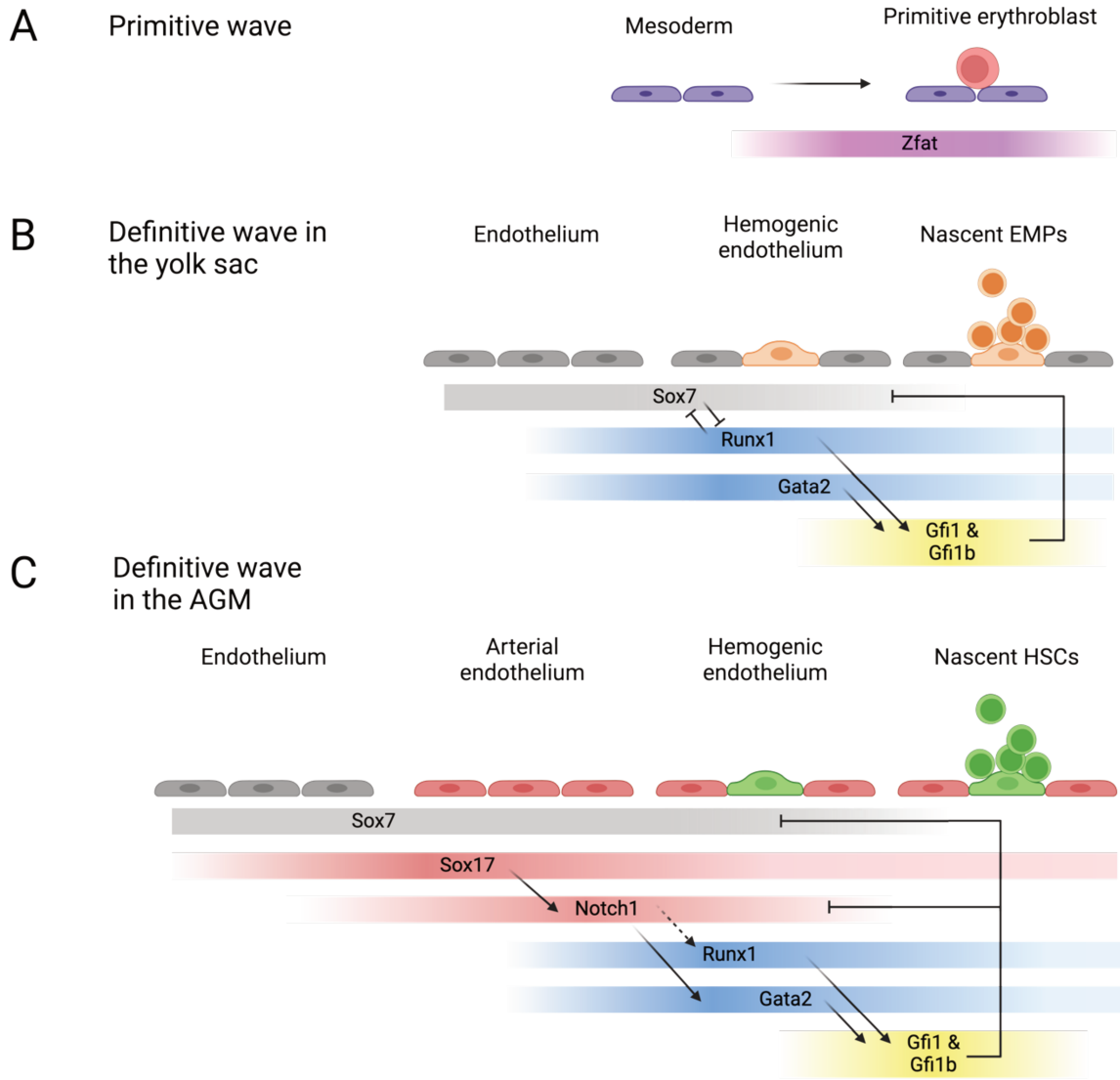

Figure 6. Molecular regulation of hematopoietic specification and emergence. (**A**) Primitive erythroblasts directly emerge from the mesoderm regulated by Zfat. (**B**)Erythro-myeloid progenitors (EMPs) emerge from hemogenic endothelial cells. (**C**) Hematopoietic stem cells (HSCs) in the aorta gonad mesonephro region (AGM) from arterial hemogenic endothelium.

SoxF family

The *SoxF* family (SRY related-HMG box family F) contains 3 transcription factors, *Sox7*, *Sox17*, and *Sox18*, that are involved in angio- and lymphangiogenesis (Francois, Koopman & Beltrame, 2010).

Sox7 is first expressed around E7.5 in the endothelial cells in the blood islands as well as in the arterial and venous endothelium of the yolk sac. Additionally, *Sox7* expression is also found in the endothelium of the dorsal aorta (Gandillet et al., 2009; Costa et al., 2012; Lilly et al., 2016). Enforced expression of *Sox7* does not affect hematopoietic specification in the endothelium but prevents maturation and differentiation of hematopoietic progenitor downstream of their emergence (Gandillet et al., 2009; Costa

et al., 2012). SOX7 inhibits hematopoiesis by physically interacting with RUNX1. This perturbs the CBFbeta-RUNX1 complex hindering the binding of RUNX1 to the DNA (Lilly et al., 2016).

Likewise, *Sox17* is expressed in hemogenic endothelium where it represses hematopoietic genes such as *Gata2* and *Runx1* (Kim, Saunders & Morrison, 2007; Corada et al., 2013; Clarke et al., 2013; Lizama et al., 2015). Contrary to *Sox7*, *Sox17* however is specific to arterial endothelium and thus is more important for HSCs than for EMPs. The conditional knockout of Sox17 in endothelial cells does not impair primitive erythropoiesis or the function of EMPs. The number of EMPs and HSCs emerging in the yolk sac and AGM, respectively, however, are decreased (Kim, Saunders & Morrison, 2007; Clarke et al., 2013).

The loss of *Sox17* during EHT in the AGM increases the emergence of hematopoietic progenitor and stem cells (Lizama et al., 2015). This increase in EHT can be rescued through overexpression of *Notch1* (Lizama et al., 2015), which places *Sox17* upstream of *Notch1* (Corada et al., 2013). Indeed, it has been demonstrated that SOX17 binds upstream of the *Notch1* 5'-untranslated region and the Notch ligand *Dll4* (Clarke et al., 2013; Corada et al., 2013; Lizama et al., 2015). Sox17 and Notch1 regulation is bidirectional since *Notch1* also counter-regulates *Sox17* (Lee et al., 2014; Lizama et al., 2015).

After hematopoietic specification, *Sox17* is crucial to regulate the survival and maintenance of fetal and neonatal HSCs but is no longer required in adult HSCs (Kim, Saunders & Morrison, 2007).

Notch1

Similar to Sox17, *Notch1* governs arterial identity and tightly regulates the balance between endothelial and hematopoietic fate (Krebs et al., 2000; Lawson et al., 2001). Increased Notch signaling promotes arterial programs in endothelial cells while inhibiting hematopoietic fate (Lizama et al., 2015; Gama-Norton et al., 2015). Notch1 is essential for the hematopoietic specification of endothelial cells in the AGM but not for primitive cells or EMPs (Kumano et al., 2003; Hadland et al., 2004).

Upon interaction with one of its ligands, Jagged 1 (*Jag1*) (Xue et al., 1999; Robert-Moreno et al., 2008), the intracellular domain of Notch1 is cleaved and translocates to the nucleus. There, it collaborates with RBPjk to activate target genes such as the hematopoietic transcription factor *Gata2* while simultaneously inhibiting endothelial genes (Robert-Moreno et al., 2005, 2008; Guiu et al., 2012; Gama-Norton et al., 2015). Since ectopic expression of *Gata2* in embryos lacking Notch signaling rescues hematopoiesis (Robert-Moreno et al., 2008), *Gata2* is placed downstream of Notch (Robert-Moreno et al., 2005; Gama-Norton et al., 2015). Other transcription factors such as *Scl* and *Runx1* are also

sensitive to Notch signaling even though they are not direct targets (Robert-Moreno et al., 2005; Gama-Norton et al., 2015).

Notably, Notch1 is only important during specification and emergence but not thereafter. In fact, to properly mature, Notch has to be downregulated in developing HSCs (Souilhol et al., 2016).

Gata2

Concurrent with the downregulation of arterial genes such as *Notch1* and *Sox17*, *Gata2*, is upregulated. GATA2 promotes the hematopoietic specification of endothelial cells in the yolk sac and major arteries and is important for HSC maturation in intra-aortic hematopoietic clusters (Tsai et al., 1994; Tsai & Orkin, 1997; Koyunlar et al., 2023). During EHT, GATA2 induces *Gfi1b*, a repressor of endothelial identity which counteracts Notch signaling (Koyunlar et al., 2023).

Gata2 has different functions and is differently required in the primitive, EMP, and HSC wave. The +9.5 *cis*-regulatory element of Gata2 is required for HSC-emergence in the AGM, but primitive erythropoiesis in the E8.0 yolk sac is normal (Johnson et al., 2012; Gao et al., 2013). While these studies did not specifically probe the effect of +9.5 knockouts on EMPs, the colony-forming potential in the E12.5 fetal liver was severely decreased. Since EMPs make up for a considerable proportion of fetal liver hematopoiesis at this stage, this may indicate that not only HSCs but perhaps also EMPs depend on the +9.5 regulatory element (Gao et al., 2013).

Additionally, mitotic bookmarking is essential for the emergence of hematopoietic progenitors in the AGM but not for EMPs in the yolk sac (Silvério-Alves et al., 2023). Forced degradation of Gata2 during mitosis (impaired bookmarking) does not affect the functional output nor the numbers of EMPs in the yolk sac at E9.5. Also, at E10.5 the output in CFU assays of fetal liver cells (mainly containing EMPs at this stage) is normal in terms of frequencies. However, the number of colonies was significantly reduced. This indicates that Gata2 bookmarking is not essential for the emergence of differentiation of EMPs but is involved in the expansion of the progenitor population. By contrast, both the number of intra-aortic hematopoietic clusters, colony output in the AGM and the long-term engraftment potential was highly impaired when Gata2 bookmarking was perturbed. This suggests that only the emergence of HSCs and not EMPs depends on Gata2 mitotic bookmarking (Silvério-Alves et al., 2023).

After the emergence from hemogenic endothelium, the dose and timing of *Gata2* expression has to be tightly regulated as the lack of timely repression of *Gata2* causes an increase in the number of HSCs with a concomitant loss of their functionality (Ling et al., 2004; Guiu et al., 2012; Eich et al., 2017).

Downstream of EHT, hematopoietic maturation, and maintenance, Gata2 is involved in lineage commitment as discussed above (Bone marrow hematopoiesis – Transcriptional regulation of lineage commitment).

Runx1

RUNX1 (Runt-related transcription factor 1, AML1, Cbfa2) is considered a master regulator of EHT as its ectopic expression in endothelial cells is sufficient to induce hematopoietic fate in the endothelium (Yzaguirre et al., 2018). RUNX1 and its non-DNA binding partner Core binding factor beta (CBFβ) are crucial for the emergence of EMPs and HSCs from the endothelium in the yolk sac and AGM, respectively. By contrast, primitive hematopoiesis is independent of RUNX1 (Wang et al., 1996a; Okuda et al., 1996; North et al., 1999; Cai et al., 2000; North et al., 2002; Lacaud et al., 2002; Chen et al., 2009; Frame et al., 2016).

Several cues such as BMP4 signaling via Smad1, shear stress, or inflammatory signaling induce R*unx1* expression (Pimanda et al., 2007; Adamo et al., 2009; Espín-Palazón et al., 2014). Importantly, Runx1, however, is not a direct target of Notch1 (Robert-Moreno et al., 2005; Gama-Norton et al., 2015). Nevertheless, since retro-viral expression of *Runx1* in *Notch1*-deficient para-aortic splanchnopleura explants rescues hematopoiesis *in vitro, Runx1* is functionally placed downstream of *Notch* (Nakagawa et al., 2006).

RUNX1 and GATA2 have overlapping functions and act in synergy in a dose-dependent manner (Wilson et al., 2010). Similar to GATA2, RUNX1 inhibits endothelial gene expression via its direct targets *Gfi1* and *Gfi1b* both in EMPs and in HSCs (Lancrin et al., 2012). Furthermore, both RUNX1 and GATA2 are not only required for the EHT process but are also part of the transcription factor heptad regulating HSC maintenance and differentiation (discussed in Transcriptional regulation of HSCs) (Wilson et al., 2010).

Conclusion

While this is not an exhaustive list of the factors governing hematopoietic specification and emergence, it illustrates that each hematopoietic wave is controlled by unique molecular mechanisms. This opens up the possibility that each wave could be disrupted differently in the event of perturbation.

1.3.2 At the cross-section between hematopoietic waves

Switch from extra- to intraembryonic hematopoiesis

The tight molecular regulation is closely tied to the strict temporal and spatial regulation of hematopoietic wave formation. The first primitive potential is detected around E7.5 and the first EMPs emerge at E8.5 in the yolk sac (Palis et al., 1999; McGrath et al., 2015; Gomez Perdiguero et al., 2015). eMPPs arise around E9.5 in the major arteries, followed by *bona fide* HSCs at E10.5 (Müller et al., 1994; De Bruijn et al., 2002; Böiers et al., 2013; Patel et al., 2022; Yokomizo et al., 2022).

Both EMPs, eMPPs and HSCs commit to immunophenotypic CMP, GMP, and MEPs (summarized as Lin$^-$ Kit$^+$ Sca-1^{neg} cells (LK)), which are progenitors with increased commitment towards erythroid and myeloid fates. The switch from EMP to intraembryonic contribution (eMPP) to these progenitor populations occurs around E14.5 (Freyer et al., 2020; Yokomizo et al., 2022).

Another 24-48 hours later (around E15.5-E16.5), the eMPP- and shortly after HSC-derived committed progenitors differentiate into mature blood and immune cells in the fetal liver superseding the EMP-derived progeny. Surprisingly, however, eMPP and HSC-derived mature blood and immune cells are not found in circulation until shortly before birth (neutrophils, red blood cells) (Freyer et al., 2020; Soares-da-Silva et al., 2021; Zhang et al., 2021; Yokomizo et al., 2022; Lazarov et al., 2024) (**Figure 7A**).

Figure 7

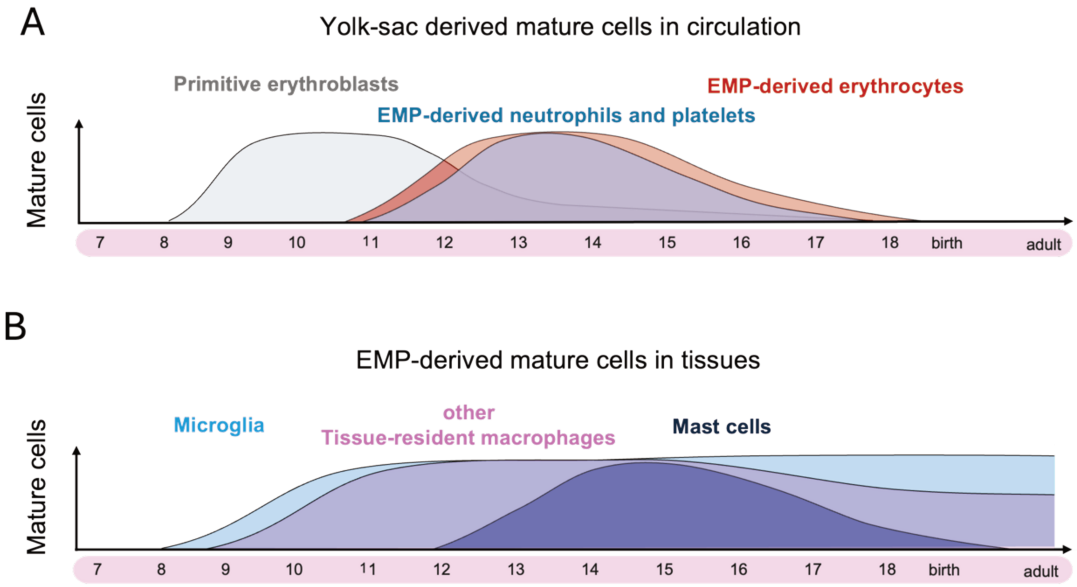

Figure 7. Contribution of yolk sac-derived mature cells during fetal life and beyond. (**A**) Primitive erythroblasts are the main source of red blood cells until E12.5 and are then superseded by EMP-derived erythrocytes. EMP-derived neutrophils circulate until late gestation. (**B**) EMP-derived microglia seed the brain around E9.5/E10.5 and persist throughout adulthood. Other tissue-resident macrophages seed tissues during development and self-maintain/are replaced in a tissue-specific manner. EMP-derived mast cells can be found in the skin after rith and are replaced by mast cells from eMPPs or HSCs during the first weeks after life.

While EMP-derived short-lived cells disappear around birth, EMP-derived tissue-resident can persist until adulthood (**Figure 7B**). This is the case for mast cells in the tongue, adipose tissue, and peritoneal cavity (Li et al., 2018; Gentek et al., 2018a; Tauber et al., 2023), and macrophages in the brain, liver, heart, lung, or skin (Ginhoux et al., 2010; Schulz et al., 2012; Hashimoto et al., 2013; Yona et al., 2013; Gomez Perdiguero et al., 2015). These tissue-resident macrophages are capable of self-maintenance throughout life, and the rate and timing of contribution of adult HSPC to their pools are organ-

specific. At one end of the spectrum, brain parenchyma microglia are almost never replaced by HSPC-derived cells in homeostatic conditions, and at the other of the spectrum, macrophages in the lamina propria are constantly renewed from bone marrow-derived monocytes (Ginhoux et al., 2010; Bain et al., 2014).

Immunophenotypic and functional differences

Initially, hematopoietic progenitor populations in the fetal liver were characterized using the definitions from the adult bone marrow. However, due to the rapid succession of different hematopoietic waves, the immunophenotypically defined progenitor populations in the fetal liver functionally do not contain the same cells as found in the adult bone marrow.

For example, at E11.5 immunophenotypic GMPs and CMPs in the fetal liver show an increased erythrocyte output compared to the adult bone marrow that steadily declines until E18.5 (Freyer et al., 2021; Monticelli et al., 2024). This could be due to a change in progenitor origin (EMP vs eMPP vs HSC). As the immunophenotypic definition of a GMP (Lin^{neg} $Sca\text{-}1^{neg}$ Kit^{high} $CD34^{+}$ $CD16/32^{+}$) corresponds to the definition of an EMP in the yolk sac, the progenitors found in the GMP gate at E11.5 or E12.5 might therefore be *bona fide* EMPs that migrated to the fetal liver whereas at later stages, when GMPs are eMPP- or HSC-derived, the same gate might contain cells with a different lineage potential. Biologically, this erythroid bias may actually be crucial in order to ensure sufficient oxygenation of the rapidly growing embryo and fetus. Intriguingly, even immunophenotypic LT-HSCs in the E14.5 fetal liver show increased erythrocyte potential compared to the adult bone marrow (Stonehouse et al., 2024).

In addition, fetal liver HSCs are more proliferative (Bowie et al., 2006) and show better reconstitution efficiency than their bone marrow counterparts (Morrison et al., 1995; He et al., 2011). Both the increased reconstitution potential and the increased erythroid output could be attributed to *Sox17* expression which is exclusively expressed in fetal but not adult HSCs (Kim, Saunders & Morrison, 2007; He et al., 2011).

Competition between extra- and intraembryonic blood cells for cytokines and growth factors

In the fetal liver, extra- and intra-embryonic-derived hematopoietic progenitors mature and differentiate side by side. As they share the same niche, they compete for cytokines and growth factors that are mainly produced by the fetal liver stroma. Compared to the bone marrow, the fetal liver, however, is a relatively low-cytokine environment (Peixoto et al., 2024).

Bona fide EMPs and EMP-derived committed progenitors outcompete intraembryonic-derived progenitors in their proliferation and differentiation potential (McGrath et al., 2015). EMPs require less erythropoietin (EPO) for erythrocyte production *in vitro* (Soares-

da-Silva et al., 2021) and produce neutrophils faster in competitive transplantation assays than HSCs (Freyer et al., 2020). Furthermore, EMPs and intraembryonic hematopoietic progenitor and stem cells depend on distinct sources of Kit Ligand (Azzoni et al., 2018). As EMPs and HSCs co-exist in the same niche their distinct dependency and sensitivity to cytokines ensures simultaneous blood cell production and HSC expansion.

Co-operation between hematopoietic waves

Sequential hematopoietic waves are not isolated but rather influence each other.

Together with our collaborators, we recently showed that the correct function of early hematopoietic waves is essential to ensure the proper maturation of later waves (Monticelli et al., 2024). By expressing ECM molecules like *perlecan*, early-wave macrophages in the fly ensure the integrity of the lymph gland and prevent the premature release of late-wave macrophages. Similarly, the maintenance of EMP-derived macrophages is important to protect HSCs from differentiating prematurely (Monticelli et al., 2024).

Additionally, early-wave myeloid cells such as EMP-derived macrophages in the mouse or primitive neutrophils in the zebrafish positively regulate HSC emergence. In mice, EMP-derived macrophages migrate to the AGM signaling where they intravasate the aortic wall (Rae et al., 2007; Stremmel et al., 2018; Mariani et al., 2019). Similarly, macrophages are found in the mesenchyme below the ventral wall of the dorsal aorta of human embryos (Travnickova et al., 2015). These macrophages are thought to facilitate the emergence of Kit^+ cells from the endothelium through pro-inflammatory TNFα and ECM remodeling through their expression of metalloproteinases MMP9 and MMP13 (Mariani et al., 2019).

This is reminiscent of findings in the zebrafish, where neutrophil-derived pro-inflammatory signals such as TNFα or Infγ positively regulate hematopoiesis (Espín-Palazón et al., 2014; Li et al., 2014; Sawamiphak, Kontarakis & Stainier, 2014). In addition, metalloproteinase MMP2, expressed by neutrophils, enables the emergence of HSPCs from the dorsal aorta by digesting ECM molecules (Theodore et al., 2017).

Finally, as macrophages are important to retain HSCs in the bone marrow (Winkler et al., 2010; Chow et al., 2011), EMP-derived macrophages may also be directly or indirectly involved in the homing of the developing bone marrow (Talk at ISEH 2023 Percin & Waskow, 2023).

1.3.3 Conclusion

Compared to adults, the developing organism faces the unique challenge of rapidly growing and forming new organs, competing with the mother for oxygen, and defending itself against potential pathogens, all while establishing a functional, life-long hematopoietic system.

Notably, when the first blood cells are required in order to supply the body with oxygen, neither hematopoietic stem cells nor the bone marrow niche are yet available. Thus, primitive erythroblasts that require few cytokines, express high-affinity globins, and transport oxygen before they are fully mature, are the rescuers in times of need (Kitchen & Brett, 1974; Palis et al., 1999). Simultaneously, the first primitive and EMP-derived platelets participate in the development of the vasculature system to ensure proper oxygenation of the body (Finney et al., 2012; Hoover et al., 2021). Furthermore, since certain developmental time windows cannot be missed for proper organogenesis, macrophages are produced rapidly so that they can seed the brain before the brain-blood-barrier closes (Risau, Hallmann & Albrecht, 1986; Bauer et al., 1993; Ginhoux et al., 2010). They also have to be ready and in place to assist in the emergence of HSCs in the AGM and to protect them during their maturation process in the fetal liver (Mariani et al., 2019; Monticelli et al., 2024).

The establishment of a complex hematopoietic system in several successive and overlapping waves that are molecularly and functionally distinct is thus the key to successful development.

2 Aims and Objectives of the Thesis

The hematopoietic system develops in a complex manner. Several successive waves ensure fetal survival, proper organ development, and maturation of hematopoietic stem cells, ready to provide lifelong hematopoiesis. The early waves (primitive cells and EMPs) sustain the fetus throughout pregnancy until shortly before birth. They are regulated by distinct molecular mechanisms and give rise to functionally different cells than *bona fide* HSCs. Intriguingly, the short-lived nature of the first blood and immune cells is reminiscent of the spontaneous resolution of some childhood blood disorders. This raises the question of whether transient hematopoietic progenitors could be the cellular origin of pediatric diseases. Thus, the objective of my PhD thesis was to decipher how perturbations affect distinct hematopoietic waves in development and whether this has consequences beyond birth. More specifically, I asked the following two main questions:

- What are the short- and long-term effects of perturbing EMPs?
- Do EMPs and HSCs respond differently to the same perturbation?

I decided to address these questions by focusing on three EMP-derived cell types each with a different lifespan. EMP-derived **MEGAKARYOCYTES** are present in the fetal liver until around E14.5 (Iturri et al., 2021), while EMP-derived **MAST CELLS** remain in tissues for several days or weeks postnatally (Gentek et al., 2018a; Tauber et al., 2023). Finally, EMP-derived **MACROPHAGES** self-maintain throughout the entire lifetime (Ginhoux et al., 2010; Yona et al., 2013; Gomez Perdiguero et al., 2015). I assessed the effect of perturbations of these cell types through three different techniques, each based on lineage tracing. Lineage tracing enables EMP-derived cells (*Csf1r*^{MeriCreMer} pulsed with 4-OHT at E8.5) to be specifically dissected from other progenitor sources (HS(P)Cs[2]: *Cdh5*^{CreERT2} pulsed with 4-OHT at E10.5).

(1) I **TRACED** EMP- and HSPC-derived megakaryocytes that both express mutant Gata1 to study potential ontogeny-specific effects of mutations.
(2) I specifically **INDUCED** a gain-of-function mutation in EMPs which drives a disease in mast cells to assess the long-term effects of perturbations in EMPs.
(3) I **DEPLETED** EMP-derived macrophages to test how perturbations in EMP hematopoiesis affect HSCs short- and long-term.

Since each of these strategies has its own advantages and pitfalls, this combination allowed me to address different complementary aspects and to gain a more comprehensive view of EMP hematopoiesis.

[2] While this strategy primarily labels HSCs (hematopoietic stem cells), a small proportion of eMPPs (embryonic multipotent progenitor cells) are also labeled. To maintain biological accuracy, I have referred to the labeled population as HSPCs (hematopoietic stem and progenitor cells) in the context of my megakaryocyte manuscript. For the sake of simplicity, however, I mainly use the term HSC in the other parts of the thesis, as the characteristics of the eMPP wave have not yet been precisely defined.

3 Results

3.1 Megakaryocytes – trace

Gata1 mutants have been demonstrated to exert stage-specific effects on megakaryocytes, particularly in the fetal liver (Li et al., 2005). Similarly, it was demonstrated that only fetal liver- and not cord blood- or bone marrow-derived megakaryocytes accumulate in the presence of only the short isoform of *Gata1*, *Gata1short* (*Gata1s*) (Gialesaki et al., 2018). The fetal liver however contains a mix of progenitors and mature cells from several different progenitor sources such as erythro-myeloid progenitors (EMPs) and hematopoietic stem and progenitor cells (HSPCs).

Here, I combined EMP- and HSPC-specific lineage tracing, to test whether the stage-specific phenotype of mutant *Gata1* is solely due to extrinsic changes in the environment over time or rather linked to distinct progenitor sources of megakaryocytes.

The following manuscript has recently been submitted and is currently awaiting the editors' and reviewers' decision.

As GATA1 regulates not only megakaryocyte, but also erythrocyte fate (Fujiwara et al., 1996), the megakaryocyte story is followed by a short section describing the effect of *Gata1*^{mCherry} on erythropoiesis. Depending on the revisions this part might either become integrated into the megakaryocyte paper or we will try to publish it as a short report.

3.1.1 Megakaryocytes

Title

Ontogeny drives stage-specific effects of a Gata1 mutation

Authors and Affiliations

Alina Sommer[1,2], Stephan Fischer[3], Laina Freyer[1], Pascal Dardenne[1], Yvan Lallemand[1] and Elisa Gomez Perdiguero[1,4]

[1]Macrophages and endothelial cells unit, Department of Developmental and Stem Cell Biology, Institut Pasteur, Université Paris Cité, UMR3738 CNRS, F-75015 Paris, France

[2]Sorbonne Université, Collège doctoral, F-75005 Paris, France

[3]Institut Pasteur, Université Paris Cité, Bioinformatics and Biostatistics Hub, F-75015 Paris, France

[4]Lead contact, elisa.gomez-perdiguero@pasteur.fr

Keywords

Developmental hematopoiesis, lineage tracing, hematopoietic stem cells, ontogeny, megakaryocytes, Gata1, yolk sac, fetal liver, hematological disorders.

Highlight

Lineage tracing reveals that cell-intrinsic differences inherited from the progenitor origin drive the stage-specific effects of a Gata1 mutant.

Abstract

Before hematopoietic stem and progenitor cells (HSPCs) emerge in the embryo, transient progenitors such as erythro-myeloid progenitors (EMPs) from the yolk sac sustain the developing fetus by producing mature blood and immune cells. While it is compelling to postulate that fetal transient progenitors contribute to the stage-specificity of pre-birth blood disorders, experimental evidence is lacking. By combining EMP- and HSPC-specific lineage tracing with a Gata1 mutation, we identified that mutant *Gata1*^{mCherry} drives transient megakaryocyte accumulation only in the EMP and not in the HSPC lineage. This accumulation depended on the progenitor origin and not on the megakaryocyte differentiation pathway or the fetal stage. Single-cell multiome sequencing revealed

ontogeny-specific transcriptional dysregulation by *Gata1*^{mCherry}, in particular of myeloid (*Cebpb)* and progenitor (*Ikzf2)* transcription regulators in erythro-megakaryocyte progenitors, leading to the development of blast-like cells exclusively in yolk sac-derived cells. This provides evidence that stage-specific diseases could be traced back to distinct progenitor origins which will improve diagnosis and treatment.

Introduction

Mutations in key transcription factors like Gata1 that govern the lineage decision-making processes of erythrocyte and megakaryocyte fate, drive transient disorders specifically in fetal development and not in adulthood (Shivdasani et al., 1997; Li et al., 2005). This stage-specificity has been attributed to environmental changes between the fetal, neonatal, and adult hematopoietic niches (Woo et al., 2013). However, it is not yet fully understood how the same somatic mutation can lead to adverse phenotypes exclusively in early life and to what extent extrinsic or intrinsic factors cause this stage specificity (Miyauchi, 2024).

Blood and immune cells at different developmental stages trace back to distinct ontogenies, as the hematopoietic system is formed from successive and overlapping progenitor waves. The first hematopoietic cells are produced from transient primitive cells and transient definitive erythro-myeloid progenitors (EMPs) that arise from the extra-embryonic yolk sac (Palis et al., 1999; McGrath et al., 2015). Around Embryonic day (E)14.5, hematopoiesis is then taken over by hematopoietic stem and progenitor cells (HSPCs) that emerge at midgestation in mice from intraembryonic hemogenic endothelium in the dorsal aorta (Müller et al., 1994; Medvinsky & Dzierzak, 1996; North et al., 1999; Iturri et al., 2021; Yokomizo et al., 2022). EMPs and HSPCs share emergence, commitment, and differentiation processes, but the underlying molecular mechanisms differ between progenitor waves (Hadland et al., 2004; Chen et al., 2011; Schulz et al., 2012; Silvério-Alves et al., 2023).

This led us to hypothesize that ontogeny, or the yolk sac- vs intraembryonic origin of progenitors, may contribute to the stage-specific effect of Gata1 mutations. Using lineage tracing and single-cell multiome sequencing, we here show that EMP- and HSPC-derived megakaryopoiesis pass through distinct differentiation trajectories at the cellular and transcriptional level. As a result, mutant Gata1 (*Gata1*^{mCherry}) affects yolk sac lineages more severely than intraembryonic-derived HSPCs. Functionally, this manifests itself in that primitive and EMP-derived, but not HSPC-derived megakaryocytes strongly accumulate in the presence of *Gata1*^{mCherry} and give rise to CD244^{+} blast-like cells. Blast-like cell development is driven by increased activity of the transcription factors CEBPB and Helios (*Ikzf2*) in *Gata1*^{mCherry} compared to wild-type conditions.

Collectively, our results show that a mutation can cause different phenotypes depending on the origin of the progenitor cells, or ontogeny. This provides groundwork to study the role of ontogeny in disease development, which may lead to a better understanding of the differences between pediatric and adult diseases.

Results

Fetal and adult megakaryopoiesis progress through immunophenotypically distinct progenitor stages.

We first characterized the different stages of megakaryocyte differentiation and maturation throughout embryonic development and across different fetal hematopoietic niches, focusing on the extraembryonic yolk sac (at embryonic day (E) 10.5) and the fetal liver (from E12.5 to E16.5), the main hematopoietic tissue in development. Adult bone marrow (BM) cells were used as a reference, where megakaryocyte progenitors (MkP) are defined as Lin^{neg} Kit^{high} $Sca\text{-}1^{neg}$ $CD41^{+}$ $CD150^{+}$ cells (Pronk et al., 2007) and megakaryocytes (Mk) as $CD41^{high}$ $CD42^{high}$ Kit^{neg} (**Fig. 1A, Supplemental Data Fig. 1A**) (Coller et al., 1983). During fetal stages, no immunophenotypic MkPs were detected (**Supplemental Data Fig. 1A**).

In contrast, two $CD41^{+}$ populations could be distinguished in fetal hematopoietic tissues based on Kit and CD41 expression levels: Kit^{+} $CD41^{+}$ and Kit^{neg} $CD41^{+}$ (**Fig. 1A**). At E12.5, both Kit^{+} $CD41^{+}$ and Kit^{neg} $CD41^{+}$ cells expressed comparable levels of CD42d (platelet glycoprotein V) and CD41 (platelet glycoprotein IIb, *Itga2b*) (**Fig. 1B**). While Kit^{+} $CD41^{+}$ cells displayed intermediate to low levels of CD45 and Kit, Kit^{neg} $CD41^{+}$ cells were mostly negative for both markers. Most Kit^{+} $CD41^{+}$ cells were 4n, 8n, or 16n, whereas most Kit^{neg} cells were mainly 8n (**Fig. 1B**).

To investigate whether $CD41^{+}$ cells were endowed with progenitor potential or rather corresponded to Mk maturation stages, we cultured single Kit^{+} and Kit^{neg} $CD41^{+}$ cells in liquid and semi-solid medium. Neither Kit^{+} nor Kit^{neg} $CD41^{+}$ cells were able to produce Mk colonies indicating that they are not progenitors (**Fig. 1C**). Hence, we named them Kit^{+} and Kit^{neg} Mk thereafter. Finally, virtually all Kit^{+} Mks were $Ki67^{+}$ and at a similar frequency as granulocyte-monocyte progenitors (GMPs), whereas only 40% of Kit^{neg} Mks were $Ki67^{+}$ (**Figure 1D**). The apparent contradiction between the inability to clone *in vitro* and the important proliferative capacity of Kit^{+} $CD41^{+}$ cells can be accounted for by endomitosis. Endomitosis is a unique feature of megakaryopoiesis, where Mks increase their ploidy by undergoing several rounds of nuclear replication without cell division (Vitrat et al., 1998). Thus, Kit^{+} Mks corresponded to maturing Mks and smaller Kit^{neg} Mks to mature Mks.

To identify the progenitor upstream of Kit^{+} $CD41^{+}$ cells endowed with Mk potential in the E12.5 fetal liver, we functionally compared GMPs (immunophenotypic equivalent to EMPs

in the yolk sac, Lin^{neg} Kit^{high} Sca-1^{neg} CD34^{+} CD16/32^{high}) and megakaryocyte-erythrocyte progenitors (MEP, Lin^{neg} Kit^{high} Sca-1^{neg} CD34^{neg} CD16/32^{neg}) (**Fig. 1C**). Potency assays demonstrated that GMPs were the fetal hematopoietic population endowed with the strongest MkP potential (with regard to Mk cloning efficiency and number of Mks per colony), particularly when compared to CD45^{+} MEPs (**Fig. 1C & Supplemental Data Fig. 1B**).

Collectively, time course analysis showed fetal Mks (Kit^{neg} CD41^{+}) are produced from Lin^{neg} Kit^{high} Sca-1^{neg} CD34^{+} CD16/32^{high} progenitors through an MEP stage only in the fetal liver. Fetal megakaryopoiesis differs from its adult counterpart due to the absence of Kit^{high} CD41^{+} CD150^{+} megakaryocyte progenitors (MkPs). Instead, fetal Mks (Kit^{neg} CD41^{+}) differentiate from an immature Kit^{+} Mk intermediate.

Yolk sac progenitors are the main source of megakaryocytes in the fetal liver until E14.5.

Since fetal blood and immune cells are produced from sequential and overlapping progenitor waves (**Fig. 1E**), we next investigated the contribution of primitive cells, EMPs, and HSPCs to fetal Mks by lineage tracing using complementary Cre drivers.

The contribution of primitive cells was assessed indirectly, as no specific Cre driver targets them. We took advantage of the constitutively active *Csf1r^{iCre}* strain, in which all definitive progenitors (EMP and HSPC) and mature myeloid cells were targeted. The contribution of yolk sac definitive progenitors (EMP) to Kit^{+} Mks was first detected at E9.0, while Kit^{neg} Mks were labeled later at E10.5 (**Fig. 1F**). This indicates that the primitive wave was the main source of Kit^{neg} Mks until E10. Notably, this also supported the developmental trajectory from Kit^{+} Mks to Kit^{neg} Mks.

EMP contribution to mature Mks was confirmed in pulse-labeling experiments using inducible *Cdh5^{CreERT2}* animals. EMPs pulsed at E7.5 with 4-hydroxytamoxifen (4-OHT) were the main source for Kit^{+} and Kit^{neg} Mks until E14.5 and E15.5, respectively. Thereafter, HSPCs (pulsed at E10.5 with 4-OHT in *Cdh5^{CreERT2}* pregnant dams) took over Mk production.

In summary, lineage tracing mouse models demonstrated that (i) the primitive wave is the main source of Mks until E10 in the yolk sac, (ii) definitive EMPs are the primary origin of Mks until late gestation (E14.5/15.5), and (iii) HSPCs supersede Mk production thereafter.

Figure 1

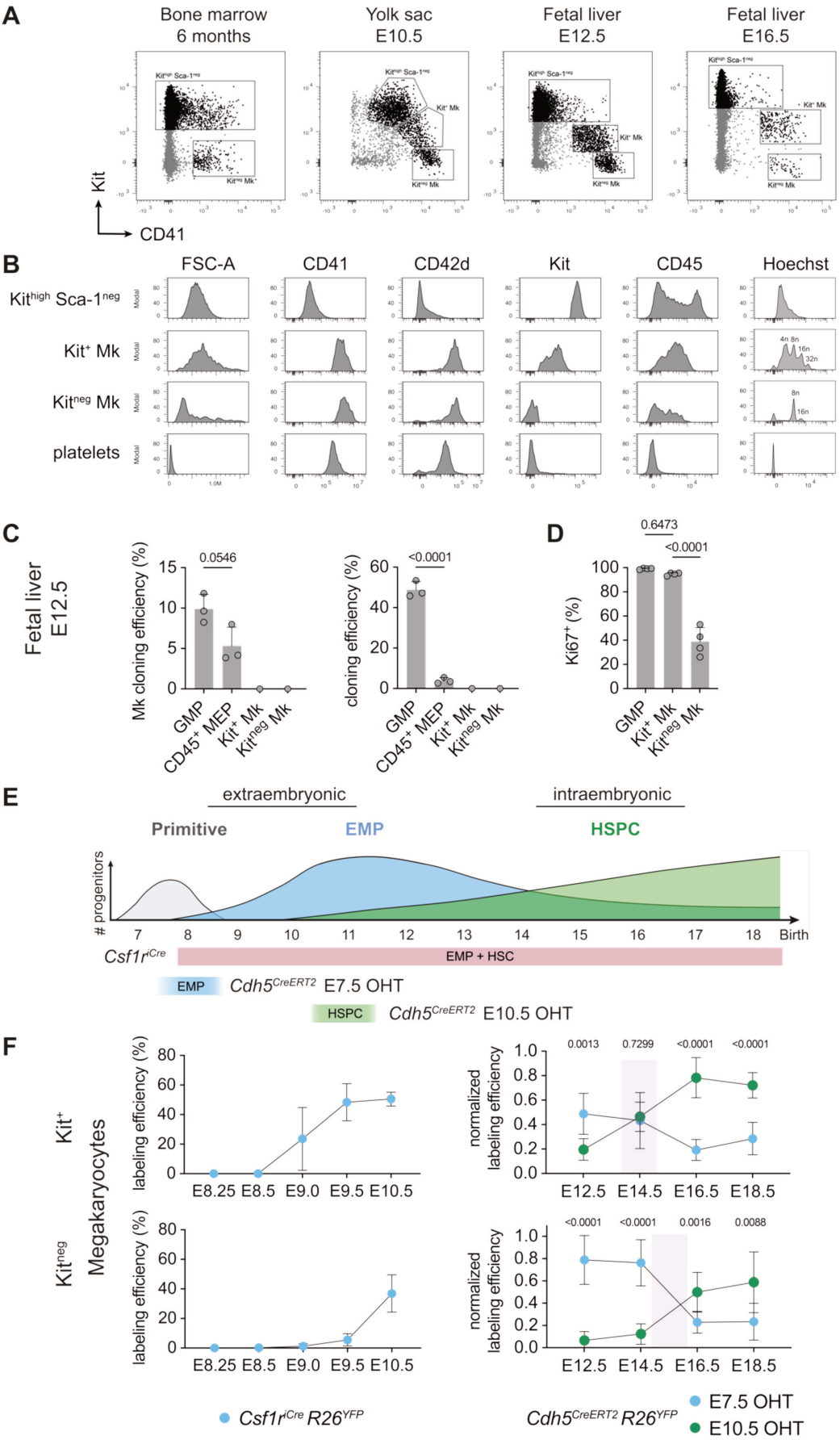
A
Bone marrow 6 months
Yolk sac E10.5
Fetal liver E12.5
Fetal liver E16.5
Kit
CD41
B
FSC-A
CD41
CD42d
Kit
CD45
Hoechst
Kithigh Sca-1neg
Kit+ Mk
Kitneg Mk
platelets
C
Fetal liver E12.5
Mk cloning efficiency (%)
0.0546
cloning efficiency (%)
<0.0001
GMP
CD45+ MEP
Kit+ Mk
Kitneg Mk
D
0.6473
<0.0001
Ki67+ (%)
E
extraembryonic
intraembryonic
Primitive
EMP
HSPC
progenitors
7 8 9 10 11 12 13 14 15 16 17 18 Birth
Csf1riCre
EMP + HSC
EMP Cdh5CreERT2 E7.5 OHT
HSPC Cdh5CreERT2 E10.5 OHT
F
Kit+ Megakaryocytes
Kitneg
labeling efficiency (%)
E8.25 E8.5 E9.0 E9.5 E10.5
normalized labeling efficiency
0.0013
0.7299
<0.0001
<0.0001
E12.5 E14.5 E16.5 E18.5
<0.0001
<0.0001
0.0016
0.0088
Csf1riCre R26YFP
Cdh5CreERT2 R26YFP
E7.5 OHT
E10.5 OHT

Figure 1. Stages and origins of megakaryopoiesis in fetal development. (**A**) Dot plots displaying Lin^{neg} Sca-1^{neg} cells from adult bone marrow (far left), E10.5 yolk sac (left), E12.5 (right), and E16.5 (far right) fetal liver. Three populations were defined based on the expression of Kit and CD41: Kit^{high} Sca-1^{neg} progenitors, Kit^{+} Mk, and Kit^{neg} Mk. (**B**) Histograms showing size (FSC-A), expression of CD41, CD42d, Kit, CD45, and ploidy (Hoechst 33342) of Kit^{high} Sca-1^{neg} progenitors, Kit^{+} and Kit^{neg} Mks and platelets in the E12.5 fetal liver as gated in **A**. (**C**) Bar plots showing the overall cloning efficiency (left) and Mk cloning efficiency (right) of immunophenotypic granulocyte-monocyte progenitors (GMPs, Lin^{neg} Kit^{high} Sca-1^{neg} CD16/32^{high} CD34^{+}), CD45+ megakaryocyte-erythrocyte progenitors (MEPs, Lin^{neg} Kit^{high} Sca-1^{neg} CD16/32^{neg} CD34^{neg}), Kit^{+} CD41^{+} Mks and Kit^{neg} CD41^{+} Mks sorted form E12.5 fetal livers and cultured for 7 days in liquid culture. 3 independent litters. One-way ANOVA excluding Kit$^{+/neg}$ Mks. (**D**) Bar plot showing the frequency of Ki67^{+} cells among GMPs, Kit^{+}, and Kit^{neg} Mks in the E12.5 fetal liver. 4 embryos from one litter. One-way ANOVA with Tukey's multiple comparisons. (**E**) Scheme representing the contribution of the four main hematopoietic waves emerging in embryonic development (primitive cells, erythro-myeloid progenitors (EMP), and hematopoietic stem and progenitor cells (HSPC)) and strategies to fate-map them. *Csf1r^{iCre}* labels all definitive hematopoietic progenitors and myeloid cells. *Cdh5^{CreERT2}* pulsed with 4-OHT at E7.5 labels EMPs and their progeny whereas when pulsed at E10.5 HSPCs and their progeny are labeled. (**F**) Graph illustrating the labeling efficiency of Kit^{+} (top left) and Kit^{neg} (bottom left) Mks in E8.25-E10.5 yolk sacs of *Csf1r^{iCre} R26^{YFP}* embryos (EMP contribution). Normalized labeling efficiency of Kit^{+} (top right) and Kit^{neg} (bottom right) Mks in E12.5-E18.5 fetal livers of *Cdh5^{CreERT2} R26^{YFP}* embryos pulsed with 4-OHT at E7.5 (blue, EMP contribution, normalized to microglia) or E10.5 (green, HSPC contribution, normalized to Lin^{neg} Sca-1^{+} Kit^{high}). n ≥3 embryos from N ≥2 litters per condition. Mixed-effects analysis with Tukey's multiple comparisons, comparing E7.5OHT versus E10.5OHT data for each time point. Data are represented as mean ± SD. See also Supplemental Data Fig. 1.

Transcriptional regulation of megakaryopoiesis differs between developmental stages.

Next, we wanted to understand whether the stage- and ontogeny-specific Mk production trajectories are transcriptionally differently regulated. To test this, we performed droplet-based paired single-cell RNA and ATAC sequencing (Chromium). We sorted cells separately at E10.5, E12.5, and E16.5 (**Fig. 2A**).

We sequenced nuclei from 10,460 wild-type Ter119^{neg} F4/80^{neg} Kit^{high} CD41^{int} and Kit$^{+/neg}$ CD41^{+} cells from a pool of 15 E10.5 yolk sacs (**Supplemental Data Fig. 2A**). From E12.5 (7,687 nuclei from 3 wild-type fetal livers) (**Supplemental Data Fig. 2B**) and E16.5 fetal livers (9,786 nuclei from 5 wild-type fetal livers), we sequenced nuclei from Lin^{neg} (Ter119, F4/80, Gr1, Nk1.1, CD3, CD19) Sca-1^{neg} Kit^{high} CD45^{+} CD16/32^{neg} CD34^{neg} (MEP) and Kit$^{+/neg}$ CD41^{+} Mks (**Supplemental Data Fig. 2C**).

Cells from all three stages were integrated and clustered using Uniform Manifold Approximation and Projection (UMAP) for dimensional reduction (**Fig. 2B, Supplemental Data Fig. 3A**). We identified multipotent progenitors, lymphoid progenitors, granulocyte-monocyte progenitors (GMPs), macrophage progenitors, granulocyte progenitors, neutrophil progenitors, mast cell progenitors, megakaryocyte-erythrocyte progenitors (MEPs), erythrocyte progenitors, 2 clusters of Mks (Mk I, Mk II), and primitive megakaryocyte-erythroblast cells (**Fig. 2B, Supplemental Data Fig. 3B**). Average

expression of key marker genes for each cluster are shown in **Supplemental Data Fig. 3C**. Multipotent progenitors comprised erythro-myeloid progenitors at E10.5, hematopoietic stem and progenitor cells at E16.5 and a mixture of both at E12.5 (**Supplemental Data Fig. 3D**).

Cells were ordered in pseudotime and we performed co-expression analysis along the Mk-differentiation trajectory from multipotent progenitors (MPPs) to Mks (**Fig. 2C, Supplemental Data Fig. 4**). At all three time points, progenitor-specific genes such as *Gata2*, *Rac2*, *Nrip1*, *Cdk19*, *Cacnb2*, *Pstpip2, Emilin2, Ptpre* were downregulated with increasing commitment and differentiation (module 1). Simultaneously, megakaryocyte-specific genes, such as *Mpl, Gucy1a1, Bin2*, *Srgap3*, and *Mmrn1,* were upregulated (module 2). Gene enrichment analysis using Enrichr (Chen et al., 2013; Kuleshov et al., 2016; Xie et al., 2021) revealed that module 1 and 2 genes collectively are involved in platelet biogenesis and were predicted to be regulated by GATA1 (**Figure 2D, Supplemental Table 1, 2**).

However, there were also significant differences between E10.5/E12.5 and E16.5. Genes such as *Hexim1*, *Alox5ap*, *Cd300a*, and *Cebpb* (Module 3) were expressed at higher levels at E10.5 and E12.5 than at E16.5 throughout the entire commitment and differentiation trajectory (**Fig. 2C, Supplemental Data Fig. 4**). These genes were predicted to be under the control of RUNX1 and NFE2L2 (**Figure 2D, Supplemental Table 3, 4**).

Module 4 genes (*Frem1*, *F13a1, Plxna4, Clec1b, Arhgap18, Arhgap45,* etc.) were expressed at higher levels at the MPP level and moderately downregulated after the MEP stage at E16.5. In contrast, at E10.5 and E12.5 module 4 genes were expressed at low levels in MPPs and upregulated after the MEP stage. Module 5 genes, such as *Lonp2*, *Zmiz1*, *Runx3*, and *Adgrg3*, were expressed at similar levels at all three time points at the MPP level. While this expression level of these genes in MPPs was sustained until the Mk stage at E16.5, it was downregulated with progressive Mk differentiation at E10.5 and E12.5 (**Fig. 2C, Supplemental Data Fig. 4A**). Amongst others, module 4 and 5 genes combined were predicted to be regulated by GATA1, EGR1, SALL4 and RUNX1, and GATA2. They are involved in the regulation of GTPase-mediated signaling and play a role in the regulation of the cytoskeleton and platelet membranes as well as coagulation (**Figure 2D, Supplemental Table 5, 6**).

Altogether, this indicates that GATA1 has common (module 1+2) but also ontogeny- and stage-specific (module 4+5) functions in yolk sac-derived and HSPC-derived Mk development.

Figure 2

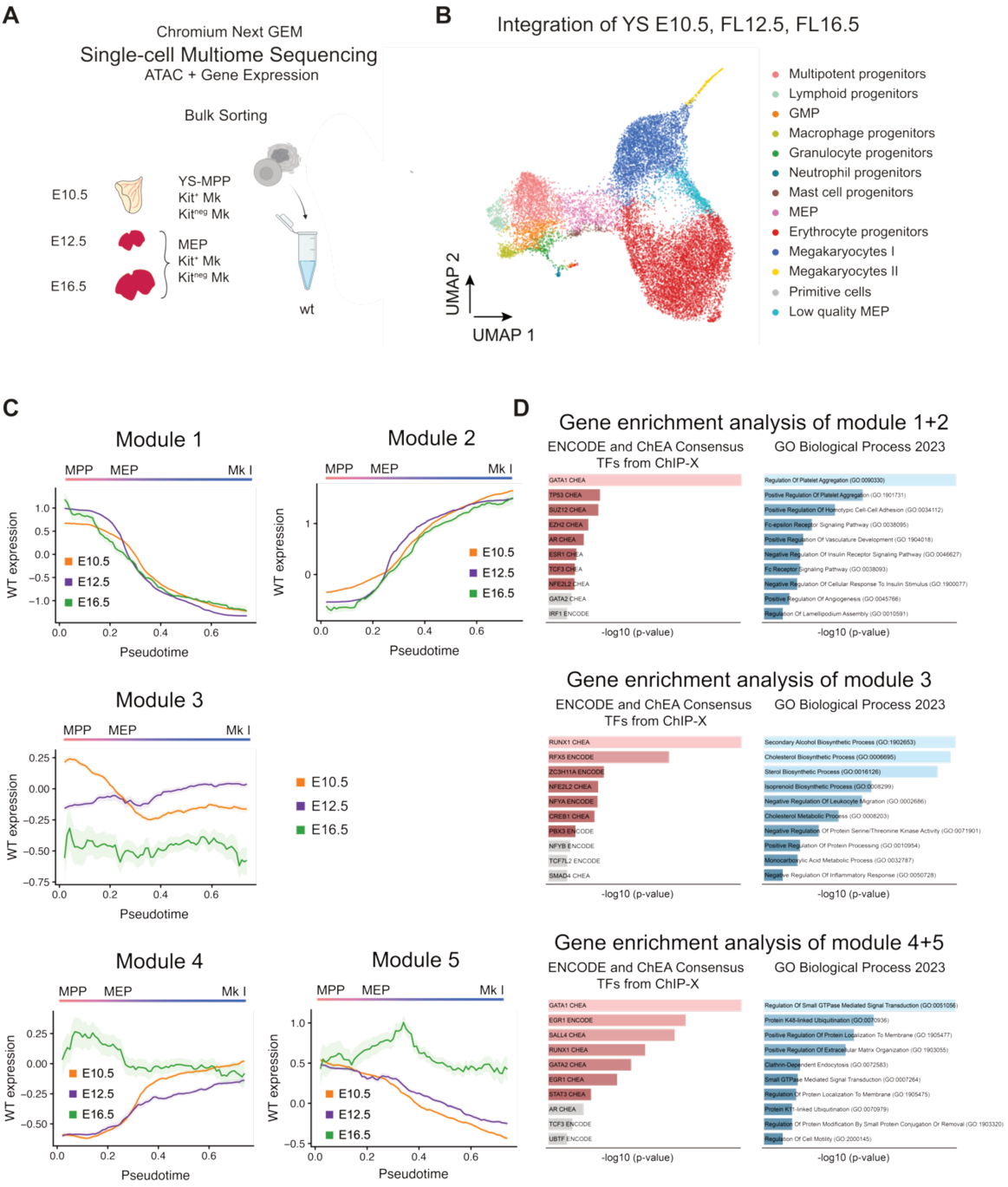

Figure 2. Single-cell multiome sequencing captures cells throughout megakaryopoiesis in fetal development. (**A**) Scheme illustrating sorting and sequencing strategy. Multipotent progenitors (Ter119^{neg} F4/80^{neg} Kit^{high} CD41^{int}), Kit^{+}, and Kit^{neg} Mks were sorted from E10.5 yolk sacs. Megakaryocyte-erythrocyte progenitors (MEP), Kit^{+}, and Kit^{neg} Mks were sorted from E12.5 and E16.5 fetal livers. Wild-type (male and female) cells were sorted separately at each time point. Cells were lysed and gene expression and ATAC libraries were prepared from nuclei following the Chromium Next Gem Single-cell Multiome Sequencing pipeline. (**B**) UMAP illustrating the integration of the single-cell RNA sequencing data from E10.5 yolk sacs, E12.5, and E16.5 fetal livers. Each color labels a different cluster. GMP = granulocyte-monocyte progenitor, MEP = megakaryocyte-erythrocyte progenitor. (**C**) Graphs showing expression of co-expression modules

1-5 along the pseudotime from multipotent progenitors (MPP) via megakaryocyte-erythrocyte progenitors (MEP) to megakaryocytes I (Mk I) in wild-type cells from E10.5 yolk sacs (orange), E12.5 (purple) and E16.5 (green) fetal livers. (**D**) Gene enrichment analysis of genes from module 1+2 (top), module 3 (middle), or module 4+5 (bottom) using EnrichR. See also Supplemental Data Fig. 2, 3, 4.

Gata1^{mCherry} causes stage-specific accumulation of Megakaryocytes.

GATA1 is a key transcription factor in megakaryopoiesis regulating Mk commitment, terminal maturation, and platelet formation (Shivdasani et al., 1997; Iwasaki et al., 2003). In line with our results on unperturbed megakaryopoiesis, mutant GATA1 perturbs megakaryopoiesis in a stage-specific manner in the fetal period (Shivdasani et al., 1997; Shimizu et al., 2001; Li et al., 2005).

Similarly, expression of *Gata1^{mCherry}*, a fusion protein of Gata1 and the fluorescent protein mCherry (Hoppe et al., 2016), caused a stage-specific accumulation of Mks in the yolk sac and the fetal liver in both male and female murine embryos (**Fig. 3A, B, Supplemental Data Fig. 5a**). No accumulation of megakaryocyte progenitors or Mks was detected in the bone marrow of 6-month-old mice (**Supplemental Data Fig. 5B, C**).

To identify the stages of megakaryopoiesis in which *Gata1^{mCherry}* exerts its effect, we characterized Lin^{neg} Kit^{high} Sca-1^{neg} CD34^{+} CD16/32^{high} progenitors (named EMP in the yolk sac, GMP in the fetal liver (Akashi et al., 2000; McGrath et al., 2015)), Mks (Kit^{+} and Kit^{neg}) and platelets in *Gata1^{mCherry}* mutant embryos. We focused on the two main fetal hematopoietic niches, the yolk sac (from E8.5 to E10.5) and fetal liver (from E12.5 to E18.5).

First, while Lin^{neg} Kit^{high} Sca-1^{neg} CD34^{+} CD16/32^{high} progenitors were modestly increased in the yolk sac, their numbers were unaffected in the fetal liver (**Fig. 3C**). However, when cultured, fetal liver Lin^{neg} Kit^{high} Sca-1^{neg} CD34^{+} CD16/32^{high} progenitors had a higher Mk output and yielded larger-sized Mk colonies (**Fig. 3D, Supplemental Data Fig. 5D**). Thus, *Gata1^{mCherry}* caused hyperproliferation downstream of Lin^{neg} Kit^{high} Sca-1^{neg} CD34^{+} CD16/32^{high} progenitors.

Accordingly, Kit^{+} Mks were affected by *Gata1^{mCherry}*. Accumulation of Kit^{+} Mks started in the yolk sac at E9.5 (5-fold increase), peaked around E12.5 in the fetal liver (7-fold increase), and decreased thereafter (**Fig. 3E, Supplemental Data Fig. 5B**). In the Fucci model, in which cells in G1 and S-G2-M can be distinguished by the presence of mCherry-Cdt or mVenus-hGem fusion proteins, respectively, no overt differences in the cell cycle of Kit^{+} Mks were found between wild-type and *Gata1^{mCherry}* embryos (**Fig. 3F**) (note that mCherry-Cdt is brighter than Gata1mCherry and the two mCherries can thus be distinguished easily). However, only *Gata1^{mCherry}* but not wild-type Kit^{+} Mks showed colony forming potential (**Supplemental Data Fig. 5E**).

Figure 3

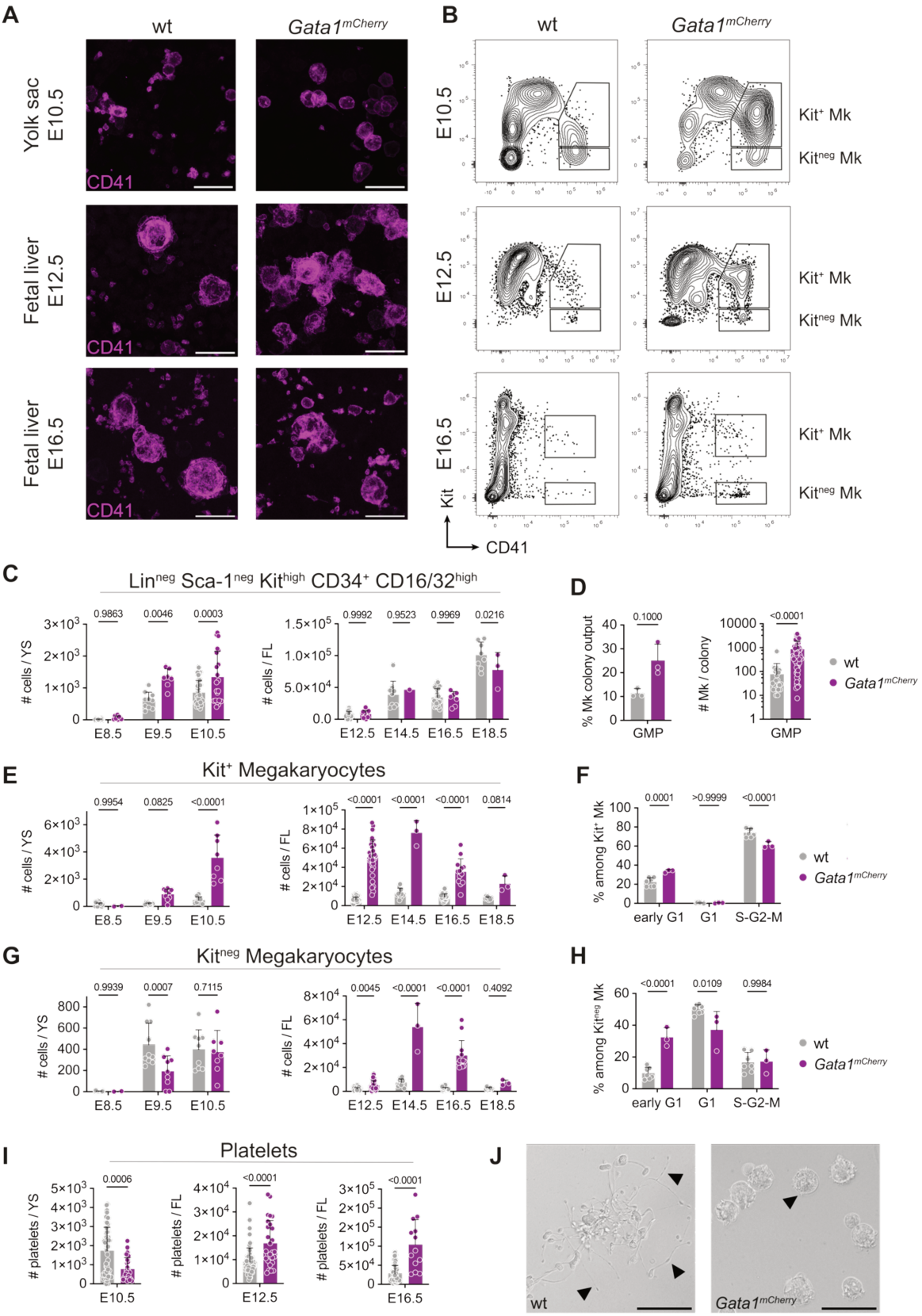

Figure 3. *Gata1*^{mCherry} causes stage-specific accumulation of Megakaryocytes. (A) Immunofluorescence of 10 µm-thick maximum projection of E10.5 yolk sacs (top), 21 µm-thick

maximum projection of E12.5 (middle), and 42 µm-thick maximum projection of E16.5 (bottom) fetal livers from wild-type (wt, left) and *Gata1*^{mCherry} (right) embryos. Mks are stained with anti-CD41 PE (magenta). Scale bar represents 25 µm. (**B**) Dot plots showing Kit^{+} and Kit^{neg} Mk gates among Lin^{neg} cells from E10.5 yolk sac (top), Kit^{+} and Kit^{neg} Mk gates among Lin^{neg} Sca-1^{neg} cells from E12.5 (middle), and E16.5 (bottom) fetal liver from wt (left) and *Gata1*^{mCherry} (right) embryos. (**C, E, G**) Bar plots showing the number of (**C**) Lin^{neg} Kit^{+} CD34^{+} CD16/32^{high} cells (immunophenotypic EMPs in the yolk sac and GMPs in the fetal liver), (**E**) Kit^{+} Mks and (**G**) Kit^{neg} Mks in E8.5-E10.5 yolk sacs (left) and E12.5-E18.5 fetal livers (right) from wt (grey) and *Gata1*^{mCherry} (purple) embryos. One-way ANOVA with Tukey's multiple comparisons. (**D**) Bar plot showing the frequency of colonies containing Mk progeny (Mk colony output, left) and size of Mk-containing colonies (right) from sorted single immunophenotypic GMPs grown in liquid cultures for 7 days from E12.5 fetal livers from wild-type (grey) or *Gata1*^{mCherry} (purple) embryos. 3 independent litters. Mann-Whitney test. (**F, H**) Bar plots showing the frequency of wt (grey) and *Gata1*^{mCherry} (purple) Kit^{+} (**F**) and Kit^{neg} (**H**) Mks in early G1 (Fucci double negative), G1 (mCherry-Cdt^{+}) and S-G2-M (mVenus-hGem^{+}) phase in E12.5 fetal livers from *PGK*^{Cre} *R26*^{Fucci2aR} embryos. n ≥3 embryos from N ≥3 litters per condition. One-way ANOVA with Tukey's multiple comparisons. (**I**) Bar plots showing the numbers of platelets in the E10.5 yolk sacs (left), E12.5 (middle), and E16.5 (right) fetal livers in wt (grey) and *Gata1*^{mCherry} (purple) embryos. n >3 embryos from N >3 litters per condition. Mann-Whitney test. (**J**) Bright-field images of Mks grown from single immunophenotypic GMPs from E12.5 fetal livers from wild-type (grey) or *Gata1*^{mCherry} (purple) embryos. Arrowheads indicate proplatelets. Scale bar represents 50 µm. Data are represented as mean ± SD. See also Supplemental Data Fig. 5.

Numbers of Kit^{neg} Mks, by contrast, were reduced at E9.5, unchanged at E10.5 in the yolk sac, and increased 6-fold at E14.5 in the fetal liver (**Fig. 3G, Supplemental Data Fig. 5C**). This accumulation was transient and resolved afterwards (**Supplemental Data Fig. 5C**). The frequency of *Gata1*^{mCherry} Kit^{neg} Mk in S-G2-M was unaffected (**Fig. 3H**), suggesting this accumulation was not due to self-amplification of the Kit^{neg} population but rather due to increased input from their upstream precursors, the Kit^{+} Mks, and decreased output by blocked maturation into platelet-producing cells.

Indeed, platelet numbers were reduced in the yolk sac at E10.5 but were increased in the fetal liver at E12.5 and E16.5 (**Fig. 3A, I**). This delay in platelet production was in line with the finding that *Gata1*^{mCherry} Mks did not form proplatelets like wild-type Mks after 7 days of incubation in liquid cultures (**Fig. 3J**).

Altogether, our findings show that *Gata1*^{mCherry} has stage-specific effects. Between E9.5 and E14.5, *Gata1*^{mCherry} blocks maturation downstream of Lin^{neg} Kit^{high} Sca-1^{neg} CD34^{+} CD16/32^{high} progenitors, causing an abnormal accumulation of Mks and a delayed production of platelets.

Primitive and EMP- but not HSPC-derived megakaryocytes accumulate in the presence of *Gata1*^{mCherry}.

The stage-specific accumulation of Mks driven by *Gata1*^{mCherry} coincided with the ontogeny switch from EMP to HSPC seen in wild-type embryos. Therefore, we tested whether the stage-specific phenotype of *Gata1*^{mCherry} was ontogeny-dependent.

First, we crossed the *Gata1*^{mCherry} allele with the *Csf1r*^{iCre} fate-mapping model described before (**Fig. 4A**) and found that primitive Kit^{+} Mks accumulated at E9.5 in *Gata1*^{mCherry} yolk sacs. In contrast, Kit^{+} and Kit^{neg} Mks accumulating at E10.5 were EMP-derived, as in control embryos (**Fig. 4, Supplemental Data Fig. 6A**).

Recently, we discovered that EMPs give rise to two distinct waves of Mks that can be distinguished by their spatiotemporal kinetics and dependency on the transcription factor c-*Myb* (Tober, McGrath & Palis, 2008; Iturri et al., 2021). Lack of *Myb* does not hamper direct Mk differentiation from EMPs in the yolk sac. However, in *Myb*-deficient embryos EMPs fail to produce bipotent CD131^{+} erythro-Mk progenitors causing a lack of erythroid and Mk generation in the fetal liver (**Supplemental Data Fig. 6B**).

We thus examined Mk numbers in double *Gata1*^{mCherry} *Myb*-deficient yolk sacs and fetal livers. Mks accumulated normally in double *Gata1*^{mCherry} *Myb* mutant yolk sacs, confirming that *Gata1*^{mCherry} affects the direct differentiation of Mks from EMPs (**Fig. 4C**). In contrast, Mk accumulation was abrogated in double *Gata1*^{mCherry} *Myb*$^{-/-}$ fetal livers (**Fig. 4C**). This demonstrated that Mks accumulating in *Gata1*^{mcherry} fetal livers arise from EMP-derived *Myb*-dependent CD131^{+} progenitors.

To test the effect of *Gata1*^{mcherry} in the production of Mks from CD131^{+} progenitors, we performed colony-forming assays. *Gata1*^{mCherry} CD131^{+} progenitors gave rise to more mixed colonies with erythrocyte and Mk output at the expense of pure erythroid and pure Mk colonies. Further, colonies containing Mks were larger in *Gata1*^{mCherry} conditions than in wild-type conditions (**Fig. 4D, Supplemental Data Fig. 6C**).

Altogether, primitive and both EMP-derived Mk pathways are affected by *Gata1*^{mCherry} and contribute to Mk accumulation in the yolk sac and fetal liver.

To specifically trace the fate of *Gata1*^{mCherry} EMPs and HSPCs in the fetal liver, we pulse-labeled EMPs at E8.5 in inducible *Gata1*^{mCherry} *Csf1r*^{MeriCreMer} *R26*^{eYFP} embryos and HSPCs at E10.5 in *Gata1*^{mCherry} *Cdh5*^{CreERT2} *R26*^{eYFP} embryos (**Fig. 4E**). EMP-derived Mks continued to accumulate until E16.5 (**Fig. 4F**). Increased labeling efficiency in both Mk subsets in *Gata1*^{mCherry} *Csf1r*^{MeriCreMer} *R26*^{eYFP} embryos associated with the decreased labeling efficiency in *Gata1*^{mCherry} *Cdh5*^{CreERT2} *R26*^{eYFP} embryos demonstrated that most of the accumulating Mks in *Gata1*^{mCherry} fetal livers were of EMP origin (**Fig. 4G, H**).

In contrast to wild-type conditions where the majority of Mks are HSPC-derived at E16.5, Kit^{neg} Mks in *Gata1*^{mCherry} embryos were still of EMP origin. Importantly, when analyzing the number of pulse-labeled cells (**Fig. 4I, J**), HSPC-traced Kit^{+} Mks did accumulate in the fetal liver at E16.5, albeit at a lower extent than EMP-derived ones. Indeed, while the number of EMP-derived Kit^{+} and Kit^{neg} Mks showed a 50-fold increase, HSPC-derived Kit^{+} Mks only increased in numbers by 2-fold, and numbers of HSPC-derived Kit^{neg} Mks were unchanged (**Fig. 4I, J**).

Figure 4

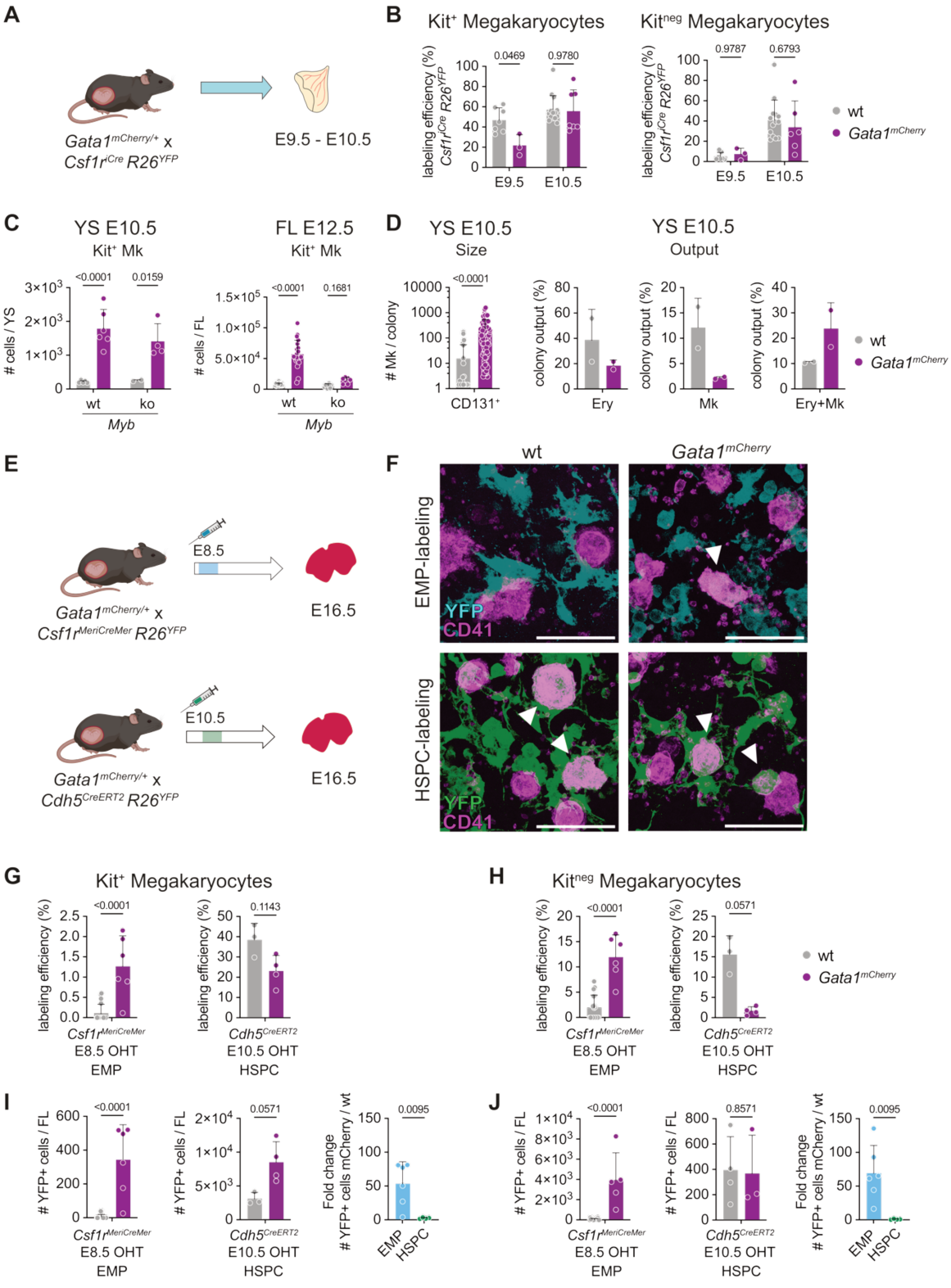

Figure 4. Primitive and EMP- but not HSPC-derived megakaryocytes accumulate in the presence of *Gata1*^{mCherry}. (**A**) Scheme illustrating fate mapping of yolk sac-derived definitive *Gata1*^{mCherry} cells in the yolk sac. (**B**) Bar plot showing labeling efficiency of Kit^{+} (left) and Kit^{neg} (right) Mks in E9.5 and E10.5 yolk sacs from wt (grey) or *Gata1*^{mCherry} (purple) embryos. n ≥ 3 embryos from N ≥ 3 litters per condition. One-way ANOVA with Tukey's multiple comparisons. (**C**) Bar plot

showing the number of Kit$^+$ Mks in E10.5 yolk sacs (left) or E12.5 fetal livers (right) from *Myb*$^{+/+}$ or *Myb*$^{-/-}$ *Gata1*$^{wild\text{-}type}$ (grey) or *Gata1*^{mCherry} (purple) embryos. n ≥ 3 embryos from N ≥ 3 litters per condition. One-way ANOVA with Tukey's multiple comparisons. (**D**) Bar plot showing the colony size of Mk-containing colonies (far left) and colony output of pure erythrocytes (Ery, left), Mks (right), and Ery+Mk mixed (far right) colonies grown from Kit^{high} CD41$^+$ CD131$^+$ cells from E10.5 yolk sacs. 2 independent experiments. (**E**) Scheme illustrating fate mapping of EMP-derived (top) and HSPC-derived (bottom) cells in the E16.5 fetal liver. (**F**) Immunofluorescence of 42 µm-thick maximum projection of E16.5 fetal livers from wild-type (wt, left) and *Gata1*^{mCherry} (right) embryos. Mks are stained with anti-CD41 PE (magenta). EMP-derived cells are fate-mapped in *Csf1r*^{MeriCreMer} *R26*^{YFP} embryos pulsed at E8.5 with 4-OHT (cyan). HSPC-derived cells are fate-mapped in *Cdh5*^{CreERT2} *R26*^{YFP} embryos pulsed at E10.5 with 4-OHT (green). Scale bar represents 50 µm. White arrow heads indicate YFP$^+$ Mks. (**G, H**) Bar plot showing labeling efficiency of EMP-derived (left) and HSPC-derived (right) Kit$^+$ (**G**) and Kit^{neg} (**H**) Mks in E16.5 fetal livers from wild-type (grey) or *Gata1*^{mCherry} (purple) embryos. n ≥ 3 embryos from N ≥ 3 litters per condition. Mann-Whitney test. (**I, J**) Bar plots showing the number of EMP- (left) and HSPC-derived (middle) YFP$^+$ Kit$^+$ (**I**) and Kit^{neg} (**J**) Mks in E16.5 fetal livers from wild-type (grey) or *Gata1*^{mCherry} (purple) embryos. Fold change (right) of *Gata1*^{mCherry} over wild-type EMP- (blue) and HSPC-derived (green) Kit$^+$ (**I**) and Kit^{neg} (**J**) Mks. n ≥ 3 embryos from N ≥ 3 litters per condition. Mann-Whitney test. Data are represented as mean ± SD. See also Supplemental Data Fig. 6.

Collectively, these data suggest that only yolk sac-derived (primitive and EMP) and not intraembryonic HSPC-derived megakaryocytes strongly accumulate in the presence of *Gata1*^{mCherry}. Moreover, analysis of double *Gata1*^{mCherry} *Myb* mutants provides evidence that the phenotype exerted by *Gata1*^{mCherry} is not dependent on the differentiation route but rather on the progenitor of origin.

Single-cell multiome sequencing captures cells throughout perturbed megakaryopoiesis in fetal development.

To understand the molecular mechanisms underlying the ontogeny-specific effects of *Gata1*^{mCherry}, we performed droplet-based single-cell RNA and ATAC sequencing (Chromium). We sorted *Gata1*^{mCherry} (male) cells separately at E10.5, E12.5, and E16.5 (**Supplemental Data Fig. 7A**).

We sequenced nuclei 13,742 *Gata1*^{mCherry} Ter119^{neg} F4/80^{neg} Kit$^+$ CD41^{int} and Kit$^{+/neg}$ CD41$^+$ cells from a pool of 9 the E10.5 yolk sacs (**Supplemental Data Fig. 2A**). From E12.5 (9,208 nuclei from 4 *Gata1*^{mCherry} fetal livers) (**Supplemental Data Fig. 2B**) and E16.5 fetal livers (5,858 nuclei from 4 *Gata1*^{mCherry} fetal livers), we sequenced nuclei from Lin^{neg} (Ter119, F4/80, Gr1, Nk1.1, CD3, CD19) Sca-1^{neg} Kit^{high} CD45$^+$ CD16/32^{neg} CD34^{neg} (MEP) and Kit$^{+/neg}$ CD41$^+$ Mks (**Supplemental Data Fig. 2C**).

Single-cell data of *Gata1*^{mCherry} cells were integrated with wild-type cells, clustered and represented using Uniform Manifold Approximation and Projection (UMAP) for dimensional reduction for each stage individually. Mutant cells were found in all clusters first identified in the wild-type dataset. In addition, mutant cells also formed a cluster of blast-like cells which did not exist in wild-type samples (**Fig. 5A, B, Supplemental Data Fig. 7B**). At all three stages, wild-type (orange) and *Gata1*^{mCherry} (purple) multipotent and

committed myeloid and lymphoid progenitors integrated well. In contrast, wild-type and mutant cells of the Mk and erythrocyte lineage integrated at E16.5 but not at E10.5 and E12.5 (**Fig. 5B**).

Gata1^{mCherry} drives stage-specific transcriptional changes in megakaryocytes.

We found stage-specific particularities when analyzing the differentially expressed genes between wild-type and *Gata1^{mCherry}* Mk I at each time point (**Fig. 5C**). A core of up-regulated genes (such as *Frem1*, *F13a1*, *Aoah*) was shared among mutant cells at all three time points (**Fig. 5C, Supplemental Data Fig. 7C**). However, the majority of downregulated genes such as *Proser2*, *Plcb1*, *Sardh*, *Sntb1*, *Vwf*, *Pf4* (2-fold reduction between *Gata1^{mCherry}* and wt at E10.5 and E12.5) were not significantly changed at E16.5 (**Fig. 5C, Supplemental Data Fig. 7C**).

Furthermore, regulon analysis revealed a *Gata1^{mCherry}*-driven change in transcription factor activity that differed between stages (**Fig. 5E**). In this regulon analysis the change of the expression level of transcription factor-target genes (RNA score) as well as the accessibility of transcription factor binding sites near these target genes (ATAC score) was evaluated. At E10.5, CEBPB was the transcription factor with the highest increase in activity in *Gata1^{mCherry}* compared to the wild-type. Helios (*Ikzf2*) and PU.1 (*Spi1*) also showed a moderate increase in activity, which soared at E12.5, with Helios being the most upregulated of all transcription factors. In parallel, CEBPB was less active at E12.5 than at E10.5.

In contrast, at E16.5 JUNB and RELB had the strongest increase in activity while these transcription factors were not significantly upregulated at E10.5 and E12.5 (**Fig. 5E**). CEBPB showed no increase in activity at E16.5 and Helios even showed decreased activity at E16.5. Intriguingly, a GATA2 binding site in a *Relb* candidate cis-regulatory element (cCRE) was shut down in wild-type MEPs and Mks at E16.5 but accessible in mutant cells (**Fig. 5F**). At E10.5 and E12.5 this GATA2 binding site was similarly accessible in mutant and wild-type MEPs and Mks. GATA2 is a transcription factor important for megakaryocyte differentiation that has unique regulatory features in yolk sac and fetal liver megakaryopoiesis compared to bone marrow megakaryopoiesis (Fujiwara et al., 2004; Huang et al., 2009).

Taken together these data suggest that *Gata1^{mCherry}* disrupts megakaryopoiesis differently and more severely at E10.5 and E12.5 compared to E16.5 at the transcriptional level.

Figure 5

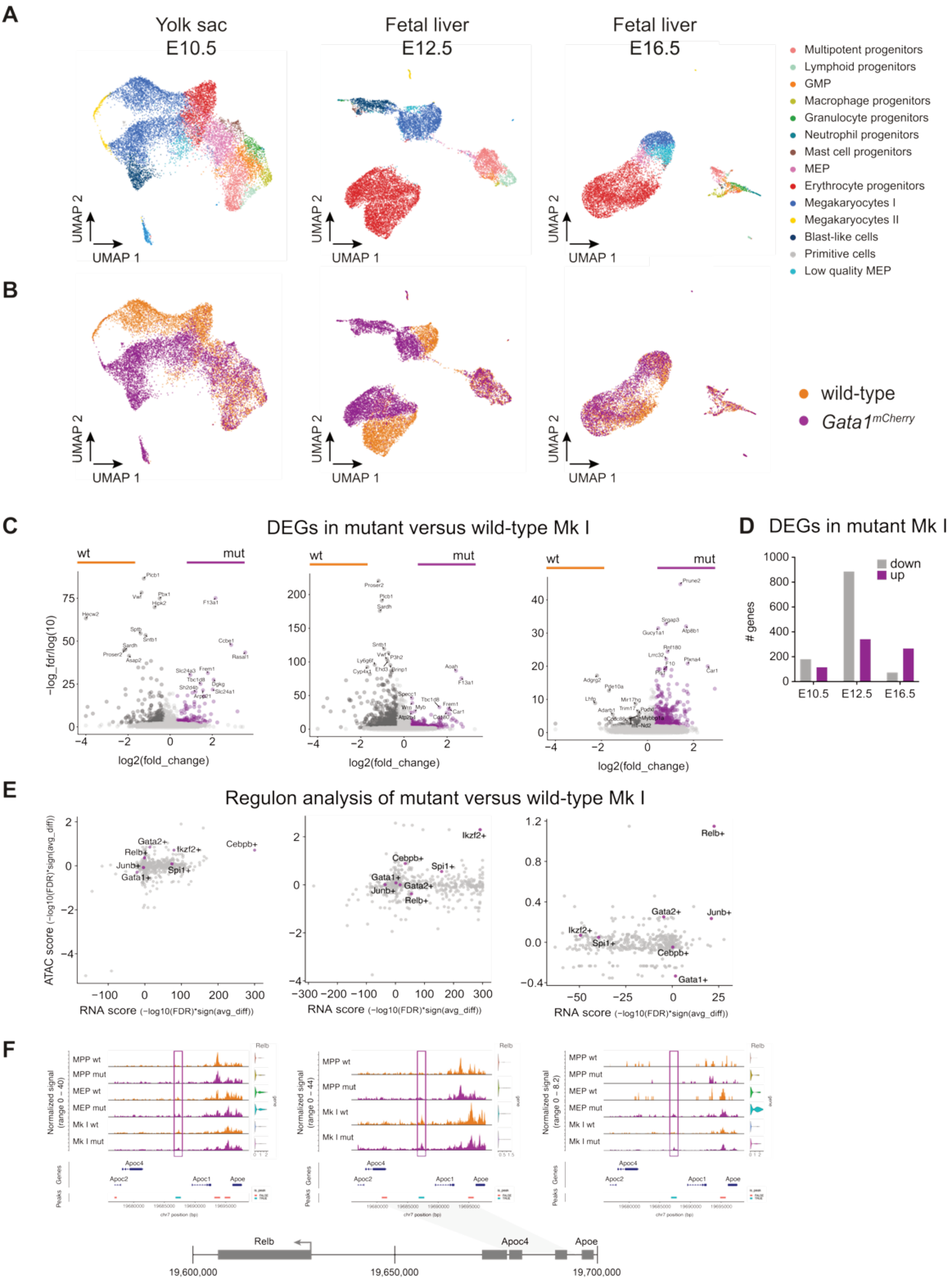

Figure 5. *Gata1*^{mCherry} drives stage-specific transcriptional changes in megakaryopoiesis. (**A**) UMAPs from E10.5 yolk sacs, E12.5, and E16.5 fetal livers featuring clusters identified in the integration of the single-cell RNA sequencing data of all three time points together. (**B**) UMAPs featuring wild-type (orange) and *Gata1*^{mCherry} (purple) cells in single-cell RNA sequencing datasets from E10.5 yolk sacs, E12.5, and E16.5 fetal livers. (**C**) Volcano plot showing up (purple) and down

(grey) regulated genes in *Gata1*^{mCherry} Mks (Mk I, purple bar) compared to wild-type (grey bar). Differentially expressed genes = DEGs. (**D**) Bar plot quantifying the genes up (purple) and down (grey) regulated between wild-type and *Gata1*^{mCherry} Mks (Mk I) at E10.5, E12.5 and E16.5. (**E**) Regulon analysis indicates the increase in transcription factor activity in *Gata1*^{mCherry} compared to wt Mks (Mk I) in E10.5 yolk sacs, E12.5, and E16.5 fetal livers. (**F**) Coverage plot illustrating chromatin accessibility of Gata2 binding site in a *Relb* candidate cis-regulatory element (cCRE). See also Supplemental Data Fig. 7.

Gata1^{mCherry}-driven formation of CD244^{+} blast-like cells occurs exclusively in yolk sac-derived megakaryopoiesis

In line with the stage-specific differences at the transcriptional and cellular level, single-cell RNA sequencing revealed a cluster of blast-like cells which were detected exclusively in *Gata1*^{mCherry} and not in wild-type embryos and only at E10.5 (30 cells in wild-type, 840 cells in *Gata1*^{mCherry}) and E12.5 (1 cell in wild-type, 819 cells in *Gata1*^{mCherry}) but not at E16.5 (0 cells in wild-type, 11 cells in *Gata1*^{mCherry}) (**Fig. 6A**).

These blast-like cells expressed typical Mk genes such as *Pf4*, *Itga2b* (CD41), *Nfe2*, and *Rap1b*, but also upregulated myeloid and pluripotency genes such as *Spi1* and *Myb* (**Supplemental Data Fig. 8A**). Likewise, blast-like cells showed similar patterns of transcription factor activity as Mks, but also abnormal activity of myeloid and pluripotency transcription factors such as PU.1, CEBPA, CEBPB, Ikaros (*Ikzf1*) and *Helios* (*Ikzf2*) at E10.5 and E12.5 (**Fig. 6B, Supplemental Data Fig. 8B**). While the activity of few transcription factors was changed at E10.5 in blast-like cells, many transcription factors had increased activity at E12.5 (**Supplemental Data Fig. 8B**).

To functionally characterize blast-like cells, we searched for cell surface markers specifically expressed in mutant blast-like cells but not wild-type or mutant Mks. *Cd244a*, a type-I transmembrane protein belonging to the signaling lymphocytic activation molecule family of receptors (SLAMF), was significantly upregulated in blast-like cells at E12.5 (**Fig. 6C**). On the contrary, *Cd244a* was barely expressed at E10.5 and absent at E16.5 (**Fig. 6D**). We validated *Cd244a* expression at the protein level using flow cytometry. CD244^{+} cells were only found in *Gata1*^{mCherry} fetal livers at E12.5 *in vivo* and were present among Kit^{+} and Kit^{neg} CD41^{+} Mks (**Fig. 6E, Supplemental Data Fig. 8C, D**). CD244^{+} Kit^{+} CD41^{+} blast-like cells showed higher protein levels of Helios and PU.1 than CD244^{-} Kit^{+} CD41^{+} cells, confirming the upregulation of myeloid and pluripotency transcription factors from the single-cell sequencing data (**Fig. 6B, F, Supplemental Data Fig. 8A, B**).

Figure 6

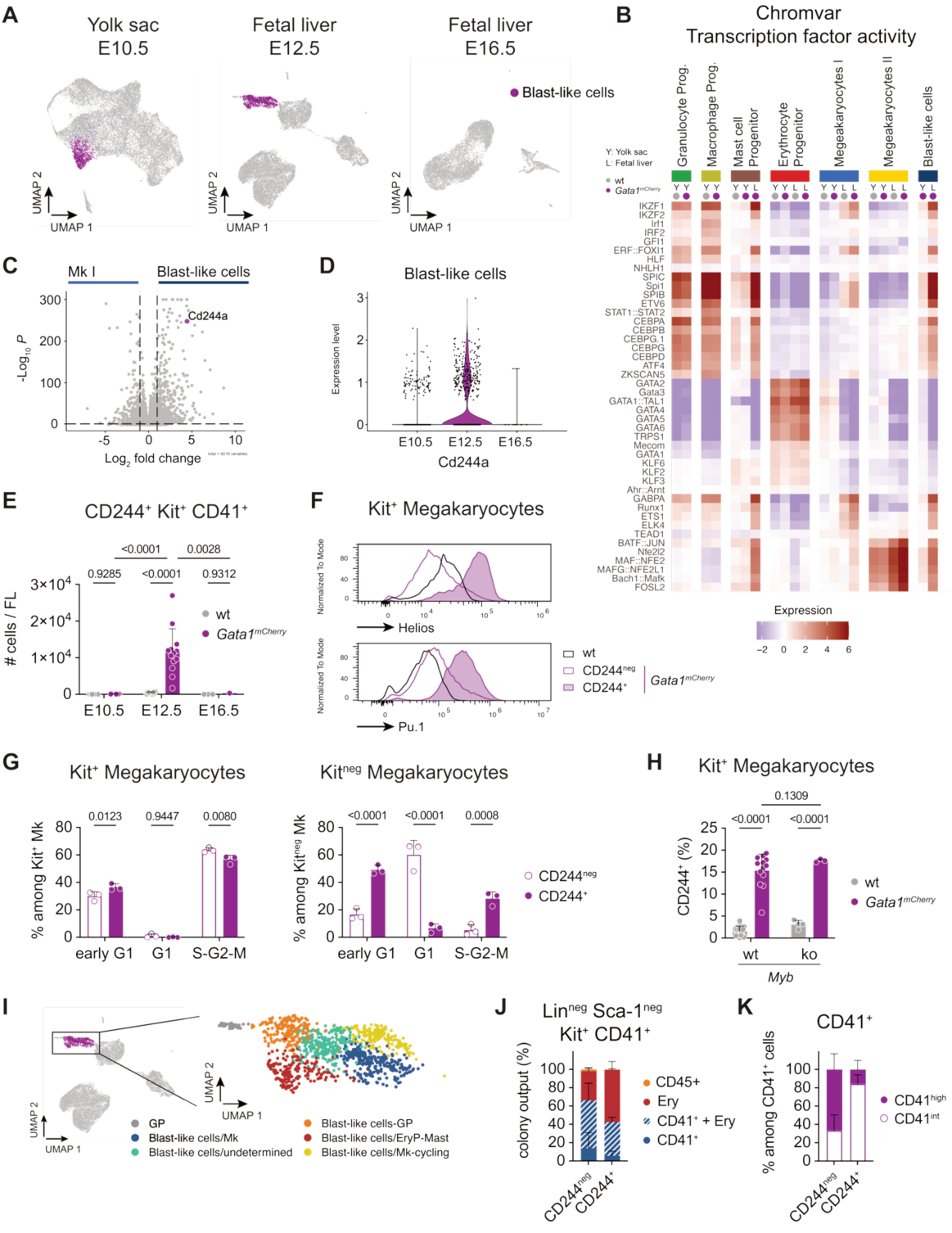

Figure 6. *Gata1*^{mCherry}-driven formation of CD244^{+} blast-like cells occurs exclusively in yolk sac-derived megakaryopoiesis. (**A**) UMAPs featuring blast-like cells (purple) in the E10.5 yolk sac, E12.5, and E16.5 fetal liver. (**B**) Heat map showing transcription factor activity calculated using Chromvar among clusters in yolk sac (Y) and fetal liver (L) wild-type (grey) and *Gata1*^{mCherry} (purple) samples. (**C**) Volcano plot comparing the gene expression between mutant blast-like cells and wild-type and mutant Mks (Mk I) in the E12.5 fetal liver. *Cd244a* is highlighted in purple. (**D**) Violin plot showing the expression level of *CD244a* among blast-like cells at E10.5, E12.5, and E16.5. (**E**)

Bar plot showing the number of CD244^{+} Kit^{+} CD41^{+} cells per E12.5 fetal liver from wild-type (grey) or *Gata1^{mCherry}* (purple) embryos. ≥ 3 embryos from ≥ 3 litters per condition except for E16.5 *Gata1^{mCherry}* (only 1 embryo). Two-way ANOVA. (**F**) Histograms showing Helios (top) and PU.1 (bottom) protein expression in wild-type (black), *Gata1^{mCherry}* CD244^{neg} (purple border), and *Gata1^{mCherry}* CD244^{+} (purple filled) cells from E12.5 fetal livers. (**G**) Bar plot showing the frequency of CD244^{neg} (purple border) and CD244^{+} (purple filled) Kit^{+} (left) and Kit^{neg} (right) Mks in early G1 (Fucci double negative), G1 (Fucci mCherry^{+}) and S-G2-M (Fucci mVenus^{+}) phase in E12.5 fetal livers from embryos with constitutive expression of *R26$^{Fucci/+}$*. n ≥3 embryos from N ≥3 litters. One-way ANOVA with Tukey's multiple comparisons. (**H**) Bar plot showing the frequency of CD244 expression among Kit^{+} Mks from *Myb$^{+/+}$* or *Myb$^{-/-}$ Gata1$^{wild-type}$* (grey) or *Gata1^{mCherry}* (purple) embryos. ≥ 3 embryos from ≥ 3 litters per condition. Two-way ANOVA. (**I**) UMAP of blast-like cells from E12.5 fetal livers featuring different subpopulations: GP = granulocyte progenitors, EryP = erythrocyte progenitor, Mk = megakaryocyte. (**J**) Stacked bar plot illustrating the colony output of CD244^{neg} and CD244^{+} Kit^{+} Mks from *Gata1^{mCherry}* E12.5 fetal livers. Detected were CD45^{+} cells, erythrocytes (Ery, CD71^{+}, Ter119^{+} cells), and CD41^{+} cells. 3 independent experiments. (**K**) Stacked bar plot showing the frequency of CD41^{high} and CD41^{int} cells among all CD41^{+} (pure CD41^{+} and CD41^{+} + Ery) cells detected in **J**. Data are represented as mean ± SD. See also Supplemental Data Fig. 8, 9.

Gata1^{mCherry}-driven blast-like cells are primed in the yolk sac and mature in the fetal liver

At E10.5, blast-like cells were detected at the transcriptional but not at the cellular level. Although E10.5 blast-like cells did not express *CD244a* mRNA, the *Cd244a* promoter was accessible in blast-like cells at both E10.5 and E12.5. In contrast, *the Cd244a* promoter was closed in both wt and *Gata1^{mCherry}* Mks at E10.5 and E12.5 (**Supplemental Data Fig. 8E**).

These data, together with the observation that the overall transcription factor activity in blast-like cells increases from E10.5 to E12.5 (**Supplemental Data Fig. 8B**), indicated that blast-like cell fate is primed in *Gata1^{mCherry}* yolk sac MPPs. In the fetal liver, these blast-like cells then mature as evidenced by the expression of CD244 protein. *Gata1^{mCherry}*-driven blast-like cell development only occurred in yolk sac-derived lineages but not in HSPC-derived megakaryopoiesis and was never observed in wild-type embryos.

Gata1^{mCherry}-driven blast-like cells are hyperproliferative cells that retain erythrocyte potential

Finally, we functionally characterized the fetal liver blast-like cells at E12.5. Kit^{+} CD244^{+} blast-like cells were as proliferative as Kit^{+} CD244^{neg} Mks, whereas Kit^{neg} CD244^{+} blast-like cells were more proliferative than Kit^{neg} CD244^{neg} Mks (**Fig. 6G**). Even though blast-like cells were highly proliferative, their development did not depend on *Myb* (**Fig. 6H**).

Further, sub-clustering of blast-like cells at E12.5 revealed their heterogeneity. While cells in the blast-like cell cluster expressed high levels of *Itga2b* (CD41) and *Gata2*, we identified sub-clusters with granulocyte (*Gria3*), megakaryocyte (*Mpl*), or erythrocyte-mast

cell (*Tgfbr3*, *Klf1*, *Ifitm1*) gene expression signatures (**Supplemental Data Fig. 9A**). *CD244a* expression was limited to non-Mk clusters (**Supplemental Data Fig. 9B**).

Despite the expression of myeloid genes such as *Spi1* at the mRNA and protein level (**Fig. 6F & Supplemental Data Fig. 9A**), Kit^{+} CD41^{+} CD244^{+} blast-like cells did not give rise to macrophages, neutrophils, or mast cells when cultured for 7 days (**Fig. 6J**). However, CD244^{+} cells did show increased red blood cell potential compared to CD244^{neg} Kit^{+} CD41^{+} cells, which came at the expense of CD41^{+} Mk output (**Fig. 6J**). Concerning the CD41^{+} progeny of cultured Kit^{+} CD41^{+} cells, Mk potential (CD41^{high} in culture) was enriched in CD244^{neg} cells, whereas CD244^{+} cells mainly produced CD41^{int} undifferentiated cells (**Fig. 6K and Supplemental data Fig. 9C**).

Collectively, accumulating *Gata1*^{mCherry} Kit^{+} Mks had cloning capacity, in stark contrast to wild-type Kit^{+} Mks. They contained at least two subsets of cells: CD244^{neg} Mks endowed with high Mk potential and CD244^{+} blast-like cells. CD244^{+} blast-like cells were less committed towards Mk fate and instead gave rise to erythrocytes and CD41^{int} undifferentiated cells. The overexpression of myeloid transcription factors such as *Spi1* did not translate into myeloid differentiation *in vitro*. Rather, the expression of these transcription factors was a sign of a *Gata1*^{mCherry}-driven delay in the lineage-commitment towards erythrocyte and Mk fate.

Discussion

In this study, we tested the hypothesis that ontogeny, i.e. progenitors emerging from different hematopoietic waves, can determine the molecular and cellular responses to a genetic perturbation, here expression of a GATA1 mutant protein. Lineage tracing revealed that indeed yolk sac-derived megakaryopoiesis, from both primitive and definitive EMP progenitors, was strongly impacted by a Gata1 mutant protein, while intra-embryonic HSPC-derived megakaryopoiesis remained mostly unaffected.

Gata1^{mCherry} phenocopies *Gata1s*

A key finding of this study is that *Gata1*^{mCherry} mice phenocopy *Gata1s (Gata1short)* mouse models (Li et al., 2005; Ling et al., 2019). Naturally, both the short and full-length isoforms of *Gata1* are expressed (Calligaris et al., 1995; Rainis et al., 2003). In *Gata1s* mice, however, somatic point mutations in exon 2 lead to the exclusive expression of the short and loss of the long isoform (Rainis et al., 2003). Both *Gata1s* and *Gata1*^{mCherry} mouse models are characterized by a transient hyperproliferation and a block in maturation that ultimately lead to the accumulation of Mks in the yolk sac and fetal liver (Li et al., 2005; Juban et al., 2021). Additionally, erythropoiesis is delayed in *Gata1s* and *Gata1*^{mCherry} embryos (data not shown for *Gata1*^{mCherry}) (Ling et al., 2019).

Gata1s lacks the N-terminal domain. This does not impact its DNA binding activity nor its interaction with other important transcription regulators, such as FOG-1 (Tsang et al.,

1998; Wechsler et al., 2002). The N-terminal domain is important in controlling proliferation and terminal Mk differentiation (Kuhl et al., 2005). Moreover, primitive and definitive hematopoiesis each require different dosages of the N-terminal domain (Shimizu et al., 2001). In contrast to *Gata1s, Gata1*^{mCherry} is a fusion protein of mCherry to the C-terminus of endogenous GATA1. Several non-mutually exclusive phenomena could explain why *Gata1*^{mCherry} phenocopies *Gata1s*. First, mCherry might sterically hinder the accessibility of the N-terminal domain and block the interaction with important binding partners. Second, mCherry might lead to the misfolding of GATA1 thereby changing the functionality of the N-terminal domain. Finally, mCherry might decrease Gata1 mRNA or protein stability. Importantly, *Gata1*^{mCherry} animals do not display the decrease in male viability observed in *Gata1*^{low} mutants (Shivdasani et al., 1997; Hoppe et al., 2016), thereby supporting that fusion of mCherry to GATA1 rather disrupts the function of GATA1 by compromising its 3D organization.

Gata1^{mCherry} drives ontogeny-specific accumulation of megakaryocytes as well as differentiation of blast-like cells

The *Gata1*^{mCherry}-driven increase in activity of the transcription factor CEBPB initiated the priming of a blast-like fate exclusively yolk sac-derived megakaryopoiesis. These blast-like cells further matured in the fetal liver, characterized by the expression of CD244 as well as increased expression and activity of several myeloid and pluripotency transcription factors such as *Spi1* and *Ikzf2*. CD244 is expressed by various immune cells such as natural killer (NK) cells as well as MPPs (Garni-Wagner et al., 1993; Kiel et al., 2005). We confirmed that blast-like cells were not NK cells (data not shown). This indicated that CD244 expression instead is a marker of loss of commitment in this case. The characterization of the cell surface receptor CD244 as a marker for at least a subset of Gata1 mutant-driven blast-like cells will allow future studies to investigate whether blast-like cells in *Gata1s* mouse models share similar transcriptomic and functional properties.

In line with human *Gata1s* expressing blasts that have the potential for eosinophils, mast cells, and megakaryocytes (Miyauchi et al., 2010; Maroz et al., 2014), CD244^{+} blast-like cells showed granulocyte, mast cell, and erythrocyte gene expression patterns. In *Gata1*^{mCherry}, however, CD244^{+} blast-like cells only differentiated into CD41^{low} undifferentiated cells and erythrocytes and not into myeloid cells *in vitro*.

Extrinsic factors influencing megakaryocyte hyperproliferation

Cell fates are usually influenced by both intrinsic and extrinsic cues in their niche. For instance, it was proposed that the higher level of type 1 interferon in the adult bone marrow compared to the fetal liver inhibits Mk hyperproliferation, thereby contributing to the lack of Mk phenotype in adult *Gata1s* animals (Woo et al., 2013). Similarly, the fetal liver but not fetal bone marrow stroma support blast growth in co-cultures (Miyauchi & Kawaguchi, 2014).

Additionally, it is conceivable that EMP- and HSPC-derived Mks may compete for cytokines and space, as recently shown for the erythroid lineage (Soares-da-Silva et al., 2021). As EMP-derived Mks emerge and colonize the FL before HSPC-derived counterparts, accumulation of EMP-derived Mks in *Gata1*^{mcherry} embryos may limit the availability of cytokines for HSPC-derived Mks, and thus prevent them from hyperproliferating. In our study, female embryos however provide evidence that this is not the case. Here we took advantage of the fact that *Gata1* is encoded on the X-chromosome and is subjected to X-inactivation. Thus, female embryos are chimeras containing both *Gata1*$^{wild\text{-}type}$- and *Gata1*^{mCherry}-expressing cells, that can be distinguished by mCherry expression. In female embryos, the hyperproliferation of *Gata1*^{mCherry} cells did not perturb the differentiation of wild-type Mks. This indicated that *Gata1*^{mCherry}-driven Mk hyperproliferation is not sufficient to inhibit megakaryopoiesis from other lineages co-existing simultaneously in the same niche.

Intrinsic differences between yolk sac- and intraembryonic-derived hematopoiesis driving stage-specific phenotypes

Fetal Mks have been described to be intrinsically more proliferative than their adult counterparts (Slayton et al., 2005). Furthermore, in humans, hematopoietic progenitors from the fetal liver, cord blood, and adult BM respond differently when a *Gata1s* mutation is introduced *in vitro* (Gialesaki et al., 2018), suggesting an intrinsic difference between fetal and adult Mks. Indeed, Klusmann and colleagues showed that IGF2 signaling was required for *Gata1s*-induced hyperproliferation in fetal liver progenitor cells but that IGF2 had no effect on bone marrow-derived cells. They showed that *Gata1s* acted downstream of the IGF2 signaling cascade by failing to repress E2F leading to the overexpression of proliferation genes such as *Myc* (Klusmann et al., 2010).

Next to different cytokine and growth factor requirements, the time duration between the emergence of the progenitor cell and the mature Mk is different in the yolk sac and HSPC-derived lineages. While EMPs arise on day E8.5 and produce Mks 24-48 hours later (Palis et al., 1999; Tober et al., 2007; Iturri et al., 2021), there are at least 4 days (96 hours) between the emergence of an HSPC and their differentiation into Mks (Medvinsky et al., 1993; Müller et al., 1994). This could provide the cells more time to compensate for the lack of full-length Gata1 and to induce alternative mechanisms that prevent hyperproliferation of Mks and the development of blast-like cells. This longer duration also indicates that in wild-type conditions the signaling processes in the differentiation and maturation of HSPC-derived Mks may be fundamentally different from that of EMP-derived Mks as we showed.

Finally, our data revealed that megakaryopoiesis is transcriptionally differently regulated and passes through distinct immunophenotypic populations at the cellular level

depending on the stage and ontogeny. This is in line with the findings of a previous study (Cortegano et al., 2019) and could explain the stage-specific nature of *Gata1* mutants.

Strikingly, different transcription factors were active in mutant conditions at E10.5 and E12.5 compared to E16.5. While in yolk sac-derived Mks (E10.5 and E12.5) CEBPB, Helios, and PU.1 showed increased activity in mutant over wild-type Mks (discussed below), JUNB and RELB had upregulated activity in mutant Mks at E16.5. *Relb* is a member of the NF-kB family. One of the direct targets of NF-kB in hematopoietic cells is *Junb* (Oeckinghaus & Ghosh, 2009). Nf-kB signaling is required for hematopoietic stem cell emergence, maintenance, and differentiation (Espín-Palazón & Traver, 2016; Nakagawa & Rathinam, 2018). Additionally, Nf-kB plays a role in Mk commitment and function (Spinelli et al., 2010; Nakagawa & Rathinam, 2018). Interestingly, in zebrafish NF-kB is only required for the emergence of definitive but not primitive hematopoietic cells by regulating Notch signaling (Espín-Palazón & Traver, 2016), a signaling pathway required only for HSPC but not EMP emergence in mice (Hadland et al., 2004; Robert-Moreno et al., 2008). This suggests that NF-kB signaling might differently affect EMP- and HSPC-derived hematopoiesis. Furthermore, we found that a Gata2 binding site in a candidate cis-regulatory element (cCRE) of *Relb* was differently accessible between mutant and wild-type cells in an ontogeny-specific manner. Curiously, it has been proposed that Gata2 has ontogeny-specific functions and can compensate for lack of Gata1 (Fujiwara et al., 2004; Huang et al., 2009; Silvério-Alves et al., 2023).

Collectively, these studies indicate that lineage commitment and differentiation from distinct hematopoietic waves are controlled by unique molecular mechanisms and respond differently to genetic perturbations.

Transcription factors inducing blast-like cell fate

We observed that CEBPB was the most active transcription factor in *Gata1*^{mCherry} Mks and CD244^{+} blast-like cells at E10.5. CEBPB is associated with myeloid and particularly granulocyte fate (Ness et al., 1993; Graf & Enver, 2009; Mancini et al., 2012; Cirovic et al., 2017). Later, at E12.5, the number of transcription factors with heightened activity in *Gata1*^{mCherry} embryos increased, with Helios (*Ikzf2*, master regulator of regulatory T cell development (Wang et al., 1996b; Hahm et al., 1998; Thornton et al., 2010)) at the top. While these transcription factors are both important for lineage commitment and differentiation, they have also been shown to be involved in the maintenance of pluripotency and the development of leukemia (Park et al., 2019; Yusenko et al., 2021; Cova et al., 2021; Klempnauer, 2022).

For example, CEBPB has been reported to cooperate with P300 and MYB in leukemic cells (Yusenko et al., 2021; Klempnauer, 2022). In our study, *Myb* deficiency did not affect blast-like cell development. This indicates that in the context of *Gata1*^{mCherry}, CEBPB regulates blast-like fate independently of MYB.

Helios has been reported to repress Mk fate in order to maintain pluripotency at the level of hematopoietic stem and progenitor cells in the adult bone marrow (Cova et al., 2021). This is in line with our finding that CD244^{+} blast-like cells which express high levels of *Ikzf2* have reduced megakaryocyte output in contrast to CD244^{neg} cells.

Prenatal origin of pediatric leukemias in humans

As in mice, the human hematopoietic system is established in several sequential and overlapping waves originating from spatiotemporally distinct regions (Calvanese et al., 2022). This led to the hypothesis that childhood leukemias might originate from fetal progenitors (Cazzola et al., 2021; Camiolo, Mullen & Ottersbach, 2024).

One example of a pre-leukemic disorder that originates *in utero* is transient myeloproliferative disorder (TMD) also called transient abnormal myelopoiesis (TAM). It is caused by mutations in the 2nd exon of *Gata1* found in around 10 % of all children with Down Syndrome. These mutations lead to the expression of only the short isoform of *Gata1*, *Gata1s(short)* (Mundschau et al., 2003; Rainis et al., 2003). *Gata1s* causes hyperproliferation of megakaryoblasts in these children already *in utero* in the fetal liver (Smrcek et al., 2001; Zipursky, 2003). In most cases, TMD spontaneously resolves within the first 3 months after birth. Only if subsequent mutations occur, TMD further develops into acute megakaryoblastic leukemia (Labuhn et al., 2019; Sato et al., 2024). It has already been demonstrated through *in vitro* experiments that only human fetal liver, but not human cord blood or human bone marrow-derived Mks accumulate in the presence of GATA1s (Gialesaki et al., 2018). Unfortunately, the current lack of tools in human embryonic research to ascribe ontogeny to fetal cells has hampered the identification of the exact progenitor origin of the studied fetal cells.

Additionally, studies performed in mice suggest that also pediatric acute lymphoid leukemias (ALLs) might originate from distinct cellular origins than adult ALL. For example, Sinha and colleagues demonstrated that MLL-ENL translocation causes a more aggressive disease when induced at E12.5 than in the bone marrow (Sinha et al., 2020). Furthermore, another study also showed that the expression of the MLL-AF4 fusion gene causes a stronger effect between E12.5 and E14.5 than at later stages (Barrett et al., 2016). This effect was associated with lymphoid-primed multipotent progenitors (LMPPs) (Böiers et al., 2013) which are a distinct population of HSPCs that most likely rely on unique molecular mechanisms. Altogether, these studies support our finding that ontogeny determines the effect a mutation exerts.

As the landscape of the different hematopoietic progenitor waves and their intrinsic particularities are being refined in mice and humans, our understanding of the origins and molecular events of the onset of infant and pediatric blood disorders will increase.

Conclusion

In summary, we provide evidence that the ontogeny or cellular origin determines which phenotype or disease a mutant/mutation will exert. This has the potential to help further elucidate the origins of infant and pediatric diseases such as leukemias.

Acknowledgment

We thank all team members for their support and constructive discussion. We thank Timm Schroeder for kindly sharing the Gata1^{mCherry} mice and Peggy Kirstetter (IGBMC, Illkrich, France) for insight into their single cell methocult protocol. We acknowledge the flow cytometry platform (Sebastien Megharba, Sandrine Schmutz, and Sophie Novault) and single cell biomarkers platform (Carolina Moraes Cabé, Valérie Seffer) of the CB UTechS at Institut Pasteur for support in conducting this study. We are grateful to all personnel of the Institut Pasteur center for Animal resources and research for their invaluable work. We thank Yann Loe Mie with support in initial analysis of the sequencing data. We thank Azimdine Habib and Marc Monot from the Biomics Platform, C2RT, Institut Pasteur, Paris, France, supported by France Génomique (ANR-10-INBS-09) and IBISA.

This work was supported by recurrent funding from Institut Pasteur, CNRS, and Revive (Investissement d'Avenir; ANR-10-LABX-73), and by an ERC investigator award (2016-StG-715320) from the European Research Council to E.G.P. A.S. was funded by a fellowship from FRM (FDT202304016740).

Methods

Mice

All mice used in this study have been previously described. Experimental procedures, housing, and husbandry were in compliance with the regulatory guidelines of the Institut Pasteur Committee for Ethics and Animal Experimentation (CETEA, dap160091 and dap190119). Strains included *Csf1r*^{iCre} (FVB background, MGI:4429470) (Deng et al., 2010), *Csf1r*^{MeriCreMer} (FVB background, MGI:J:186831) (Qian et al., 2011), *Cdh5*^{CreERT2} (C57Bl/6 background, MGI:3848982) (Sörensen, Adams & Gossler, 2009), *PGK*^{Cre} transgenic mice (C57Bl/6 background, MGI:2178050) (Lallemand et al., 1998), *Gata1*^{mCherry} (kind gift from Timm Schroeder, ETH Zürich, C57Bl/6 background) (Hoppe et al., 2016), *c-Myb* mutant (Mucenski et al., 1991), *Rosa26*$^{(e)YFP}$ (C57Bl/6 background, MGI:J:80963) (Srinivas et al., 2001) and *Rosa26*^{Fucci2aR} (C57Bl/6 background, MGI:5645798) (Mort et al., 2014). Timed matings were performed and the date of the vaginal plug was considered E0.5. Embryonic stages were validated using somite counting and morphological landmarks.

Genotyping

PCR genotyping of *Csf1r*^{iCre} (Deng et al., 2010), *Csf1r*^{MeriCreMer} (Qian et al., 2011), *Cdh5*^{CreERT2} (Sörensen, Adams & Gossler, 2009), *Gata1*^{mCherry} (Hoppe et al., 2016), *c-Myb* (Mucenski et al., 1991), and *R26*^{Fucci2aR} (Mort et al., 2014) , *R26*^{YFP} (Srinivas et al., 2001) embryos, and mice was performed according to protocols described earlier and are available upon request.

4-OHT preparation and injection

4-hydroxytamoxifen (4-OHT) (Sigma, H7904-25MG) was dissolved in equal parts of ethanol and Kolliphor (Sigma C5135-500G) using sonication. 10 mg/mL stocks of progesterone (P3972-5G) were prepared by resuspending in ethanol and sunflower oil (Sigma S5007-250ML) and co-injected with OHT to reduce the risk of abortion. For pulse-labeling using the *Csf1r*^{MeriCreMer} strain, females were weighed on day 8 of pregnancy and injected with 75 µg/g (body weight) OHT and 37.5 µg/g (body weight) progesterone at 1 pm. For pulse-labeling using the *Cdh5*^{CreERT2} strain, females were weighed on day 7 or 10 of pregnancy and injected with 50 µg/g (body weight) OHT and 25 µg/g (body weight) progesterone at 1 pm.

Flow cytometry

Pregnant mice were killed by cervical dislocation and embryos were dissected in cold PBS. Fetal peripheral blood was collected in 2 mM EDTA by severing the vitelline and umbilical vessels after removing the placenta and extraembryonic membranes. Fetal organs were enzymatically dissociated in digestion buffer composed of PBS with 1 mg/mL collagenase D (Sigma 11088882001), 100 U/mL DNaseI (DN25-100mg), and 3% Fetal Bovine Serum for 30 minutes at 37 °C. Fetal organs were passed through 100 µm strainers

by mashing with the piston of a 2 mL syringe and then collected in ice-cold filtered FACS Buffer (0.5% BSA and 2mM EDTA in PBS). Blocking was performed with 5% FBS and 1:20 mouse IgG (Interchim 015-000-003) in FACS Buffer followed by 30 minutes of antibody staining (antibodies listed below). Cells were washed and incubated with fluorescently-conjugated streptavidin for 20 minutes when applicable. Stained cells were passed on the Cytoflex LX (Beckman Coulter) or BD Symphony A5 (BD Biosciences). To quantify cells, the following formula was used : (# of cells acquired) x (volume of resuspended cells after staining and washing/volume of cells acquired) x (volume of cell suspension in blocking buffer before staining/volume of cells plated for staining). Results were analyzed and plots were generated using FlowJo™ v10.10.0 Software (BD Life Sciences).

Antigen	Clone
CD16/32	2.4G2
CD45	30-F11
CD41	MWReg30
F4/80	BM8
Ly6G	1A8
Ly6C	HK1.4
Sca1	D7
CD34	RAM34
Ter119	TER-119
CD71	C2
CD19	1D3
CD3e	145-2C11
Gr1	RB6-8C5
NK1.1	PK136
Kit	2B8
CD11b	M1/70
CD150	mShad150
CD48	HM48-1
CD244.2	REAL493
CD42d	1C2
Ki67	B56
PU.1	E.388.3
Helios	22F6

Intracellular staining for flow cytometry

Cells were prepared for flow cytometry as described above. After cell surface staining, cells were fixed and permeabilized for 1 h using the FoxP3 kit (Invitrogen 00-5523-00) by following the manufacturer's instructions. Afterward, cells were washed and stained for 1 h with primary antibody in permeabilization buffer at room temperature on a shaker (1:100 rabbit anti-PU.1 (Invitrogen MA5-15064, clone E.388.3), 1:100 Ki67-AF647

(BD558615, clone B56), or 1:100 Helios-APC (Biolegend 137222, clone 22F6)) and washed again. In the case of the PU.1 staining, secondary antibody staining was performed for 1 h in permeabilization buffer under the same conditions as the primary antibody (anti-rabbit AF647 (Invitrogen 10123672), 1:100).

Hoechst staining for polyploidy assay

Cells were prepared for flow cytometry as described above. Cells were then incubated with FACS buffer containing 1:100 Hoechst 33342 (Miltenyi 130-111-569) in a shaking incubator at 37 °C with 100 rpm for 40 min. Single cell suspensions were washed and acquired on the flow cytometer.

Immunofluorescence of yolk sac whole mounts

Yolk sacs were fixed in 10 % Formalin solution containing 4 % formaldehyde (Sigma) for 2 h at 4 °C and washed 3 times in 1x PBS at room temperature. Yolk sacs were then permeabilized and blocked in 10 % Normal Goat Serum in PBS-Triton 0.5% (PBS-T) for 2 h at room temperature and stained in blocking buffer containing rat anti-CD41-PE (1:100; clone MWREg 30 Biolegend) overnight at 4 °C. Finally, yolk sacs were washed 3 times for 10 min in PBS-T at room temperature and mounted in ProLong™ Gold antifade (Life technologies, P36930). Z-stacks were acquired on a *Leica SP8* confocal microscope with a 40x/1.30NA objective (immersion oil). Maximum projections were generated in *Fiji* (Schindelin et al., 2012) and PE exposure was adapted for better visibility of the signal.

Immunofluorescence of thick fetal liver sections

Fresh 100 µm thick E12.5 or E16.5 fetal liver sections were prepared as previously described (Peixoto et al., 2024). Dissected fetal livers (FL) were fixed in 5 % Formalin solution containing 2 % formaldehyde (Sigma, HT5014) in PBS at 4 °C overnight and washed 3 times in PBS for 15 min each. 100 µm thick sections were cut in PBS using a vibratome (Leica, VT 1200S). For E16.5 samples, sections were permeabilized and blocked in 10% Normal Goat Serum in PBS-Triton 0.5% (PBS-T) for 2 h at room temperature, washed 3x 20 min in 0.1 % PBS-T, incubated with chicken anti-GFP (1:100; Abcam ab13970) in blocking solution overnight at 4 °C and finally washed again 3x 20 min in 0.1 % PBS-T. Secondary staining was performed by incubation with anti-chicken AF488 (1:500; Invitrogen #10286672) and rat anti-CD41-PE (1:100; clone MWREg 30 Biolegend) in 0.1 % PBS-T for 2 h at room temperature in the dark. FL sections were washed 3x 20 min in 0.1 % PBS-T and cleared in RapiClear (1.52; Sunjin Lab RC152001) overnight. For E12.5 samples, the same protocol was followed but staining was only performed using rat anti-CD41-PE. All sections were mounted in RapiClear and z-stacks were acquired as described above.

Single cell liquid culture

Fetal livers were dissected and blocked as described above. Lineage cells ($Ter119^+$ $CD19^+$ $CD3e^+$ $CD4^+$ $CD8^+$ $NK1.1^+$ $F4/80^+$ $Gr1^+$) were depleted using magnetic anti-biotin

Microbeads (1:5) (Miltenyi Biotec 130-090-485) and MS columns (Miltenyi Biotec 130-042-201). Single cells were sorted using a FACSAria III (Diva software) into flat-bottom 96-well plates containing pre-warmed and equilibrated differentiation medium (0.1% **β**-mercaptoethanol, 1X Penicillin/Streptomycin, 10% FBS, 1:125 SCF, 5ng/µL GM-CSF, 5ng/µL M-CSF, 2ng/µL EPO and 5ng/µL TPO in Opti-MEM with Glutamax). SCF was supplied from myeloma cell line supernatant. Cells were grown at 37°C with 5% CO_2 for 7 days. Colonies were manually scored to detect small megakaryocyte colonies before collecting them by scratching with a pipette tip for flow cytometry analysis. The overall cloning efficiency was defined as the number of sorted single cells that give rise to colonies. The Mk cloning efficiency was defined as the number of sorted single cells that give rise to Mk containing colonies. The colony output was calculated by dividing the number of colonies of one type, i.e. erythrocytes, by the number of all colonies grown.

Single-cell MethoCult culture

Single cells were sorted into 96-well plates containing 50 µL of MethoCult™ GF M3434 (Stemcell Technologies, 03434) as described above. Cells were grown at 37 °C with 5 % CO_2 for 10 days. Colonies were manually scored to detect small colonies before washing them twice with 1x PBS and staining them for flow cytometry analysis.

Single-cell multiome experiment

Library preparation

Cells were sorted using a Symphony S6 (BD Biosciences) with an 85 µL m nozzle into 350 µL PBS containing 5 % FBS. Paired scRNA-and scATAC-seq libraries were prepared using the 10x Genomics Single Cell Multiome ATAC + Gene Expression kit according to the manufacturer's instructions. The initial lysis step was performed for 4 min. ATAC sample index PCR was run with 8 cycles, the cDNA amplification step with 9 cycles, and the GEX sample index PCR with 11 cycles.

Libraries were sequenced with paired-end 100-bp reads on a NextSeq 2000 (Illumina) to a target depth of 25,000 read pairs per nucleus for the ATAC library and 25,000 read pairs per nucleus for the GEX library.

Analysis and annotation of the 10x multiome dataset

Sequencing reads from the six multiome samples were processed using 10X's Cell Ranger ARC pipeline (mm10-2020A genome) to produce count matrices, which were then further processed using the R packages Seurat (Hao et al., 2021) and Signac (Stuart et al., 2021). To combine datasets from the same time points, we computed time-point-specific consensus peak sets by merging overlapping peaks from the two conditions, keeping all peaks smaller than 10 kbp. We then re-quantified the count matrices using Signac's FeatureMatrix function. Low-quality cells were filtered out according to the following criteria: >100,000 RNA counts, >100,000 ATAC counts, <30% reads in peaks, >5% of

ATAC reads mapping to ENCODE blacklisted regions (Amemiya, Kundaje & Boyle, 2019), >2 nucleosome signal, <2 TSS enrichment, doublet score >0.75 (assessed using DoubletFinder (McGinnis, Murrow & Gartner, 2019) for RNA and scDblFinder for ATAC (Germain et al., 2022)). We used the following sample-specific minimal thresholds: >1,500 genes for E10.5-wt, E10.5-*Gata1*^{mCherry}, E12.5-wt, >1,000 genes for E12.5- *Gata1*^{mCherry} and E16.5- *Gata1*^{mCherry}, >500 genes for E16.5 wt, >5,000 ATAC counts for E12.5- *Gata1*^{mCherry}, >2,000 ATAC counts for all other datasets.

We ran two analyses: an unintegrated analysis of each time point that highlights fine biological distinctions and an integrated analysis of the RNA modality to harmonize annotations and visualize all data in a single embedding. For each time point, we combined the RNA and ATAC count matrices (without integration). For the RNA modality, we computed log-normalized counts (counts per 10K), variable features (top 2000 genes, excluding mitochondrial genes and gene models), scaling, PCA, UMAP, SNN, and Louvain clustering. For the ATAC modality, we computed the TF-IDF normalization, SVD (removing the first component), UMAP, SNN, and Louvain clustering. We computed Seurat's WNN analysis (Hao et al., 2021) to obtain a multiome UMAP and clustering. We chose to use the unintegrated RNA analysis to display fine differences at each time point as the RNA modality produced the finest clustering and visualization results, while systematic differences between conditions (technical effects, sex) were negligible compared to biological effects at all time points (good mixing of samples around the MPP compartment, perfect mixing of males and females). To obtain harmonized annotations and visualizations for all time points and conditions, we combined and re-processed the RNA modality of all six samples. We applied Harmony integration (Korsunsky et al., 2019) to obtain a joint PCA-like embedding, then computed UMAP, SNN, and Louvain clustering. We manually annotated the resulting clusters using known marker genes.

Analysis and annotation of the 10x multiome dataset

To mitigate batch effects (ambient content, male vs female differences), we used generalized linear models with the following formula:

$$g(Y) = \alpha.cell\_type + \beta.sample + \gamma.cell\_type.sample + \delta.log\_counts$$

where Y are expression values (normalized or counts depending on the modality), $cell\_type$ is an indicator function (one-vs-all setting, 1 for the cell type of interest, 0 for cells from other types), log_counts is the per-cell log number of counts (used when the model is fit on counts). Coefficient α captures cell-type related effects, β captures systematic biological and technical variablity, γ captures cell-type specific conditional effects. In the paper, we focused on the interpretation of α (cell-type effects) and γ (within cell-type conditional effects). GLM computations and p-value estimations were performed independently at each time point using the fastglm package (Huling et al., 2022), then

FDR-corrected (Benjamini & Hochberg, 1995). For the RNA modality, we applied a plain linear model on ranked normalized expression. For the ATAC modality, we used a Poisson model on counts, keeping only peaks detected in >100 cells.

Gene regulatory networks

To compute transcription factor activity at the single-cell level in the ATAC modality, we ran ChromVAR (Schep et al., 2017) using Signac's RunChromVAR function on the JASPAR 2024 motif set (all mammals, (Rauluseviciute et al., 2024)). To compare differential activity at the cluster level, we fit two sets of linear models: across cell types (pooled conditions, one cell type against all others) and across conditions (one model per cell type). For each model, we used the log number of fragments as a covariable to adjust for sequencing depth.

To compute gene regulatory networks (GRNs), we applied Pando (Fleck et al., 2023) at each time point, pooling conditions. Pando finds triplets of transcription factors, candidate cis-regulatory elements (cCREs), and target genes using a generalized linear model at the single-cell level (independently of clusters) that directly combines RNA and ATAC information. To focus on regulations on the megakaryocyte branch, we subsetted the data to MEPs, megakaryocytes and megakaryocyte progenitors. To obtain robust results, we aggregated cells into metacells using the Louvain algorithm at a resolution of 20 (~50 cells per metacell) and ran Pando with the XGB algorithm on all genes detected in >1% cells. We used the JASPAR 2024 motif set to initiate the GRN. For each TF, the XGB algorithm finds a regulon consisting of up to 50 cCREs and target genes. We then estimated the activity of each regulon at the single-cell level for each modality: on the RNA side, we computed an AUCell-like score (Aibar et al., 2017) using a standard Area under the ROC Curve (scoring the rank of target genes among all genes); on the ATAC side, we computed the ChromVAR score for the top cCREs of each TF. Finally, we computed differential regulon activity across cell types and conditions using linear models (see ChromVAR differential activity), using the log number of fragments as a covariable for the ATAC, without covariable for the RNA.

Pseudotime and co-expression analysis

We computed pseudotime values using Palantir (Setty et al., 2019) on the joint Harmony embedding, with multipotent progenitors as the starting point and all other clusters except MEP as endpoints. To focus on expression differences along the megakaryocyte branch, we extracted Mk I and Mk II, then re-computed markers for each cell type and condition combination at each time point using MetaMarkers (Fischer & Gillis, 2021). We extracted all genes with both high cell-type variability (AUROC>0.6, FDR<10^{-5} in any cell-type by condition combination) and high conditional variability (log2FC>0.5, FDR<0.01 specifically for the WT vs mutant Mk I comparison). We then grouped these genes by co-

expression along the MEP to megakaryocyte differentiation path: we computed the Pearson correlation of expression values in MEP, Mk I, and Mk II at each time point, rank-normalized the resulting co-expression matrices, then averaged the matrices across the 3 timepoints. We obtained co-expression modules by applying the dynamic tree cut algorithm (Langfelder, Zhang & Horvath, 2008) to the hierarchical clustering with average linkage of the average coexpression matrix. Finally, we computed the average expression of each module in all cells using the MetaMarkers score_cells function. To account for sequencing depth differences, the sum of expression across modules was normalized to 1 for each cell, then module expression scores were z-scored across cells. For visualization purposes, module scores were smoothed along pseudotime using a window size of 0.2. We performed gene enrichment analysis of the genes of module 1+2, 3 and 4+5 using Enrichr (Chen et al., 2013; Kuleshov et al., 2016; Xie et al., 2021).

Statistics and Graphs

Statistical analysis was performed with GraphPad Prism v10.1.1. Figures were created with GraphPad Prism v10.1.1, Biorender.com and Adobe Illustrator v27.9.1.

Data availability

Paired single cell RNA and ATACseq data will be made available on a public repository.

Code availability

The code of our single cell RNA and ATACseq data will be made available.

Author contributions

Conceptualization: A.S and E.G.P.

Methodology and data collection: Flow cytometry and animal breeding: A.S., L.F., and P.D.; scMultiome-seq data analysis: S.F., A.S., and E.G.P.

Writing - Original Draft: A.S.; Writing - Review & Editing: A.S., S.F., L.F., and E.G.P.

Funding Acquisition: E.G.P.

Supervision: E.G.P.

Competing interests

The authors declare no competing interests.

Supplemental Data

Supplemental Data Figure 1

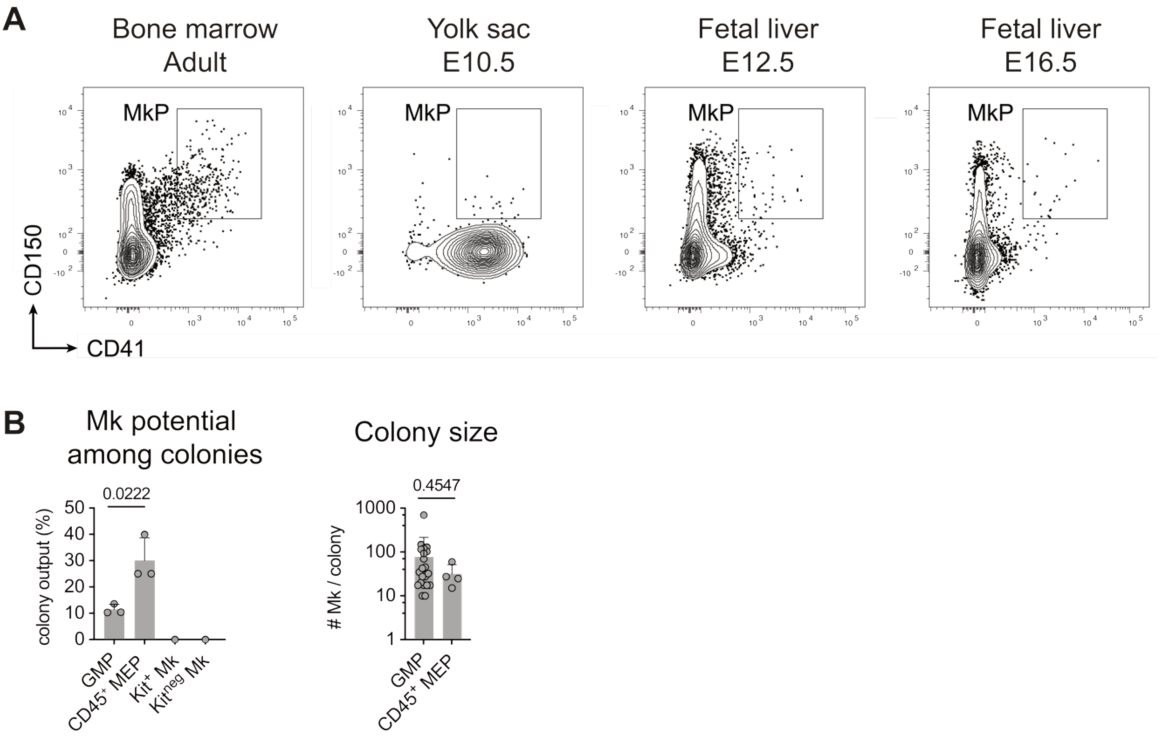

Supplemental Data Figure 1, to Figure 1. (**A**) Dot plot of Lin^{neg} Kit^{high} Sca-1^{neg} cells in the adult bone marrow, E10.5 yolk sac, E12.5 fetal liver, and E16.5 fetal liver. Gate corresponds to CD150^{+} CD41^{+} Megakaryocyte progenitors (MkPs). (**B**) Mk potential among colonies (Mk cloning efficiency) (left, One-way ANOVA, excluding Kit^{+} and Kit^{neg} Mks) and colony size (right, Mann-Whitney test) grown from E12.5 fetal liver-derived immunophenotypic granulocyte-monocyte progenitors (GMPs, Lin^{neg} Kit^{high} Sca-1^{neg} CD16/32^{high} CD34^{+}), CD45^{+} megakaryocyte-erythrocyte progenitors (MEPs, Lin^{neg} Kit^{high} Sca-1^{neg} CD16/32^{neg} CD34^{neg}), Kit^{+} CD41^{+} and Kit^{neg} CD41^{+} Mks from 3 independent litters.

Supplemental Data Figure 2

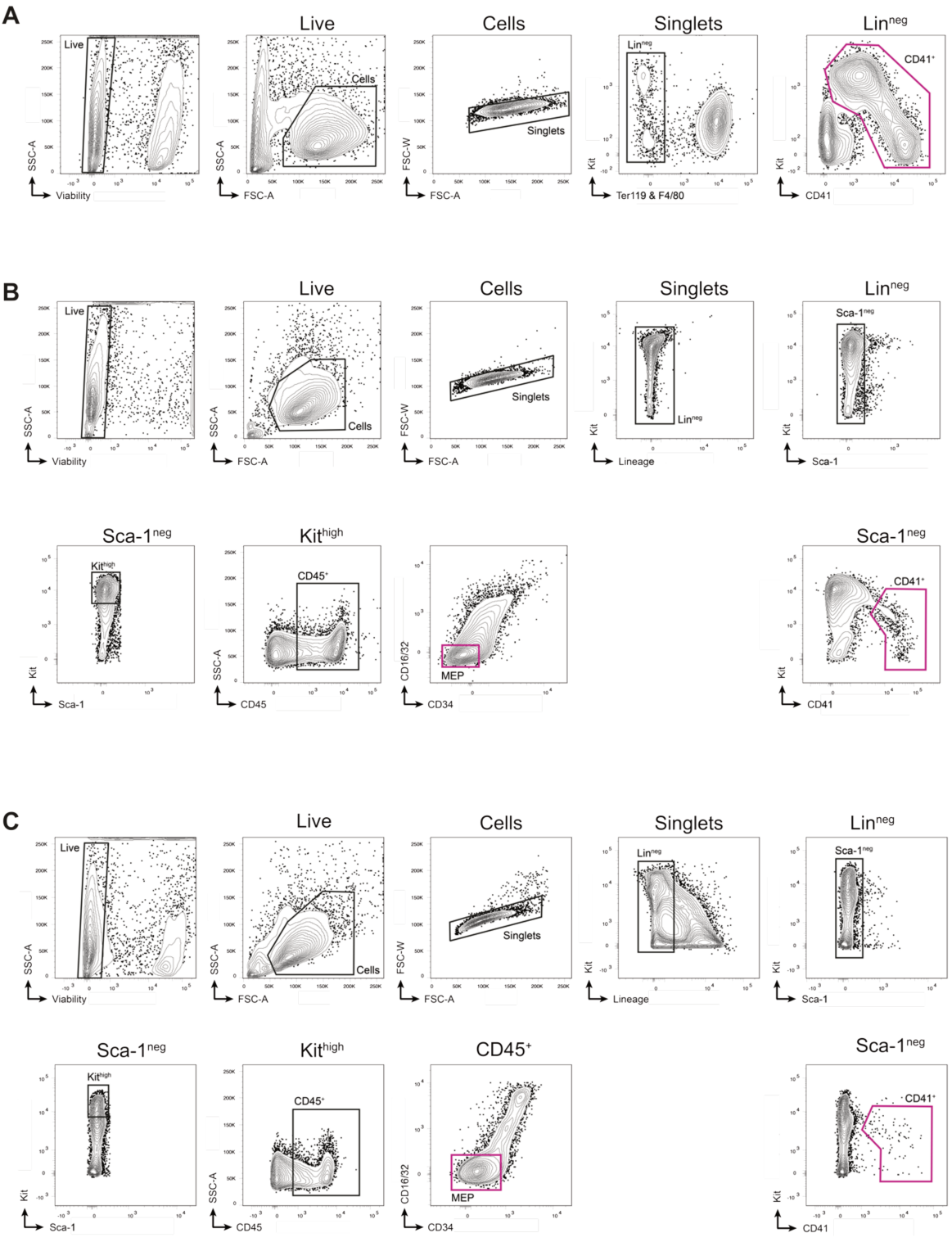

Supplemental Data Figure 2, to Figure 2. Gating strategy used for cell sorting prior to single-cell RNA and single-cell ATAC (multiome) sequencing. Purple gates indicate sorted cells from E10.5 yolk sacs (**A**) E12.5 (**B**), and E16.5 (**C**) fetal livers.

Supplemental Data Figure 3

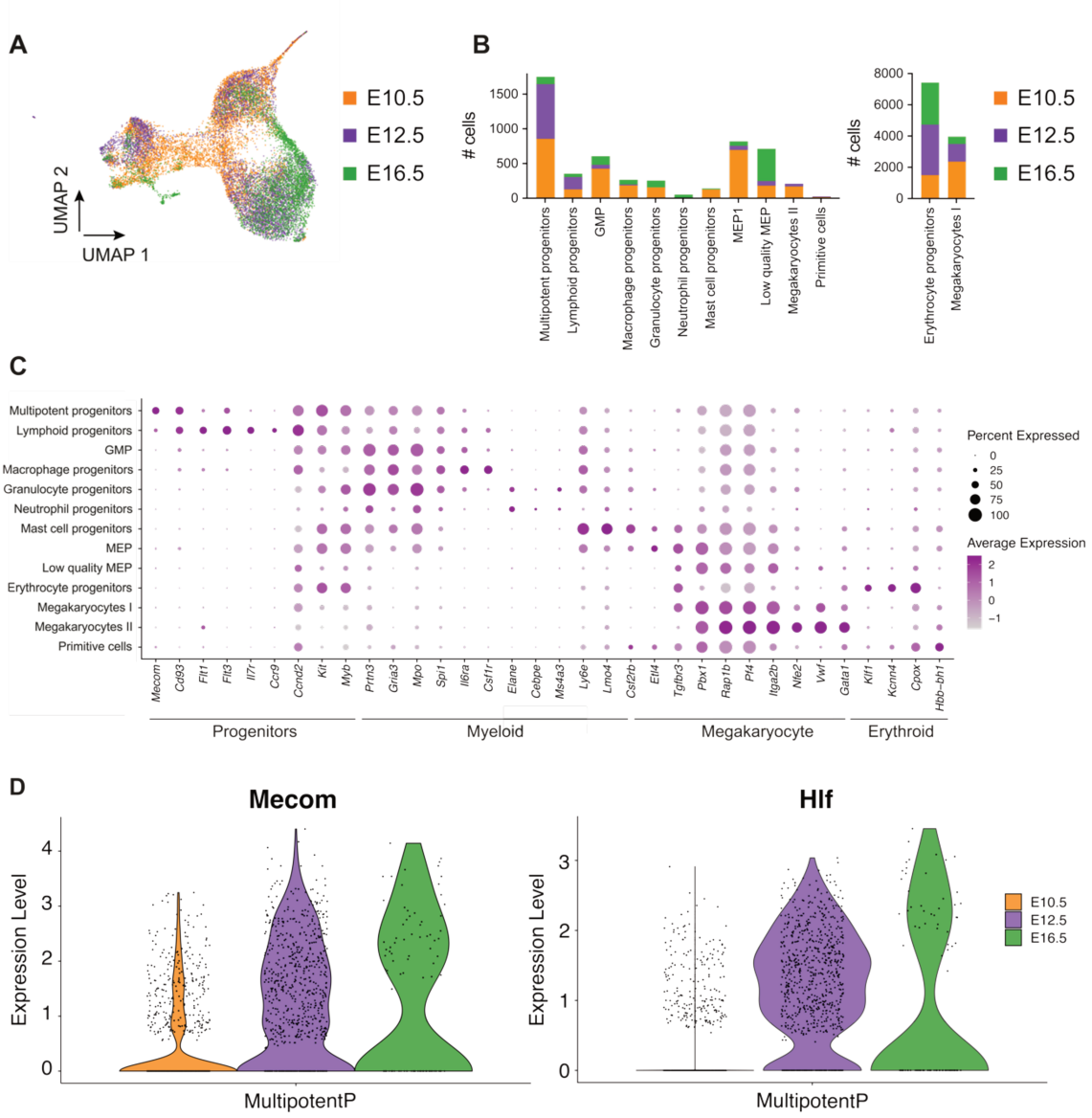

Supplemental Data Figure 3, to Figure 2. Integration of single-cell RNA seq data of wild-type (wt) and *Gata1*^{mCherry} (mut) cells from E10.5 yolk sacs, E12.5 fetal livers, and E16.5 fetal livers. (**A, B**) UMAP (**A**) and number of cells per cluster and sample (**B**). E10.5 wt (orange), E12.5 wt (purple), E16.5 wt (green). (**C**) Dot plot showing average expression level (color intensity) and frequency of expression (dot size) of cell type-specific genes among clusters. (**D**) Violin plot illustrating expression levels of *Mecom* (top) and *Hlf* (bottom) in multipotent progenitors (MultipotentP or MPP) at E10.5, E12.5, and E16.5.

Supplemental Data Figure 4

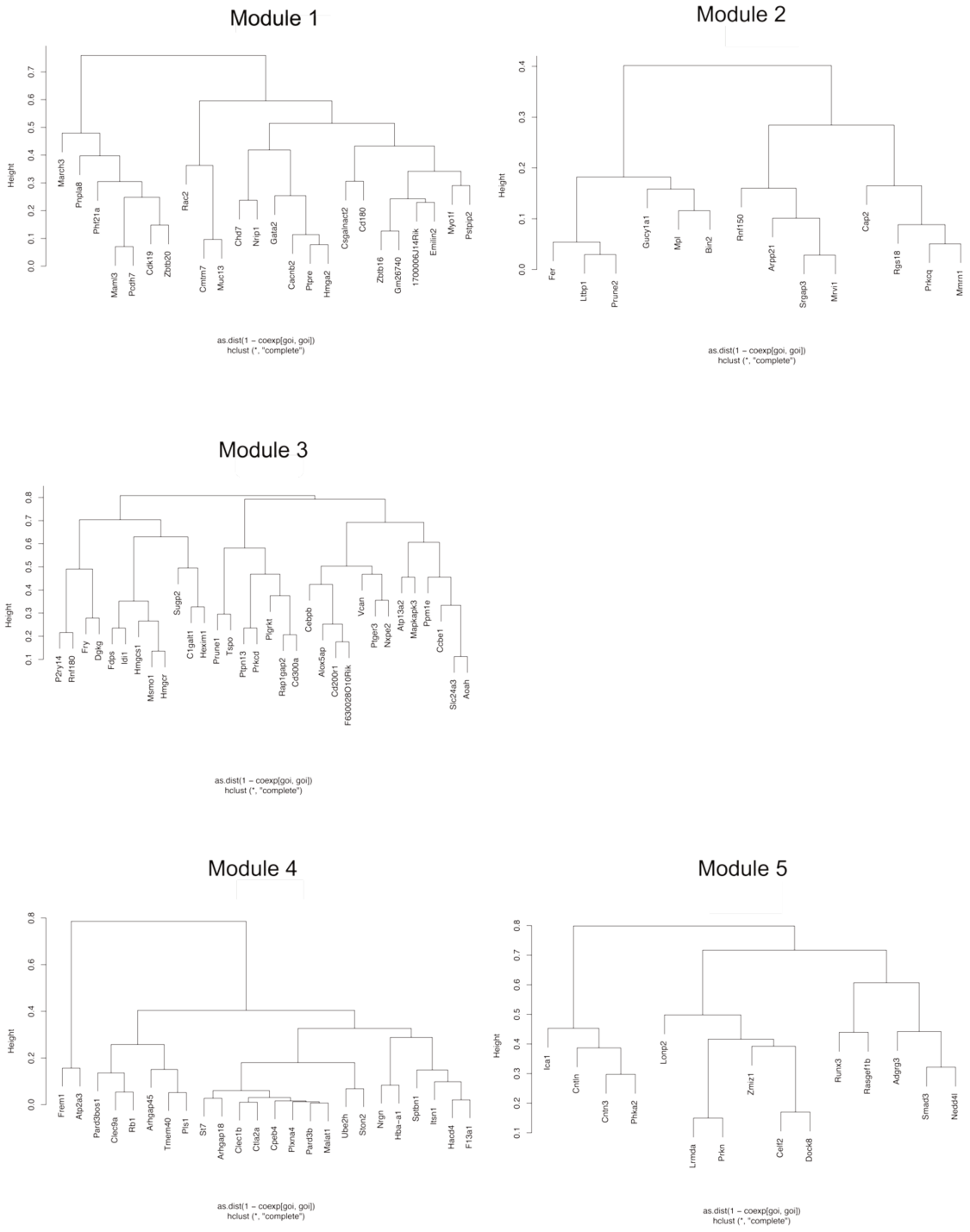

Supplemental Data Figure 4, to Figure 2. Dendrograms showing the genes co-expressed in modules 1-5.

Supplemental Data Figure 5

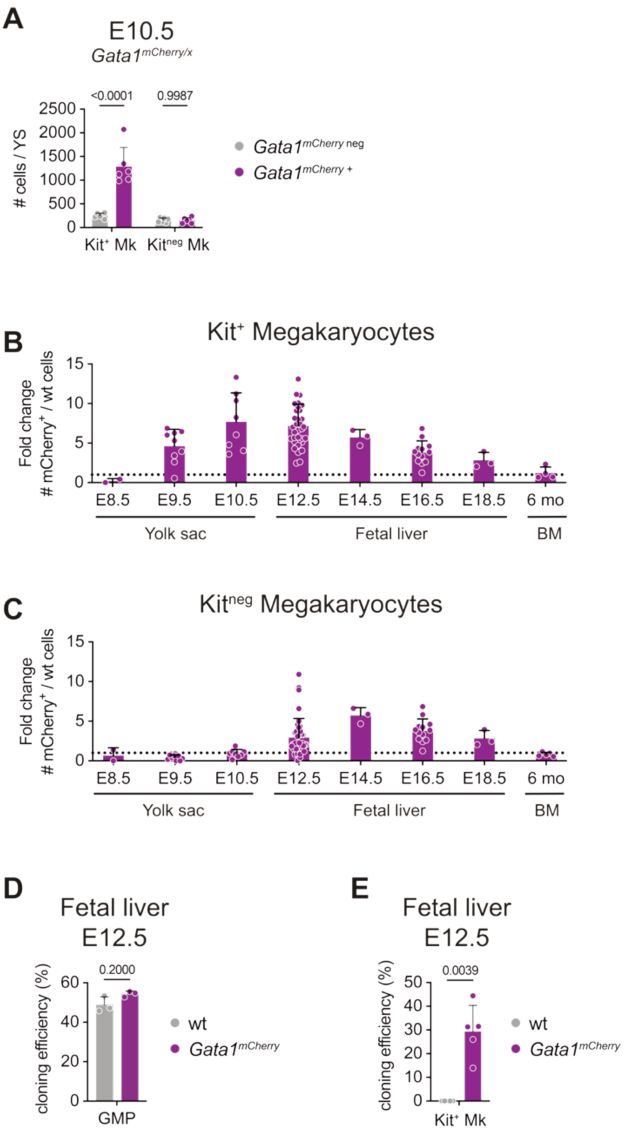

Supplemental Data Figure 5, to Figure 3. (**A**) Bar plot showing the number of *Gata1*$^{mCherry\ neg}$ (grey) and *Gata1*$^{mCherry+}$ (purple) Kit^{+} and Kit^{neg} Mks in E10.5 yolk sacs from *Gata1*$^{mCherry/x}$ female embryos. ≥ 3 embryos from ≥ 3 litters per condition. One-way ANOVA with Tukey's multiple comparisons (**B**) Bar plot showing the fold change of numbers of *Gata1*^{mCherry} over wild-type Kit^{+} Mks in the yolk sac (E8.5-E10.5), fetal liver (E12.5-E18.5) and bone marrow (6 months). Dotted line indicates the value "1". ≥ 3 embryos from ≥ 3 litters per condition (**C**) Bar plot showing the fold change of numbers of *Gata1*^{mCherry} over wild-type Kit^{neg} Mks in the yolk sac (E8.5-E10.5), fetal liver (E12.5-E18.5) and bone marrow (6 months). Dotted line indicates the value "1". ≥ 3 embryos from ≥ 3 litters per condition. (**D**) Bar plot showing the cloning efficiency of single immunophenotypic granulocyte-monocyte progenitors (GMPs, Lin^{neg} Kit^{high} Sca-1^{neg} CD16/32^{high} CD34^{+}) sorted from E12.5 fetal livers from wild-type (grey) or *Gata1*^{mCherry} (purple) embryos. 3 independent litters. (**E**) Bar plot showing the cloning efficiency of single Kit^{+} Mks sorted from E12.5 fetal livers from wild-type (grey) or *Gata1*^{mCherry} (purple) embryos. 5 independent litters.

Supplemental Data Figure 6

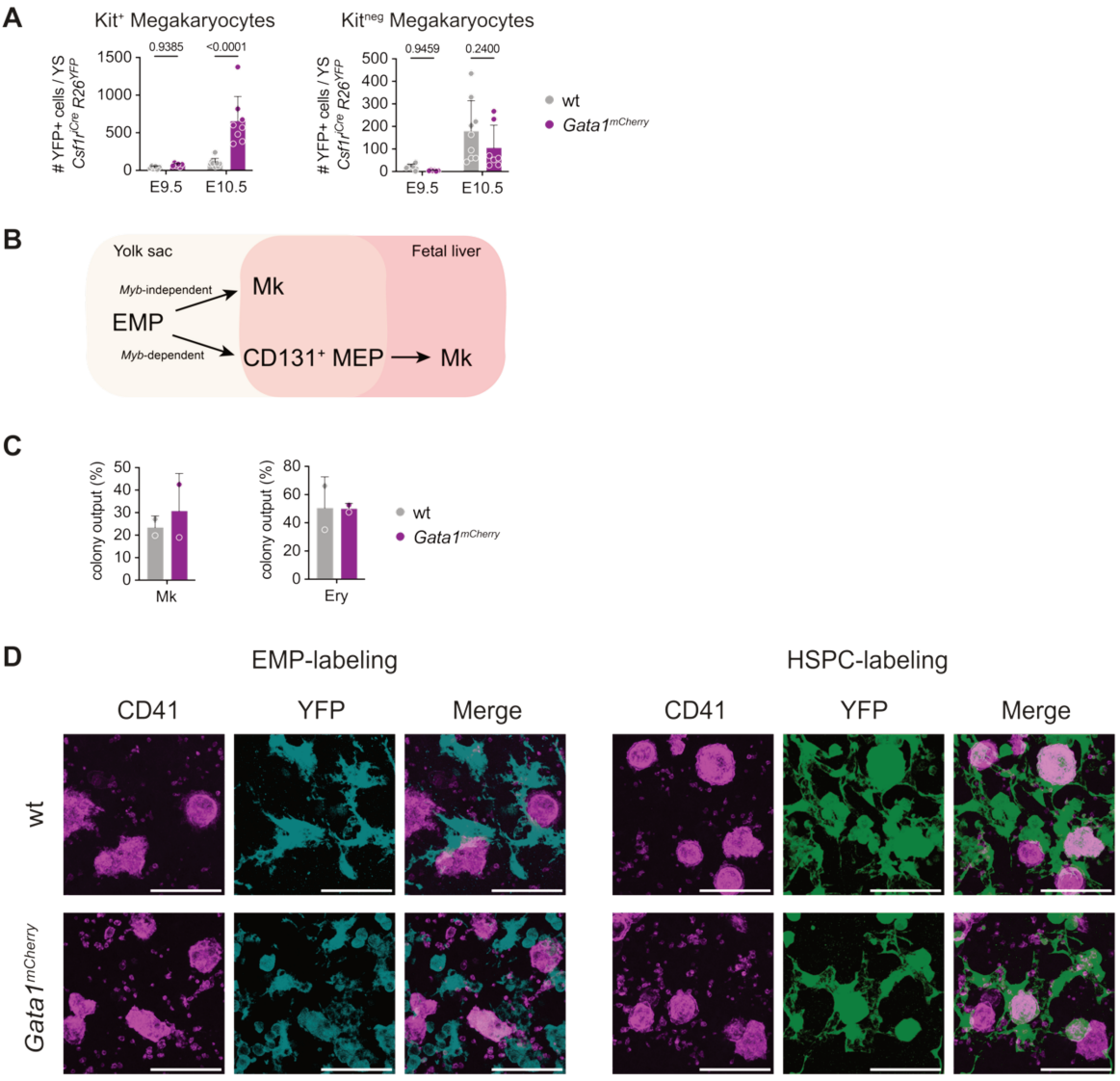

Supplemental Data Figure 6, to Figure 4. (**A**) Number of YFP^{+} Kit^{+} (left) and YFP^{+} Kit^{neg} (right) Mks in E9.5 and E10.5 yolk sacs from *Csf1r*^{iCre} *R26*^{YFP} *Gata1*$^{wild\text{-}type}$ (grey) or *Gata1*^{mCherry} (purple) embryos. > 3 embryos from ≥ 3 litters per condition. One-way ANOVA with Tukey's multiple comparisons. (**B**) Scheme illustrating EMP-derived *Myb*-independent and *Myb*-dependent megakaryocyte differentiation in the yolk sac and fetal liver. (**C**) Bar plot showing megakaryocyte (Mk) and erythrocyte (Ery) output in colonies grown after from Kit^{high}, CD41^{+} CD131^{+} cells from E10.5 yolk sacs. 2 independent experiments. (**D**) Immunofluorescence of 42 µm-thick maximum projection of E16.5 fetal livers from wild-type (wt, top) and *Gata1*^{mCherry} (bottom) embryos. Mks are stained with anti-CD41 PE (magenta). EMP-derived cells were fate-mapped in *Csf1r*^{MeriCreMer} *R26*^{YFP} embryos pulsed at E8.5 with 4-OHT (cyan, left). HSPC-derived cells were fate-mapped in *Cdh5*^{CreERT2} *R26*^{YFP} embryos pulsed at E10.5 with 4-OHT (green, right). Scale bar represents 50 µm.

Supplemental Data Figure 7

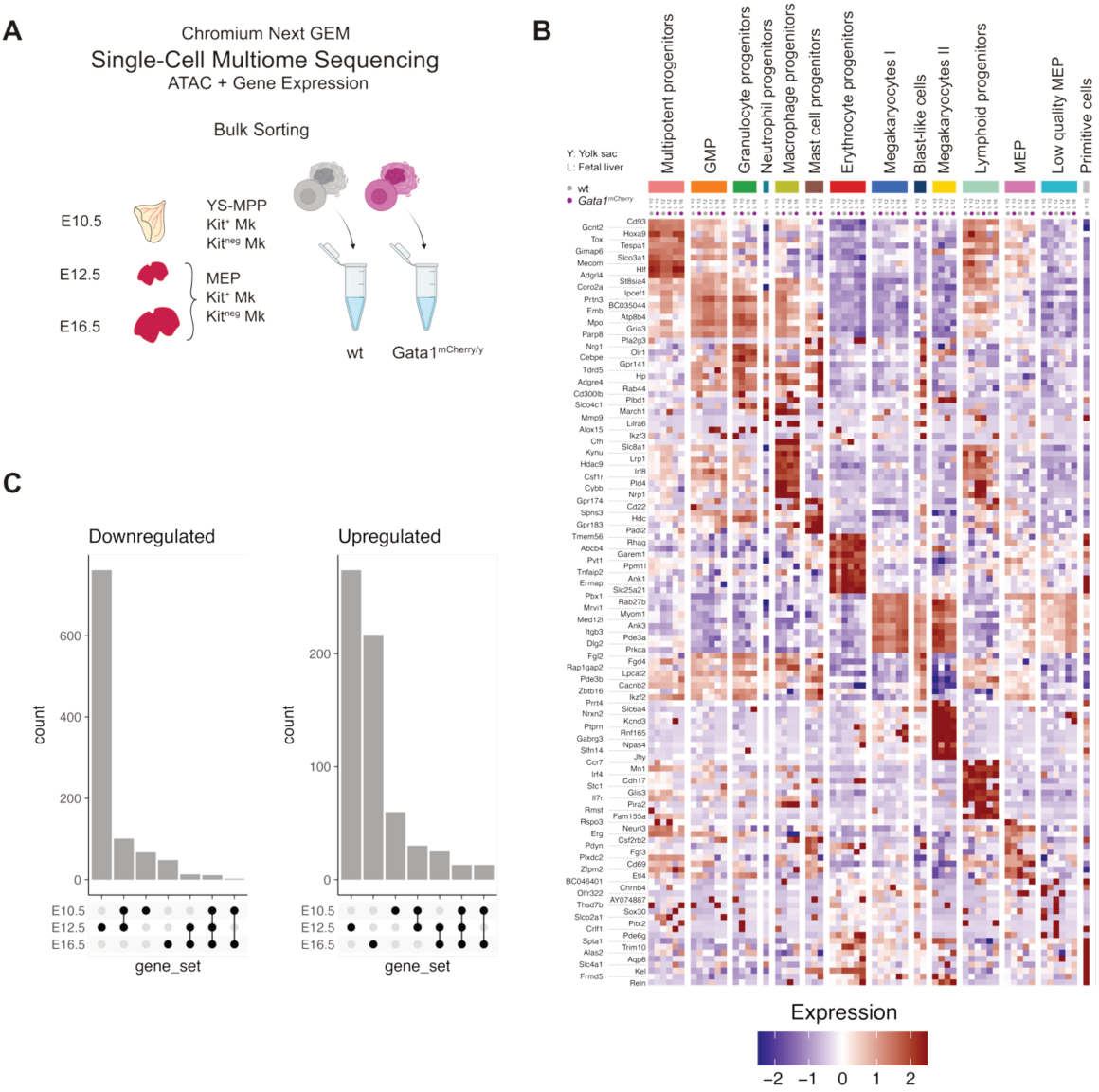

Supplemental Data Figure 7, to Figure 5. Integration of single-cell RNA seq data of wild-type (wt) and *Gata1*^{mCherry} (mut) cells from E10.5 yolk sacs, E12.5 fetal livers, and E16.5 fetal livers. (**A**) Scheme illustrating sorting and sequencing strategy. Multipotent progenitors (Ter119^{neg} F4/80^{neg} Kit^{high} CD41^{int}), Kit^{+}, and Kit^{neg} Mks were sorted from E10.5 yolk sacs. Megakaryocyte-erythrocyte progenitors (MEP), Kit^{+}, and Kit^{neg} Mks were sorted from E12.5 and E16.5 fetal livers. Wild-type (male and female) and *Gata1*^{mCherry} (only male) cells were sorted separately at each time point. Cells were lysed, and gene expression and ATAC libraries were prepared from nuclei following the Chromium Next Gem Single-Cell Multiome Sequencing pipeline. (**B**) Heat map showing Top 10 expressed genes per cluster GMP = granulocyte-monocyte progenitor, MEP = megakaryocyte-erythrocyte progenitor. (**C**) Up-set plot highlighting down- and upregulated genes in *Gata1*^{mcherry} cells compared to wt cells shared by E10.5, E12.5, and E16.5 samples.

Supplemental Data Figure 8

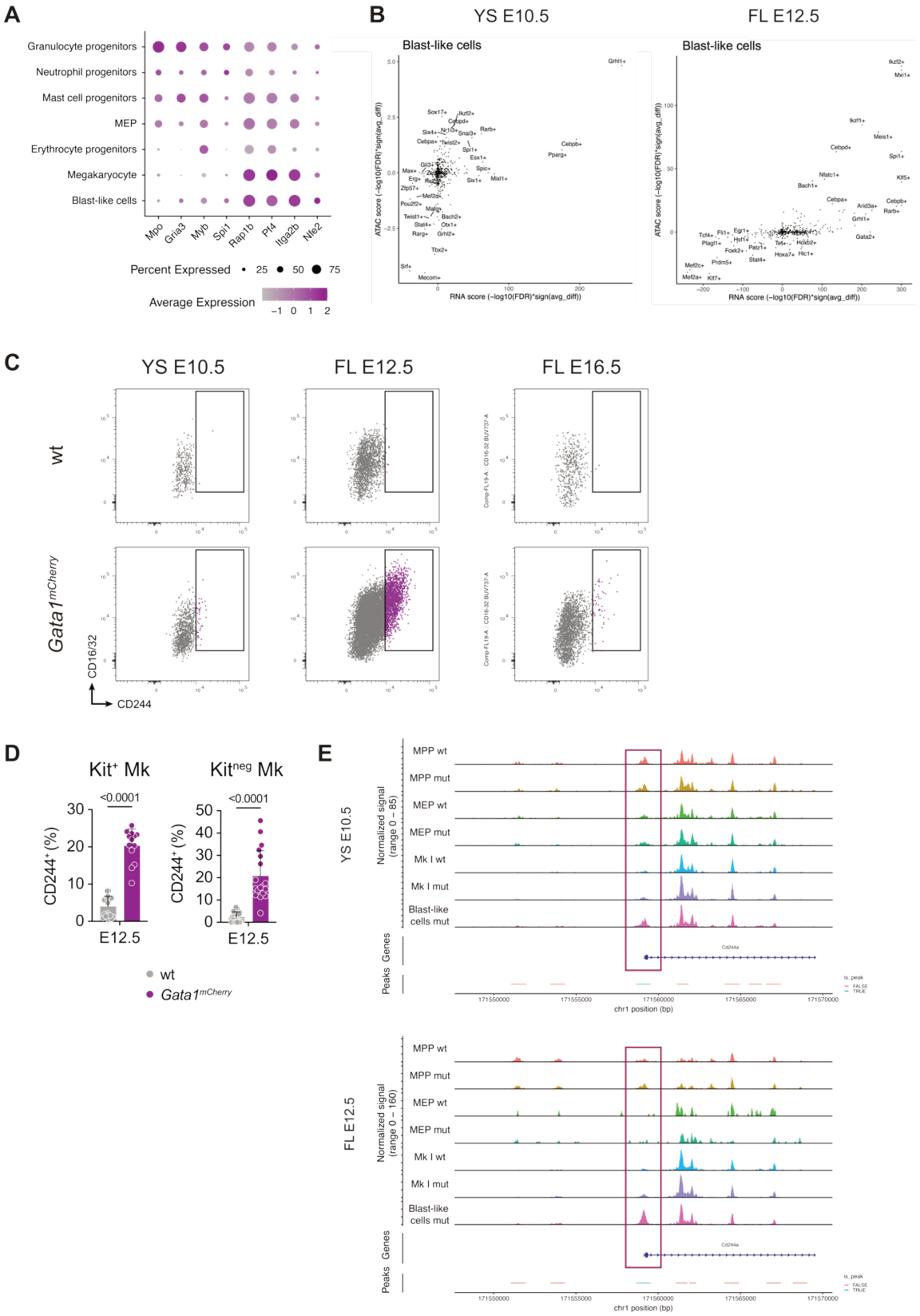

Supplemental Data Figure 8, to Figure 6. (**A**) Dot plot showing average expression level (color intensity) and frequency of expression (dot size) of selected genes among clusters. (**B**) Regulon analysis indicates transcription factors with increased activity in blast-like cells compared to other

clusters in E10.5 yolk sacs and E12.5 fetal livers. (**C**) Dot plots showing gating of CD244^{+} cells (purple) among Kit^{+} Mks in E10.5 yolk sacs, E12.5 and E16.5 fetal livers. (**D**) Bar plot showing the frequency of CD244^{+} cells among Kit^{+} (left) and Kit^{neg} (right) Mks in E12.5 fetal livers. > 3 embryos from ≥ 3 litters per condition. Mann-Whitney test. Error bars represent standard deviation. (**E**) Coverage plot illustrating chromatin accessibility of the *Cd244a* gene in multipotent progenitors (MPP), megakaryocyte-erythrocyte progenitors (MEP), megakaryocytes (Mk I), and blast-like cells from in wild-type (wt) and *Gata1*^{mCherry} (mut) E10.5 yolk sacs and E12.5 fetal livers.

Supplemental Data Figure 9

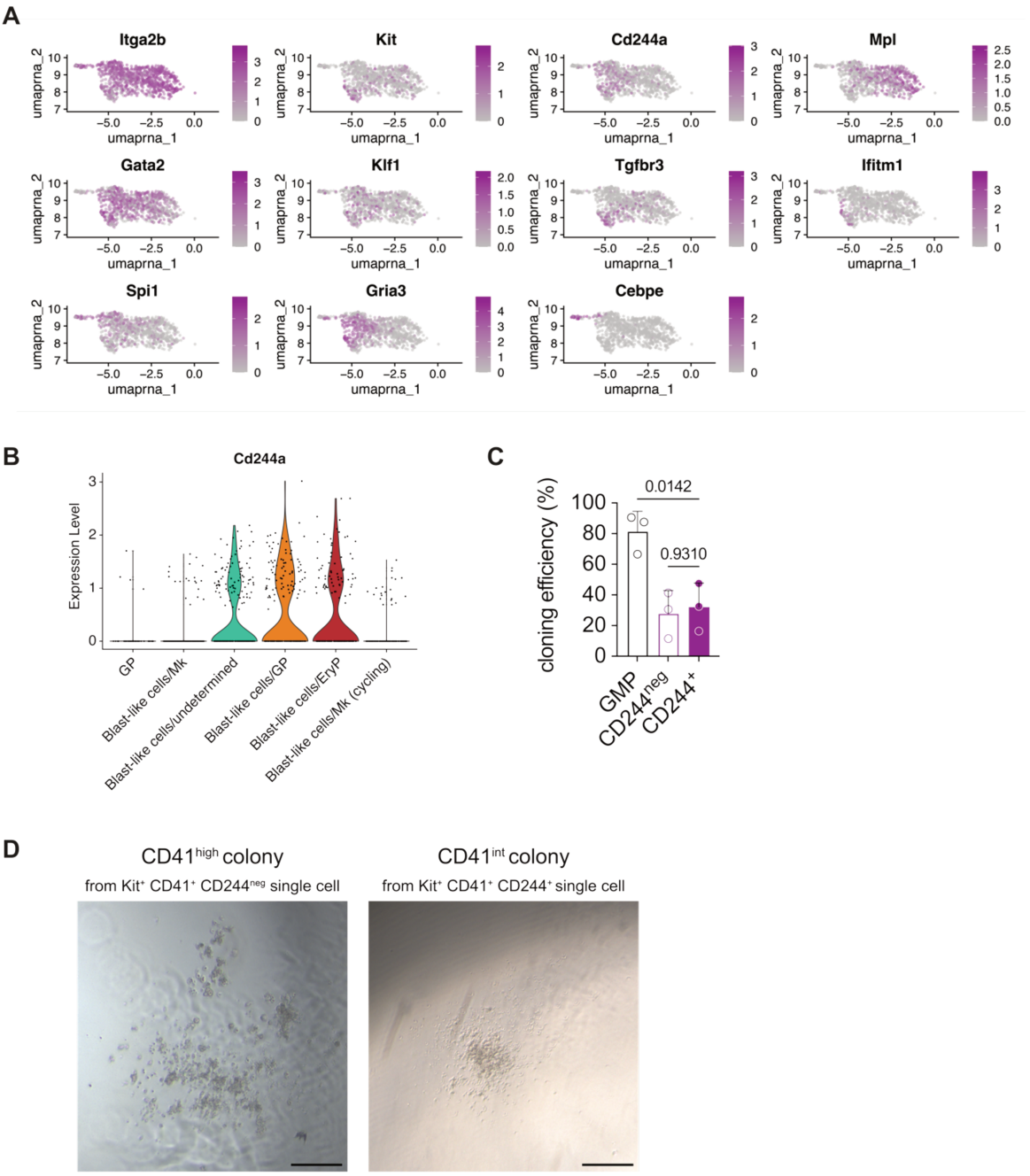

Supplemental Data Figure 9, to Figure 6. (**A**) UMAPs displaying gene expression levels in blast-like cells sequenced from E12.5 fetal livers. (**B**) Violin plot showing *Cd244a* expression among sub-clusters in blast-like cells. (**C**) Bar plot showing the cloning efficiency of single immunophenotypic granulocyte-monocyte progenitors (GMPs, Lin^{neg} Kit^{high} Sca-1^{neg} CD16/32^{high} CD34^{+}, black border), Kit^{+} CD41^{+} CD244^{neg} (purple border) or Kit^{+} CD41^{+} CD244^{+} (purple filled) sorted from E12.5 *Gata1^{mCherry}* fetal livers embryos. 3 independent litters. One-way ANOVA with Tukey's multiple comparisons. (**D**) Bright-field image of CD41^{high} colony grown in methocult for 10 days from a single Kit^{+} CD41^{+} CD244^{neg} cell (left) and CD41^{int} colony grown from a single Kit^{+} CD41^{+} CD244^{+} cell (right) from a E12.5 *Gata1^{mCherry}* fetal liver. Scale bar represents 250 µm.

Supplemental Table 1. ENCODE and ChEA Consensus TFs from ChIP-X predicted to be regulating module 1+2 genes.

Term	P-value	Adjusted P-value	Odds Ratio	Combined Score	Genes
GATA1 CHEA	1,45E-09	7,98E-08	12,553	255,473	RGS18; PCDH7; ZBTB16; PRUNE2; CD180; GATA2; LTBP1; PHF21A; PTPRE; RAC2; MRVI1; PRKCQ; MAML3
TP53 CHEA	0,003	0,066	7,338	42,486	FER; PCDH7; CD180; LTBP1
SUZ12 CHEA	0,004	0,066	3,388	19,062	CACNB2; PTPRE; PCDH7; ZBTB16; EMILIN2; HMGA2; PRKCQ; RNF150; GATA2
EZH2 CHEA	0,010	0,140	7,226	33,127	CACNB2; ZBTB16; RNF150
AR CHEA	0,016	0,179	3,249	13,374	FER; CD180; HMGA2; MAML3; PHF21A; CAP2
ESR1 CHEA	0,035	0,294	7,240	24,365	NRIP1; CAP2
TCF3 CHEA	0,040	0,294	2,870	9,207	CDK19; ZBTB16; CHD7; NRIP1; SRGAP3
NFE2L2 CHEA	0,043	0,294	2,822	8,893	CDK19; PCDH7; ZBTB20; MRVI1; CAP2
GATA2 CHEA	0,058	0,353	2,940	8,388	ZBTB16; RAC2; PRKCQ; GATA2
IRF1 ENCODE	0,089	0,489	4,193	10,147	FER; NRIP1

Supplemental Table 2. GO Biological Processes (2023) predicted to be modulated by module 1+2 genes.

Term	P-value	Adjusted P-value	Odds Ratio	Combined Score	Genes
Regulation Of Platelet Aggregation (GO:0090330)	1,41E-05	0,006	77,688	867,512	MMRN1; EMILIN2; PRKCQ
Positive Regulation Of Platelet Aggregation (GO:1901731)	1,91E-04	0,038	123,167	1054,544	MMRN1; EMILIN2
Positive Regulation Of Homotypic Cell-Cell Adhesion (GO:0034112)	4,15E-04	0,055	79,159	616,469	MMRN1; EMILIN2
Fc-epsilon Receptor Signaling Pathway (GO:0038095)	7,93E-04	0,060	55,394	395,517	FER; PRKCQ
Positive Regulation Of Vasculature Development (GO:1904018)	1,01E-03	0,060	16,855	116,272	EMILIN2; HMGA2; GATA2
Negative Regulation Of Insulin Receptor Signaling Pathway (GO:0046627)	1,11E-03	0,060	46,153	313,996	PTPRE; PRKCQ
Fc Receptor Signaling Pathway (GO:0038093)	1,11E-03	0,060	46,153	313,996	FER; PRKCQ
Negative Regulation Of Cellular Response To Insulin Stimulus (GO:1900077)	1,20E-03	0,060	44,304	298,064	PTPRE; PRKCQ
Positive Regulation Of Angiogenesis (GO:0045766)	1,49E-03	0,066	14,665	95,467	EMILIN2; HMGA2; GATA2
Regulation Of Lamellipodium Assembly (GO:0010591)	1,79E-03	0,071	35,719	225,974	FER; RAC2

Supplemental Table 3. ENCODE and ChEA Consensus TFs from ChIP-X predicted to be regulating module 3 genes.

Term	P-value	Adjusted P-value	Odds Ratio	Combined Score	Genes
RUNX1 CHEA	1,39E-04	0,010	5,689	50,519	HEXIM1; CD300A; P2RY14; PTGER3; C1GALT1; ALOX5AP; ATP13A2; AOAH; FRY
RFX5 ENCODE	0,002	0,066	6,490	40,991	IDI1; CEBPB; HMGCS1; TSPO; HMGCR
ZC3H11A ENCODE	0,018	0,305	10,415	41,816	MAPKAPK3; PTGER3
NFE2L2 CHEA	0,022	0,305	3,451	13,165	CEBPB; VCAN; C1GALT1; PRKCD; ALOX5AP
NFYA ENCODE	0,023	0,305	2,635	9,999	HEXIM1; IDI1; FDPS; HMGCS1; MAPKAPK3; MSMO1; HMGCR; SUGP2
CREB1 CHEA	0,025	0,305	2,974	10,960	HEXIM1; IDI1; FDPS; CEBPB; MSMO1; HMGCR
PBX3 ENCODE	0,049	0,471	2,740	8,248	HEXIM1; HMGCS1; MSMO1; PTPN13; SUGP2
NFYB ENCODE	0,059	0,471	1,995	5,640	HEXIM1; IDI1; FDPS; PLGRKT; HMGCS1; MAPKAPK3; C1GALT1; MSMO1; HMGCR; PTPN13
TCF7L2 ENCODE	0,065	0,471	3,458	9,426	HEXIM1; IDI1; PLGRKT
SMAD4 CHEA	0,066	0,471	3,452	9,395	MAPKAPK3; AOAH; FRY

Supplemental Table 4. GO Biological Processes (2023) predicted to be modulated by module 3 genes.

Term	P-value	Adjusted P-value	Odds Ratio	Combined Score	Genes
Secondary Alcohol Biosynthetic Process (GO:1902653)	7,36E-06	0,002	98,261	1161,394	HMGCS1; MSMO1; HMGCR
Cholesterol Biosynthetic Process (GO:0006695)	8,35E-06	0,002	93,790	1096,660	HMGCS1; MSMO1; HMGCR
Sterol Biosynthetic Process (GO:0016126)	1,19E-05	0,002	82,523	935,996	HMGCS1; MSMO1; HMGCR
Isoprenoid Biosynthetic Process (GO:0008299)	6,90E-05	0,007	221,800	2125,076	IDI1; HMGCR
Negative Regulation Of Leukocyte Migration (GO:0002686)	8,87E-05	0,007	190,105	1773,816	CD200R1; CD300A
Cholesterol Metabolic Process (GO:0008203)	1,66E-04	0,011	32,172	279,965	HMGCS1; MSMO1; HMGCR
Negative Regulation Of Protein Serine/Threonine Kinase Activity (GO:0071901)	2,81E-04	0,016	26,723	218,508	HEXIM1; CD300A; PRKCD
Positive Regulation Of Protein Processing (GO:0010954)	4,63E-04	0,021	73,889	567,334	CCBE1; PLGRKT
Monocarboxylic Acid Metabolic Process (GO:0032787)	4,95E-04	0,021	21,872	166,451	TSPO; MSMO1; AOAH
Negative Regulation Of Inflammatory Response (GO:0050728)	7,34E-04	0,029	19,023	137,292	CD200R1; PRKCD; AOAH

Supplemental Table 5. ENCODE and ChEA Consensus TFs from ChIP-X predicted to be regulating module 4+5 genes.

Term	P-value	Adjusted P-value	Odds Ratio	Combined Score	Genes
GATA1 CHEA	0,001	0,048	5,409	39,162	SMAD3; ZMIZ1; CELF2; ATP2A3; ICA1; RUNX3; PLXNA4
EGR1 ENCODE	0,003	0,100	5,534	31,607	ZMIZ1; RASGEF1B; NEDD4L; LONP2; MALAT1
SALL4 CHEA	0,004	0,100	6,573	35,555	UBE2H; CELF2; DOCK8; SPTBN1
RUNX1 CHEA	0,010	0,168	3,277	15,071	SMAD3; CELF2; DOCK8; ATP2A3; ICA1; ARHGAP18; NRGN
GATA2 CHEA	0,015	0,198	3,792	15,979	ZMIZ1; DOCK8; ST7; ITSN1; ICA1
EGR1 CHEA	0,022	0,243	5,398	20,667	SMAD3; RASGEF1B; ST7
STAT3 CHEA	0,044	0,426	6,282	19,554	RUNX3; PARD3B
AR CHEA	0,055	0,459	2,623	7,620	RASGEF1B; ST7; F13A1; NEDD4L; CNTLN
SUZ12 CHEA	0,096	0,472	2,043	4,788	ZMIZ1; DOCK8; PLXNA4; PARD3B; PLS1; CNTLN
UBTF ENCODE	0,085	0,472	2,116	5,210	RB1; SMAD3; ZMIZ1; DOCK8; ATP2A3; NEDD4L

Supplemental Table 6. GO Biological Processes (2023) predicted to be modulated by module 4+5 genes.

Term	P-value	Adjusted P-value	Odds Ratio	Combined Score	Genes
Regulation Of Small GTPase Mediated Signal Transduction (GO:0051056)	7,28E-05	0,036	20,483	195,162	DOCK8; ITSN1; ARHGAP18; ARHGAP45
Protein K48-linked Ubiquitination (GO:0070936)	3,17E-04	0,065	25,452	205,037	PRKN; UBE2H; NEDD4L
Positive Regulation Of Protein Localization To Membrane (GO:1905477)	4,53E-04	0,065	22,428	172,689	PRKN; SPTBN1; PLS1
Positive Regulation Of Extracellular Matrix Organization (GO:1903055)	0,001	0,065	69,257	522,697	RB1; SMAD3
Clathrin-Dependent Endocytosis (GO:0072583)	0,001	0,076	44,304	298,064	ITSN1; STON2
Small GTPase Mediated Signal Transduction (GO:0007264)	0,001	0,076	15,612	104,355	RB1; RASGEF1B; ARHGAP18
Regulation Of Protein Localization To Membrane (GO:1905475)	0,001	0,076	42,598	283,480	PRKN; SPTBN1
Protein K11-linked Ubiquitination (GO:0070979)	0,001	0,076	41,019	270,085	PRKN; UBE2H
Regulation Of Protein Modification By Small Protein Conjugation Or Removal (GO:1903320)	0,001	0,076	41,019	270,085	PRKN; ZMIZ1
Regulation Of Cell Motility (GO:2000145)	0,002	0,081	14,173	90,922	ADGRG3; ARHGAP18; PLXNA4

---End of megakaryocyte manuscript---

3.1.2 Erythrocytes

Gata1 is not only involved in the megakaryocyte fate but also essential for erythrocytes (Fujiwara et al., 1996). It has already been described in the literature that *Gata1s* not only perturbs megakaryocyte development but that it also delays erythrocyte differentiation (Ling et al., 2019, 2023). We therefore assessed how *Gata1^{mCherry}* affects erythropoiesis.

Gata1^{mCherry} delays erythrocyte commitment and differentiation

Our lab previously identified 4 subpopulations among Kit$^+$ CD41$^+$ cells in the yolk sac representing cells with progressive commitment to the erythroid fate (Iturri et al., 2021). Population A contains mainly multipotent and myeloid progenitors (Kit$^+$ CD41$^+$ CD34$^+$ AA4.1$^+$), population B a mix of multipotent, myeloid and erythroid committed progenitors (Kit$^+$ CD41$^+$ CD34$^+$ AA4.1^{neg}), population C early erythroid committed progenitors (Kit$^+$ CD41$^+$ CD34^{neg} AA4.1^{neg} CD16/32$^+$ CD45$^+$), and population D contains exclusively late erythroid committed progenitors (Kit$^+$ CD41$^+$ CD34^{neg} AA4.1^{neg} CD16/32^{neg} CD45^{neg}). In the presence of *Gata1^{mCherry}*, the frequencies of populations A and B among Kit$^+$ CD41$^+$ cells were unchanged. On the other hand, there was an increase in frequency of population C at the expense of population D indicating a delay in erythroid commitment in the yolk sac at E10.5 (**Figure 8A**). In the E12.5 fetal liver the numbers of CMPs, GMPs, and MEPs by contrast were unaffected by *Gata1^{mCherry}* (**Figure 8A**).

Similar to the delay of erythroid progenitors in the yolk sac, the number of mature Ter119$^+$ erythrocytes was significantly decreased between E9.5 to E16.5 in the yolk sac and fetal liver (**Figure 8B**). Following a similar gating strategy as Ling and colleagues (R1-R5) allowed us to get a better resolution of the delay of erythrocyte differentiation (**Figure 9A**) (Ling et al., 2019). At E12.5 the numbers of R1 (CD71$^+$ Ter119^{neg}) cells were similar between wild-type and mutant whereas R2-3 and R4-5 were reduced (**Figure 8C**). By contrast, at E16.5 only R4-5 was reduced (**Figure 8C**) leading to the recovery of all Ter119$^+$ cells by E18.5 (**Figure 8B**). This suggested that the delay in erythroid commitment observed at the level of progenitor cells in the yolk sac spanned the entire course of erythroblast maturation but started to recover around E16.5.

Gata1^{mCherry} delays the ontogeny switch from primitive to EMP to HSPC erythropoiesis

In unperturbed development, erythroblasts in the bloodstream are mainly of primitive origin until E12.5 (Kingsley et al., 2004). Afterward, EMPs are the primary source of erythrocytes in the fetal liver from E11.5 to E14.5 and in the circulation between E13.5 and E18.5. Finally, HSPCs supersede erythrocyte production in the fetal liver around E16.5 (Soares-da-Silva et al., 2021). In *Gata1^{mCherry}* embryos, however, EMPs barely contributed to CD71$^+$ or Ter119$^+$ cells at E12.5 in the fetal liver. This indicates that at E12.5 most of the erythrocytes are instead of primitive origin in *Gata1^{mCherry}* embryos (**Figure 8D**). At E16.5 red blood cells were now mainly EMP-derived (**Figure 8E,F, 9B, C**). At the same time, the contribution of HSPCs to erythrocytes was significantly reduced in all

erythrocyte populations compared to wild-type fetuses at E16.5. Collectively, this suggests that the delay in maturation is accompanied by a delay in the ontogeny switch from primitive- to EMP- to HSPC-origin by at least 48 hours.

Interestingly, the recovery of erythrocyte maturation coincided with the onset of EMP contribution to the erythrocyte pool. Potentially, this could indicate a distinct role of *Gata1*^{mCherry} in primitive versus EMP-derived erythropoiesis.

In the blood of wild-type embryos, EMP-derived erythrocytes are a large part of all circulating red blood cells until at least E18.5 (Soares-da-Silva et al., 2021). Even though we did not analyze fate-mapped embryos beyond E16.5 the fact that the contribution of EMPs to erythrocytes in fetal liver is extended by at least 48 hours suggests that *Gata1*^{mCherry} probably causes EMP-derived erythrocytes to be present several days after birth. This emphasizes that mutations in EMP-derived cells can impact mice beyond birth.

Conclusion

In summary, these data show that *Gata1*^{mCherry} phenocopies *Gata1s* both in the megakaryocyte and erythrocyte lineage. *Gata1*^{mCherry} causes a delay in erythropoiesis which manifests itself in various stages of erythropoiesis in the yolk sac and fetal liver. Additionally, in the presence of *Gata1*^{mCherry}, the switch between the different origins of erythrocytes is delayed by at least 48 hours. This could be caused by delayed maturation and also potentially by prolonged survival of erythrocytes. Importantly, it should be noted that the kinetics of the delay in ontogeny switch are different between megakaryocytes and erythrocytes. The only time point at which we observed a reduction in the EMP contribution to Kit^{+} megakaryocytes was at E9.5 in the yolk sac but not thereafter. Curiously, the effect of *Gata1s* was also different between megakaryocytes and erythrocytes in human HSPCs in the study by Gialesaki and colleagues. They found that erythrocytes only accumulated in neonatal HSPCs and not fetal HSPCs, while for megakaryocytes the opposite was the case (Gialesaki et al., 2018).

Overall, these results show that mutations can prolong the period in which transient hematopoietic waves contribute to mature cells.

Figure 8

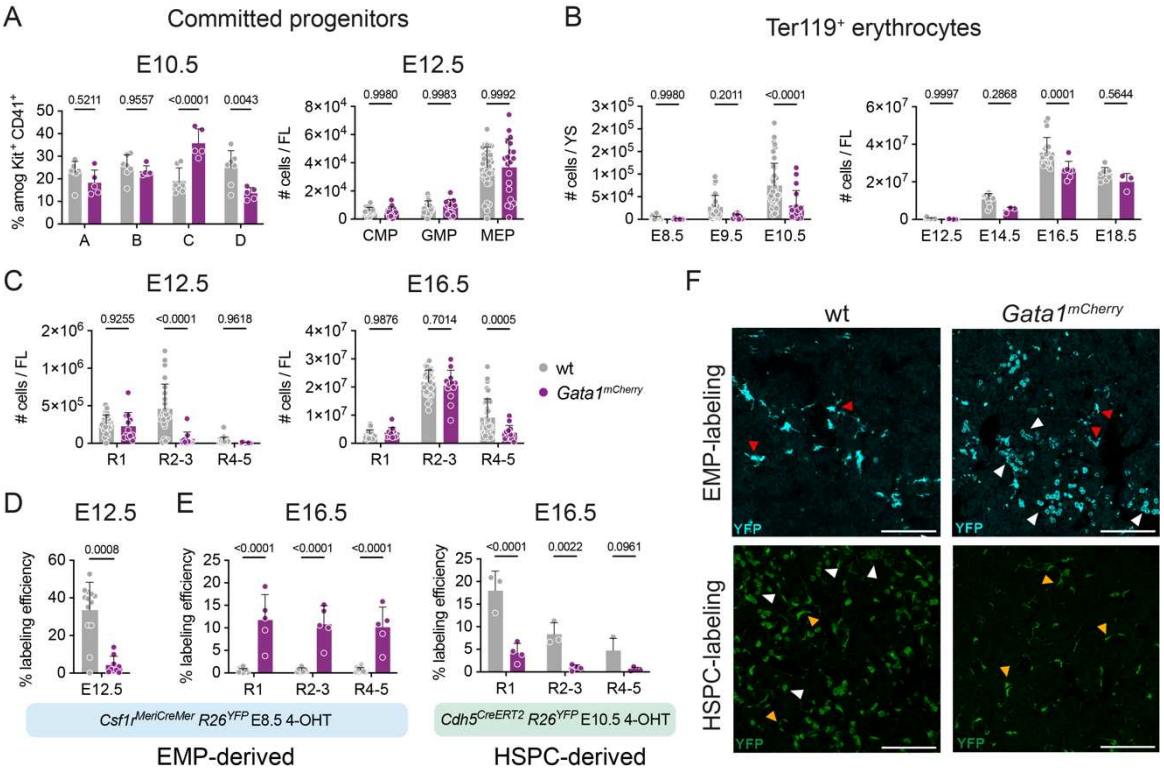

Figure 8. *Gata1*^{mCherry} delays the ontogeny switch from EMP to HSPC erythropoiesis. (**A**) Bar plot the frequency of populations A (Kit^{+} CD41^{+} CD34^{+} AA4.1^{+}), B (Kit^{+} CD41^{+} CD34^{+} AA4.1^{neg}), C (Kit^{+} CD41^{+} CD34^{neg} AA4.1^{neg} CD16/32^{+} CD45^{+}), D (Kit^{+} CD41^{+} CD34^{neg} AA4.1^{neg} CD16/32^{neg} CD45^{neg}) among Kit^{+} CD41^{+} hematopoietic progenitors in the yolk sac at E10.5 in wild-type (wt, grey) or *Gata1*^{mCherry} (purple) embryos (left). Bar plot showing the number of common myeloid progenitors (CMPs, Lin^{neg} Kit^{high} Sca-1^{neg} CD34^{+} CD16/32^{neg}), granulocyte-monocyte progenitors (GMPs, Lin^{neg} Kit^{high} Sca-1^{neg} CD34^{+} CD16/32^{+}), and megakaryocyte-erythrocyte progenitors (MEP, Lin^{neg} Kit^{high} Sca-1^{neg} CD34^{neg} CD16/32^{neg}) per fetal liver (FL) at E12.5 in wild-type (grey) or *Gata1*^{mCherry} (purple) embryos (right). One-way ANOVA with Tukey's multiple comparisons. (**B**) Bar plots showing the number of Ter119^{+} erythrocytes per yolk sac (YS, left) or fetal liver (FL, right) between E8.5 and E18.5. One-way ANOVA with Tukey's multiple comparisons. (**C**) Bar plot showing the number of cells in populations R1 (CD71^{+} Ter119^{neg}), R2-3 (CD71^{+} Ter119^{+}), and R4-5 (CD71^{neg} Ter119^{+}) in the E12.5 (left) or E16.5 (right) fetal liver in wild-type (grey) or *Gata1*^{mCherry} (purple) embryos (right). One-way ANOVA with Tukey's multiple comparisons. (**D**) Bar plot showing the YFP labeling efficiency of R1-5 combined in wild-type (grey) or *Gata1*^{mCherry} (purple) fetal livers of *Csf1r*^{MeriCreMer} *R26*^{YFP} in embryos at E12.5 pulsed with 4-OHT at E8.5. Mann-Whitney test. (**E**) Bar plot showing the YFP labeling efficiency in populations R1, R2-3, or R4-5 in the E16.5 fetal liver in wild-type (grey) or *Gata1*^{mCherry} (purple) embryos (right) in the *Csf1r*^{MeriCreMer} (left) or *Cdh5*^{CreERT2} (right) model pulsed with 4-OHT at E8.5 or E10.5, respectively. One-way ANOVA with Tukey's multiple comparisons. (**F**) Immunofluorescence images of 11 µm-thick z-stacks showing YFP^{+} cells in the E16.5 fetal liver from wild-type (left) or *Gata1*^{mCherry} (right) embryos in the *Csf1r*^{MeriCreMer} *R26*^{YFP} (top, YFP in cyan) or *Cdh5*^{CreERT2} *R26*^{YFP} (bottom, YFP in green) model pulsed with 4-hydroxytamoxifen (4-OHT) at E8.5 or E10.5, respectively. Red arrowheads highlight macrophages. White arrowheads indicate erythroid cells (CD71^{+}, see Supplemental Figure 9). Orange arrowheads highlight endothelial cells. The scale bar represents 100 µm. Data are represented as mean ± SD. See also Supplemental Figure 9.

Figure 9

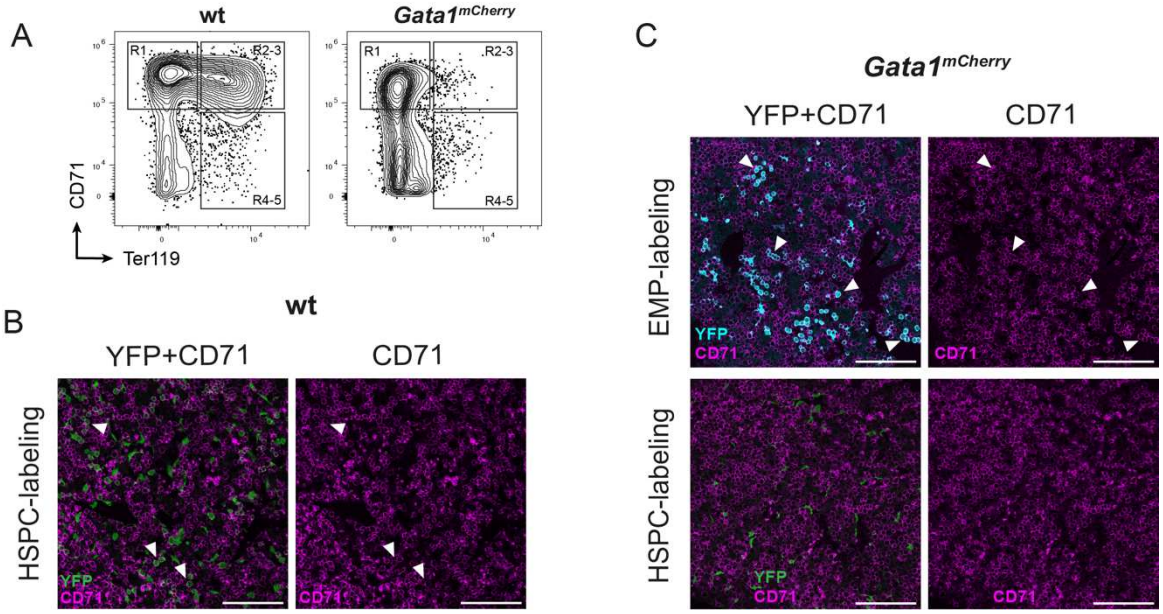

Supplemental Figure 9. Supplemental Figure to Figure 8. (**A**) Dotplots showing the gating strategy of populations R1 ($CD71^{+}$ $Ter119^{neg}$), R2-3 ($CD71^{+}$ $Ter119^{+}$) and R4-5 ($CD71^{neg}$ $Ter119^{+}$) among Lin^{neg} cells ($F4/80^{neg}$ $Gr\text{-}1^{neg}$ $Nk1.1^{neg}$) in the E12.5 fetal liver of wild-type (left) or *Gata1*^{mCherry} (right) embryos. (**B-C**) Immunofluorescence images showing CD71 staining (magenta) of the same sections that are displayed in Figure 7D. The left panels show the merge of YFP (green) and CD71 (magenta). The right panels show only CD71 (magenta) staining. White arrowheads indicate YFP^{+} $CD71^{+}$ erythroid cells. The scale bar represents 100 μm. (**B**) Immunofluorescence images of 11 μm-thick z-stacks showing YFP^{+} cells of the E16.5 fetal liver from wild-type embryos in the *Cdh5*^{CreERT2} *R26*^{YFP} (bottom, YFP in green) model pulsed with 4-hydroxytamoxifen (4-OHT) at E10.5, respectively. (**C**) Immunofluorescence images of 11 μm-thick z-stacks showing YFP^{+} cells of the E16.5 fetal liver from *Gata1*^{mCherry} embryos in the *Csf1r*^{MeriCreMer} *R26*^{YFP} (top, YFP in cyan) or *Cdh5*^{CreERT2} *R26*^{YFP} (bottom, YFP in green) model pulsed with 4-OHT at E8.5 or E10.5, respectively.

3.2 Mast cells – induce

This project was initiated by me, and I performed the pilot experiments while supervising my interns Julia Sanchez Viladevall and Abigail Jolteus. I would like to thank Clarisabel Garcia for her technical assistance. Follow-up experiments were performed by Alesia Arifi under the supervision of Ramy Elsaid. More experiments will be required to complete the project as discussed in the future perspectives.

3.2.1 Introduction

In 1878, Paul Ehrlich discovered cells containing large granules filled with histamine and heparin (Ehrlich, 1878). Due to the high number of granules, he termed these cells mast cells from the German term "Mast" meaning the process of fattening farm animals. Mast cells are involved in a vast array of functions such as immune responses, tissue repair, interaction with the nervous system, angiogenesis, allergies, and autoimmunity. These functions are mediated (1) via the high-affinity receptor FcER1 that binds IgE antibodies, (2) via pattern recognition receptors (PRRs) like TLRs and NOD-like receptors, (3) via Mas-related gene (Mrg) receptor Mrgprb2 that is activated by secretagogues and neurokinins, or (4) via the IL33-receptor (ST2). The binding of ligands to these receptors leads to (1) exocytosis of secretory granules (degranulation) filled with different pre-formed molecules like histamine, proteases (chymase, trypatase), and many more, (2) *de novo* synthesis of chemokines, growth factors, and cytokines which can be released without degranulation, or (3) to secretion of extracellular vesicles (exosomes) (reviewed by da Silva et al., 2014; Olivera et al., 2018).

The first mast cells arise from EMPs, a transient hematopoietic progenitor population that emerges from the yolk sac and does not seed the bone marrow (Palis et al., 1999; Li et al., 2018; Gentek et al., 2018a; Iturri et al., 2021). No markers have been identified so far to distinguish progenitors with mast cell potential from progenitors with other lineage potentials before E10.5. After the onset of fetal liver hematopoiesis, around E11.5, committed mast cell progenitors throughout the body start to express integrin β-7 (*Itgb7*) (Li et al., 2018). Whether migration to the fetal liver is required for mast cell commitment and differentiation remains elusive (reviewed in Chia et al., 2023).

In the adult bone marrow, mast cells have been thought to commit through a myeloid progenitor (GMP) but recent single-cell experiments have suggested that mast cells rather branch off from the erythroid lineage upstream of GMPs (Arinobu et al., 2005; Drissen et al., 2016; Tusi et al., 2018; Dahlin et al., 2018; Ahmed et al., 2020; Wanet et al., 2021). Interestingly, mast cells require both PU.1 and GATA2 (Walsh et al., 2002). As mast cell commitment and differentiation are still being unraveled in adulthood, even less is known about mast cell development in embryonic and fetal life.

EMP-derived mast cells seed tissues such as the skin (dermis), tongue, and peritoneal cavity. These first mast cells are superseded by a second wave of mast cells in a tissue-specific manner. Additionally, this second wave also gives rise to mast cells in other organs like the gut that were omitted by the first wave (Li et al., 2018; Tauber et al., 2023). It remains under investigation which hematopoietic waves, eMPPs or HSCs, are the source of the second wave of mast cells in the fetal period (Li et al., 2018; Gentek et al., 2018a). Depending on the tissue, second-wave mast cells maintain themselves throughout life, such as in the dermis (Kitamura et al., 1979; Hatanaka, Kitamura & Nishimune, 1979; Gentek et al., 2018a; Weitzmann et al., 2020; Tauber et al., 2023), or are regularly replaced by bone marrow-derived cells as in the gut (Du et al., 1996; Li et al., 2018). Curiously, this tissue-specific turnover is reminiscent of the kinetics of tissue-resident macrophages (Merad et al., 2002; Bain et al., 2014; Gomez Perdiguero et al., 2015).

Depending on the stage and tissue of residence, mast cells are characterized by different markers (Msallam et al., 2020; Tauber et al., 2023). While fetal and adult mast cells express CD16/32 and CD200r, and contain heparin-filled granules, only adult mast cells express CD63. Additionally, FcER1 is detected at low levels in the fetus and at high levels on mast cells in adulthood. Fetal mast cells on the other hand have higher levels of Itgb7 and CX3CR1 (Msallam et al., 2020). Furthermore, tissue-specific expression has been described for Mas-related G-protein coupled receptor X2 (*MRGPRX2*) which is expressed by human dermal but not polyp mast cells in the lung (Dwyer & Boyce, 2021).

Expression of Kit (Stem cell factor receptor), however, is a hallmark of mast cells, regardless of the stage or tissue, as Kit signaling is indispensable for mast cell development and survival (Grimbaldeston et al., 2005; Tsai, Valent & Galli, 2022). Upon binding of Stem Cell Factor (SCF, Kit ligand), two Kit monomers dimerize which leads to autophosphorylation of intracellular tyrosine residues initiating a signaling cascade (Blume-Jensen et al., 1991).

A point mutation in the Kit gene (A to T substitution at nt 2468) that causes the amino acid exchange of aspartic acid to valine in position 816 (Kit^{D816V} in humans, Kit^{D814V} in mice) in a tyrosine residue leads to ligand-independent Kit signaling (Nagata et al., 1995). This results in an abnormal accumulation and uncontrolled degranulation of mast cells, which manifests as brown or red lesions on the skin and flushing, anaphylaxis after bee or wasp stings, gastrointestinal cramping, and diarrhea in the case of a chronic course of disease (Hartmann et al., 2016; Valent et al., 2017).

This disease, called mastocytosis, has different pathology in children compared to adults. In children, mastocytosis is usually limited to the skin and spontaneously regresses by adolescence (cutaneous mastocytosis). Adults, on the other hand, develop systemic mastocytosis, a chronic disease affecting not only the skin but the entire body including the bone marrow, spleen, lymph nodes, and gastrointestinal tract (Caplan, 1963;

Hartmann et al., 2016; Valent et al., 2017). While mastocytosis is not life-threatening though discomforting for children, the prognosis can be poor for patients with systemic mastocytosis depending on the severity of their symptoms (Valent et al., 2017).

Interestingly, the transient kinetic of cutaneous (pediatric) mastocytosis is reminiscent of the transient contribution of EMPs to skin mast cells. Additionally, EMPs don't seed the bone marrow which matches the absence of bone marrow infiltration in cutaneous mastocytosis.

This led me and others (Mass & Gentek, 2021; Chia et al., 2023) to hypothesize that the *Kit*^{D816V} mutation might hit distinct progenitor waves (EMPs versus HSPCs) in cutaneous and systemic mastocytosis, respectively. By inducing *Kit*^{D814V} specifically in EMPs, I expected to see a transient increase in the number of mast cells in the skin in the postnatal period, without mast cell infiltration in the bone marrow. Additionally, I expected to observe only a local increase in mast cell degranulation and no systemic symptoms.

The aim of this project was therefore to first better understand how EMPs produce mast cells in health, and how they contribute to disease. By performing single-cell cultures with EMPs, I studied the mast cell commitment process in the yolk sac. Afterward, I tested whether inducing the mastocytosis-driving mutation *Kit*^{D814V} specifically in EMPs would have postnatal effects and cause a disease phenotype mimicking cutaneous mastocytosis.

3.2.2 Results and Discussion

a. Mast cell commitment

Mast cell potential increases with time in the YFP$^+$ EMP population

To study the initial steps of mast cell commitment in the yolk sac, I labeled EMPs at two different time points by pulsing *Csf1r*^{MeriCreMer} *R26*^{YFP} embryos with 4-OHT either at E8.5 or E9.5 (Gomez Perdiguero et al., 2015; Iturri et al., 2021). Single pulse-labeled EMPs (YFP$^+$ Kit$^+$ CD41$^+$ CD34$^+$ AA4.1^{neg}) were then sorted from yolk sacs into 96 well plates 24 h, 48 h, or 72 h after injection and cultured for 7 days. 24 h after the 8.5 and E9.5 pulse, EMPs gave rise to pure myeloid (granulocyte and/or macrophages), erythrocyte, megakaryocyte, and mast cell colonies but also to mixed colonies containing both erythroid, myeloid, and/or mast cells (**Figure 10A**). The cloning efficiency was similar between all conditions and stages (**Figure 10B**). Interestingly YFP$^+$ cells pulsed at 9.5 had an increased myeloid output. At 9.5 EMPs have already started to commit towards erythroid and myeloid fates. Since Csf1r is expressed by myeloid progenitors, the 9.5 pulse therefore potentially captures nascent EMPs but also committed myeloid progenitors which could explain the increased myeloid output.

Colonies containing a mix of erythroid and myeloid cells were virtually absent at time points later than 24 h after pulse. This is a consequence of the progressive commitment and loss of multipotency of EMPs over time.

The frequency of pure mast cells increased from 5 % 24 h after pulse (E8.5 and E9.5 4-OHT), to 20 % 48 h after pulse, and to 50 % at 72 h post pulse. At the same time, erythrocyte potential was significantly reduced 72 h after pulse.

Mast cell potential is found in erythroid and myeloid colonies

Interestingly, mast cell potential was detected not only in pure mast cell colonies but also in combination with erythroid, myeloid, or mixed erythroid-myeloid colonies before E11.5 irrespective of the time of EMP labelling (**Figure 10C**). The fraction of colonies containing erythroid and mast cells was twice as high as colonies with mixed myeloid and mast cell output. The number of mast cells per colony were similar in pure mast cell, erythroid-mast cell, and myeloid-mast cell colonies with a slight tendency to smaller colonies in the pure mast cell colonies (**Figure 10D**).

Figure 10

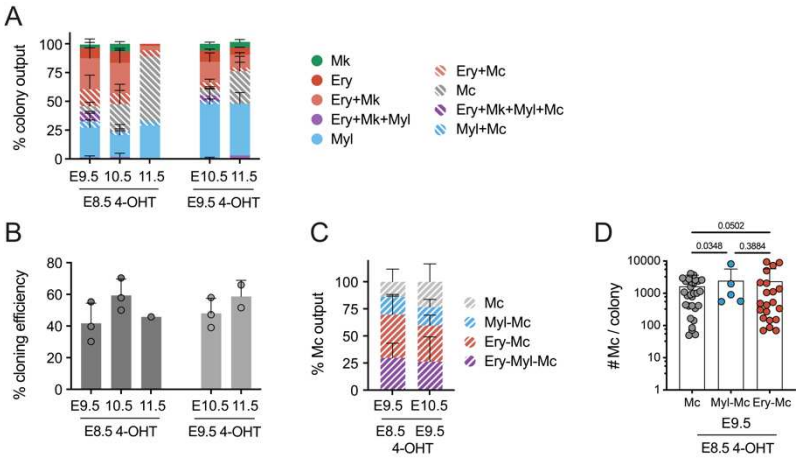

Figure 10. Mast cell potential of yolk sac-derived EMPs. (**A**) Stacked bar plot showing the colony output of single YFP^{+} Kit^{+} CD41^{+} CD34^{+} AA4.1^{neg} cells isolated from yolk sacs at E9.5, E10.5, or E11.5 from Csf1r$^{MeriCreMer/+}$ R26$^{YFP/+}$ embryos with 4-hydroxytamoxifen (4-OHT) pulsed at E8.5 or E9.5. Cells detected in the colonies were megakaryocytes (Mk) erythrocytes (Ery), myeloid cells (Myl, macrophages and neutrophils), and mast cells (Mc). Mast cell colonies are highlighted with white stripes. (**B**) Bar plot showing the cloning efficiency of YFP^{+} Kit^{+} CD41^{+} CD34^{+} AA4.1^{neg} cells isolated from yolk sacs at E9.5, E10.5, or E11.5 from *Csf1r$^{MeriCreMer/+}$ R26$^{YFP/+}$* embryos with 4-hydroxytamoxifen (4-OHT) pulsed at E8.5 or E9.5. (**C**) Stacked bar plot showing the frequency of different mast cell-containing colonies among all mast cell-producing colonies grown from single YFP^{+} Kit^{+} CD41^{+} CD34^{+} AA4.1^{neg} cells from yolk sacs pulsed with 4-OHT at E8.5 or E9.5 and sorted at E9.5 or E10.5, respectively. (**D**) Bar plot showing the number of mast cells per colony in pure mast cell (Mc), myeloid-mast cell mixed (Myl-Mc), or erythroid-mast cell mixed (Ery-Mc) colonies grown from single YFP^{+} Kit^{+} CD41^{+} CD34^{+} AA4.1^{neg} cells from yolk sacs pulsed with 4-OHT at E8.5 and sorted at E9.5.

Conclusion and Discussion

The fact that 24 hours after pulse-labeling EMPs, mast cell output is barely found in pure colonies but is rather mixed with other lineages shows that mast cells originate from *bona fide* multipotent EMPs and not from an independent progenitor population. Pure mast cell colonies significantly increased 48 hours after pulse, which aligns with single-cell RNA sequencing data from our lab, where a distinct mast cell progenitor or precursor cluster is detected at E10.5 but not at E9.5 (**Figure 11A**) (Iturri et al., 2021). Importantly, the kinetic of increasing numbers of pure mast cell colonies was consistent between EMPs pulsed at E8.5 and E9.5. This shows that it intrinsically takes approximately 48 hours, from emergence to mast cell commitment.

Figure 11

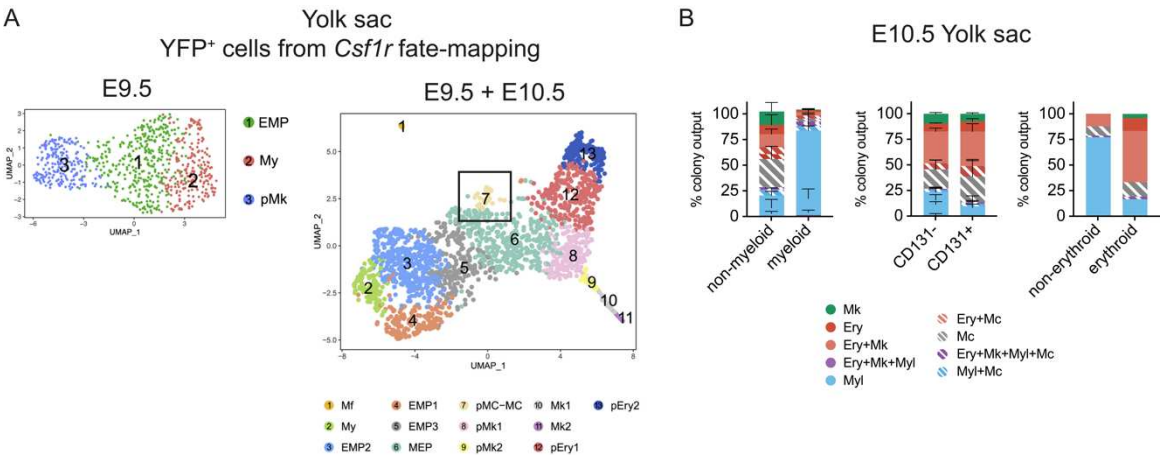

Figure 11. Supporting data for mast cell commitment discussion. (**A**) UMAP representation of YFP$^+$ cells from E9.5 *Csf1r*^{icre}*Rosa*^{yfp} (left) and YFP$^+$ cells from E9.5 *Csf1r*^{icre}*Rosa*^{yfp} integrated with YFP$^+$ cells from E10.5 *Csf1r*^{MericreMer} *Rosa*^{yfp} pulsed at E8.5 (right). Mf, macrophage; My, myeloid progenitor; MEP, megakaryocyte-erythroid progenitor; pMC-MC, mast cell progenitor and/or mast cell; pMK, Mk progenitor; pEry, erythroid progenitor. (**B**) Stacked bar plots showing the colony output of non-myeloid and myeloid progenitors (left), CD131^{neg} versus CD131$^+$ Kit$^+$ CD41$^+$ cells (middle), and non-erytrhoid and erytrhoid progenitors (right) sorted from the E10.5 yolk sac and cultured for 7 days in liquid cultures.

As expected, by E11.5 more than 50 % of the Kit$^+$ CD41$^+$ YFP$^+$ cells had pure mast cell potential and no multipotential was detected. This is in line with other studies showing that *bona fide* EMP multipotential is gone by E11.5. It is also in line with the finding that mast cell potential peaks in the yolk sac at E11.5 (Sonoda, Hayashi & Kitamura, 1983; Palis et al., 1999).

Furthermore, my findings suggest that mast cells might potentially commit through both a myeloid and an erythroid pathway. This is in line with the debate on adult mast cell commitment in the bone marrow that positions mast cells either closer to the erythroid (Drissen et al., 2016; Tusi et al., 2018) or the myeloid lineage (Arinobu et al., 2005; Ahmed et al., 2020; Wanet et al., 2021). Interestingly, mast cell potential was preferentially mixed with erythroid output. This is in line with other unpublished results from our lab that

showed that mast cell potential is specifically enriched in the non-myeloid fraction (**Figure 11 B**). In CD131^{+} cells in the yolk sac, a population that we previously identified as progenitors enriched in erythroid potential (Iturri et al., 2021), showed a slight increase in mast cell output compared to CD131^{neg} cells. Additionally, mast cells were relatively evenly distributed between erythroid and non-erythroid progenitors (n=1!). Collectively, our data argues for a closer relationship with the erythroid lineage but further research will be required to fully understand mast cell commitment in the yolk sac.

b. Effects of mutations in EMP-derived mast cells

Next, to test whether mutations in EMP-derived mast cells cause post-natal effects, I induced the gain-of-function mutation *Kit^{D814V}* specifically in EMPs by pulsing littermate *Csf1r^{MeriCreMer} R26^{YFP} Kit$^{LSL\text{-}D814V}$* (Kit mutant) and *Csf1r^{MeriCreMer} R26^{YFP}* (Kit wild-type) embryos at E8.5 with 4-hydroxytamoxifen (4-OHT) (Srinivas et al., 2001; Gerbaulet et al., 2011; Qian et al., 2011; Gomez Perdiguero et al., 2015). The inducible *Kit$^{LSL\text{-}D814V}$* gene is a transgene. This means upon Cre-mediated excision of the loxP-Stop-loxP site, the expression of *Kit^{D814V}* is activated while the endogenous Kit alleles remain unaffected.

Accumulation of mast cells

First, we tested whether *Kit^{D814V}* increases the number of mast cells in the skin. In pups, the number of mast cells per ear was unchanged. (**Figure 12A**). In the adults, however, we detected a sex-specific effect. While males showed only a mild but not significant increase in mast cell numbers in the ear, mutant female adults showed an almost 2-fold increase compared to wild-type litter mates. (**Figure 12A**).

Precocious maturation of EMP-derived mutated mast cells

At early fetal and postnatal stages, mast cells only express low levels of FcER1 (Msallam et al., 2020). However, inducing the *Kit^{D814V}* mutation in EMPs, caused precocious expression of FcER1α among Kit^{+} ST2^{+} or Kit^{+} CD200r^{+} mast cells in the back skin dermis (BSD) and ear skin dermis (ESD), respectively, of 8-day-old pups (Postnatal day 8, P8) (**Figure 12B**). As expected, virtually all mast cells in the adult ear skin dermis expressed FcER1α.

Prolonged survival of EMP-derived mutated mast cells in pups

To trace mast cells back to their origin, we performed fate-mapping using the inducible *Csf1r^{MeriCreMer}* model pulsed with 4-OHT at E8.5. Since Cre recombination never occurs in 100 % of the targeted cells, controls are required to interpret labeling efficiencies. Microglia are tissue-resident macrophages that emerge in the yolk sac and self-maintain throughout life without contribution from other ontogenies (Ginhoux et al., 2010). Since microglia are a stable population that is highly labeled in the E8.5-pulsed *Csf1r^{MeriCreMer}* model, they serve as a positive control to estimate the initial recombination efficiency. On the other hand, LSKs in the bone marrow are not EMP-derived and therefore serve as a negative control.

In wild-type and mutant mice, microglia were labeled around 15 % or 25 % in animals analyzed at P8 or in adulthood, respectively. As expected, no LSKs in the bone marrow were labeled (**Figure 12C**). This indicates that we successfully induced the mutation specifically in EMPs and spared HSCs.

Mast cells in the BSD and ESD of mutant pups showed dramatically higher labeling efficiency (BSD: 15%, ESD: 10%) in contrast to wild-type littermates (BSD: 7%, ESD: 1.7%) (**Figure 12D**). Surprisingly, the labeling efficiency of around 15 % of the dermal mast cells in mutant 8-day-old pups equilibrated with the labeling efficiency of the microglia. This indicated that in mutant but not in the wild-type pups, most mast cells in the skin are EMP-derived.

In wild-type adult mice (3-6 months old), barely any mast cells showed YFP labeling, indicating the absence of EMP-derived mast cells in the skin, in line a previous study (Gentek et al., 2018a). In mutant adults, on the other hand, YFP$^+$ mast cells were detected in the ear skin dermis of males and females (**Figure 12D)**. YFP$^+$ mast cells, however, were only found in 50 % of all adult mice analyzed. A potential explanation for this is that mast cells are regulated in clonal territories (Weitzmann et al., 2020). Perhaps only in 50% of the animals, YFP$^+$ mast cells expressing the *Kit*^{D814V} mutation initially seeded the analyzed ear. It should be noted that *Kit*$^{LSL\text{-}D814V}$ and *R26*$^{LSL\text{-}YFP}$ are not necessarily recombined in the same cell. This means that ears without YFP$^+$ mast cells in the skin might nevertheless contain EMP-derived mast cells expressing the *Kit*^{D814V} mutation. On the contrary, given the fact that control animals showed almost no YFP labeling in skin mast cells, all YFP$^+$ mast cells detected in the mutant adults most likely expressed the *Kit*^{D814V} mutation.

Mast cells in other tissues

Next to the skin, also the tongue had an increased contribution of EMP-derived mast cells in mutant compared to wild-type mice both in pups and adults (**Figure 12E**). Similarly, mast cells of the peritoneal cavity showed higher labeling efficiency in mutant than in wild-type adults (**Figure 12E**). This indicates that the induction of *Kit*^{D814V} expression specifically in EMPs *in utero* dramatically extends the survival of EMP-derived mast cells not only in the skin as described above, but also in peritoneal cavity, and tongue by several months.

EMP-derived *Kit*^{D814V} mutated mast cells cause ulcerative dermatitis in adult mice

Curiously, around six months of age, mutant but not wild-type mice developed ulcerative dermatitis in the neck region (5 observations out of 5 mutant mice) (**Figure 12F**). YFP labeling efficiencies in all analyzed tissues were similar to 3-month-old mice that had no signs of ulceration (**Figure 12D**). Ulcerative dermatitis is a disease in mice caused by an increase in the numbers and the degranulation of dermal mast cells (De Biase et al., 2019; Gozalo et al., 2023). Ulceration is thought to be a result of intense scratching caused by histamine-driven pruritus (itchy skin) (Gozalo et al., 2023). This suggests that *Kit*^{D814V}

mutant mice have elevated histamine levels in the skin, which could be due to an increase in (EMP-derived) mast cell numbers or heightened degranulation (mast cell activation) both caused by ligand-independent Kit signaling.

Figure 12

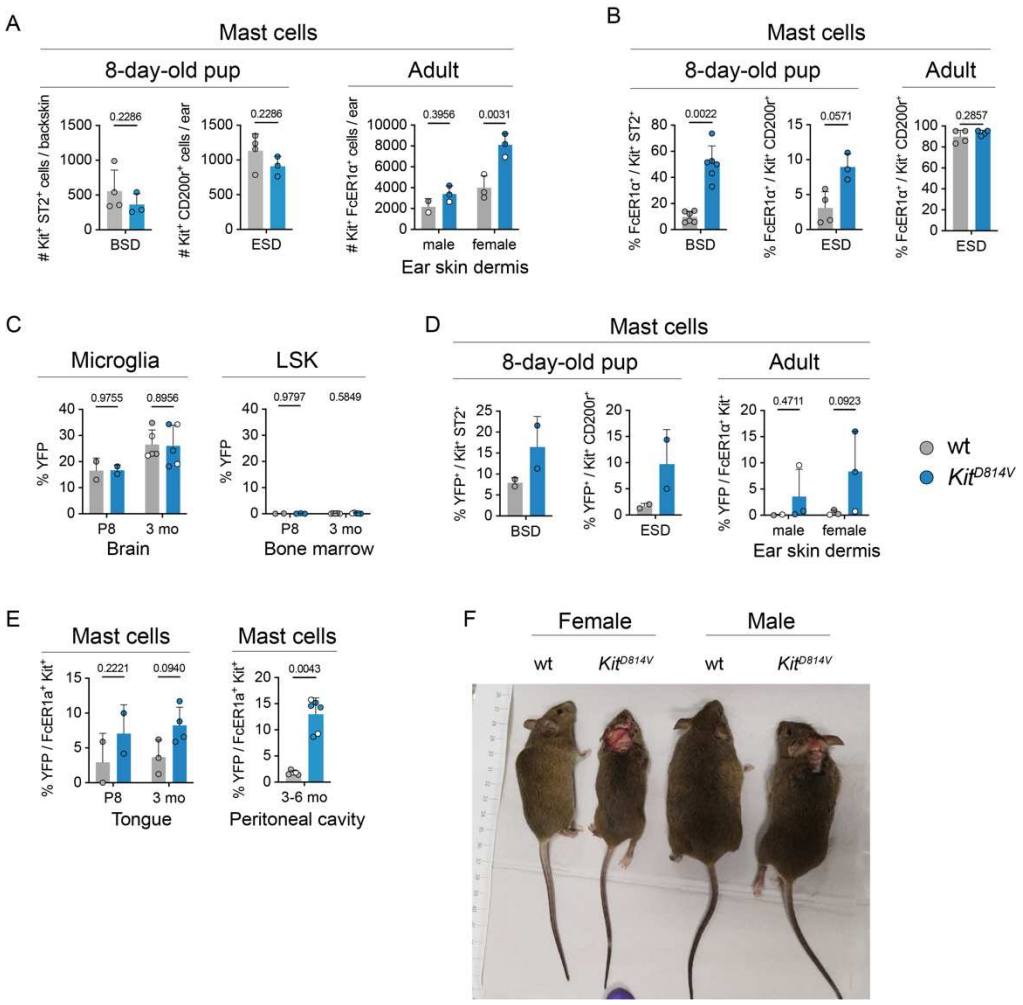

Figure 12. Kit^{D814V} mutation in EMPs causes precocious maturation, prolonged survival of mast cells, and ulcerative dermatitis in adulthood. Analysis of *Csf1r*$^{MeriCreMer/+}$ *R26*$^{YFP/+}$ *Kit*$^{LSL-D814V/+}$ (Kit mutant, blue) and *Csf1r*$^{MeriCreMer/+}$ *R26*$^{YFP/+}$ (Kit wild-type, wt, grey) mice pulsed at E8.5 with 4-OHT. (**A**) Bar plots showing the number of mast cells per patch of back skin dermis (BSD, mast cells gated as Kit$^+$ ST2$^+$, left) at P8 (left) or per ear (ESD, mast cells gated as Kit$^+$ CD200r$^+$) at P8 (middle) and of 3-6 months (right). (**B**) Bar plots showing the frequency of FcER1α$^+$ cells among mast cells in BSD at P8, ESD at P8 (middle) or 3 months (right). (**C**) Bar plots showing the frequency of YFP$^+$ cells among CD45$^+$ CD11b$^+$ F4/80$^+$ microglia in the brian (left) or Lin^{neg} Kit^{high} Sca-1$^+$ hematopoietic stem and progenitor cells (LSK) in the bone marrow (right) at P8 or 3 to 6 months. (**D**) Bar plots showing the frequency of YFP$^+$ cells among mast cells in BSD at P8, ESD at P8 (middle) or 3 months (right). (**E**) Bar plots showing the frequency of YFP$^+$ cells among mast cells in the tongue (left) or peritoneal cavity (right) at P8 and 3 to 6 months. (**F**) Photo of 6-month-old wild-type (wt) and Kit^{D814V} mutant female and male mice. Mutant mice show ulceration in the head and neck region. White data points highlight 6-month-old mice in contrast to 3-month-old mice. Statistics: Mann-Whitney test or One-way ANOVA with Tukey's multiple comparisons. Data are represented as mean ± SD.

Conclusion

The goal of the project was to test whether induction of the mastocytosis driving *Kit*^{D814V} mutation specifically in EMPs, a transient hematopoietic wave, could mimic the unique features of cutaneous mastocytosis compared to systemic mastocytosis. Indeed, the expression of *Kit*^{D814V} led to the precocious maturation of EMP-derived mast cells. Contrary to what was expected, these mutated mast cells, however, did not disappear around puberty but remained in the skin until adulthood. In accordance with the pathology of cutaneous mastocytosis in humans, we did not observe mast cell infiltration in the bone marrow (data not shown). Nevertheless, we detected increased numbers of EMP-derived mast cells in the peritoneal cavity which might cause systemic effects.

Even though this means that inducing the mutation *Kit*^{D814V} in EMPs does not faithfully mimic pediatric mastocytosis, our study provides a proof of concept that in mice inducing a mutation specifically in EMPs has adverse effects far beyond the developmental period even until the age of 6 months.

c. Future perspectives

To further characterize the effect of *Kit*^{D814V} mutation in EMP-derived mast cells in future experiments we could quantify the number of mast cells in ear skin whole mounts or back skin sections in histology as well as the tryptase levels in the serum of wild-type and mutant mice with or without ulcerative dermatitis.

Additionally, functional mast cell assays such as passive systemic or passive cutaneous anaphylaxis (PCA) could provide insight into the local and systemic effects of mast cell degranulation in the presence of *Kit*^{D814V}. In PCA, mice are systemically (intraperitoneally) or locally (intradermally in the ear) sensitized with IgE anti-DNP-HSA (mouse dinitrophenylated human serum albumin, Sigma Aldrich D8406) and challenged with DNP-HAS 24-48 hours later. A systemic anaphylactic reaction is measured by assessing the rectal temperature every 10 min for one hour (Gouel-Chéron et al., 2023). The speed and amplitude of temperature drop (hypothermia) would be expected to be steeper and stronger in *Kit*^{D814V} mice compared to control mice. To read out a local reaction in the ear skin, the swelling of the ear will be measured and the formation of edema will be quantified by injecting Evans blue and measuring its extravasation from vessels using spectrometry. These experiments could potentially be done with 6-week-old adult mice.

So far, we only induced the mutation in EMPs by taking advantage of the *Csf1r*^{MeriCreMer} model pulsed with 4-OHT at E8.5. It would, however, also be interesting to test whether inducing the mutation in HSPCs leads to a more systemic phenotype with infiltration of mast cells in the bone marrow. This could be achieved by crossing *Kit*$^{LSL-D814V}$ mice with *Cdh5*^{CreERT2} and pulsing with 4-OHT at E10.5. It will also allow us to elucidate whether *Kit*^{D814V} in HSPCs drives a later disease onset or whether it causes the same precocious maturation of mast cells in pups as seen in the EMP wave.

d. Materials and Methods

Mice

All mice used in this study have been previously described. Experimental procedures, housing, and husbandry were in compliance with the regulatory guidelines of the Institut Pasteur Committee for Ethics and Animal Experimentation (CETEA, dap160091 and dap190119). Strains included *Csf1r*^{MeriCreMer} (FVB background, MGI:J:186831) (Qian et al., 2011), *Rosa26*$^{(e)YFP}$ (C57Bl/6 background, MGI:J:80963) (Srinivas et al., 2001), and $^{KitLSL\text{-}D814V}$ (C57Bl/6 background, MGI:4942357) (Gerbaulet et al., 2011). Timed matings were performed and the date of the vaginal plug was considered E0.5. Embryonic stages were validated using somite counting and morphological landmarks. Pups were born naturally or by C-section when necessary at E19.5. Genotypes were determined by PCR of tail biopsies.

4-OHT preparation and injection

4-hydroxytamoxifen (4-OHT) (Sigma, H7904-25MG) was dissolved in equal parts of ethanol and Kolliphor (Sigma C5135-500G) using sonication. 10 mg/mL stocks of progesterone (P3972-5G) were prepared by resuspending in ethanol and sunflower oil (Sigma S5007-250ML) and co-injected with OHT to reduce the risk of abortion. For pulse-labeling using the *Csf1r*^{MeriCreMer} strain, females were weighed on day 8 of pregnancy and injected with 75 µg/g (body weight) OHT and 37.5 µg/g (body weight) progesterone at 1 pm.

Flow cytometry

Mice were sacrificed by cervical dislocation. The fluid of the peritoneal cavity was harvested by removing abdominal skin, injecting 5 mL of ice-cold FACS buffer (0.5% BSA and 2mM EDTA in PBS) into the peritoneal cavity, massaging the mouse for 1 min, opening the peritoneum with scissors, and collecting the fluid in a 50 mL Falcon tube. For ear skin dissection, epidermal sheets were first separated from the dermis after incubation for 1h at 37°C in 2.4 mg/ml of Dispase II in PBS and the dermis was further digested for 30 min in PBS containing 1 mg/ml collagenase D, 100 U/ml DNase I, 2.4 mg/ml of Dispase II and 3% FBS at 37°C and passed through a 100 µm strainer by mashing with the piston of a 2mL syringe and then collected in cold filtered FACS buffer. Bone marrow was flushed from the femur and tibia using a 25G needle. For red blood cell lysis of bone marrow samples, cells were resuspended in 1 ml of red blood cell lysis buffer (155 mM NH_4Cl, 10 mM $NaHCO_3$, and 0.1 mM EDTA). The reaction was terminated after 5 min by adding 3 ml of FACS buffer. Single cell suspensions from all tissues were pelleted by centrifugation at 320*g* for 7 minutes. Blocking was performed with 1:50 Fc-block (anti-CD16/32) in FACS Buffer followed by 30 minutes of antibody staining. Stained cells were passed on the Cytoflex LX (Beckman Coulter). Results were analyzed and plots generated using FlowJo.

Single cell liquid culture

Pregnant mice were killed by cervical dislocation and embryos were dissected in cold PBS. Yolk sacs were dissected and enzymatically dissociated in digestion buffer composed of PBS with 1 mg/mL collagenase D (Sigma 11088882001), 100 U/mL DNaseI (DN25-100mg), and 3% Fetal Bovine Serum for 30 minutes at 37 °C. Yolk sacs were passed through 100 µm strainers by mashing with the piston of a 2 mL syringe and then collected in ice-cold filtered FACS Buffer (0.5% BSA and 2mM EDTA in PBS). Blocking was performed with 5% FBS and 1:20 mouse IgG (Interchim 015-000-003) in FACS Buffer followed by 30 minutes of antibody. Single YFP^+ Kit^+ $CD41^+$ $CD34^+$ $AA4.1^{neg}$ cells were sorted using a FACSAria III (Diva software) into flat-bottom 96-well plates containing pre-warmed and equilibrated differentiation medium (0.1% β-mercaptoethanol, 1X Penicillin/Streptomycin, 10% FBS, 1:125 SCF, 5ng/µL GM-CSF, 5ng/µL M-CSF, 2ng/µL EPO and 5ng/µL TPO in Opti-MEM with Glutamax). SCF was supplied from myeloma cell line supernatant. Cells were grown at 37°C with 5% CO_2 for 7 days. Colonies were manually scored to detect small megakaryocyte colonies before collecting them by scratching with a pipette tip for flow cytometry analysis. The overall cloning efficiency was defined as the number of sorted single cells that give rise to colonies. The colony output was calculated by dividing the number of colonies of one type, i.e. erythrocytes, by the number of all colonies grown.

e. Acknowledgment

I want to thank William Worral from the lab of Laurent Reber (Toulouse Institute for Infectious and Inflammatory Diseases (Infinity)) for insightful discussions about protocols for mast cell isolation from the back skin and the IgE-mediated anaphylaxis assay.

3.3 Macrophages – deplete

This project was a collaboration between the lab of Angela Giangrande, a reknown expert in developmental hematopoiesis in Drosophila melanogaster, and our lab. While Sara Monticelli, a Postdoc in the lab of Angela conducted experiments in *Drosophila*, I designed, managed, and performed experiments in the mouse model. I would like to express my gratitude for the technical help from Clarisabel García, Kémy Adé, and my intern Corentin Guichen.

3.3.1 Introduction

Reminiscent of vertebrates, the hematopoietic system of the fly is established by two successive waves during development (**Article Figure 1A-B**). In the fly, early-wave macrophages colonize the fly embryo and are the active immune cells during the larval stage. They are followed by late-wave macrophages that arise in the lymph glands of the larva and are released into circulation at the beginning of the pupal stage. The aim of this project was to identify how the depletion of early-wave (EMP-derived) macrophages can affect subsequent late-wave (HSC) hematopoiesis in the fly larva and mouse fetus.

3.3.2 Summary and discussion of the results

Sara and her colleagues discovered that the depletion of early-wave macrophages led to the accelerated development of the lymph glands (**Article Figure 2&3**) as well as the precocious release of late-wave macrophages due to defects in the extracellular matrix. The defects in the ECM in the fly were directly related to the absence of early-wave macrophages, which express *perlecan*, an extracellular matrix protein (**Article Figure 7**).

PLX specifically depletes EMP-derived macrophages

We wondered whether this role of interplay between early and late hematopoiesis observed in *Drosophila* was evolutionarily conserved in species with a more complex hematopoietic system. Therefore, we tested the effect of depletion of EMP-derived (early-wave) macrophages on HSC-derived (late-wave) macrophages and HSC hematopoiesis in general. To deplete EMP-derived macrophages, we fed pregnant dams the Csf1r-inhibitor PLX5622 (PLX) (Spangenberg et al., 2019) between E11.5 and E14.5 to avoid impacting HSC emergence in the AGM (Mariani et al., 2019) (**Article Figure 4A-B, C-E top**).

The effect on EMP and HSC-derived cells was probed by using the *Cdh5*^{CreERT2} fate-mapping model with the *R26*^{tdTomto} reporter line. Pregnant females were pulsed with 4-hydroxytamoxifen (4-OHT) at either E7.5 (labels mostly EMPs and very few eMPPs) or E10.5 (labels mostly HSCs and few eMPPs). Usually, we use *R26*^{YFP} reporters in lineage

tracing experiments. Injecting 4-OHT into pregnant dams led to pregnancy termination around E15.5 in more than 50 % regardless of the stage of 4-OHT injection. *R26*^{tdTomato} recombines more efficiently than *R26*^{YFP}. Since we were particularly interested in stages after E15.5, I decided to use the *R26*^{tdTomato} line and at the same time reduce the injected 4-OHT dose by half to improve pregnancy outcomes. This however unfortunately did not affect the rate of fetal survival nor the number of successful births.

Monocytes and neutrophils were barely affected by Csf1r inhibition (**Article Figure 4F-H, S5C-D**). Surprisingly, also the numbers of the few HSC-derived macrophages present at E14.5 remained unchanged. By contrast, EMP-derived macrophages were efficiently depleted (**Article Figure 4C, bottom**), reminiscent of the *Csf1r*$^{\Delta FIRE/\Delta FIRE}$ phenotype (Rojo et al., 2019). While it is known that macrophage populations in different tissues have distinct requirements of CSF1 (Cecchini et al., 1994; Percin et al., 2018), this observation indicates that Csf1r-signaling dependency also is ontogeny-specific.

Depletion of EMP-derived macrophages accelerates HSC myelopoiesis in the fetus

We found that after the depletion of EMP-derived macrophages, HSCs differentiated into macrophages around 48 h earlier than in control conditions. These HSC-derived macrophages seeded the brain, skin, and fetal liver (**Article Figure 4 C-E, middle and bottom**). More proliferative cells were found among HSC- than EMP-derived macrophages (**Article Figure S5G**). Additionally, precocious HSC differentiation was also accompanied by a transient increase in the numbers of myeloid progenitors (**Article Figure B, C, middle and bottom, S6E**).

Long-term fate of Tom$^+$ macrophages in PLX-treated mice

Curiously, even though HSCs gave rise to increased numbers of macrophages in the fetus, the contribution of HSCs to resident macrophage pools in the adult was similar between PLX-treated and control offspring (**Article Figure 4 C-E, middle and bottom**). This indicates that the increased ratio of Tom$^+$ over Tom^{neg} macrophages in PLX-treated fetuses is not maintained long-term. Two conceivable scenarios could explain this observation:

(1) Tom$^+$ (HSC-derived) macrophages cannot self-maintain and disappear with time. Instead, Tom^{neg} (EMP-derived) macrophages with distinct intrinsic features fully replenish the niche and self-maintain as tissue-resident macrophages. A small fraction of Tomato labeling is still observed, similar to control mice, since some macrophages are constantly replaced by Tom$^+$ HSC-derived monocytes from the bone marrow.

(2) Tom$^+$ (HSC-derived) macrophages can self-maintain and remain in the tissue long-term. As the tissue however grows, Tom^{neg} macrophages replenish the niche more efficiently than the tissue-resident Tom$^+$ macrophages. Tom^{neg} macrophages could be EMP-derived or unlabeled HSC-derived macrophages from the bone

marrow. In the latter case, however, it would be expected that both Tom^{+} and Tom^{neg} bone marrow-derived monocytes equally infiltrate the tissue and differentiate into tissue macrophages. This would entail an overall increase in Tomato labeling compared to control mice.

Both scenarios are in line with the notion that EMP- and HSC-derived macrophages are intrinsically different.

A simple experiment that would shed light on the origin of the replenishing macrophages would be to repeat the experiments by tracing the EMP instead of the HSC progeny. This could be achieved by either using the *Cdh5*^{CreERT2} model pulsed at E7.5 or the *Csf1r*^{MeriCreMer} pulsed with 4-OHT at E8.5.

Long-lasting effects of PLX depletion on HSC hematopoiesis

Both E16.5 fetal and 8-week adult CMPs gave rise to larger neutrophil and myeloid colonies *in vitro* after PLX treatment *in utero* without affecting the overall proportions of colony output (**Article Figure 4 D, E**). Additionally, lymphoid-biased MPPs (MPP4) were reduced in numbers in the adult bone marrow. Frequencies of B and T cells in the blood however were unaffected (**Article Figure S6D, data not shown**). This showed that the macrophage depletion *in utero* caused a long-term impact on the HSC hematopoiesis.

In the mouse, it is uncertain how the effect of macrophage depletion *in utero* affects HSCs, such that hematopoiesis is impaired in the long term. In line with the results on the fly, we observed an overall downregulation of ECM molecules in the fetal liver after PLX treatment (**Article Figure 5G**) and preliminary data suggested a difference in the collagen network in the fetal liver (**Article Figure 5F**).

Other scenarios, however, cannot be excluded. First, the pressure to upregulate macrophage production might have indirectly caused a "stress-memory" in HSCs that led to the long-term reduction of lymphoid progenitors and the increased efficiency in myeloid cell production, reminiscent of the effects on hematopoiesis seen in inflammation or aging (Li et al., 2023b).

Alternatively, the lack of macrophages might have affected HSC by disrupting a direct cross-talk between macrophages and HSCs. Macrophages are spatially closely associated with HSCs both in the AGM macrophages where they support HSC emergence and in the bone marrow, where they are essential for maintaining hematopoiesis (Winkler et al., 2010; Manneken & Currie, 2023). As we

Even though the PLX treatment did not cause dramatic inflammation, apoptosis of EMP-derived macrophages may have released signals that could have been sensed by HSC.

Finally, the PLX5622 might have also directly affected HSCs, MPPs, or other lymphoid populations *in utero*. However, Csf1r expression in HSCs, CLPs or lymphocytes has not been detected (Grabert et al., 2020). A direct effect of PLX on HSCs is therefore unlikely.

Conclusion

Collectively, our findings show intrinsic differences between EMP- and HSC-derived macrophages in regard to Csf1r-dependency and replenishment speed. Particularly, in combination with the data in *Drosophila* our results indicate that late hematopoietic waves (HSCs) rely and depend on the integrity of earlier hematopoietic waves (EMPs). Finally, our findings suggest that perturbations during development can have long-term impact on HSC hematopoiesis.

Article

Developmental Cell

Early-wave macrophages control late hematopoiesis

Graphical abstract

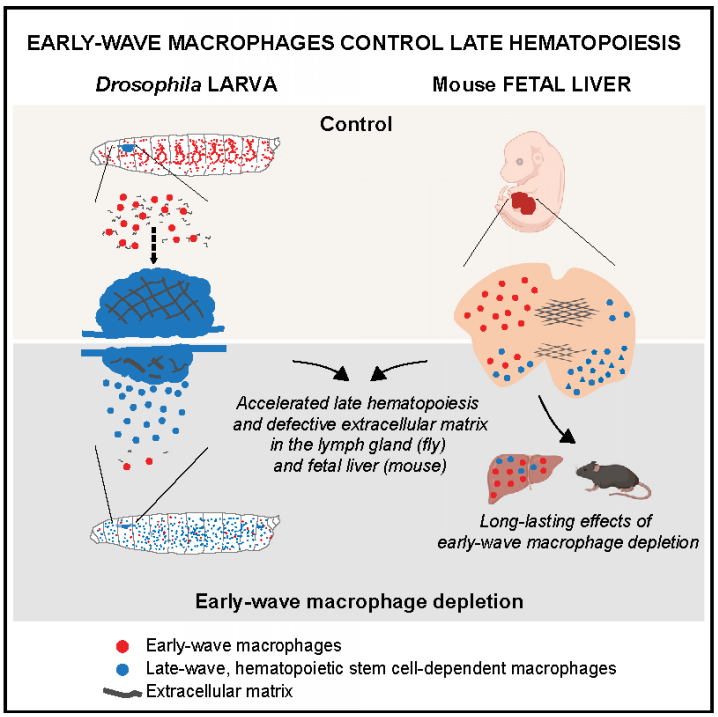

Highlights

- Macrophages remodel the developing hematopoietic environment throughout evolution
- Early-wave macrophage depletion accelerates late, stem-cell-dependent hematopoiesis
- Early-wave-derived extracellular matrix molecules control the fly late hematopoiesis
- Early-wave macrophage depletion has long-lasting effects on hematopoiesis

Authors

Sara Monticelli, Alina Sommer, Zeinab AlHajj Hassan, ..., Claude Delaporte, Elisa Gomez Perdiguero, Angela Giangrande

Correspondence

elisa.gomez-perdiguero@pasteur.fr (E.G.P.), angela@igbmc.fr (A.G.)

In brief

Monticelli et al. investigate the interaction between hematopoietic waves during development. Depletion of early-wave macrophages accelerates late, stem-cell-dependent hematopoiesis in flies and mice, which relies on extracellular matrix molecules derived from early-wave macrophages.

Monticelli et al., 2024, Developmental Cell 59, 1284–1301
May 20, 2024
https://doi.org/10.1016/j.devcel.2024.03.013

CellPress

CellPress

Developmental Cell

Article

Early-wave macrophages control late hematopoiesis

Sara Monticelli,[1,2,3,4] Alina Sommer,[5,6] Zeinab AlHajj Hassan,[1,2,3,4] Clarisabel Garcia Rodriguez,[5,6] Kémy Adé,[5] Pierre Cattenoz,[1,2,3,4] Claude Delaporte,[1,2,3,4] Elisa Gomez Perdiguero,[5,7,*] and Angela Giangrande[1,2,3,4,7,8,*]

[1]IGBMC, Institut de Génétique et de Biologie Moléculaire et Cellulaire, 67400 Illkirch, France
[2]Centre National de la Recherche Scientifique, UMR 7104, 67400 Illkirch, France
[3]Institut National de la Santé et de la Recherche Médicale, UMR, S 1258, 67400 Illkirch, France
[4]Université de Strasbourg, IGBMC UMR 7104- UMR-S 1258, 67400 Illkirch, France
[5]Macrophages and endothelial cells unit, Department of Developmental and Stem Cell Biology, Institut Pasteur, Université Paris Cité, UMR3738 CNRS, 75015 Paris, France
[6]Sorbonne Université, Collège doctoral, 75005 Paris, France
[7]These authors contributed equally
[8]Lead contact
*Correspondence: elisa.gomez-perdiguero@pasteur.fr (E.G.P.), angela@igbmc.fr (A.G.)
https://doi.org/10.1016/j.devcel.2024.03.013

SUMMARY

Macrophages constitute the first defense line against the non-self, but their ability to remodel their environment in organ development/homeostasis is starting to be appreciated. Early-wave macrophages (EMs), produced from hematopoietic stem cell (HSC)-independent progenitors, seed the mammalian fetal liver niche wherein HSCs expand and differentiate. The involvement of niche defects in myeloid malignancies led us to identify the cues controlling HSCs. In *Drosophila*, HSC-independent EMs also colonize the larva when late hematopoiesis occurs. The evolutionarily conserved immune system allowed us to investigate whether/how EMs modulate late hematopoiesis in two models. We show that loss of EMs in *Drosophila* and mice accelerates late hematopoiesis, which does not correlate with inflammation and does not rely on macrophage phagocytic ability. Rather, EM-derived extracellular matrix components underlie late hematopoiesis acceleration. This demonstrates a developmental role for EMs.

INTRODUCTION

The immune system of adult vertebrates is sustained throughout life by a classical differentiation cascade from hematopoietic stem cells (HSCs), which are maintained and regulated through interactions with their micro-environment or niche. As the pool of HSCs is established during development, with no *de novo* generation during adulthood, embryonic perturbations can affect the development of HSCs, thereby leading to long-lasting changes in the capacity of organisms to respond later on to (immune) challenges. It is thus crucial to understand the cellular and molecular events regulating HSC homeostasis during development, and here, we focused on the function of macrophages in this process. Indeed, before the emergence of HSCs, macrophages produced by earlier (HSC-independent) progenitor waves colonize the embryo and participate to key physiological processes such as metabolism; development; and tissue remodeling by phagocytosing debris/apoptotic cells and by secreting a wide range of molecules, including extracellular matrix (ECM) components/-modifying enzymes, growth factors, and cytokines.[1] They are very abundant in the fetal hematopoietic niche where HSCs expand and differentiate and are thus ideal candidates to modulate HSC micro-environment. The establishment of the immune system by successive waves is evolutionarily conserved. We combined the advantages of two model organisms, the invertebrate *Drosophila melanogaster* and the mammalian mouse model, for complementary and synergetic investigation of the contribution of early, HSC-independent macrophages to the establishment of the adult immune system.

Mouse hematopoiesis occurs in at least three distinct waves during embryogenesis, with macrophages being generated during each wave. Macrophages from the first two waves (primitive and erythro-myeloid progenitors (EMPs) emerging from the extra-embryonic yolk sac) migrate to the embryo proper and colonize, among other tissues, the nascent fetal liver (FL) starting at embryonic day (E) 9.[2–5] The third hematopoietic wave starts intra-embryonically at around E9.5, when embryonic multipotent progenitors (eMPPs) followed by HSCs emerge from the aorta-gonado-mesonephros region and major arteries[6,7] and migrate to the FL to expand and differentiate[8] (Figure 1A). Contrary to what was initially thought, fetal HSCs do not contribute to mature blood cell production until birth.[9–12] Before birth, HSCs migrate to the bone marrow niche, where they are maintained throughout adulthood and generate all blood cell types[13,14](Figure 1A). Throughout fetal life, macrophages are generated from yolk-sac-derived HSC-independent progenitors and are thus referred to as embryonic or early-wave macrophages (EMs). Murine HSCs thus expand in a FL already colonized by EMs, recently reported to be potentially involved in HSC emergence in mouse embryos.[15] However, whether mouse EMs modulate

Developmental Cell
Article

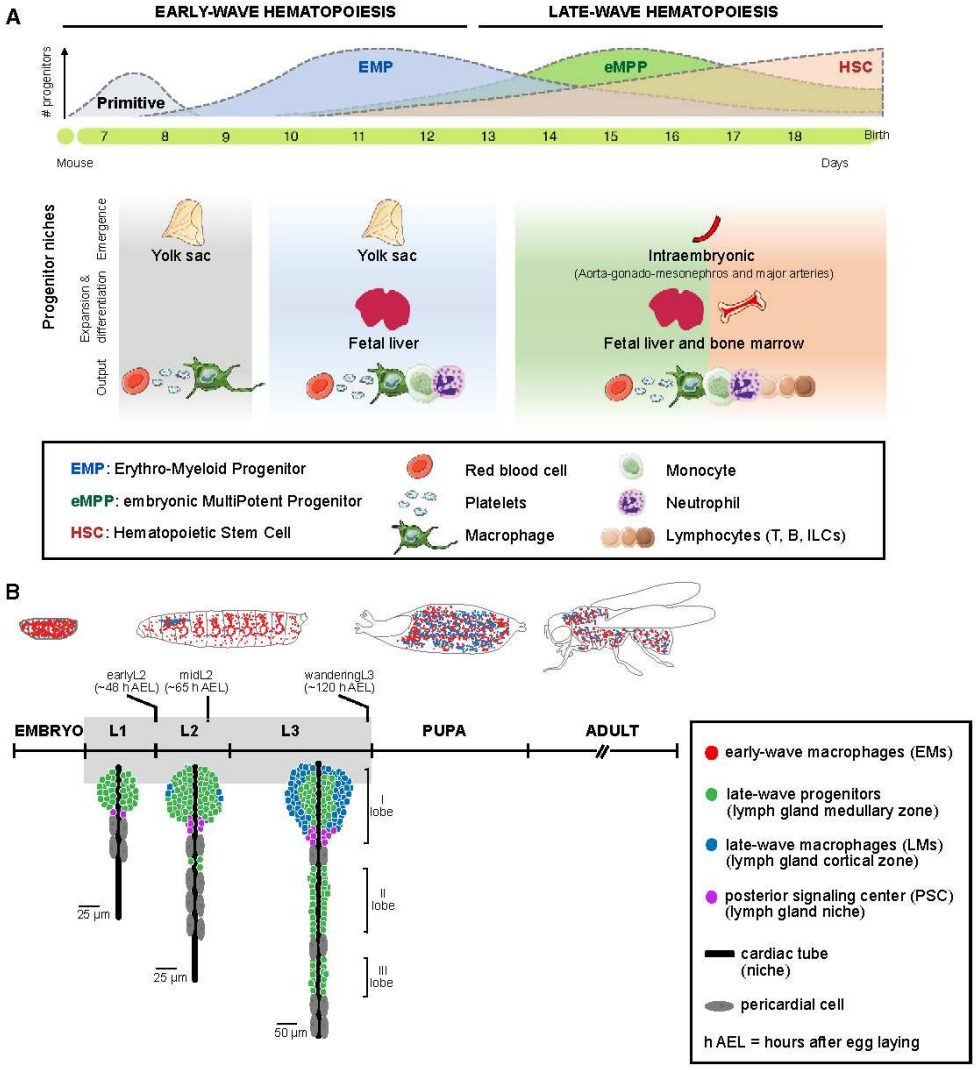

Figure 1. Mammalian and *Drosophila* hematopoiesis

Schematics representing early and late hematopoietic waves in (A) mammals and (B) *Drosophila*.

HSC-derived hematopoiesis after HSC emergence is currently unknown.

The immune system of *Drosophila* is simpler, with few cell types accounting for innate immunity only (generally called hemocytes). Under normal conditions, macrophages (also called plasmatocytes) comprise 90%–95% of *Drosophila* hemocytes, while crystal cells, platelet-like cells helping the wound healing process, account for 2%–5% of the hemocytes. For the sake of simplicity, we will refer to hemocytes as macrophages. *Drosophila* macrophages are produced during two distinct waves. Primitive or Ems differentiate from the procephalic mesoderm of the early embryo and colonize the whole organism. Late-wave macrophages (LMs) originate from a specialized hematopoietic organ, the lymph gland, which reaches maturation and releases LMs after the larval stages. LMs and Ems co-exist in the adult at a 1:2 ratio (for a recent review, see Banerjee et al.[16]) (Figure 1B). The progenitor cells of the lymph gland are considered as bona fide HSC-like cells, and their maintenance/differentiation relies on niche-derived cues that also regulate mammalian HSCs in the FL and bone marrow niches (e.g., Hh,[17,18] Dpp/BMP,[19,20] Wg/Wnt,[21,22] Slit/Robo,[23] and Col/Ebf[24,25] pathways). Whether EMs interact with the lymph gland and regulate late hematopoiesis is not known. Nevertheless, EMs are free to circulate in the hemolymph (analogous of the vertebrate blood), bathing all the organs of the *Drosophila* larva, including the developing lymph gland. Moreover, EMs impact the immune response mounted by the late hematopoietic wave,[26] calling for homeostatic interactions between the two waves.

Here, we show that EMs play a key role in modulating late hematopoiesis and that this role is evolutionarily conserved. The

CellPress

Developmental Cell
Article

depletion of *Drosophila* EMs accelerates the maturation of the lymph gland and LM differentiation. This phenotype does not rely on inflammation or on EMs' phagocytic function but rather on EM-derived ECM molecules ensuring proper architecture of the lymph gland. Similarly, EM depletion during mouse FL hematopoiesis triggers premature differentiation of HSCs not only into macrophages but also into monocytes and neutrophils in the FL, whose ECM is defective. Importantly, transient EM depletion *in utero* leads to long-lasting changes in adult HSCs, with increased myeloid potential at the expense of lymphoid-biased progenitors. Revealing the so far largely unexplored link between the hematopoietic waves opens important perspectives in basic and medical science, with the potential role of HSC-independent hematopoiesis in shaping the adult immune system, thus influencing the risk of developing diseases after birth.

RESULTS

Fly late hematopoiesis is affected by EM depletion

To assess how late hematopoiesis responds to the loss of EMs in *Drosophila*, we depleted the larva of macrophages and examined the state of the lymph gland.

The lymph gland is a paired organ sitting on the cardiac tube and consisting of lobes named from primary to tertiary (or more) by proceeding antero-posteriorly (Figure 1B). Primary lobes start differentiating at mid second larval instar (midL2), whereas the posterior lobes mature only at pupal stage, when the primary lobes undergo histolysis and release LMs.[27,28] Under normal conditions, the primary lobes are fully mature, yet still intact, at wandering third larval instar (wL3) and mainly consist of a cortical zone containing differentiated LMs; a medullary zone containing progenitors; and the posterior signaling center (PSC), the lymph gland signaling niche[16] (Figure 1B).

Previous works have shown that genetic macrophage depletion throughout larval development (from the first larval instar [L1] to wL3) triggers a severe loss of macrophages in wL3 larvae[29–33] and precocious rupture of the lymph gland primary lobes.[33] To deplete macrophages, we hence used a similar approach, upon expressing the cell death gene *head involution defective* (*UAS-hid*)[34] (together with that of the GFP, *UAS-GFP*) under the control of the macrophage-specific *Hemolectin* (*Hml*) Gal4 driver (*Hml⊿Gal4*) (Figures S1A–S1H). *Hml⊿Gal4* is active from L1 onward,[35,36] allowing postembryonic depletion of macrophages and preventing the embryonic lethality induced by earlier macrophage depletion.[30,37] We confirmed the histolysis of the primary lobes and showed that the lymph gland posterior lobes are oversized and show increased cell differentiation (Figures S1E–S1H). This approach, however, does not allow to disclose the contribution of EMs on lymph gland development because by midL2 *Hml* starts being expressed in differentiating LMs.[38,39] These cells are likely targeted by the depletion strategy and undergo apoptosis, leading to inflammation, as documented by the presence of activated immune cells, called lamellocytes and marked with Atilla[40] and L4,[41] in wL3 lymph gland and hemolymph (Figures S1H and S1I).[31,33]

To assess whether the specific loss of EMs affects late hematopoiesis, we depleted Hml^{+} macrophages and analyzed midL2 larvae (~65 h after egg laying [AEL]) (Figure 2A) before massive differentiation of Hml^{+} LMs in the lymph gland (Figure 2G). Depleted larvae show no Hml^{+} EMs (Figure 2B), and the number of EMs per larva is drastically reduced (~25%, Figure 2C), with only few cells detected by immunolabeling (Figure 2D). This suggests that EM numbers could be overestimated by brightfield counting due to the presence of dying cells and cell debris that are washed out during the labeling protocol. Consistently, the hemolymph of depleted larvae shows labeling with the apoptotic marker cleaved caspase Dcp-1 (Dcp1)[42] (Figure 2E). The few remaining cells are labeled by macrophage markers, such as Peroxidasin (Pxn) and Hemese (He)[33,43,44] and do not express *Hml* (Figures 2D and 2E). However, these cells do not resemble canonical macrophages, and quantitative reverse-transcription PCR (RT-qPCR) assays performed at the beginning of the second larval instar (earlyL2, ~48 h AEL) reveal a poor expression of *Pxn* and of the phagocytic receptor encoding genes *eater* and *NimC1*[45,46] (Figure 2F). This suggests that the Pxn signal revealed by immunolabeling at midL2 likely results from a high stability of the protein, and the cells left after EM depletion lose macrophage marker expression and possibly phagocytic function, which is hardly assessable due to the scarce number of macrophages surviving the depletion.

We next analyzed the midL2 lymph gland, consisting mostly of the sole primary lobes[16] (Figures 1B and 2G). The volume of the lymph gland from depleted larvae is almost doubled, and the primary lobe cellularity is significantly higher than in controls (Figures 2G and 2H). Increased cell proliferation is detected by earlyL2 using the mitotic marker phosphorylated Ser10 of histone 3 (PH3)[47] but not by midL2 (Figures S2A–S2D),[39] suggesting earlyL2 as the phenocritic phase for the over-proliferation of the larval hematopoietic organ. This phenotype is unlikely to be caused by the expression of Hid in the few Hml^{+} LMs normally present in the earlyL2 lymph gland (14.75 ± 3.46 Hml^{+} cells out of 450 ± 28 DAPI^{+} nuclei; mean ± standard error) (Figure 3C). Moreover, several Hml^{+} and/or Pxn^{+} LMs are present in the midL2 lymph gland upon EM depletion, and they spread throughout the primary lobes (Figure 2G), indicating a premature differentiation that overrides the proper patterning of the lymph gland (Figure 1B).

Extensive cell death occurs in the midL2 lymph gland of depleted animals (Figure 2I). This phenotype may have different origins. The premature appearance of Hml^{+} macrophages in the lymph gland could induce *hid* expression in LMs. Dying LMs could also trigger apoptosis in neighboring cells in a non-cell-autonomous manner.[48] Precocious and strong differentiation of the organ could also indirectly lead to apoptotic events. In line with these non-mutually exclusive hypotheses, we detect Dcp1 expression in Hml^{+} and Hml macrophages, some of which are close to dying Hml^{+} macrophages (Figure 2I). Finally, several lamellocytes are detected in the lymph gland of depleted larvae (Figure 2J), indicating an inflammatory state likely resulting from the widespread apoptosis.[31]

Overall, these experiments reveal that depleting EMs leads to overgrowth and premature differentiation of the late hematopoiesis organ, which also shows inflammatory phenotypes.

Fly EM depletion accelerates the physiological development of the lymph gland

To formally discriminate whether the observed precocious maturation of the lymph gland is due to inflammation-related

Developmental Cell
Article

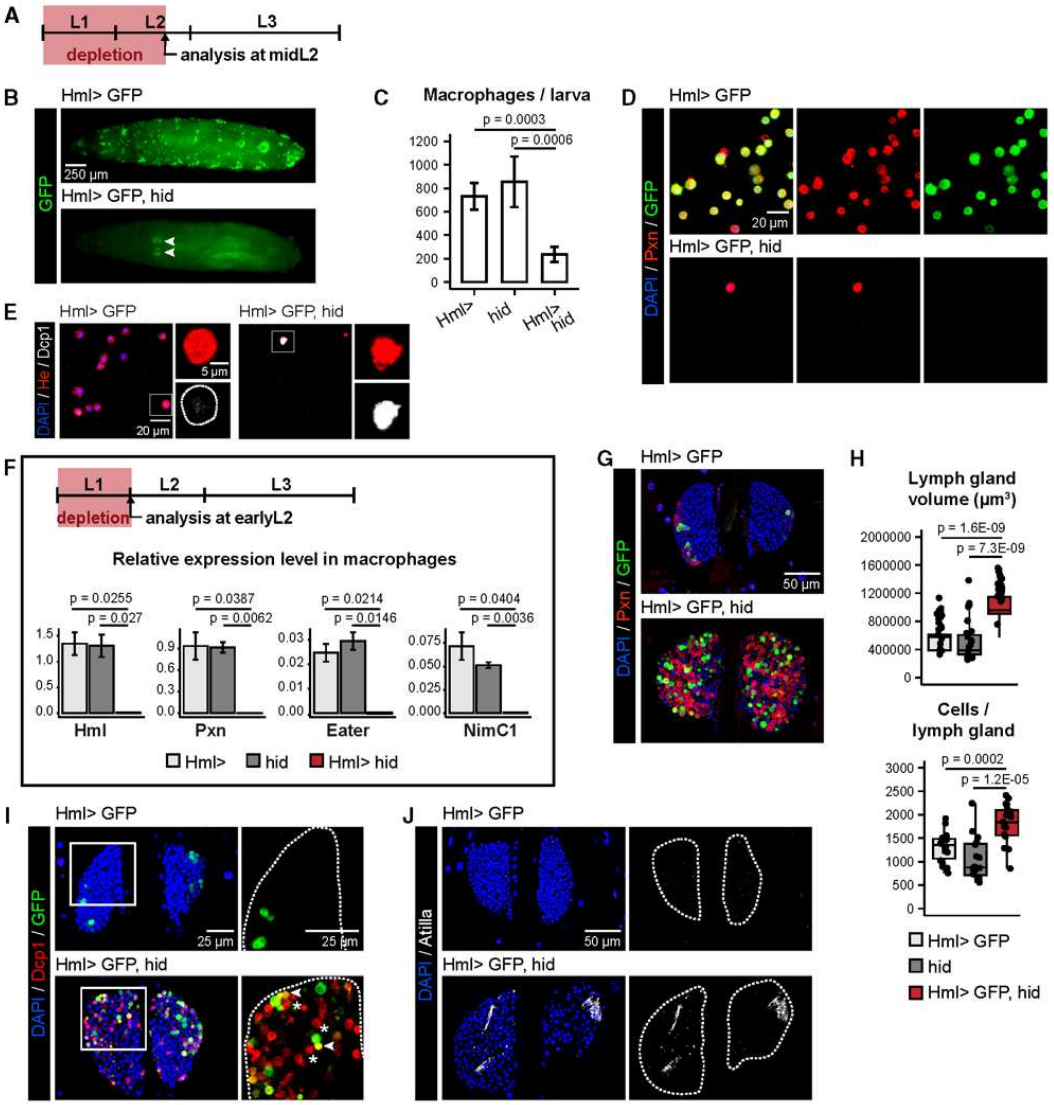

Figure 2. Fly late hematopoiesis is affected by early-wave macrophage (EM) depletion

(A) Experimental setup adopted in (B)–(E) and (G)–(J). The *Hml⊿Gal4* driver was used to express the cell death gene *hid* in macrophages from the beginning of the larval life until mid-second larval instar (midL2) ~65 h after egg laying (AEL) with animals raised at 25°C. Only in (F), the depletion was carried out until early second larval instar (earlyL2) ~48 h AEL. Both settings ensure specific depletion of early-wave macrophages (EMs) in the larva. A reporter GFP was used to reveal *Hml* expression.

(B) Dorsal view of a control larva and an EM-depleted larva (anterior on the left, posterior on the right). Arrowheads point the lymph gland primary lobes.

(C) Number of macrophages per larva (mean ± standard deviation [SD]) assessed by brightfield counting (N ≥ 3).

(D and E) Immunolabeling of bled macrophages. (D) The anti-Pxn macrophage marker is in red, anti-GFP in green; **(E)** the anti-He macrophage marker is in red, the anti-Dcp1 apoptotic marker is in gray. Nuclei are labeled with DAPI in blue.

(F) Top: experimental setup. Bottom: relative expression level (mean ± standard error [SE]) of Hml, Pxn, Eater, and NimC1 assessed by RT-qPCR on macrophages bled from control or EM-depleted larvae (3 independent replicates).

(G) Lymph gland immunolabeling. Anti-Pxn is in red, and anti-GFP in green; nuclei are labeled with DAPI in blue. N ≥ 15.

(H) Lymph gland primary lobes' volume (top) and number of cells (bottom) (N ≥ 16).

(I and J) Lymph gland immunolabeling with (I) anti-Dcp1 in red, anti-GFP in green (J) the anti-Atilla lamellocyte marker in gray; nuclei are labeled with DAPI in blue. (I) White squares define the area shown in the insets as Dcp1 and GFP merge. Dashed lines indicate the perimeter of the lymph gland lobes, arrowheads point $Hml^{+}Dcp1^{+}$ macrophages, asterisks point $Hml^{-}Dcp1^{+}$ macrophages (N ≥ 8). Detailed genotypes: *w;Hml⊿Gal4,UAS-2XEGFP/+;+* (Hml > GFP), *w;UAS-hid/+;+* (hid), *w;Hml⊿Gal4,UAS-2XEGFP/UAS-hid;+* (Hml > GFP, hid), *w;Hml⊿Gal4/+;+* (Hml>), *w; Hml⊿Gal4/UAS-hid;+* (Hml > hid). Confocal images are shown as full-stack projections for bled macrophages and representative single sections for lymph glands unless otherwise specified. Statistics: two-tailed unpaired t test.

CellPress
Developmental Cell
Article

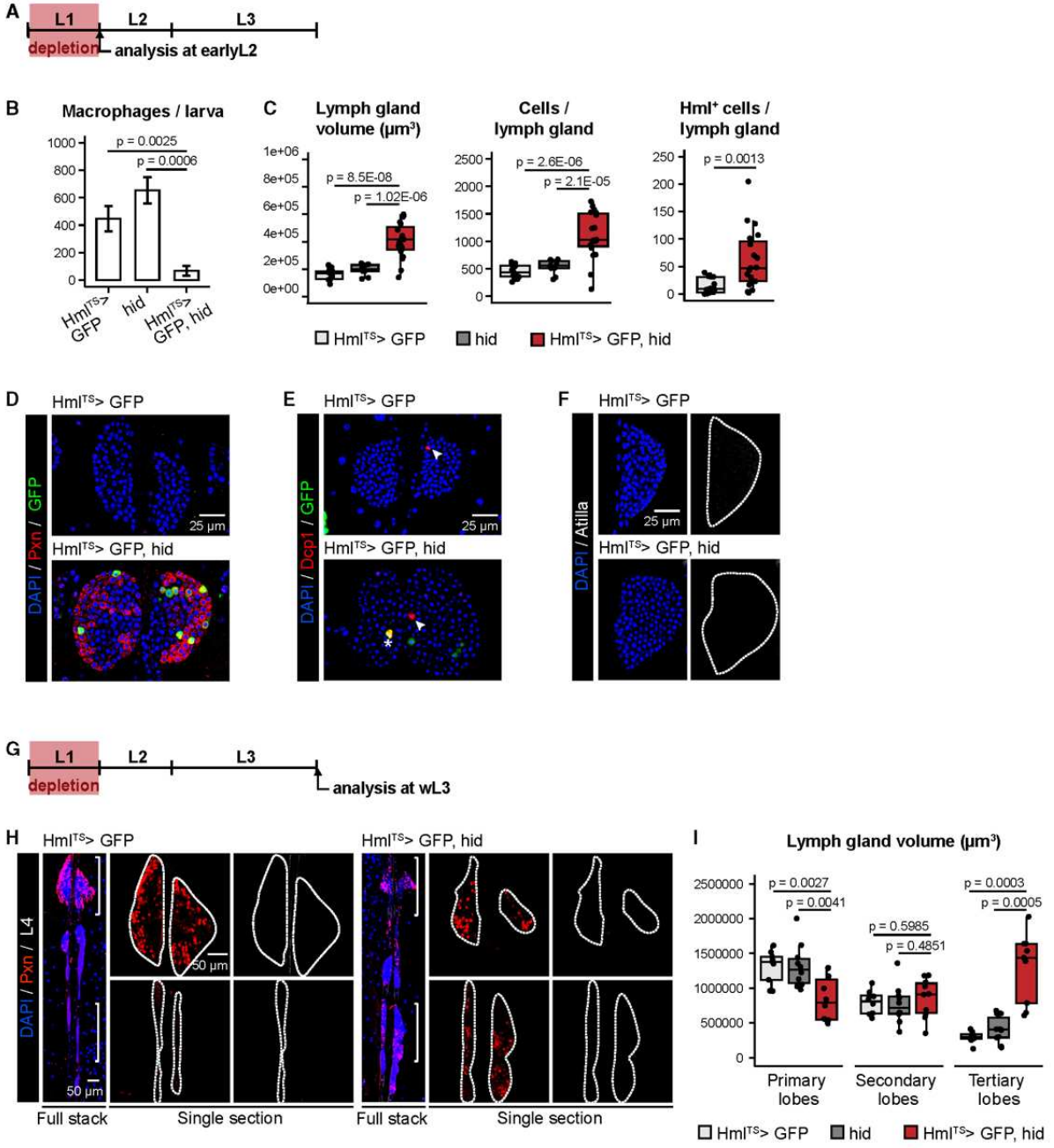

Figure 3. Fly EM depletion accelerates the physiological development of the lymph gland

(A) Experimental setup adopted in (B)–(F). The genetic depletion was restricted to the first larval instar (L1) using a thermosensitive inhibitor of Gal4 (*tubulinGal80^{TS}*), active at 18°C and inactive at higher temperature (≥25°C). Embryos and L1 larvae were raised at 25°C to trigger the expression of *hid* and reporter GFP under the control of *Hml*Δ*Gal4* and (B–F) analyzed right after depletion at earlyL2 (~48 h AEL) or (H–I) shifted at 18°C at earlyL2 (~48 h AEL) to avoid further macrophage depletion and analyzed at wandering third larval instar (wL3) ~120 h AEL.

(B) Number of macrophages per larva (mean ± SD) assessed by brightfield counting (N ≥ 3).

(C) Lymph gland primary lobes' volume, number of cells and Hml^{+} cells (N ≥ 11).

(D–F) Lymph gland immunolabeling with (D) anti-Pxn in red and anti-GFP in green (N ≥ 11), (E) anti-Dcp1 in red and anti-GFP in green (N ≥ 6), and (F) anti-Atilla in gray (N ≥ 6); nuclei are labeled with DAPI in blue. In **(E),** arrowheads point Dcp1^{+} Hml^{-} cells, and the asterisk indicates a Dcp1^{+} Hml^{+} cell.

(G) Experimental setup adopted in (H) and (I).

(legend continued on next page)

Developmental Cell
Article

CellPress

processes or to accelerated physiological development, we depleted EMs only before *Hml* is expressed in the lymph gland and in a time-restricted fashion, using a thermosensitive Gal4 inhibitor (*tubulinGal80^{TS}*). Animals were raised at 25°C (*tubulinGal80^{TS}* not active) throughout L1 to induce cell death in EMs, then shifted at 18°C (*tubulinGal80^{TS}* active) at earlyL2 to avoid expression of *hid* in the Hml^{+} cells that start differentiating in the lymph gland. Larvae were analyzed at earlyL2 (i.e., before the temperature shift) (Figures 3A–3F) and at wL3 (Figures 3G–3I). At earlyL2, the EM pool is reduced to less than 20% (Figure 3B), and the lymph gland already shows overgrowth compared with controls (Figures 3C–3F). Enhanced LM differentiation is also observed, with increased Hml^{+} and/or Pxn^{+} cells mostly located in the cortical zone (Figures 3C and 3D), indicating preserved lymph gland patterning. Importantly, we do not detect apoptosis or inflammation in the lymph gland of depleted larvae (Figures 3E and 3F). With regard to the hemolymph, no lamellocytes were detected upon bleeding and brightfield counting (3 independent replicates), and RT-qPCR assays on the bled macrophages did not reveal any increase in the expression level of the pro-inflammatory cytokines Upd2 and Upd3[49,50] upon depletion (Figures S2E and S2F). Thus, early postembryonic EM depletion is sufficient to trigger premature, yet physiological, lymph gland maturation without inducing evident inflammation.

Then, we asked whether the accelerated development persists also at a later stage, leading to precocious rupture of the wL3 lymph gland, or whether it is rescued by compensatory processes. Notably, albeit still present, the primary lobes of the wL3 lymph gland are partially histolyzed (therefore smaller) in the depleted larvae, and the posterior lobes are oversized and more differentiated (Figures 3H and 3I). In line with the ongoing histolysis, the deficit of hemolymph macrophages observed at earlyL2 (Figure 3B) is compensated by wL3 (Figures S2G and S2H). These phenotypes resemble those observed upon constitutive EM depletion (Figures S1C and S1E–S1H). Yet, while the latter protocol triggers inflammation, as evidenced by the presence of lamellocytes (Figures S1H and S1I), lamellocytes are absent in the lymph gland (Figure 3H) and in the hemolymph (brightfield counting, 3 independent replicates) upon L1-restricted depletion.

In sum, the lack of EMs during the early maturation period of the lymph gland accelerates late hematopoiesis.

Murine EM depletion leads to an increased contribution of HSCs to the macrophage pools

The presence of sequential waves of hematopoietic progenitors during development from invertebrates to mammals[51] prompted us to ask whether the interaction observed in *Drosophila* between hematopoietic waves is an evolutionarily conserved process. Hence, we assessed whether murine EMs control HSC-dependent hematopoiesis (Figure 1A). To achieve EM depletion, pregnant dams were fed with CSF1R inhibitor Plexxikon 5622[52] (PLX)-containing chow between E11.5 (after HSC emerge from the aorta) and E14.5, when hematopoiesis is active in the mouse FL (Figure 4A). PLX treatment efficiently depleted EMs by inducing apoptosis in the E14.5 FL (Figures 4B and S7A), while the number of lineage-traced HSC-dependent macrophages (LM) was unaffected (Figures 4C–4E). EM depletion *in utero* did not lead to increased inflammation[53] (Figure S5A). Rather, key inflammation pathways were downregulated in the E14.5 FL (*Tnf*, *Ifn gamma*, *Il1a/b*, *Il18*, and *Il10*), while negative regulators of cytokine signaling (*Socs1&2*) were upregulated.

After withdrawal of CSF1R inhibition, macrophages rebound to control numbers 48 h after (E16.5) in FL and 96 h after (E18.5) in brain and skin (Figures 4C–4E, upper panel). The specific contribution of late-wave (HSC-derived) hematopoiesis was investigated in *Cdh5^{CreERT2} Rosa26^{Tomato}* embryos pulsed at E10.5 with 4OHT (Figure 4A), which labels endothelial cells after E10.5, including the hemogenic endothelium giving rise to HSCs.[54] An increased HSC contribution (measured by the labelling efficiency of macrophages) was observed as early as E14.5 and maintained throughout development in PLX-treated FL (Figures 4C and 4D, middle panel). HSC contribution to peripheral tissue macrophages increased 2 days later than in FL, at E16.5. The number of LM in FL and brain increased dramatically between E14.5 and E16.5 and was stable between E16.5 and E18.5 (Figures 4C and 4D, lower panel). In contrast to skin and FL, there was only a transient HSC contribution to brain macrophages (microglia), in line with the moderate fetal HSC contribution to microglia pools.[55]

The contribution of surviving EMs to the repopulation was quantified in *Cdh5^{CreERT2} Rosa26^{tdTomato}* embryos pulsed at E7.5 to distinguish EMs (EMP-derived, Tomato positive) from LMs (Tomato negative). At E16.5, both EMs and LMs proliferate and contribute to the repopulation of macrophage pools in the FL and brain, albeit at different extents (Figure S5G). This may explain why macrophage numbers overshot at E18.5, both in the brain and FL, but returned to normal numbers by 6 weeks after birth (Figures 4C–4E, upper panel).

Surprisingly, HSC contribution to resident macrophages decreased over time to return to control levels in adulthood. In all three organs, the labeling efficiency of liver Kupffer cells, brain microglia, and epidermal Langerhans cells was not different between offspring from control and PLX-treated dams. This suggests that although HSC-derived LMs outperform EMs in their proliferative capacity in the acute recovery phase after PLX, they are incapable of long-term self-maintenance and are hence eventually replaced by EMs.

Monocytes, often viewed as macrophage precursors, were unaffected in FL, brain, and blood at the end of the PLX treatment (Figures 4F–4H, upper panel), as were neutrophils, also produced during both early- and late-wave hematopoiesis (Figures S5C and S5D). In regard to their ontogeny, HSC contribution to circulating monocytes and neutrophils was barely detectable at E14.5 in control and PLX-treated embryos

(H) Lymph gland immunolabeling with anti-Pxn in red and the anti-L4 lamellocyte marker in gray; nuclei labeled with DAPI in blue. Brackets indicate the lobes represented in the blow-up, and dashed lines mark the perimeter of the lymph gland lobes (N ≥ 8).
(I) Lymph gland lobes' volume (N ≥ 9). Detailed genotypes: *w;HmlΔHmlΔGal4,UAS-2XEGFP/+;tubGal80^{TS}/+* (Hml^{TS} > GFP), *w;UAS-hid/+* (hid), *w;HmlΔGal4,UAS-2XEGFP/UAS-hid;tubulinGal80^{TS}/+* (Hml^{TS} > GFP, hid). Confocal images are shown as representative single sections unless otherwise specified. Statistics: two-tailed unpaired t test.

CellPress

Developmental Cell
Article

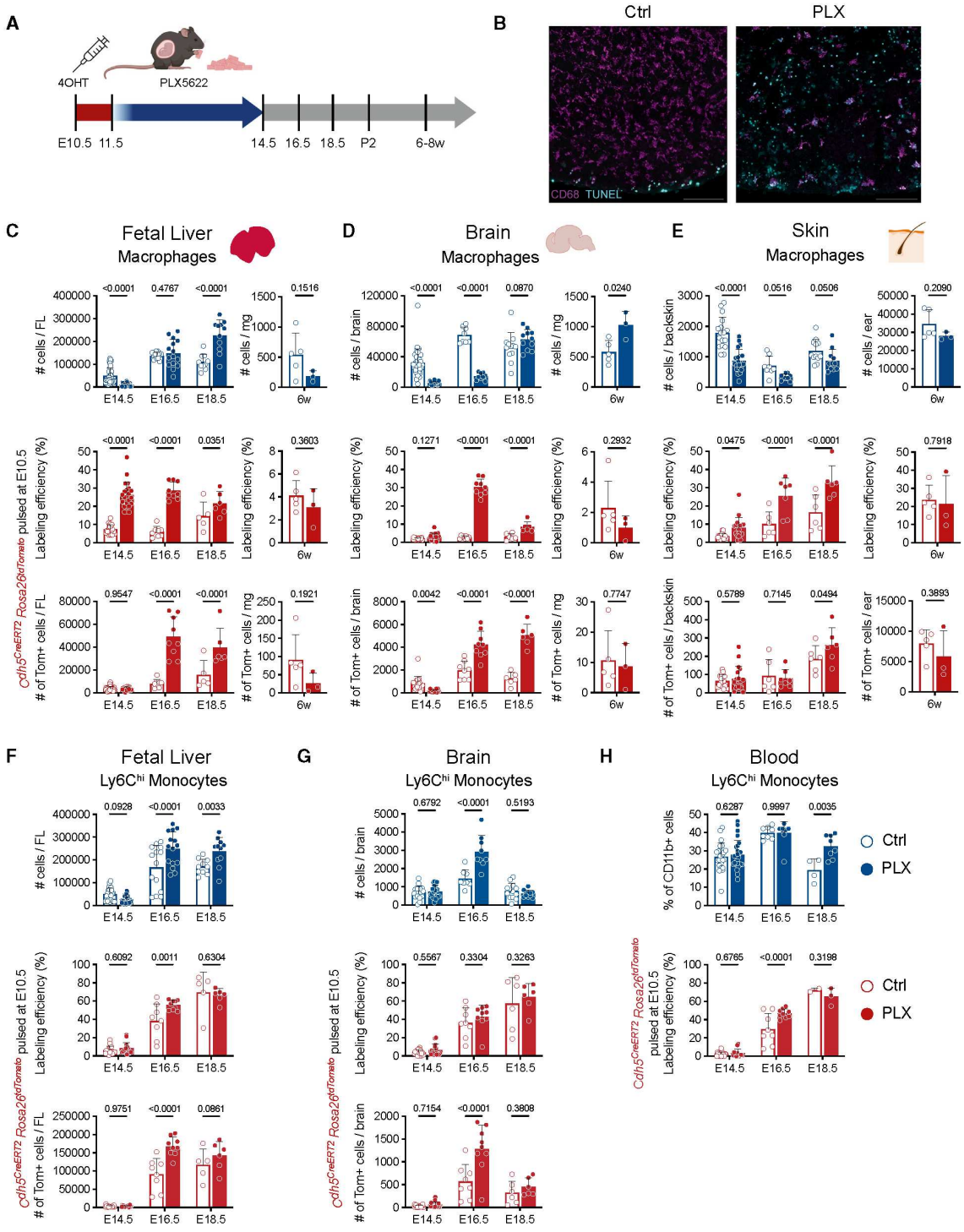

Figure 4. Murine EM depletion leads to an increased contribution of HSCs to macrophage pools

(A) *Cdh5*^{CreERT2} *Rosa26*^{tdTomato} pregnant dams were pulsed with 4OHT at E10.5 to lineage trace hematopoietic progenitors born from endothelium after E10.5 and placed the next day on control (Ctrl) or CSF1R inhibitor-containing chow (PLX5622, PLX) for 3 days. Hematopoiesis was then assessed on the last day of CSF1R inhibition (E14.5) and after withdrawal of CSF1R inhibition.

(legend continued on next page)

Developmental Cell
Article

CellPress

(Figures 4F, S5C, and S5D, respectively). During the PLX recovery phase, HSC contribution to Ly6C^{hi} monocytes increased at E16.5 in the blood and FL of PLX-treated embryos and plateaued at E18.5 with controls (Figures 4F–4H, middle panel), having reached the maximum efficiency of the system. Thus, HSC produced larger numbers of monocytes ahead of time after EM depletion (Figures 4F and 4G, lower panel). Furthermore, increased monocyte output by HSCs in EM-depleted embryos was not short lived, and Ly6C^{hi} monocytes were increased in blood at E18.5 and after birth (post-natal day [P] 2) but were back to control values by 8 weeks (Figure S4E). Notably, the 2-fold increase in FL monocytes was detected 2 days after the doubling in size of the FL macrophage population (Figures 4C and 4F), suggesting that the increase in monocyte numbers is not due to an overcompensation to repopulate macrophage pools in peripheral tissues or FL but rather the read-out of a more global change in late-wave hematopoiesis. Similarly, the contribution of late-wave hematopoiesis to neutrophils was increased in FL at E16.5, which resulted in increased neutrophil numbers at E18.5 (Figure S5C), indicating an overproduction of neutrophils that accumulate in the FL. While blood neutrophils were unaffected throughout development, in ontogeny and frequency (Figure S5D), neutrophil numbers were increased in blood after birth and at P2 but were back to control values in adulthood (Figure S5F).

Altogether, these data suggest enhanced or accelerated HSC differentiation toward monocytes and neutrophils after transient depletion of EM macrophages *in utero*. Thus, murine EM depletion drives an earlier contribution of HSC hematopoiesis to myeloid cells (neutrophils, monocytes, and macrophages) as in *Drosophila*.

Murine EM depletion triggers precocious HSC commitment and differentiation

To assess how HSC-derived hematopoiesis was affected by the loss of EMs, we quantified the number of progenitors in the E14.5 FL after EM depletion. Within the Lin neg Sca1+ Kit+ (LSK) compartment, short-term (ST-) HSCs,[56] as well as lymphoid-biased multi-potent progenitors (MPP4), were not affected. In contrast, long-term (LT-) HSCs and erythroid-biased MPPs (MPP2) were upregulated, while myeloid-biased MPPs (MPP3) were reduced in numbers. These changes were only transient, and progenitor populations were back to control levels by E18.5, except for MPP2 (Figures 5A and 5B). This demonstrates that HSC-derived hematopoiesis is altered by EM depletion and suggests an increased commitment of HSCs into downstream progenitors. To investigate this further, we characterized committed myeloid progenitors. The differentiation cascade in early-wave (from EMPs) and late-wave (from HSC) hematopoiesis toward myeloid cells is summarized in Figure 5A. By E14.5, the progenitors upstream of the myeloid differentiation cascade (common myeloid progenitors [CMPs] and granulocyte-monocyte progenitor [GMP]) are significantly increased in numbers, while more committed downstream progenitors (macrophage/dendritic cell progenitor [MDP], common monocyte progenitor [cMoP]) are unaffected (Figure 5C). Intriguingly, not only myeloid progenitors but also megakaryocyte-erythroid progenitors (MEPs) were increased in numbers at E14.5 (Figure S6C). The changes in progenitors persisted until E18.5 in the FL. Thus, PLX treatment does not deplete hematopoietic progenitors, instead it enhances progenitor production.

Moreover, EM depletion leads to long-lasting changes in HSC-derived hematopoiesis. Bone marrow (BM) colonization by HSCs at P2 was unaffected in EM-depleted embryos (Figure S6D). While most progenitor cell numbers were unchanged, lymphoid-biased MPP4 were reduced at P2 and in adulthood (Figures S6D and S6E). Furthermore, when single CMPs from adult (6–8 weeks) BM (Figures 5D and 5E) were sorted and cultured for 7 days in liquid culture, they produced larger macrophage and neutrophil colonies if they had undergone transient EM depletion *in utero*. Although tissue macrophages, circulating monocytes, and neutrophil numbers in adult mice were normal (Figures 4C–4E, S5E, and S5F), these results show a long-term increased myeloid differentiation potential of HSC-derived progenitors after transient macrophage depletion in the developmental period at the expense of lymphoid potential.

The acceleration of late hematopoiesis caused by fly EM depletion does not rely on inflammation or on EM phagocytic ability

EM depletion causes acceleration of late hematopoiesis in both flies and mice, suggesting that layered hematopoiesis plays an important and conserved function in adjusting immune system development. Next, we asked what the underlying mechanisms are, and we first took advantage of the fly model to narrow down the specific macrophage function at play.

To further exclude the involvement of inflammation, we reduced the EM number by preventing their proliferation. The String/Cdc25 (Stg) tyrosine protein phosphatase required for cell-cycle progression[57] was knocked down in EMs by expressing a *stg RNAi* transgene[58] under the control of *HmlΔGal4* until midL2, when lymph glands were analyzed (Figures 6A–6G).

(B) Representative immunolabeling of E14.5 fetal livers from control and PLX-treated embryos. Anti-CD68 (macrophages, magenta); TUNEL (cyan). Scale bar represents 100 μm.
(C) Number of CD45+ CD11b+ F4/80+ CD64+ Tim4+ macrophages (top), frequency (middle), and number (bottom) of tdTomato+ fetal liver macrophages per fetal liver or per mg of 6-week-old adult liver.
(D) Number of CD45+ CD11b+ F4/80+ CD64+ macrophages (top), frequency (middle), and number (bottom) of tdTomato+ macrophages per fetal brain or per mg of 6-week-old adult brain.
(E) Number of CD45+ CD11b+ F4/80+ CD64+ macrophages (top), frequency (middle), and number (bottom) of tdTomato+ macrophages per fetal backskin or per ear skin epidermis of one ear of 6-week-old adults.
(F and G) Number of CD45+ CD11b+ F4/80- Ly6Chi monocytes (top), frequency (middle), and number (bottom) of tdTomato+ monocytes per fetal liver (F) and brain (G).
(H) Frequency of CD115+ Ly6Chi monocytes among blood CD11b+ cells (top) and frequency of tdTomato+ blood Ly6Chi monocytes (bottom). (C–H) Mean ± SD; control (Ctrl, blue border) and macrophage-depleted (PLX, blue fill) embryos. Symbols correspond to individual embryos from at least two independent litters per time point and per treatment group. Tukey multiple comparisons test (embryos) and unpaired t test (adults).

CellPress
Developmental Cell
Article

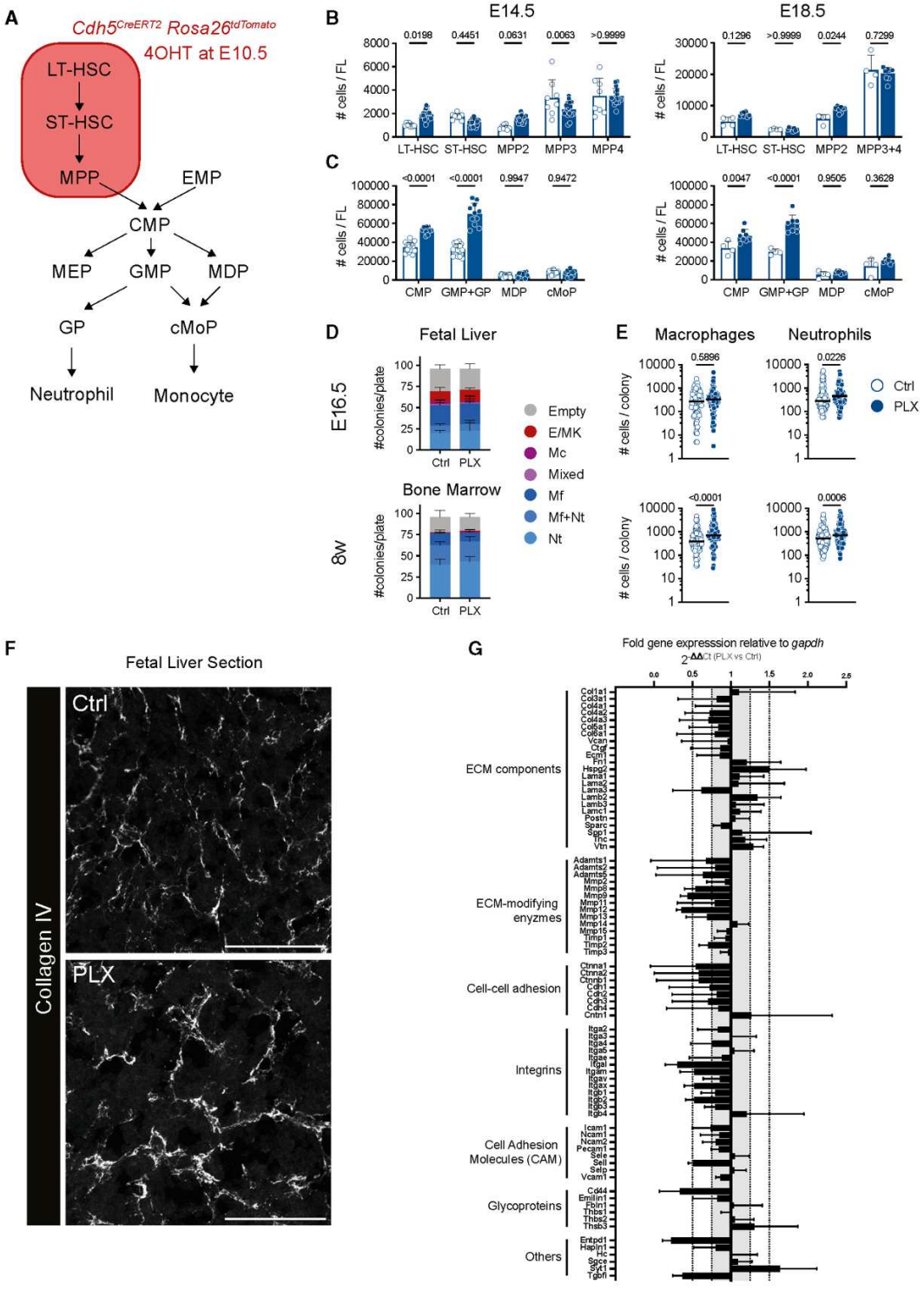

Figure 5. Murine EM depletion alters fetal liver hematopoiesis and ECM organization

(A) Simplified representation of myeloid commitment and differentiation from definitive multipotent progenitors toward neutrophil and monocyte fates. A 4OHT pulse at E10.5 in *Cdh5*^{CreERT2} *Rosa26*^{tdTomato} embryos labels hematopoietic stem and progenitor cells emerging after E10.5 (red square) and their progeny.

(legend continued on next page)

Developmental Cell
Article

CellPress

This strategy avoids inducing *stg RNAi* in lymph gland Hml^{+} cells and allows the comparison with midL2 lymph glands dissected after EM depletion (Figures 2G–2J). Upon *stg RNAi*, the number of EMs per larva drops drastically, similar to what observed upon depletion (Figures 6B and 2C). However, while EMs are barely detectable by immunolabeling upon depletion (Figures 2D and 2E), EMs from *stg RNAi* larvae have normal morphology and are mostly Hml , and their numbers are in accordance with those obtained by brightfield counting (Figure 6C). This likely accounts for the milder phenotype induced by *stg RNAi* compared with that induced by cell depletion (see below). No lamellocytes were detected by brightfield counting (4 independent replicates), indicating the absence of inflammatory states. Even in these conditions, however, the lymph gland is increased in size and shows precocious cell differentiation, mostly in the cortical zone (Figures 6D and 6E), without signs of apoptosis or inflammation (Figures 6F and 6G) as in the L1-restricted depletion (Figures 3E, 3F, and 3H).

Since the accelerated lymph gland development triggered by EM loss does not rely on inflammatory mechanisms, a specific EM function, namely phagocytosis and/or secretion, might be involved. Downregulating the expression of the phagocytic receptor Eater in EMs (*eater RNAi*[59] expressed under the control of *HmlΔGal4*) does not impact EM number or accelerate lymph gland development at midL2 (Figures 6H–6K), suggesting that the EM phagocytic function does not underlie the modulation of late hematopoiesis.

ECM molecules from fly EMs control lymph gland development

In the lymph gland, cells are interweaved with ECM that also separate the organ from the hemolymph.[28,38,41,60] ECM integrity is crucial for proper cell-cell interactions and to convey homeostatic signaling regulating progenitor maintenance/differentiation. Animals mutant for the ECM component *trol* (ortholog of the mammalian Perlecan) show severe defects in the lymph gland ECM along with precocious differentiation of the organ.[60] EMs produce and secrete several ECM molecules[61,62] such as Trol,[63] the collagen IV subunits Col4alpha1[64] and Viking/Col4alpha2,[65] laminin,[66] and SPARC.[67] We hence asked whether EMs modulate late hematopoiesis through the ECM pathway

We knocked down the expression of Trol in EMs by expressing a *trol RNAi* (Figure S4A) under the control of *HmlΔGal4* until midL2 (before massive differentiation of Hml^{+} cells in the lymph gland), and we analyzed the lymph gland phenotype (Figure 7A). *trol RNAi* triggers a significant increase of the lymph gland volume, along with increased lymph gland cellularity and LM differentiation (Figures 7B and 7C). Similar results were obtained upon knocking down *vkg* (*vkg RNAi*) in EMs (Figures S3A–S3C), further proving the involvement of the ECM pathway in mediating the EM-dependent modulation of late hematopoiesis. The enhanced number of Hml^{+} macrophages observed upon *trol RNAi* may trigger *trol* silencing *in loco*, causing indirect effects. To avoid that, lymph glands were also analyzed at an earlier stage (early-midL2, ~45 h AEL) from larvae raised at 29°C to optimize RNAi efficiency[68] (Figures 7D and S3D). At this stage, no increase of Hml^{+} cells was detected in the lymph glands of *trol RNAi* larvae, yet the organ is already enlarged (Figures 7E, 7F, S3E, and S3F). Of note, *trol* downregulation in EMs does not impinge on the main patterning of the developing lymph gland. At early-midL2, a medullary zone populated by Domeless^{+} (dome) and E-cadherin^{+} (E-cad) progenitors[38,60,69,70] is present and similar to what observed in controls. Furthermore, the precociously differentiated LMs are cortically located, and the PSC, immunolabeled by Antennapedia (Antp),[18] does not show evident defects (Figures 7E,7F, and S3G). Importantly, the patterning is well preserved also at later stages. Upon using the thermosensitive approach to confine *trol* knockdown at L1 and early L2 stages (thus avoiding possible cell autonomous effects) (Figure 7G), in feeding L3 (fL3) lymph glands, we observed a preserved E-cad^{+}, βPS integrin^{+},[71] and wingless^{+} (wg)[22] medullary zone as well as a Pxn^{+} cortical zone at the periphery of the primary lobes (Figures 7H, 7I, S3I, and S3J).

We then assessed the status of the lymph gland ECM of early-midL2 larvae, at the onset of the lymph gland phenotype (Figure 7J). The ECM of controls is clearly organized in a network surrounding single macrophages or small groups of cells. By contrast, this regular architecture is disrupted upon *trol RNAi*: ECM filaments are not properly connected, and wide gaps in the ECM surrounding groups of cells are visible (Figure 7K). Similar defects were scored by immunolabeling the ECM with the anti-Col4alpha1 antibody (Figure S3H). To gain better resolution on the lymph gland ECM structure, we performed transmission electron microscopy (Figure 7L). In control lymph glands, the macrophages appear packed, and the cleft between neighboring cells are generally filled with highly organized ECM filaments. Moreover, the outermost ECM layer coating the lymph gland lobe tightly adheres to the cells in control lymph gland. Upon *trol* downregulation, this external ECM layer is more

LT- and ST- HSCs, long-term and short-term HSCs; MPP, multipotent progenitors; EMP, erythro-myeloid progenitors; CMPs, common myeloid progenitors; MEPs, megakaryocyte-erythroid progenitors; GMP, granulocyte-monocyte progenitor; GP, granulocyte progenitor; MDP, macrophage/dendritic cell progenitor; cMoP, common monocyte progenitor.

(B and C) Number (mean ± SD) of LT-HSC, ST-HSC and MPP2 (CD150+ CD48+ CD135- LSK, erythroid-biased), MPP3 (CD150- CD48+ CD135- LSK, myeloid-biased), MMP4 (CD150- CD48+ CD135+ LSK, lymphoid-biased) (B) and of CMP, GMP + GP, MDP, and cMoP (C) per fetal liver at E14.5 (left) and E18.5 (right). Mean ± SD; control (Ctrl, blue border) and macrophage-depleted (PLX, blue fill) embryos. Symbols correspond to individual embryos from at least two independent litters per time point and per treatment group. Statistics: one-way ANOVA.

(D) Stacked bar charts (mean ± SD) representing the number and types of colonies in CFC assay of CMP from E16.5 fetal liver (top) and 8-week-old bone marrow (bottom). Empty wells, erythrocyte-megakaryocyte- (E/Mk), mast cell- (Mc), mixed- (E/Mk and/or Mc and/or Mf and/or Nt), macrophage- (Mf), neutrophil- (Nt), and neutrophil-macrophage- (Nt + Mf) containing colonies.

(E) Scatter dot plot (median) representing the number of cells (macrophages or neutrophils) in single colonies from E16.5 (top) and adult CMP (bottom). Statistics: Mann-Whitney.

(F) Representative anti-Coll IV (gray) immunolabeling of E14.5 fetal liver from control and PLX-treated embryos. Scale bar represents 100 μm.

(G) Fold gene expression (mean ± SD) relative to *gadph* in E14.5 control and EM-depleted FL.

CellPress
Developmental Cell
Article

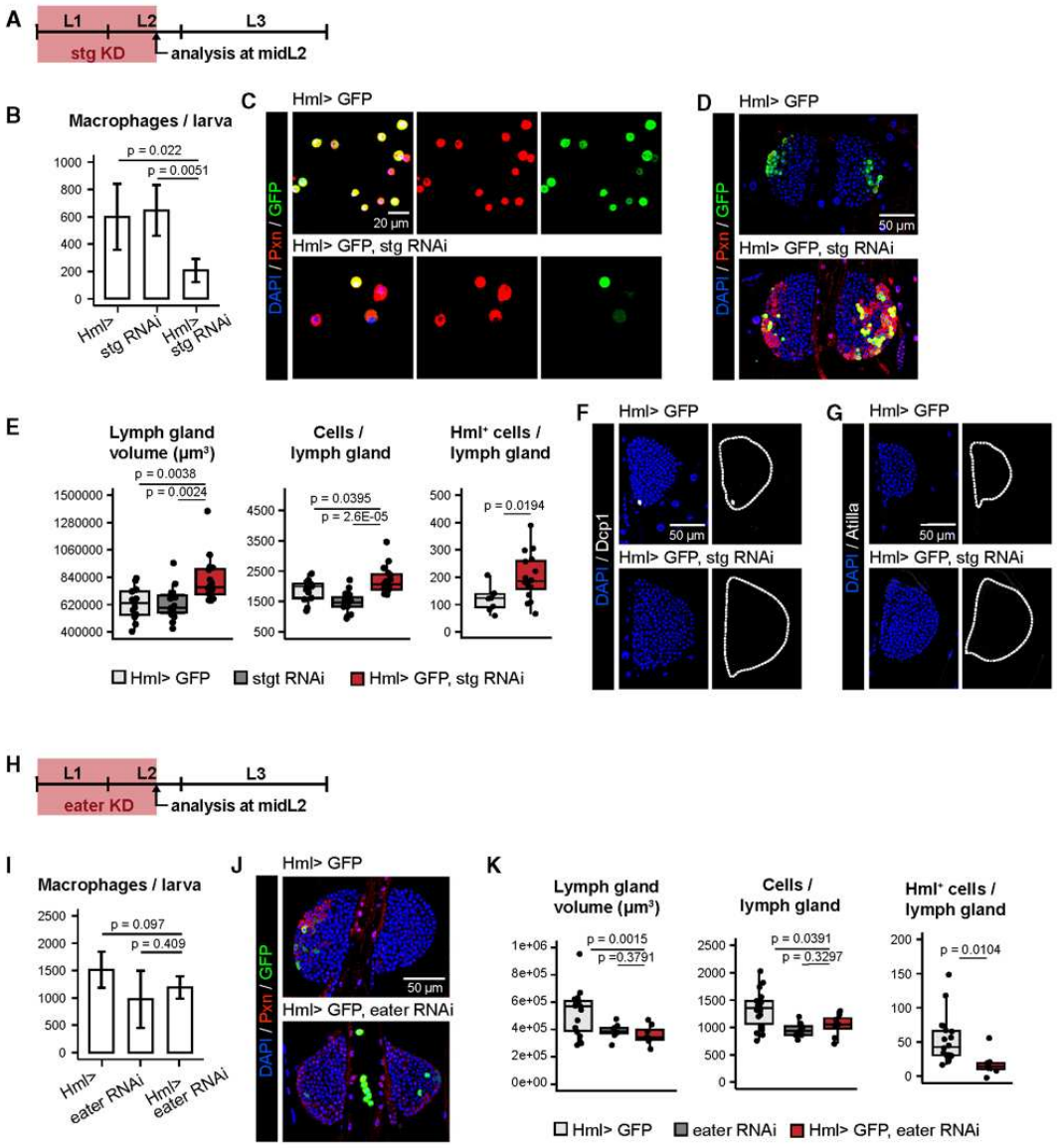

Figure 6. The acceleration of late hematopoiesis caused by fly EM depletion does not rely on inflammation or on EM phagocytic ability

(A) Experimental setup adopted in (B)–(G). The *HmlΔGal4* driver was used to knock down (KD) *string/cdc25* (*stg RNAi*), a positive regulator of cell-cycle progression, in EMs from the beginning of the larval life until midL2 (~65 h AEL) with animals raised at 25°C. *Hml* expression was revealed through a reporter GFP.

(B) Number of macrophages per larva (mean ± SD) assessed by brightfield counting (N ≥ 3).

(C) Immunolabeling of bled macrophages. Anti-Pxn is in red, anti-GFP in green, and nuclei are labeled with DAPI in blue.

(D–F) Lymph gland immunolabeling with (D) anti-Pxn in red and anti-GFP in green (N ≥ 14), (F) anti-Dcp1 in gray (N ≥ 8), and (G) anti-Atilla in gray (N = 6); nuclei are labeled with DAPI in blue. Dashed lines mark the perimeter of the lymph gland lobes. (E) Lymph gland primary lobes' volume, number of cells, and number of Hml^{+} cells (N ≥ 13). Both sexes in a 1:1 ratio were used for the lymph gland analysis upon *stg RNAi*.

(H) Experimental setup adopted in (I)–(K). The phagocytic receptor *eater* was knocked down (*eater RNAi*) in EMs under the control of *HmlΔGal4* from the beginning of the larval life until midL2 (~65 h AEL) with animals raised at 25°C. *Hml* expression was revealed through a reporter GFP.

(I) Number of macrophages per larva (mean ± SD) assessed by brightfield counting (N ≥ 3).

(J) Lymph gland immunolabeling with anti-Pxn in red and anti-GFP in green; nuclei are labeled with DAPI in blue (N ≥ 8).

(K) Lymph gland primary lobes' volume, number of cells and number of Hml^{+} cells (N ≥ 8). Detailed genotypes: *w;HmlΔGal4,UAS-2XEGFP/+;+* (Hml > GFP), *w;stg RNAi/+;+* (stg RNAi), *w;HmlΔGal4,UAS-2XEGFP/stg RNAi;+* (Hml > GFP, stg RNAi), *w;HmlΔGal4/+;+* (Hml>), *w; HmlΔGal4/stg RNAi;+* (Hml > stg RNAi), *w;+;eater RNAi/+* (eater RNAi), *w;HmlΔGal4,UAS-2XEGFP/+;eater RNAi/+* (Hml > GFP, eater RNAi), *w; HmlΔGal4/+;eater RNAi/+* (Hml> eater RNAi). Confocal images are shown as full-stack projections for bled macrophages and representative single sections for lymph glands unless otherwise specified. Statistics: two-tailed unpaired t test.

Developmental Cell
Article

CellPress

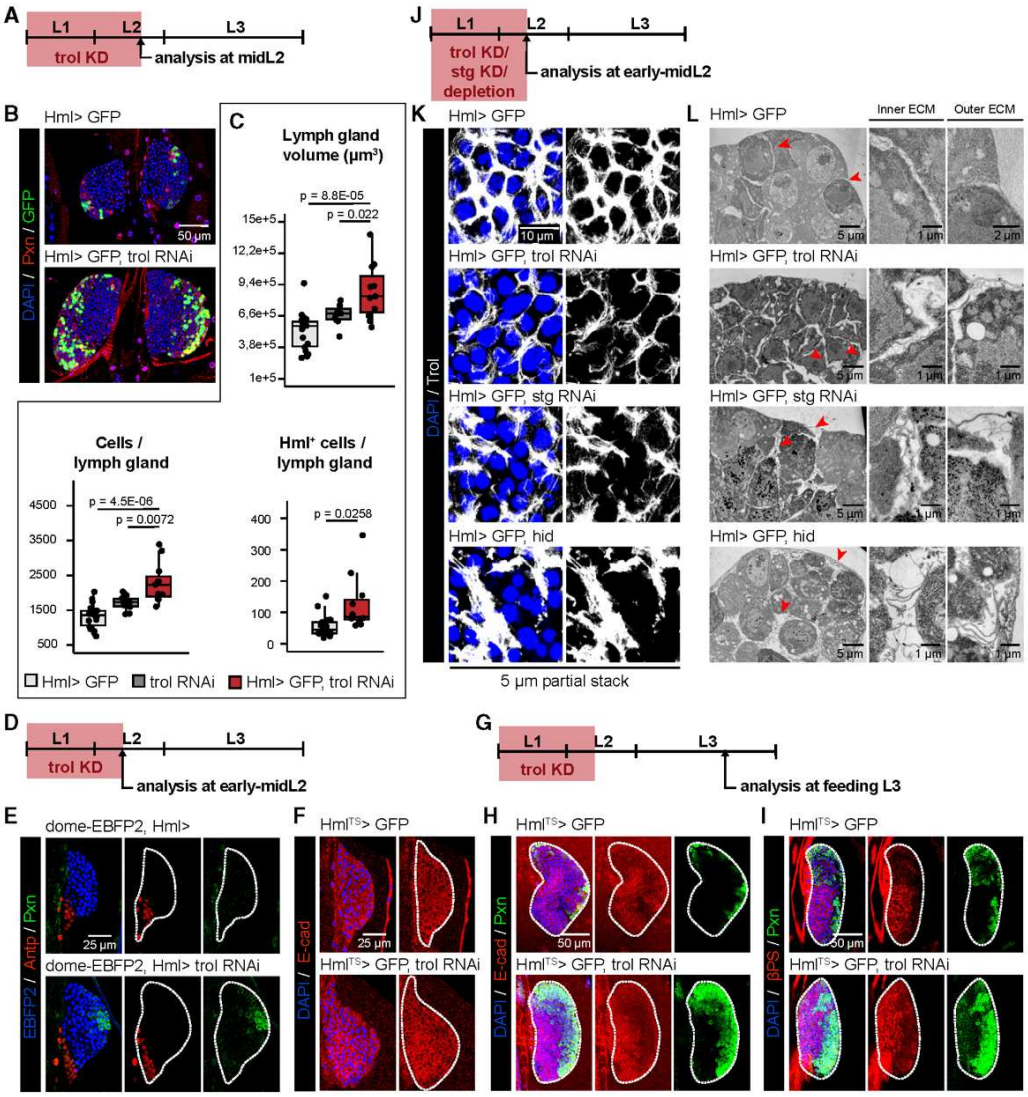

Figure 7. The downregulation of extracellular matrix (ECM) molecules in fly EMs accelerates the lymph gland development and affects the lymph gland ECM organization without altering the patterning

(A) Experimental setup adopted in (B) and (C). The *Hml⊿Gal4* driver was used to express a reporter GFP and knock down the ECM molecule Trol (*trol RNAi*) in EM from the beginning of the larval life until midL2 (~65 h AEL) with animals raised at 25°C.

(B) Lymph gland immunolabeling with anti-Pxn in red, anti-GFP in green, and nuclei labeled with DAPI in blue. N ≥ 10.

(C) Lymph gland primary lobes' volume, number of cells, and number of Hml^{+} cells in control and *trol RNAi* larvae. N ≥ 10.

(D) Experimental setup adopted in (E) and (F). The *Hml⊿Gal4* driver was used to knock down *trol* (*trol RNAi*) in EMs from the beginning of the larval life until early-mid second larval instar (early-midL2) ~45 h AEL, with animals raised at 29°C to increase the UAS-Gal4 system efficiency.

(E) Lymph gland immunolabeling in control and *trol RNAi* larvae. A *domeless* reporter labels the medullary zone in blue (EBFP2), the posterior signaling center marker Antp (Antennapedia) is in red, and anti-Pxn in green. N = 6. dashed lines: perimeter of the lymph gland primary lobes.

(F) Lymph gland immunolabeling with the medullary zone marker E-cad in red and nuclei labeled in blue with DAPI. N ≥ 11. Despite the presence of a *tubulinGal80^{TS}*, no temperature shift was performed to reproduce the conditions used in (E).

(G) Experimental setup adopted in (H) and (I). *trol* knock down was restricted to L1 and beginning of L2 using a thermosensitive inhibitor of Gal4 (*tubulinGal80^{TS}*), which is active at low temperature (18°C) and inactive at higher temperature (≥25°C). Embryos and larvae were raised at 29°C until early-midL2 (~45 h AEL) to trigger *trol* knock down and expression of a GFP reporter under the control of the Hml. Then, animals were shifted at 18°C and analyzed at feeding third larval instar (fL3).

(H and I) Lymph gland immunolabeling with anti-Pxn in green, anti-E-cadherin (E-cad) **(H)** and βPS integrin (βPS) **(I)** in red, and nuclei labeled in blue with DAPI. N ≥ 5.

(legend continued on next page)

CellPress

Developmental Cell
Article

convoluted, with gaps between cells or scarce ECM filaments around them. Similar ECM was detected upon downregulating EM proliferation (*stg RNAi*), and it was even more evident upon EM depletion (Figures 7K and 7L).

Overall, these results demonstrate that the secretion of ECM molecules such as Trol and collagen IV by EMs contribute to the integrity of the lymph gland ECM and that the loss of this ECM source accelerates the physiological course of late hematopoiesis.

Murine EM depletion modifies the ECM of the FL niche

We finally probed whether the modulation of HSC hematopoiesis by murine EMs also involved changes in ECM remodeling in the fetal hematopoietic niche, as evidenced in the fly lymph gland. By E14.5, the FL ECM is mostly composed of laminins, nidogen, fibronectin, HSPG, and type IV Collagen.[72] Analysis of E14.5 FL sections revealed changes to the fine structure of the ECM, with a reduction of the Collagen IV network in PLX-treated embryos (Figures 5F and S7B). We thus probed the expression of ECM-related genes and found that out of 79 tested genes, expression of only 4 genes is upregulated (>1.2-fold increase; *Syt1*, *Vtn*, *Lamb2*, and *Hspg2*). In contrast, 40 genes are downregulated (<0.8-fold change), among them ECM key components (Collagens, Laminins, and Versican) and ECM-modifying enzymes (Mmp8, 9, 12, and 13; Adamts 1,2 and 5; and Timp2). Furthermore, several genes coding for key adhesion molecules (belonging to Cadherin, Integrin, and CAM families) are also downregulated in PLX-treated embryos (Figure 5G).

Thus, macrophage depletion between E11.5 and E14.5 leads to profound changes in ECM organization in the E14.5 FL, demonstrating that ECM alteration at the site of late hematopoiesis is evolutionarily conserved upon EM depletion.

DISCUSSION

Multiple hematopoietic waves have been observed throughout evolution, and macrophages from different waves co-exist during development and then adult life.[73] This has sparked a renewed interest in macrophage function during tissue repair, infection, and tumor growth[74–85] in light of their two possible origins and maintenance mechanisms: prenatal EMs that self-renew versus continuously recruited HSC-derived macrophages. Although macrophages from early waves colonize the embryo including the hematopoietic niches, little is known about their developmental function in late hematopoietic waves. Since these macrophages experience varied physiological/pathological stimuli, we asked whether homeostatic interactions occur between the different waves as an evolutionarily conserved mechanism to adjust late hematopoiesis and ensure a proper blood cell repertoire. We here identify EMs as key regulators of late hematopoiesis throughout evolution, and we uncover the ECM as an important mediator of the process. Our study demonstrates that EMs work as signaling hubs for HSC-dependent hematopoiesis.

EMs control late hematopoiesis

Drosophila LMs are generated in the lymph gland, whose development is tightly regulated by well-described signals exchanged between PSC (the signaling niche), progenitor cells, and mature LMs (reviewed in Banerjee et al.[16]). Organs outside the lymph gland, i.e., cardiac tube, brain, and fat body (equivalent to the mammalian liver), also contribute to the process.[86–89] Here, we reveal EMs as an additional source of cues regulating lymph gland maturation under physiological conditions. The constitutive loss of EMs not only boosts growth and LM differentiation in the lymph gland but also results in increased cell death and the presence of activated immune cells. This is due to an indirect effect rather than being triggered by EM loss, as LMs precociously expressing *Hml* in the lymph gland die and trigger the inflammatory state. By contrast, the analysis of early-stage lymph glands upon EM depletion already displays increased cell proliferation and precocious cell differentiation, in the absence of apoptosis and lamellocytes. Moreover, similar phenotypes are triggered by decreasing EM proliferation. Thus, the loss of EMs at the beginning of lymph gland development accelerates a bona fide physiological maturation of the lymph gland, which maintains a wild-type-like patterning.

Previous works hint at the involvement of embryonic macrophages in modulating vertebrate late hematopoiesis. Zebrafish embryonic macrophages facilitate the entry of HSCs into circulation from their site of emergence, whereas murine embryonic macrophages participate to the emergence of HSCs from the aorta-gonado-mesonephros region.[15,90] Here, we reveal the role of EMs in HSC expansion and differentiation. Inhibition of signaling downstream of the main macrophage growth factor receptor (CSF1R) during embryonic development leads to macrophage depletion, without affecting CSF1R+ hematopoietic progenitors or monocytes. After withdrawal of CSF1R inhibition, macrophages return to normal levels, first in the FL and then in peripheral tissues (brain and skin). However, EM depletion profoundly impacts fetal HSC behavior. Macrophage repopulation from HSC-derived cells was driven by the increase in HSC differentiation into erythro-myeloid cells. Of note, the few LMs present at E14.5 surviving the treatment could also contribute to the repopulation through local proliferation. Thus, HSC commitment and differentiation into myeloid cells, not only

(J) Experimental setup adopted in (K) and (L). The *HmlΔGal4* driver was used to knock down *trol* (*trol RNAi*) or *stg* (*stg RNAi*) or express the cell death gene *hid* in EMs from the beginning of the larval life until early-midL2 (~45 h AEL, animals raised at 29°C).

(K) Lymph gland immunolabeling in control (N ≥ 10), *trol RNAi* (N ≥ 10), *stg RNAi* (N ≥ 6), or depleted larvae (N ≥ 6). Anti-Trol is in gray, and nuclei are labeled with DAPI in blue.

(L) Transmission electron microscopy micrographs of lymph glands from control, *trol RNAi*, *stg RNAi*, or depleted larvae. Low magnified images are on the left, and red arrowheads point the fields represented at higher magnification on the right, which are centered on the inner or outer lymph gland ECM. Detailed genotypes: *w;HmlΔGal4,UAS-2XEGFP/+;+* (Hml > GFP), *w;+;trol RNAi/+* (trol RNAi), *w;HmlΔGal4,UAS-2XEGFP/+;trol RNAi/+* (Hml > GFP, trol RNAi), *w;HmlΔGal4,UAS-2XEGFP/stg RNAi;+* (Hml > GFP, stg RNAi), *w;HmlΔGal4,UAS-2XEGFP/UAS-hid;+* (Hml > GFP, hid), *w,domeMeso-EBFP2/+;HmlΔG4/+* (dome-EBFP2, Hml>), *w,domeMeso-EBFP2/+;HmlΔG4/+;trol RNAi/+* (dome-EBFP2, Hml > trol RNAi), *w;HmlΔGal4,UAS-2XEGFP/+;tubulinGal80TS/+* (HmlTS > GFP), *w;HmlΔGal4,UAS-2XEGFP/+;tubulinGal80TS/trol RNAi* (HmlTS > GFP, trol RNAi). Confocal images are shown as representative single sections unless otherwise specified. Statistics: two-tailed unpaired t test.

Developmental Cell
Article

CellPress

monocyte/macrophages but also neutrophils, is accelerated. In contrast to the limited differentiation of HSCs into myeloid cells at E14.5 in unperturbed development, EM depletion leads to an earlier contribution of HSCs to upstream multipotent and myeloid progenitors. 4 days after the withdrawal of CSF1R inhibition, increased myeloid output of HSC is evidenced by the doubling of myeloid progenitors (GMPs and granulocyte progenitors [GP]), monocytes, and neutrophils in the FL. Importantly, the increased myeloid-bias of HSCs is still present in the post-natal and adult bone marrow, raising important questions on the long-lasting contribution of pre-natal challenges into adult homeostasis, such as how the hematopoietic system of PLX-treated offspring would respond to secondary challenges.

Despite the different cellular hematopoietic mechanisms linked to specific developmental schemes and lifespan extent (lack of extraembryonic and adult hematopoiesis in flies) between flies and vertebrates, our findings strengthen the hypothesis that layered hematopoiesis is a beneficial strategy that the organism has adopted to face the different environments and needs encountered during development.

ECM components secreted by EMs regulate late hematopoiesis

In flies, the appropriate deposition of the ECM throughout the organ is essential for lymph gland development. It ensures proper local environments, allowing cell-to-cell interactions and controlled diffusion of signals that regulate progenitor maintenance/differentiation. *trol*/*Perlecan* encodes an heparan sulfate proteoglycan of the ECM, and its silencing in lymph gland progenitors leads to a mild increase of LM differentiation at late larval stage. This phenotype is much more severe when *trol* is downregulated ubiquitously,[60] suggesting that additional sources of ECM proteins impinge on lymph gland development. Here, we show that EM-derived ECM molecules contribute to lymph gland maturation. Knocking down *trol* or *viking* (a Collagen IV subunit) expression in EMs leads to defective ECM organization in early-stage lymph gland and accelerates lymph gland growth and differentiation while preserving organ patterning, similar to what we observed upon EM loss. These phenotypes cannot be explained by cell autonomous effects, since *trol* mutation or downregulation in the lymph gland does not phenocopy our results.[60] The involvement of pathways other than the ECM in the regulation of late hematopoiesis by EMs cannot be excluded, but the EM function at play is most likely the secretory one, since reducing the expression of the phagocytic receptors Eater does not have evident impact on the lymph gland.

We did not discriminate between direct and indirect effects on the lymph gland in this study. Nevertheless, we searched for a potential role of macrophages in depositing Trol on the fat body, which is close to the lymph gland and is known to be a signaling hub. Upon overexpressing Trol in EMs (Figure S4A), we could observe a more refined Trol pattern in the fat body compared with controls (Figures S4B and S4C), calling for possible indirect effects. The fact that the phenotype is not 100% penetrant underlines again the complexity of the process, which may involve additional tissues. Of note, Trol overexpression in EMs induced lymph gland phenotypes similar to those induced by *trol* knockdown (Figure S4D), indicating that it is the balance of the Trol molecule that matters.

The mouse model does not allow dissecting different macrophage functions (phagocytosis/secretion). Thus, benefiting from the hypothesis tested in the fly larva, we could show that embryonic macrophage depletion in mice also leads to profound changes in the hematopoietic niche ECM. The FL ECM in depleted embryos shows downregulation of key ECM components (e.g., type IV Collagen, Laminins). In regard to ECM production by macrophages, available RNA-seq datasets of embryonic liver macrophages[91] show the expression of several collagen family members (*Col1a1*, *Col3a1*, *Col4a1-2*, *Col5a1-2*, and *Col6a1-2*) and other ECM genes (*Lama3*, *Sparc*, and *Spp1*), all of which are downregulated in the E14.5 FL upon macrophage depletion. In contrast, while embryonic liver macrophages do express *Hspg2, Vtn*, and *Fn1*, overall expression of these genes in EM-depleted FL is upregulated, suggesting compensatory mechanisms by other liver populations. *Vtn* and *Fn1* are expressed by fetal hepatocytes.[92] In addition, embryonic macrophages express several key ECM-modifying enzymes during development from the Adamts, Timp, and MMP families, thus suggesting that depletion of embryonic macrophages could lead to changes not only in the ECM composition but also in its organization or ability to present/release growth factors and cytokines. Importantly, there appears to be a global dysregulation of cell-cell and cell-ECM adhesion, as evidenced by the downregulation of integrin genes, E-cadherin (*Cdh1*), N-cadherin (*Cdh2*), cadherins 3 and 4, and downstream catenins that connect them to the actin cytoskeleton. Thus, whether murine EMs are a cellular source for ECM components, are involved in ECM remodeling, or rather have an indirect effect through cross-talk with other FL cell populations needs to be further explored.

In sum, the acceleration of LM differentiation upon EM depletion is evolutionarily conserved, and we disclose the ECM pathway as an important mediator of this process. The role of EMs in controlling late hematopoiesis improves the current knowledge of the homeostatic function of macrophages, well beyond immunity. Our findings also open important perspectives to understand the etiology of pediatric diseases and to design therapeutic approaches for diseases involving macrophage dysfunctions.

Limitations of the study

This study discloses the impact of EMs on the late immune system development. Further experiments are required to assess whether this is a direct or indirect effect and to characterize additional tissues and pathways possibly regulating late hematopoiesis.

It is also important to note that two hypotheses still need to be further investigated, (1) the respective contribution to the repopulation of surviving LMs versus newly differentiated LMs from monocytes and (2) the contribution of the change of ontogeny in FL macrophages to the HSC phenotype.

STAR★METHODS

Detailed methods are provided in the online version of this paper and include the following:

- KEY RESOURCES TABLE
- RESOURCE AVAILABILITY

CellPress

Developmental Cell
Article

SUPPLEMENTAL INFORMATION

Supplemental information can be found online at https://doi.org/10.1016/j.devcel.2024.03.013.

ACKNOWLEDGMENTS

We thank I. Ando, J. Shim, A. González Reyes, and S. Noselli for kindly sharing fly lines and antibodies. In addition, fly stocks obtained from the Bloomington Drosophila Stock Center (NIH P40OD018537) and antibodies from the Developmental Studies Hybridoma Bank (DSHB) created by the NICHD of the NIH and maintained at the University of Iowa (Department of Biology, Iowa City, IA 52242) were used in this study. We thank the Imaging and electron microscopy facility of the IGBMC and N. Massaddeq for technical assistance. This work was supported by INSERM, CNRS, UDS, Ligue Régionale contre le Cancer, Hôpital de Strasbourg, ARC, CEFIPRA, ANR grants and by the CNRS/University LIA Calim. E.G.P. and A.G. were supported by the EMAC ANR PRC grant. S.M. is funded by CEFIPRA, ANR, and FRC; PhD program of Z.A.H. is supported by FRM. The IGBMC was also supported by a French state fund through the ANR Labex. This work of the Interdisciplinary Thematic Institute IMCBio+, as part of the ITI 2021-2028 program of the University of Strasbourg, CNRS, and Inserm, was supported by IdEx Unistra (ANR-10-IDEX-0002) and by SFRI-STRAT'US project (ANR-20-SFRI-0012) and EUR IMCBio (ANR-17-EURE-0023) under the framework of the France 2030 Program. We appreciate the technical support of the Institut Pasteur core facilities, notably the cytometry platform (UTECHS CB) and the Center for Animal Resources and Research. We thank P. Dardenne, Y. Lallemand, C. Guichen, and M. Peixoto for their technical support. This work was also funded by Revive (Investissement d'avenir; ANR-10-LABX-0073) and the European Research Council ERC investigator award (2016-StG-715320 to E.G.P.).

AUTHOR CONTRIBUTIONS

S.M., A.S., P.C., A.G., and E.G.P. designed the experiments; S.M., A.G., A.S., and E.G.P. co- wrote the manuscript; S.M., Z.A.H., and C.D. performed the experiments in *Drosophila*; A.S., C.G.R., and K.A. performed the experiments in mice.

DECLARATION OF INTERESTS

The authors declare no competing interests.

Received: July 6, 2023
Revised: January 8, 2024
Accepted: March 7, 2024
Published: April 2, 2024

REFERENCES

1. Mosser, D.M., Hamidzadeh, K., and Goncalves, R. (2021). Macrophages and the maintenance of homeostasis. Cell. Mol. Immunol. *18*, 579–587. https://doi.org/10.1038/s41423-020-00541-3.
2. Kieusseian, A., Brunet de la Grange, P.B., Burlen-Defranoux, O., Godin, I., and Cumano, A. (2012). Immature hematopoietic stem cells undergo maturation in the fetal liver. Development *139*, 3521–3530. https://doi.org/10.1242/dev.079210.
3. Perdiguero, E.G., and Geissmann, F. (2016). The development and maintenance of resident macrophages. Nat. Immunol. *17*, 2–8. https://doi.org/10.1038/ni.3341.
4. Bertrand, J.Y., Jalil, A., Klaine, M., Jung, S., Cumano, A., and Godin, I. (2005). Three pathways to mature macrophages in the early mouse yolk sac. Blood *106*, 3004–3011. https://doi.org/10.1182/blood-2005-02-0461.
5. Stremmel, C., Schuchert, R., Wagner, F., Thaler, R., Weinberger, T., Pick, R., Mass, E., Ishikawa-Ankerhold, H.C., Margraf, A., Hutter, S., et al. (2018). Yolk sac macrophage progenitors traffic to the embryo during defined stages of development. Nat. Commun. *9*, 75. https://doi.org/10.1038/s41467-017-02492-2.
6. de Bruijn, M.F., Speck, N.A., Peeters, M.C., and Dzierzak, E. (2000). Definitive hematopoietic stem cells first develop within the major arterial regions of the mouse embryo. EMBO J. *19*, 2465–2474. https://doi.org/10.1093/emboj/19.11.2465.
7. Medvinsky, A., and Dzierzak, E. (1996). Definitive Hematopoiesis Is Autonomously Initiated by the AGM Region. Cell *86*, 897–906. https://doi.org/10.1016/S0092-8674(00)80165-8.
8. Ema, H., and Nakauchi, H. (2000). Expansion of hematopoietic stem cells in the developing liver of a mouse embryo. Blood *95*, 2284–2288. https://doi.org/10.1182/blood.V95.7.2284.
9. Gomez Perdiguero, E., Klapproth, K., Schulz, C., Busch, K., Azzoni, E., Crozet, L., Garner, H., Trouillet, C., de Bruijn, M.F., Geissmann, F., and Rodewald, H.R. (2015). Tissue-resident macrophages originate from yolk-sac-derived erythro-myeloid progenitors. Nature *518*, 547–551. https://doi.org/10.1038/nature13989.
10. Freyer, L., Iturri, L., Biton, A., and Perdiguero, E.G. (2020). Overlapping Definitive Progenitor Waves Divide and Conquer to Build a Layered Hematopoietic System. Preprint at bioRxiv. https://doi.org/10.1101/2020.12.24.424302.
11. Yokomizo, T., Ideue, T., Morino-Koga, S., Tham, C.Y., Sato, T., Takeda, N., Kubota, Y., Kurokawa, M., Komatsu, N., Ogawa, M., et al. (2022). Independent origins of fetal liver haematopoietic stem and progenitor cells. Nature *609*, 779–784. https://doi.org/10.1038/s41586-022-05203-0.
12. Soares-da-Silva, F., Freyer, L., Elsaid, R., Burlen-Defranoux, O., Iturri, L., Sismeiro, O., Pinto-do-Ó, P., Gomez-Perdiguero, E., and Cumano, A. (2021). Yolk sac, but not hematopoietic stem cell-derived progenitors, sustain erythropoiesis throughout murine embryonic life. J. Exp. Med. *218*, e20201729. https://doi.org/10.1084/jem.20201729.
13. Christensen, J.L., Wright, D.E., Wagers, A.J., and Weissman, I.L. (2004). Circulation and Chemotaxis of Fetal Hematopoietic Stem Cells. PLOS Biol. *2*, E75. https://doi.org/10.1371/journal.pbio.0020075.
14. Mikkola, H.K.A., and Orkin, S.H. (2006). The journey of developing hematopoietic stem cells. Development *133*, 3733–3744. https://doi.org/10.1242/dev.02568.

Developmental Cell
Article

15. Mariani, S.A., Li, Z., Rice, S., Krieg, C., Fragkogianni, S., Robinson, M., Vink, C.S., Pollard, J.W., and Dzierzak, E. (2019). Pro-inflammatory Aorta-Associated Macrophages Are Involved in Embryonic Development of Hematopoietic Stem Cells. Immunity *50*, 1439–1452.e5. https://doi.org/10.1016/j.immuni.2019.05.003.

16. Banerjee, U., Girard, J.R., Goins, L.M., and Spratford, C.M. (2019). Drosophila as a Genetic Model for Hematopoiesis. Genetics *211*, 367–417. https://doi.org/10.1534/genetics.118.300223.

17. Lemos, T., and Merchant, A. (2022). The hedgehog pathway in hematopoiesis and hematological malignancy. Front. Oncol. *12*, 960943. https://doi.org/10.3389/fonc.2022.960943.

18. Mandal, L., Martinez-Agosto, J.A., Evans, C.J., Hartenstein, V., and Banerjee, U. (2007). A Hedgehog- and Antennapedia-dependent niche maintains Drosophila haematopoietic precursors. Nature *446*, 320–324. https://doi.org/10.1038/nature05585.

19. Crisan, M., Kartalaei, P.S., Vink, C.S., Yamada-Inagawa, T., Bollerot, K., van IJcken, W., van der Linden, R., de Sousa Lopes, S.M., Monteiro, R., Mummery, C., and Dzierzak, E. (2015). Monteiro, R., Mummery, C., et al. (2015). BMP signalling differentially regulates distinct haematopoietic stem cell types. Nat. Commun. *6*, 8040. https://doi.org/10.1038/ncomms9040.

20. Pennetier, D., Oyallon, J., Morin-Poulard, I., Dejean, S., Vincent, A., and Crozatier, M. (2012). Size control of the Drosophila hematopoietic niche by bone morphogenetic protein signaling reveals parallels with mammals. Proc. Natl. Acad. Sci. USA *109*, 3389–3394. https://doi.org/10.1073/pnas.1109407109.

21. Austin, T.W., Solar, G.P., Ziegler, F.C., Liem, L., and Matthews, W. (1997). A Role for the Wnt Gene Family in Hematopoiesis: Expansion of Multilineage Progenitor Cells. Blood *89*, 3624–3635. https://doi.org/10.1182/blood.V89.10.3624.

22. Sinenko, S.A., Mandal, L., Martinez-Agosto, J.A., and Banerjee, U. (2009). Dual role of Wingless signaling in stem-like hematopoietic precursor maintenance in Drosophila. Dev. Cell *16*, 756–763. https://doi.org/10.1016/j.devcel.2009.03.003.

23. Morin-Poulard, I., Sharma, A., Louradour, I., Vanzo, N., Vincent, A., and Crozatier, M. (2016). Vascular control of the Drosophila haematopoietic microenvironment by Slit/Robo signalling. Nat. Commun. *7*, 11634. https://doi.org/10.1038/ncomms11634.

24. Benmimoun, B., Polesello, C., Haenlin, M., and Waltzer, L. (2015). The EBF transcription factor Collier directly promotes Drosophila blood cell progenitor maintenance independently of the niche. Proc. Natl. Acad. Sci. USA *112*, 9052–9057. https://doi.org/10.1073/pnas.1423967112.

25. Kieslinger, M., Hiechinger, S., Dobreva, G., Consalez, G.G., and Grosschedl, R. (2010). Early B Cell Factor 2 Regulates Hematopoietic Stem Cell Homeostasis in a Cell-Nonautonomous Manner. Cell Stem Cell *7*, 496–507. https://doi.org/10.1016/j.stem.2010.07.015.

26. Bazzi, W., Cattenoz, P.B., Delaporte, C., Dasari, V., Sakr, R., Yuasa, Y., and Giangrande, A. (2018). Embryonic hematopoiesis modulates the inflammatory response and larval hematopoiesis in Drosophila. eLife *7*, e34890. https://doi.org/10.7554/eLife.34890.

27. Lanot, R., Zachary, D., Holder, F., and Meister, M. (2001). Postembryonic Hematopoiesis in Drosophila. Dev. Biol. *230*, 243–257. https://doi.org/10.1006/dbio.2000.0123.

28. Grigorian, M., Mandal, L., and Hartenstein, V. (2011). Hematopoiesis at the onset of metamorphosis: terminal differentiation and dissociation of the Drosophila lymph gland. Dev. Genes Evol. *221*, 121–131. https://doi.org/10.1007/s00427-011-0364-6.

29. Charroux, B., and Royet, J. (2009). Elimination of plasmatocytes by targeted apoptosis reveals their role in multiple aspects of the Drosophila immune response. Proc. Natl. Acad. Sci. US A *106*, 9797–9802. https://doi.org/10.1073/pnas.0903971106.

30. Shia, A.K.H., Glittenberg, M., Thompson, G., Weber, A.N., Reichhart, J.-M., and Ligoxygakis, P. (2009). Toll-dependent antimicrobial responses in Drosophila larval fat body require Spätzle secreted by haemocytes. J. Cell Sci. *122*, 4505–4515. https://doi.org/10.1242/jcs.049155.

31. Arefin, B., Kucerova, L., Krautz, R., Kranenburg, H., Parvin, F., and Theopold, U. (2015). Apoptosis in Hemocytes Induces a Shift in Effector Mechanisms in the Drosophila Immune System and Leads to a Pro-Inflammatory State. PLOS ONE *10*, e0136593. https://doi.org/10.1371/journal.pone.0136593.

32. Tomar, A., Madhwal, S., and Mukherjee, T. (2020). Immune Control of Animal Growth in Homeostasis and Nutritional Stress in Drosophila. Front. Immunol. *11*, 1528. https://doi.org/10.3389/fimmu.2020.01528.

33. Shin, M., Cha, N., Koranteng, F., Cho, B., and Shim, J. (2020). Subpopulation of Macrophage-Like Plasmatocytes Attenuates Systemic Growth via JAK/STAT in the Drosophila Fat Body. Front. Immunol. *11*, 63. https://doi.org/10.3389/fimmu.2020.00063.

34. Grether, M.E., Abrams, J.M., Agapite, J., White, K., and Steller, H. (1995). The head involution defective gene of Drosophila melanogaster functions in programmed cell death. Genes Dev. *9*, 1694–1708. https://doi.org/10.1101/gad.9.14.1694.

35. Sinenko, S.A., and Mathey-Prevot, B. (2004). Increased expression of Drosophila tetraspanin, Tsp68C, suppresses the abnormal proliferation of ytr-deficient and Ras/Raf-activated hemocytes. Oncogene *23*, 9120–9128. https://doi.org/10.1038/sj.onc.1208156.

36. Goto, A., Kadowaki, T., and Kitagawa, Y. (2003). Drosophila hemolectin gene is expressed in embryonic and larval hemocytes and its knock down causes bleeding defects. Dev. Biol. *264*, 582–591. https://doi.org/10.1016/j.ydbio.2003.06.001.

37. Defaye, A., Evans, I., Crozatier, M., Wood, W., Lemaitre, B., and Leulier, F. (2009). Genetic Ablation of *Drosophila* Phagocytes Reveals Their Contribution to Both Development and Resistance to Bacterial Infection. J. Innate Immun. *1*, 322–334. https://doi.org/10.1159/000210264.

38. Jung, S.H., Evans, C.J., Uemura, C., and Banerjee, U. (2005). The Drosophila lymph gland as a developmental model of hematopoiesis. Development *132*, 2521–2533. https://doi.org/10.1242/dev.01837.

39. Mondal, B.C., Mukherjee, T., Mandal, L., Evans, C.J., Sinenko, S.A., Martinez-Agosto, J.A., and Banerjee, U. (2011). Interaction between Differentiating Cell- and Niche-Derived Signals in Hematopoietic Progenitor Maintenance. Cell *147*, 1589–1600. https://doi.org/10.1016/j.cell.2011.11.041.

40. Honti, V., Kurucz, E., Csordás, G., Laurinyecz, B., Márkus, R., and Andó, I. (2009). In vivo detection of lamellocytes in Drosophila melanogaster. Immunol. Lett. *126*, 83–84. https://doi.org/10.1016/j.imlet.2009.08.004.

41. Irving, P., Ubeda, J.M., Doucet, D., Troxler, L., Lagueux, M., Zachary, D., Hoffmann, J.A., Hetru, C., and Meister, M. (2005). New insights into Drosophila larval haemocyte functions through genome-wide analysis. Cell. Microbiol. *7*, 335–350. https://doi.org/10.1111/j.1462-5822.2004.00462.x.

42. Song, Z., McCall, K., and Steller, H. (1997). DCP-1, a Drosophila Cell Death Protease Essential for Development. Science *275*, 536–540. https://doi.org/10.1126/science.275.5299.536.

43. Nelson, R.E., Fessler, L.I., Takagi, Y., Blumberg, B., Keene, D.R., Olson, P.F., Parker, C.G., and Fessler, J.H. (1994). Peroxidasin: a novel enzyme-matrix protein of Drosophila development. EMBO J. *13*, 3438–3447. https://doi.org/10.1002/j.1460-2075.1994.tb06649.x.

44. Kurucz, E., Zettervall, C.-J., Sinka, R., Vilmos, P., Pivarcsi, A., Ekengren, S., Hegedüs, Z., Ando, I., and Hultmark, D. (2003). Hemese, a hemocyte-specific transmembrane protein, affects the cellular immune response in Drosophila. Proc. Natl. Acad. Sci. USA *100*, 2622–2627. https://doi.org/10.1073/pnas.0436940100.

45. Kocks, C., Cho, J.H., Nehme, N., Ulvila, J., Pearson, A.M., Meister, M., Strom, C., Conto, S.L., Hetru, C., Stuart, L.M., et al. (2005). Eater, a Transmembrane Protein Mediating Phagocytosis of Bacterial Pathogens in Drosophila. Cell *123*, 335–346. https://doi.org/10.1016/j.cell.2005.08.034.

46. Kurucz, E., Márkus, R., Zsámboki, J., Folkl-Medzihradszky, K., Darula, Z., Vilmos, P., Udvardy, A., Krausz, I., Lukacsovich, T., Gateff, E., et al. (2007). Nimrod, a Putative Phagocytosis Receptor with EGF Repeats in

CellPress

Developmental Cell
Article

Drosophila Plasmatocytes. Curr. Biol. *17*, 649–654. https://doi.org/10.1016/j.cub.2007.02.041.

47. Pérez-Cadahía, B., Drobic, B., and Davie, J.R. (2009). H3 phosphorylation: dual role in mitosis and interphase. Biochem. Cell Biol. *87*, 695–709. https://doi.org/10.1139/O09-053.
48. Pérez-Garijo, A., Fuchs, Y., and Steller, H. (2013). Apoptotic cells can induce non-autonomous apoptosis through the TNF pathway. eLife *2*, e01004. https://doi.org/10.7554/eLife.01004.
49. Agaisse, H., Petersen, U.M., Boutros, M., Mathey-Prevot, B., and Perrimon, N. (2003). Signaling Role of Hemocytes in Drosophila JAK/STAT-Dependent Response to Septic Injury. Dev. Cell *5*, 441–450. https://doi.org/10.1016/S1534-5807(03)00244-2.
50. Yang, H., Kronhamn, J., Ekström, J.-O., Korkut, G.G., and Hultmark, D. (2015). JAK/STAT signaling in Drosophila muscles controls the cellular immune response against parasitoid infection. EMBO Rep. *16*, 1664–1672. https://doi.org/10.15252/embr.201540277.
51. Elsaid, R., Soares-da-Silva, F., Peixoto, M., Amiri, D., Mackowski, N., Pereira, P., Bandeira, A., and Cumano, A. (2020). Hematopoiesis: A Layered Organization Across Chordate Species. Front. Cell Dev. Biol. *8*, 606642. https://doi.org/10.3389/fcell.2020.606642.
52. Spangenberg, E., Severson, P.L., Hohsfield, L.A., Crapser, J., Zhang, J., Burton, E.A., Zhang, Y., Spevak, W., Lin, J., Phan, N.Y., et al. (2019). Sustained microglial depletion with CSF1R inhibitor impairs parenchymal plaque development in an Alzheimer's disease model. Nat. Commun. *10*, 3758. https://doi.org/10.1038/s41467-019-11674-z.
53. Elmore, M.R.P., Najafi, A.R., Koike, M.A., Dagher, N.N., Spangenberg, E.E., Rice, R.A., Kitazawa, M., Matusow, B., Nguyen, H., West, B.L., and Green, K.N. (2014). Colony-Stimulating Factor 1 Receptor Signaling Is Necessary for Microglia Viability, Unmasking a Microglia Progenitor Cell in the Adult Brain. Neuron *82*, 380–397. https://doi.org/10.1016/j.neuron.2014.02.040.
54. Gentek, R., Ghigo, C., Hoeffel, G., Bulle, M.J., Msallam, R., Gautier, G., Launay, P., Chen, J., Ginhoux, F., and Bajénoff, M. (2018). Hemogenic Endothelial Fate Mapping Reveals Dual Developmental Origin of Mast Cells. Immunity *48*, 1160–1171.e5. https://doi.org/10.1016/j.immuni.2018.04.025.
55. De, S., Van Deren, D., Peden, E., Hockin, M., Boulet, A., Titen, S., and Capecchi, M.R. (2018). Two distinct ontogenies confer heterogeneity to mouse brain microglia. Development *145*, dev152306. https://doi.org/10.1242/dev.152306.
56. Kiel, M.J., Yilmaz, O.H., Iwashita, T., Yilmaz, O.H., Terhorst, C., and Morrison, S.J. (2005). SLAM Family Receptors Distinguish Hematopoietic Stem and Progenitor Cells and Reveal Endothelial Niches for Stem Cells. Cell *121*, 1109–1121. https://doi.org/10.1016/j.cell.2005.05.026.
57. Edgar, B.A., and O'Farrell, P.H. (1989). Genetic control of cell division patterns in the Drosophila embryo. Cell *57*, 177–187. https://doi.org/10.1016/0092-8674(89)90183-9.
58. Neves, A., and Eisenman, R.N. (2019). Distinct gene-selective roles for a network of core promoter factors in Drosophila neural stem cell identity. Biol. Open *8*, bio042168. https://doi.org/10.1242/bio.042168.
59. Okuda, K., Tong, M., Dempsey, B., Moore, K.J., Gazzinelli, R.T., and Silverman, N. (2016). Leishmania amazonensis Engages CD36 to Drive Parasitophorous Vacuole Maturation. PLOS Pathog. *12*, e1005669. https://doi.org/10.1371/journal.ppat.1005669.
60. Grigorian, M., Liu, T., Banerjee, U., and Hartenstein, V. (2013). The proteoglycan Trol controls the architecture of the extracellular matrix and balances proliferation and differentiation of blood progenitors in the Drosophila lymph gland. Dev. Biol. *384*, 301–312. https://doi.org/10.1016/j.ydbio.2013.03.007.
61. Matsubayashi, Y., Louani, A., Dragu, A., Sánchez-Sánchez, B.J., Serna-Morales, E., Yolland, L., Gyoergy, A., Vizcay, G., Fleck, R.A., Heddleston, J.M., et al. (2017). A Moving Source of Matrix Components Is Essential for De Novo Basement Membrane Formation. Curr. Biol. *27*, 3526–3534.e4. https://doi.org/10.1016/j.cub.2017.10.001.
62. Cattenoz, P.B., Sakr, R., Pavlidaki, A., Delaporte, C., Riba, A., Molina, N., Hariharan, N., Mukherjee, T., and Giangrande, A. (2020). Temporal specificity and heterogeneity of Drosophila immune cells. EMBO J. *39*, e104486. https://doi.org/10.15252/embj.2020104486.
63. Lindner, J.R., Hillman, P.R., Barrett, A.L., Jackson, M.C., Perry, T.L., Park, Y., and Datta, S. (2007). The Drosophila Perlecan gene trol regulates multiple signaling pathways in different developmental contexts. BMC Dev. Biol. *7*, 121. https://doi.org/10.1186/1471-213X-7-121.
64. Fessler, J.H., and Fessler, L.I. (1989). Drosophila Extracellular Matrix. Annu. Rev. Cell. Biol. *5*, 309–339. https://doi.org/10.1146/annurev.cb.05.110189.001521.
65. Yasothornsrikul, S., Davis, W.J., Cramer, G., Kimbrell, D.A., and Dearolf, C.R. (1997). viking: identification and characterization of a second type IV collagen in Drosophila. Gene *198*, 17–25. https://doi.org/10.1016/S0378-1119(97)00274-6.
66. Kusche-Gullberg, M., Garrison, K., MacKrell, A.J., Fessler, L.I., and Fessler, J.H. (1992). Laminin A chain: expression during Drosophila development and genomic sequence. EMBO J. *11*, 4519–4527. https://doi.org/10.1002/j.1460-2075.1992.tb05553.x.
67. Martinek, N., Zou, R., Berg, M., Sodek, J., and Ringuette, M. (2002). Evolutionary conservation and association of SPARC with the basal lamina in Drosophila. Dev. Genes Evol. *212*, 124–133. https://doi.org/10.1007/s00427-002-0220-9.
68. Brand, A.H., and Perrimon, N. (1993). Targeted gene expression as a means of altering cell fates and generating dominant phenotypes. Development *118*, 401–415. https://doi.org/10.1242/dev.118.2.401.
69. Gao, H., Wu, X., and Fossett, N. (2013). Drosophila E-Cadherin Functions in Hematopoietic Progenitors to Maintain Multipotency and Block Differentiation. PLOS ONE *8*, e74684. https://doi.org/10.1371/journal.pone.0074684.
70. Evans, C.J., Liu, T., and Banerjee, U. (2014). Drosophila hematopoiesis: Markers and methods for molecular genetic analysis. Methods *68*, 242–251. https://doi.org/10.1016/j.ymeth.2014.02.038.
71. Khadilkar, R.J., Ho, K.Y.L., Venkatesh, B., and Tanentzapf, G. (2020). Integrins Modulate Extracellular Matrix Organization to Control Cell Signaling during Hematopoiesis. Curr. Biol. *30*, 3316–3329.e5. https://doi.org/10.1016/j.cub.2020.06.027.
72. Shiojiri, N., and Sugiyama, Y. (2004). Immunolocalization of extracellular matrix components and integrins during mouse liver development. Hepatology *40*, 346–355. https://doi.org/10.1002/hep.20303.
73. Mahony, C.B., and Bertrand, J.Y. (2019). How HSCs Colonize and Expand in the Fetal Niche of the Vertebrate Embryo: An Evolutionary Perspective. Front. Cell Dev. Biol. *7*, 34. https://doi.org/10.3389/fcell.2019.00034.
74. Ajami, B., Bennett, J.L., Krieger, C., McNagny, K.M., and Rossi, F.M.V. (2011). Infiltrating monocytes trigger EAE progression, but do not contribute to the resident microglia pool. Nat. Neurosci. *14*, 1142–1149. https://doi.org/10.1038/nn.2887.
75. Misharin, A.V., Morales-Nebreda, L., Reyfman, P.A., Cuda, C.M., Walter, J.M., McQuattie-Pimentel, A.C., Chen, C.-I., Anekalla, K.R., Joshi, N., Williams, K.J.N., et al. (2017). Monocyte-derived alveolar macrophages drive lung fibrosis and persist in the lung over the life span. J. Exp. Med. *214*, 2387–2404. https://doi.org/10.1084/jem.20162152.
76. Bajpai, G., Bredemeyer, A., Li, W., Zaitsev, K., Koenig, A.L., Lokshina, I., Mohan, J., Ivey, B., Hsiao, H.-M., Weinheimer, C., et al. (2019). Tissue Resident CCR2− and CCR2+ Cardiac Macrophages Differentially Orchestrate Monocyte Recruitment and Fate Specification Following Myocardial Injury. Circ. Res. *124*, 263–278. https://doi.org/10.1161/CIRCRESAHA.118.314028.
77. Shechter, R., London, A., Varol, C., Raposo, C., Cusimano, M., Yovel, G., Rolls, A., Mack, M., Pluchino, S., Martino, G., et al. (2009). Infiltrating Blood-Derived Macrophages Are Vital Cells Playing an Anti-inflammatory Role in Recovery from Spinal Cord Injury in Mice. PLOS Med. *6*, e1000113. https://doi.org/10.1371/journal.pmed.1000113.

Developmental Cell
Article

78. Duffield, J.S., Forbes, S.J., Constandinou, C.M., Clay, S., Partolina, M., Vuthoori, S., Wu, S., Lang, R., and Iredale, J.P. (2005). Selective depletion of macrophages reveals distinct, opposing roles during liver injury and repair. J. Clin. Invest. *115*, 56–65. https://doi.org/10.1172/JCI22675.

79. Weinberger, T., Esfandyari, D., Messerer, D., Percin, G., Schleifer, C., Thaler, R., Liu, L., Stremmel, C., Schneider, V., Vagnozzi, R.J., et al. (2020). Ontogeny of arterial macrophages defines their functions in homeostasis and inflammation. Nat. Commun. *11*, 4549. https://doi.org/10.1038/s41467-020-18287-x.

80. Blériot, C., Dupuis, T., Jouvion, G., Eberl, G., Disson, O., and Lecuit, M. (2015). Liver-Resident Macrophage Necroptosis Orchestrates Type 1 Microbicidal Inflammation and Type-2-Mediated Tissue Repair during Bacterial infection. Immunity *42*, 145–158. https://doi.org/10.1016/j.immuni.2014.12.020.

81. Wang, T., Zhang, J., Wang, Y., Li, Y., Wang, L., Yu, Y., and Yao, Y. (2023). Influenza-trained mucosal-resident alveolar macrophages confer long-term antitumor immunity in the lungs. Nat. Immunol. *24*, 423–438. https://doi.org/10.1038/s41590-023-01428-x.

82. Madsen, D.H., Jürgensen, H.J., Siersbæk, M.S., Kuczek, D.E., Grey Cloud, L.G., Liu, S., Behrendt, N., Grøntved, L., Weigert, R., and Bugge, T.H. (2017). Tumor-Associated Macrophages Derived from Circulating Inflammatory Monocytes Degrade Collagen through Cellular Uptake. Cell Rep. *21*, 3662–3671. https://doi.org/10.1016/j.celrep.2017.12.011.

83. Zhu, Y., Herndon, J.M., Sojka, D.K., Kim, K.-W., Knolhoff, B.L., Zuo, C., Cullinan, D.R., Luo, J., Bearden, A.R., Lavine, K.J., et al. (2017). Tissue-Resident Macrophages in Pancreatic Ductal Adenocarcinoma Originate from Embryonic Hematopoiesis and Promote Tumor Progression. Immunity *47*, 323–338.e6. https://doi.org/10.1016/j.immuni.2017.07.014.

84. Hutter, G., Theruvath, J., Graef, C.M., Zhang, M., Schoen, M.K., Manz, E.M., Bennett, M.L., Olson, A., Azad, T.D., Sinha, R., et al. (2019). Microglia are effector cells of CD47-SIRPα antiphagocytic axis disruption against glioblastoma. Proc. Natl. Acad. Sci. USA *116*, 997–1006. https://doi.org/10.1073/pnas.1721434116.

85. Loyher, P.L., Hamon, P., Laviron, M., Meghraoui-Kheddar, A., Goncalves, E., Deng, Z., Torstensson, S., Bercovici, N., Baudesson de Chanville, C., Combadière, B., et al. (2018). Macrophages of distinct origins contribute to tumor development in the lung. J. Exp. Med. *215*, 2536–2553. https://doi.org/10.1084/jem.20180534.

86. Destalminil-Letourneau, M., Morin-Poulard, I., Tian, Y., Vanzo, N., and Crozatier, M. (2021). The vascular niche controls Drosophila hematopoiesis via fibroblast growth factor signaling. eLife *10*, e64672. https://doi.org/10.7554/eLife.64672.

87. Shim, J., Mukherjee, T., and Banerjee, U. (2012). Direct sensing of systemic and nutritional signals by haematopoietic progenitors in Drosophila. Nat. Cell Biol. *14*, 394–400. https://doi.org/10.1038/ncb2453.

88. Shim, J., Mukherjee, T., Mondal, B.C., Liu, T., Young, G.C., Wijewarnasuriya, D.P., and Banerjee, U. (2013). Olfactory control of blood progenitor maintenance. Cell *155*, 1141–1153. https://doi.org/10.1016/j.cell.2013.10.032.

89. Cho, B., Spratford, C.M., Yoon, S., Cha, N., Banerjee, U., and Shim, J. (2018). Systemic control of immune cell development by integrated carbon dioxide and hypoxia chemosensation in Drosophila. Nat. Commun. *9*, 2679. https://doi.org/10.1038/s41467-018-04990-3.

90. Travnickova, J., Tran Chau, V., Julien, E., Mateos-Langerak, J., Gonzalez, C., Lelièvre, E., Lutfalla, G., Tavian, M., and Kissa, K. (2015). Primitive macrophages control HSPC mobilization and definitive haematopoiesis. Nat. Commun. *6*, 6227. https://doi.org/10.1038/ncomms7227.

91. Mass, E., Ballesteros, I., Farlik, M., Halbritter, F., Günther, P., Crozet, L., Jacome-Galarza, C.E., Händler, K., Klughammer, J., Kobayashi, Y., et al. (2016). Specification of tissue-resident macrophages during organogenesis. Science *353*, aaf4238. https://doi.org/10.1126/science.aaf4238.

92. Han, X., Wang, R., Zhou, Y., Fei, L., Sun, H., Lai, S., Saadatpour, A., Zhou, Z., Chen, H., Ye, F., et al. (2018). Mapping the Mouse Cell Atlas by Microwell-Seq. Cell *172*, 1091–1107.e17. https://doi.org/10.1016/j.cell.2018.02.001.

93. Yoon, S., Cho, B., Shin, M., Koranteng, F., Cha, N., and Shim, J. (2017). Iron Homeostasis Controls Myeloid Blood Cell Differentiation in Drosophila. Mol. Cells *40*, 976–985. https://doi.org/10.14348/molcells.2017.0287.

94. Kurucz, E., Váczi, B., Márkus, R., Laurinyecz, B., Vilmos, P., Zsámboki, J., Csorba, K., Gateff, E., Hultmark, D., and Andó, I. (2007). Definition of Drosophila hemocyte subsets by cell-type specific antigens. Acta Biol. Hung. *58* (suppl), 95–111. https://doi.org/10.1556/ABiol.58.2007.Suppl.8.

95. Díaz-Torres, A., Rosales-Nieves, A.E., Pearson, J.R., Santa-Cruz Mateos, C., Marín-Menguiano, M., Marshall, O.J., Brand, A.H., and González-Reyes, A. (2021). Stem cell niche organization in the Drosophila ovary requires the ECM component Perlecan. Curr. Biol. *31*, 1744–1753.e5. https://doi.org/10.1016/j.cub.2021.01.071.

96. Van De Bor, V., Zimniak, G., Papone, L., Cerezo, D., Malbouyres, M., Juan, T., Ruggiero, F., and Noselli, S. (2015). Companion Blood Cells Control Ovarian Stem Cell Niche Microenvironment and Homeostasis. Cell Rep. *13*, 546–560. https://doi.org/10.1016/j.celrep.2015.09.008.

97. Schindelin, J., Arganda-Carreras, I., Frise, E., Kaynig, V., Longair, M., Pietzsch, T., Preibisch, S., Rueden, C., Saalfeld, S., Schmid, B., et al. (2012). Fiji: an open-source platform for biological-image analysis. Nat. Methods *9*, 676–682. https://doi.org/10.1038/nmeth.2019.

98. Peixoto, M.M., Soares-da-Silva, F., Bonnet, V., Ronteix, G., Santos, R.F., Mailhe, M.-P., Feng, X., Pereira, J.P., Azzoni, E., Anselmi, G., et al. (2023). Spatiotemporal dynamics of cytokines expression dictate fetal liver hematopoiesis. Preprint at bioRxiv. https://doi.org/10.1101/2023.08.24.554612.

CellPress

Developmental Cell
Article

STAR★METHODS

KEY RESOURCES TABLE

REAGENT or RESOURCE	SOURCE	IDENTIFIER
Antibodies		
chicken anti-GFP	abcam	Cat# 13970; RRID: AB_300798
rabbit anti-Peroxidasin	gift from Jiwon Shim, Hanyang University (Yoon et al.[93])	N/A
mouse anti-Hemese	gift from István Andó, HUN Biological Research Centre (Kurucz et al.[44])	N/A
mouse anti-PH3	Millipore	Cat# 05-806; RRID: AB_310016
rabbit ati-Dcp1	Cell signaling	Cat# 9578; RRID: AB_2721060
mouse anti-Atilla	gift from István Andó, HUN Biological Research Centre (Kurucz et al.[94])	N/A
mouse anti-L4	gift from István Andó, HUN Biological Research Centre (Kurucz et al.[94])	N/A
rabbit anti trol	gift from Acaimo González-Reyes, CSIC/Universidad Pablo de Olavide/JA (Díaz-Torres et al.[95])	N/A
rabbit anti Cg25c	gift from Stéphane Noselli, University of Nice Sophia Antipolis, Institut de Biologie Valrose (Van De Bor et al.[96])	N/A
mouse anti-Antp	DSHB	Cat# anti-Antp 4C3; RRID: AB_528082
mouse anti-Antp	DSHB	Cat# anti-Antp 8C11; RRID: AB_528083
Rat anti-E-Cadherin	DSHB	Cat# DCAD2; RRID: AB_528120
mouse anti-βPS integrin	DSHB	Cat# cf.6g11; RRID: AB_528310
mouse anti-Wg	DSHB	Cat# 4d4; RRID: AB_528512
donkey anti-chicken FITC	Jackson ImmunoResearch	Cat# 703-095-155; RRID: AB_2340356
goat anti-mouse Alexa Fluor 647	Jackson ImmunoResearch	Cat# 115-605-166; RRID: AB_2338914
donkey anti-rabbit Cy3	Jackson ImmunoResearch	Cat# 711-165-152; RRID: AB_2307443
CD16/32 BUV737 (Clone 2.4G2)	BD Biosciences	Cat# 612783; RRID:AB_2870112
CD16/32 BV711 (Clone 2.4G2)	Biolegend	Cat# 101337; RRID:AB_2565637
CD16/32 Fc Block™ (Clone 2.4G2)	BD Biosciences	Cat# 553142; RRID:AB_394657
CD45 BUV395 (Clone 30-F11)	BD Biosciences	Cat# 564279; RRID:AB_2651134
CD45 BV510 (Clone 30-F11)	BD Biosciences	Cat# 563891 ; RRID:AB_2734134
CD45 FITC (Clone 30-F11)	BD Biosciences	Cat# 553080 ; RRID:AB_394610
F4/80 BV785 (Clone BM8)	Biolegend	Cat# 123141; RRID:AB_2563667
F4/80 BV421 (Clone BM8)	Sony Biotechnology Inc.	Cat# 1215660; RRID: AB_11203717
F4/80 biotin (Clone BM8)	Biolegend	Cat# 123106; RRID:AB_893501
Ly-6G BV711 (Clone 1A8)	BD Biosciences	Cat# 563979; RRID:AB_2738520
Ly-6G BV421 (Clone 1A8)	BD Biosciences	Cat# 562737; RRID:AB_2737756
Ly-6C BV510 (Clone HK1.4)	Biolegend	Cat# 128033 ; RRID:AB_2562351
Ly-6C eF450 (Clone HK1.4)	eBioscience	Cat# 15321810
Sca-1 BV711 (Clone D7)	Biolegend	Cat# 108131; RRID:AB_2562241
Sac-1 BV510 (Clone D7)	Biolegend	Cat# 108129; RRID:AB_2561593
CD34 eF450 (Clone RAM34)	eBioscience	Cat# 48-0341-82; RRID:AB_2043837

(Continued on next page)

Developmental Cell
Article

CellPress

Continued

REAGENT or RESOURCE	SOURCE	IDENTIFIER
CD34 eF660 (Clone RAM34)	eBioscience	Cat# 50-0341-80; RRID:AB_10609352
Ter119 BV785 (Clone TER-119)	Biolegend	Cat# 116245; RRID:AB_2650921
Ter119 biotin (Clone TER-119)	Biolegend	Cat# 116204; RRID:AB_313705
CD19 biotin (Clone 1D3)	BD Biosciences	Cat# 553784; RRID:AB_395048
CD3e biotin (Clone 145-2C11)	BD Biosciences	Cat# 553060; RRID:AB_394593
Gr1 biotin (Clone RB6-8C5)	BD Biosciences	Cat# 553124; RRID:AB_394640
NK1.1 biotin (Clone PK136)	Biolegend	Cat# 108704; RRID:AB_313391
CD115 FITC (Clone AFS98)	TONBObiosciences	Cat# TNB35-1152-U025
CD115 PE (Clone AFS98)	eBioscience	Cat# 12-1152-83; RRID:AB_465809
CD115 PE-CF594 (Clone AFS98)	Biolegend	Cat# 135527; RRID:AB_2566522
CD115 APC (Clone AFS98)	eBioscience	Cat# 17-1152-82; RRID:AB_1210789
Flt3 PE-CF594 (Clone A2F10)	BD Biosciences	Cat# 562537 ; RRID:AB_2737639
Kit BV711 (Clone 2B8)	BD Biosciences	Cat# 563160; RRID:AB_2722510
Kit PE (Clone 2B8)	BD Biosciences	Cat# 553355; RRID:AB_394806
Kit APC-Cy7 (Clone 2B8)	Sony Biotechnology Inc.	Cat# 1129130; RRID: AB_1626278
CD11b PE (Clone M1/70)	Biolegend	Cat# 101208; RRID:AB_312791
CD11b PE-Cy7 (Clone M1/70)	BD Biosciences	Cat# 552850; RRID:AB_394491
CD11b BB515 (Clone M1/70)	BD Biosciences	Cat# 564454; RRID:AB_2665392
CD11b APC-Cy7 (Clone M1/70)	BD Biosciences	Cat# 557657; RRID:AB_396772
CD11b AF700 (Clone M1/70)	BD Biosciences	Cat# 557960; RRID:AB_396960
CD150 PE-Cy7 (Clone mShad150)	eBioscience	Cat# 25-1502-80; RRID:AB_10804766
CD48 BUV395 (Clone HM48-1)	BD Biosciences	Cat# 740236; RRID:AB_2739984
CD64 BV711 (Clone X54-5/7.1)	Biolegend	Cat# 139311 ; RRID:AB_2563846
CD64 PE-Cy7 (Clone X54-5/7.1)	Sony Biotechnology Inc.	Cat# 1296570; RRID:AB_2917921
CD64 APC (Clone X54-5/7.1)	Biolegend	Cat# 139306; RRID:AB_11219391
CD41 BUV395 (Clone MWReg30)	BD Biosciences	Cat# 752966; RRID: AB_2917921
Tim4 BUV737 (Clone RMT4-54)	BD Biosciences	Cat# 749134; RRID:AB_2873523
Tim4 PE-Cy7 (Clone RMT4-54)	Biolegend	Cat# 130010; RRID:AB_2565719
IL33Ra (ST2) PE/Dazzle (Clone DIH9)	Biolegend	Cat# 145314; RRID:AB_2687364
Ki67 AlexaFluor647 (Clone B56)	BD Biosciences	Cat# 558615; RRID:AB_647130
Streptavidin BUV737	BD Biosciences	Cat# 564293; RRID: AB_2869560
Streptavidin BV785	Biolegend	Cat# 405249
rat anti-mouse CD68	Biorad	Cat# MCA1957; RRID:AB_322219
rabbit anti-mouse Collagen IV	Biorad	Cat# 2150-1470; RRID:AB_2082660
goat anti-rat AF555	Invitrogen	Cat# A-21434; RRID:AB_1417833
goat anti-rabbit AF555	Invitrogen	Cat# A-21429; RRID:AB_2535850
Chemicals, peptides, and recombinant proteins		
N-Phenylthiourea	Sigma-Aldrich	P7629
PFA	Electron Microscopy Sciences	50-980-487
NGS	Vector Laboratories	Cat# S-10000
DAPI	Sigma-Aldrich	Cat# D9542
Vectashield	Vector Laboratories	H-1000-10
TRI-reagent	Molecular Research Center	TR 118
AIN-76A Rodent Diet With 1,200 mg PLX5622 (Free Base)/kg	Research Diets, Inc.	Cat# D11100404i; Lot: 21121410A5HSi
4-Hydroxytamoxifen	Sigma	Cat# H7904-25MG
Kolliphor EL	Sigma	Cat# C5135-500G
Progesterone	Sigma	Cat# P3972-5G
Sunflower oil	Sigma	Cat# S5007-250ML

(*Continued on next page*)

Continued

REAGENT or RESOURCE	SOURCE	IDENTIFIER
0.5M EDTA pH 8.0	Invitrogen	Cat# AM9260G
Collagenase D	Sigma	Cat# 11088882001
DNase I	Sigma	Cat# DN25-100MG
Dispase II	Invitrogen	Cat# 17105-041
Liberase DL	Roche	Cat# 5466202001
Collagenase I	Gibco	Cat# 17018029
ChromPure Mouse IgG	Jackson ImmunoResearch	Cat# 015-000-003; RRID:AB_2337188
Sytox™ Green dead cell stain	Invitrogen	Cat# S34860
RNAprotect	Qiagen	Cat# 76104
Stainless steel bead	Qiagen	Cat# 69989
Tissue Lyser II	Qiagen	Cat# 85300
Formalin solution, neutral buffered, 10%	Sigma	Cat# HT5014-1CS
O.C.T™	Tissue-Tek®	Cat# 4583
Dapi (mouse experiments)	Invitrogen	Cat# 10116287
NGS (mouse experiments)	Gibco	Cat# 16210064
RapiClear® 1.52	SUNJin Lab	Cat# RC152001
ProLong™ Gold Antifade Mounting	Invitrogen	Cat# P36930
Stem Cell Factor (Kit ligand)	N/A	N/A
Mouse Granulocyte Macrophage Colony Stimulating Factor (mGM-CSF)	Cell Signaling Technology	Cat# 70343
Mouse Macrophage Colony Stimulating Factor (mM-CSF)	Cell Signaling Technology	Cat# 33444
rmEpo (Recombinant Mouse Erythropoietin)	R&D Systems	Cat# 959-ME-010
rmTpo (Recombinant Mouse Thrombopoietin)	R&D Systems	Cat# 488-TO-025
OptiMEM-I W/Glutamax	Gibco	51985026
2-Mercaptoethanol	Gibco	31350010
Penicillin Streptomycin Solution	Gibco	15070063
Critical commercial assays		
DNase I recombinant RNase free	Roche	Cat# 04716728001
Super-Script IV	Invitrogen	Cat# 18091050
SYBR Green I Master Mix	Roche	Cat# 04673492001
RNeasy Plus Mini Kit	Qiagen	Cat# 74134
PrimeScript™ RT Reagent Kit	Takara	Cat# RR037A
TaqMan™ Fast Advanced Master Mix	Applied Biosystems™	Cat# 12634225
Mouse Immune array	Applied Biosystems™	Cat# 4418724
Customized mouse Extracellular Matrix and Adhesion molecules plates	Applied Biosystems™	N/A
BD Cytofix/Cytoperm™	BD Biosciences	Cat# 554714
In Situ Cell Death Detection Kit, TMR red	Roche	Cat# 12156792910
Anti-Biotin MicroBeads	Miltenyi Biotec	Cat# 130-090-485
MS columns	Miltenyi Biotec	Cat# 130-042-201
Experimental models: Organisms/strains		
Fly: *w^{1118}*	BDSC	5905
Fly: *HmlΔGal4, UAS-2XEGFP*	BDSC	30140
Fly: *HmlΔGal4*	BDSC	30139
Fly: *UAS-hid*	BDSC	65403
Fly: *stg* RNAi	BDSC	36094
Fly: *eater RNAi*	BDSC	25863
Fly: *trol RNAi*	BDSC	29440

(*Continued on next page*)

Developmental Cell
Article

CellPress

Continued

REAGENT or RESOURCE	SOURCE	IDENTIFIER
Fly: *vkg RNAi*	BDSC	50895
Fly: *UAS-trol*	BDSC	65273
Fly: *UbiGal4*	BDSC	32551
Fly: *domeMeso-EBFP2*	gift from Jiwon Shim, Hanyang University (Evans et al.[70])	N/A
Mouse: *Cdh5*^{CreERT2}	Gift from Ralf H Adams, Max Planck Institute for Molecular Biomedicine.	MGI:3848982
Mouse: *Rosa26*^{tdTomato}	Institut Pasteur animal facility	MGI:3809524
Mouse: C57BL/6JRj	Janvier	RRID:IMSR_RJ:C57BL-6JRJ
Oligonucleotides		
Act5C (F) GCAAGAGGATCAGGATCGGG *(R)* TGCTGCACTCCAAACTTCCA	Sigma-Aldrich	N/A
Rp49 (F) GACGCTTCAAGGGACAGTA *(R)* AAACGCGGTTCTGCATGAG	Sigma-Aldrich	N/A
Hml (F) AATCGAGAGCACCCGGAAAG *(R)* GCCACAACTGATGGGACAGA	Sigma-Aldrich	N/A
Pxn (F) AACTGCCCCAGGATACACAAA *(R)* TAAGCCAGCTCGTTGTCGTT	Sigma-Aldrich	N/A
Eater (F) ATGGCTGTAGCAACGGAGTTT *(R)* CTTGCAAACAGGAGTGCAGAC	Sigma-Aldrich	N/A
NimC1 (F) ATCGAGTGGTCAACTGGTGTG *(R)* GTCAGGAATCCGTACCTCAGC	Sigma-Aldrich	N/A
Upd2 (F) ACAACCTGCGACTCTTCTCC *(R)* CAGATTGCCGTACTCCAGGG	Sigma-Aldrich	N/A
Upd3 (F) TCTGGACTGGGAGAACACCT *(R)* CTCACTGTGGCCAGCTTGT	Sigma-Aldrich	N/A
Trol (F) TACTCCTGCGTTGCCGAAAA *(R)* AATCTTTACACTCGGCCGCT	Sigma-Aldrich	N/A
Viking (F) TTCTGGGCGTCGTTTATCTGT *(R)* CTTTGCAGTCGCATAGCGTT	Sigma-Aldrich	N/A
Col4alpha1 (F) AGGCTTAAGTGCATAGGGCAT *(R)* TTGTAGTGTTTCACGGAGTCCT	Sigma-Aldrich	N/A
Software and algorithms		
Fiji	N/A	RRID:SCR_002285; https://fiji.sc/
IMARIS	Oxford Instruments	RRID:SCR_007370
CytExpert software	Beckman Coulter	RRID:SCR_017217
BD FACSDiva Software	BD (Becton Dickinson)	RRID:SCR_001456
GraphPad Prism v10.1	GraphPad Software Inc.	RRID:SCR_002798; https://www.graphpad.com/scientific-software/prism/

(*Continued on next page*)

CellPress

Developmental Cell
Article

Continued

REAGENT or RESOURCE	SOURCE	IDENTIFIER
FlowJo™ v10.10.0	FlowJo Inc.	RRID:SCR_008520; https://www.flowjo.com/solutions/flowjo/downloads
Biorender.com	Biorender	RRID:SCR_018361; https://www.biorender.com
Adobe Illustrator v27.9.1	Adobe	RRID:SCR_010279; https://www.adobe.com/products/illustrator.html
Leica Application Suite X	Leica	RRID: SCR_013673; https://www.leica-microsystems.com/products/microscope-software/details/product/leica-las-x-ls/

RESOURCE AVAILABILITY

Lead contact

Further information and requests for reagents should be directed to and will be fulfilled by corresponding authors E. Gomez Perdiguero (elisa.gomez-perdiguero@pasteur.fr) and A. Giangrande (angela@igbmc.fr). The lead contact is A. Giangrande.

Materials availability

This study did not generate new unique reagents.

Data and code availability

- Data reported in this paper will be shared by the lead contact upon request.
- This paper does not report original codes.
- Any additional information required to reanalyze the data reported in this paper is available from the lead contact upon request.

EXPERIMENTAL MODEL AND STUDY PARTICIPANT DETAILS

Fly lines

All flies were raised on standard media at 25°C. The following strains were used: w^{1118}(reference line), *HmlΔGal4, UAS-2XEGFP* (BDSC #30140), *HmlΔGal4* (BDSC #30139), *UAS-hid* (BDSC #65403), *stg* RNAi (BDSC 36094), *eater RNAi* (BDSC #25863), *trol RNAi* (BDSC 29440), *vkg RNAi* (BDSC 50895), *UAS-trol* (BDSC 65273), *UbiGal4* (BDSC #32551), *domeMeso-EBFP2* (gift from Jiwon Shim[70]). Optimized conditions were used to obtain stage-synchronized progeny. Adult flies were let lay on apple juice agar plates for 3 h at 25°C. The plates were transferred at 25°C or 29°C according to the experimental set up. L1 larvae were selected 24 h after egg lay, transferred in batches of 100 larvae on fresh medium and raised at the desired temperature until the stage of the analysis. Unless otherwise specified, male larvae were used to avoid gender-related variability since males and females show different organs/body size and macrophage number.

Mouse lines

All mice used in this study have been previously described. Experimental procedures, housing and husbandry were in compliance with the regulatory guidelines of the Institut Pasteur Committee for Ethics and Animal Experimentation (CETEA, dap160091). Strains included $Cdh5^{CreERT2}$ transgenic (C57Bl6 background, MGI:3848982) and $Rosa26^{tdTomato}$ mice. Timed matings were performed and the date of vaginal plug was considered E0.5. Embryonic stage was validated using morphological landmarks. Genotyping procedures are available upon request. To deplete macrophages, we used the selective CSF1R-inhibitor PLX5622. Control and PLX5622 (1200 ppm formulated in AIN-76A standard chow, Research Diets, Inc.) chows were kindly provided by Plexxikon Inc (Berkeley, CA) and administered to pregnant dams.

METHOD DETAILS

Fly macrophage immunolabeling

Macrophages were collected upon bleeding larvae in cold PBS 1X added with N-Phenylthiourea (Sigma-Aldrich P7629) to avoid cell melanization. The amount was adjusted according to the stage in analysis: 10 wL3 larvae were bled in 100 µl, 20 midL2 larvae were bled in 50 µl. Cells were let decant on the slide for 20 min at room temperature (RT) or cytospinned at 500 rpm for 3 min for lamellocyte immunolabeling due to the poor adhesion of lamellocytes to the slide by decantation. The cells were then fixed in 4% paraformaldehyde (PFA)/PBS 1X for 10 min, washed three times with PTX (0.3% Triton X-100 in PBS 1X) for 10 min, incubated 1 h in PTXN

Developmental Cell
Article

CellPress

(NGS 5% in PTX, Vector Laboratories), incubated ON at 4°C in primary antibodies diluted in PTXN. Cells were then washed with PTX for 10 min, incubated 1 h in secondary antibodies diluted in PTXN, incubated 1 h with DAPI (1:5000, Sigma-Aldrich), washed with PTX and then mounted with Vectashield mounting medium. The following primary antibodies were used: chicken anti-GFP (1:500, abcam ab13970), rabbit anti-Peroxidasin (1:2000, gift from J. Shim[93]), mouse anti-Hemese (1:50, gift from I. Ando[44]), mouse anti-PH3 (1:1000, Millipore 3H10), rabbit ati-Dcp1 (1:200, Cell signaling 9578), mouse anti-Atilla and mouse anti-L4 (1:50, gift from I. Ando[94]). The donkey anti-chicken FITC (Jackson ImmunoResearch # 703 095 155) and goat anti-mouse Alexa Fluor 647 (Jackson ImmunoResearch # 115 605 166), donkey anti-rabbit Cy3 (Jackson ImmunoResearch # 711-165-152) secondary antibodies were used at 1:400. For each marker, at least two independent experiments were performed.

Lymph gland immunolabeling

Lymph glands were dissected in PBS 1X, fixed in 4% PFA/PBS 1X for 30 min, washed three times with PTX for 10 min, incubated 1 h in PTXN, incubated ON at 4°C in primary antibodies diluted in PTXN. After 3 washes with PTX of 10 min each, lymph glands were incubated 20 min in PTXN, incubated 2 h in secondary antibodies diluted in PTXN, incubated 30 min with DAPI, washed twice with PTX, then transferred in PBS 1X and mounted with Vectashield mounting medium. The following primary antibodies were used in addition to those previously mentioned: rabbit anti trol (1:1000, gift from A. González Reyes[95]), rabbit anti Cg25c (1:500, gift from S. Noselli[96]), mouse anti-Antp (1:50, DSHB 4C3, DSHB 8C11), Rat anti-E-Cadherin (1:50, DSHB DCAD2), mouse anti-βPS integrin (1:50, DSHB CF.6G11), mouse anti-Wg (1:5, DSHB 4D4). See above for secondary antibodies.

Image acquisition on fly macrophages and lymph glands

Images were acquired using a Leica SP8 inverted-based confocal microscope equipped with 20, 40 and 63X objectives. A647/Cy5 was excited at 633 nm and emission signal was collected with 650-700 filters. GFP/FITC was excited at 488 nm and the emission signal was collected with 500-550 filters. RFP/Cy3 was excited at 561 nm and the emission signal was collected with 570-620 filters. Z-series images were acquired using a Z-step size between 0.5 and 2μm and applying identical settings for control and experimental genotypes. Confocal images were analyzed with Fiji software (RRID:SCR_002285).[97]

Transmission electron microscopy

Samples for transmission electron microscopy were prepared according to published protocols.[28] Briefly, early-midL2 larvae (~45 h after egg laying) raised at 29°C were dissected in 4% PFA/PBS 1X and incubated in a fixative solution of 3.2% EM grade PFA and 3.125% Glutaraldehyde at 4°C for at least 1 day. Post-fixation was carried out in 1% osmium tetroxide. Tissue was dehydrated through acetone series at 4°C, embedded with a graded series of epon:acetone mixtures at room temperature in flexible plastic mold and finally polymerized at 60 °C for 48 h. Ultra-thin serial sections of 70 nm were picked up on grids, contrasted with uranyl acetate and lead citrate and examined using a CM12 TEM electron microscope 100Kv (FEI) equipped with a CCD ORIUS 1000 Gatan Camera.

RNA extraction and RT-qPCR on fly macrophages and larvae

To assess the expression levels of genes of interest in macrophages, at least 30 earlyL2 (~48 h after egg laying) larvae from both sexes were bled in 100 μl of cold PBS 1X added with N-Phenylthiourea. RNA extraction was performed as follows. 1 ml of TRI-reagent (Molecular Research Center) was added to the collected macrophages, and the samples were left at RT for 5 min to ensure complete dissociation. 0.2 ml of chloroform was added to each sample followed by centrifugation at 12,000 g for 15 min at 4°C. The upper aqueous phase containing the RNA was collected and transferred to a fresh autoclaved tube. 0.5 ml of 2-propanol was added, and the samples were incubated for 10 min at RT. The RNA was precipitated by centrifugation, washed with 1 ml of 75% ethanol, precipitated again, and air-dried. 20 μl of RNase-free water was used to resuspend the pellet and the samples were incubation at 55°C for 15 min to facilitate the resuspension. The extracted RNA was then treated with DNase I recombinant RNase free (Roche) and the reverse transcription was done using the Super-Script IV (Invitrogen) with random primers. The cycle program used for the reverse transcription is 65°C for 10 minutes, 55°C for 20 minutes, 80°C for 10 minutes. The qPCR was performed using SYBR Green I Master (Roche). Actin5C (Act5C) and Ribosomal protein 49 (Rp49) were used to normalize the data.

To assess the expression levels of the ECM components *trol*, *vkg* and *Col4alpha1* upon ubiquitous induction of *trol RNAi*, total RNA from 4 control or *trol RNAi* wandering L3 larvae was extracted and treated as above described.

4OHT Preparation and Injection

4-hydroxytamoxifen (4OHT) (Sigma, H7904-25MG) was dissolved in equal parts of ethanol and Kolliphor EL (Sigma C5135-500G) by sonication. 10mg/mL stocks of progesterone (P3972-5G) were prepared by resuspending in ethanol and sunflower oil (Sigma S5007-250ML). For pulse-labeling, females were weighed on day 7 or 10 and 37.5μg/g (body weight) 4OHT were co-injected with 18.75μg/g (body weight) progesterone to reduce the risk of abortion.

Flow Cytometry

Pregnant mice were killed by cervical dislocation and embryos were dissected in cold PBS. Fetal peripheral blood was collected in 2mM EDTA by severing the vitelline and umbilical vessels after removing the placenta and extraembryonic membranes. Organs were enzymatically dissociated in digestion buffer composed of PBS with 1mg/mL collagenase D (Sigma 11088882001), 100 U/mL DNaseI

CellPress
Developmental Cell
Article

(DN25-100mg) and 3% Fetal Bovine Serum. Cells were passed through 100μm strainers by mashing with the piston of a 2mL syringe and then collected in cold filtered FACS Buffer (0.5% BSA and 2mM EDTA in PBS). Cells were then pelleted by centrifugation at 320*g* for 7 minutes. Blocking was performed with 5% FBS and 1:20 Mouse IgG (Interchim 015-000-003) or in 1:50 Fc-block (anti-CD16/32) in FACS Buffer followed by 30 minutes of antibody staining. Cells were washed and incubated with fluorescently-conjugated streptavidin for 20 minutes. For experiments with adult mice, blood was collected by retro-orbital bleeding. After sacrificing mice by cervical dislocation perfusion was performed by gentle intracardiac injection of 10 ml prewarmed (37°C) PBS. Adult tissues were minced with scissors before enzymatical digestion in digestion buffer composed of PBS with 1mg/mL collagenase D (Sigma 11088882001), 100 U/mL DNaseI (DN25-100mg), 2.4mg Dispase II (Invitrogen 17105-041) and 3% Fetal Bovine Serum. For livers, hepatocyte removal was performed by centrifugation of the whole liver single cell suspension at 50*g* for 3 minutes. For earskin, epidermal sheets were first separated from the dermis after incubation for 1h at 37°C in 2.4 mg/ml of Dispase II in PBS and the epidermis was further digested for 30 min in PBS containing 1 mg/ml collagenase D, 100 U/ml DNase I, 2.4 mg/ml of Dispase II and 3% FBS at 37°C. Bone marrow was flushed from the femur and tibia using a 25G needle. For red blood cell lysis, cells were resuspended in 1 ml of Red blood cell lysis buffer (155 mM NH_4Cl, 10 mM $NaHCO_3$, and 0.1 mM EDTA). The reaction was terminated after 5 min by adding 3 ml of FACS buffer. Lysis was performed once for adult livers and bone marrows and twice for adult blood samples. Stained cells were passed on the Cytoflex LX (Beckman Coulter). Results were analyzed and plots generated using FlowJo.

RNA extraction and quantitative qPCR on mouse fetal liver

Fetal livers were dissected in ice-cold PBS and directly transferred to RNAprotect (Qiagen, 76104) for short term-storage. After transfer of 10mg of fetal liver tissue into RLT buffer (RNeasy Plus Mini Kit, Qiagen, 74134) with 1% beta-Mercaptoethanol, livers were lysed and homogenized by bead-milling with a 5 mm stainless steel bead (Qiagen, 69989) in the TissueLyserII (Qiagen) twice for 2 min at 30 Hz. Total RNA was extracted from whole tissue lysate using the RNeasy Plus Mini Kit (Qiagen, 74134), using 50 % ethanol in step 5. cDNA was reverse transcribed using PrimeScript™ RT Reagent Kit (Perfect Real Time) (Takara, RR037A) and following manufacturer's instructions. Taqman assays (Mouse Immune array- Applied BiosystemsTM, 4418724 or customized mouse Extracellular Matrix and Adhesion molecules plates) were performed on a Quantstudio 3 thermocycler (Applied Biosystems, 50 °C 2 min, 95 °C 20 sec, 40 cycles : 95 °C 3 sec and 60 °C 30 sec, 60 °C 30 sec) using 20 ng of cDNA in 1x TaqMan™ Fast Advanced Master Mix (Applied Biosystems™, 12634225) per well. Gene expression was normalized to *gapdh* or *hprt1* and relative expression was calculated using the $2^{-\Delta\Delta}$ method.

Fetal liver immunolabeling

Dissected fetal livers were fixed in 5 % Formalin solution containing 2 % formaldehyde (Sigma) in PBS at 4 °C overnight, washed 3 times in PBS, immersed in 30% sucrose overnight, cryoembedded in OCT (Tissue-Tek) and stored at -80 °C. 12μm thin sections were cut on a Leica Cryostat at -25 °C. Sections were washed in PBS for 5 min, permeabilized in PBS-Triton 0.5% (PBS-T) for 5 min, washed in PBS for 5 min and finally blocked in 5 % normal goat serum in 0.1 % PBS-T for 1 hour. Fetal liver sections were stained with primary antibodies in blocking solution for 1 hour (rabbit anti-mouse Collagen IV 1:200 (Biorad, 2150-1470)), washed 3 times in 0.1 % PBS-T for each 5 min, stained with secondary antibodies (goat anti-rabbit AF555 1:500 (Invitrogen, A-21429)) and washed 3 times in 0.1 % PBS-T. Permeabilization, blocking and staining were all performed at room temperature. Stained sections were covered with ProLong™ Gold Antifade Mounting (Invitrogen, P36930). Sections were imaged as z-stacks of 8 μm depth (9 planes with a distance of 1 μm) in tilescans using an inverted Leica SP8 confocal microscope with a HC PL APO 20x/0,75 CS2 objective (Leica, 11506517) and the LasX software. AF555 was excited at 552 nm and the emission signal was collected with a HyD detector set at 562-600nm. Final image processing (flipping of images and adding of scale bars) was performed in Fiji.[97]

Fetal Liver TUNEL Assay

Fresh 100μm thick fetal liver (FL) sections were prepared as mentioned elsewhere.[98] Sections were permeabilized and blocked in 10% Normal Goat Serum in PBS-Triton 0.5% (PBS-T) for 2 hours at room temperature, incubated with rat anti-mouse CD68 (1:100) in bocking solution overnight at 4C and finally washed 3x 20 min in 0.1% PBS-T. Secondary staining was performed by incubation with goat anti-rat AF555 (1:500) in 0.1 % PBS-T for 2h at room temperature in the dark. FL sections were washed 3x 20 min in 0.1% PBS-T. Thick sections were incubated in 200μL of TUNEL reaction mix (Roche, Cat. No. 12156792910) for 1h at 37°C, washed 2x15 min in PBS and cleared in RapiClear (1.52) overnight. Sections were mounted in RapiClear and imaged with a *Leica SP8* confocal microscope with a 63x objective (immersion oil) and a 40μm deep z-stack was acquired. Maximum projections were generated in *Fiji*[97] and CD68 AF555 exposure was enhanced for better visibility of the signal.

Proliferation assay

To assay proliferation, single cell suspensions were stained for cell surface proteins as described above. Following the staining, cells were fixed and permeabilized in 4% Fixation/Permeabilization buffer (BD, Cat. No. 554714) for 20 minutes on ice, washed, then stained with intracellular markers (Ki67, 1:50; SYTOX green, 1:1000) in BD Perm/Wash™ for 1 hour on ice, washed in BD Perm/Wash™ and finally resuspended in FACS buffer. Stained cells were passed on the Cytoflex LX and SYTOX green was recorded in linear.

Developmental Cell
Article

CellPress

Single cell liquid culture

Single cell suspensions from fetal livers and adult bone marrows were prepared and blocked as described above. Lineage positive cells (Ter119$^+$ CD19$^+$ CD3e$^+$ CD4$^+$ CD8$^+$ NK1.1$^+$ F4/80$^+$ Gr1$^+$) were depleted using magnetic anti-biotin Microbeads (1:5) (Miltenyi Biotec 130-090-485) and MS columns (Miltenyi Biotec 130-042-201). CMPs (Live (SYTOX green, Thermo Fisher), Lin$^-$ Kit$^+$ Sca-1$^-$ CD127$^-$ CD34$^+$ CD16/32^{int}) were sorted using a FACSAria III (Diva software) and cloned into flat-bottom 96-well plates (UpcellNUNC) containing pre-warmed and equilibrated differentiation medium (0.1% β-mercaptoethanol, 1X Penicillin/Streptomycin, 10% FBS, 1:125 SCF, 5ng/μL GM-CSF, 5ng/μL M-CSF, 2ng/μL EPO and 5ng/μL TPO in Opti-MEM with Glutamax). SCF was supplied from myeloma cell line supernatant. Cells were grown at 37 °C with 5% CO_2 for 7 days. Colony analysis was performed first by manually scoring wells for the presence of colonies and identification of Megakaryocytes (Mk), centrifugating plates at 320*g* for 7 minutes at 4 °C and staining each colony for 1 hour at 4 °C with 40 μL of antibody mix containing 1:400 Fc-block (anti-CD16/32) and 1:400 anti-CD45, -CD11b, -Ly6G, -Ly6C, -IL33Ra(ST2), -Kit, -Ter119, -CD41. Stained colonies were collected for flow cytometry analysis by scratching. Cells were identified by the following markers: Macrophages: CD45$^+$ CD11b$^+$, F4/80$^+$, Monocytes: Neutrophils: CD45$^+$, CD11b$^+$, Ly6G$^+$, Mast cells: CD45$^+$ Kit$^+$ IL33Ra (ST2)$^+$, Red blood cells: CD45$^-$ Ter119$^+$, Megakaryocytes: CD41$^+$.

QUANTIFICATION AND STATISTICAL ANALYSIS

Quantification

Fly lymph gland's volume, cellularity (number of DAPI$^+$ nuclei) as well as number of PH3$^+$, Hml$^+$, Antp$^+$ cells were measured with IMARIS software (RRID:SCR_007370) based on confocal images. For fly macrophage counting, 10 larvae were bled in 100 μl (wL3) or 50 μl (L2) of cold PBS 1X added with few crystals of N-Phenylthiourea. The bleeding was performed by peeling the dorsal and ventral cuticle of the larva in order to release macrophages. Cells were then counted in brightfield with a hemocytometer (volume of counting: 1 μl) and the following formula was used to estimate the number of macrophages/larva: (# of macrophages counted in 1 μl) x (bleeding volume)/10. For flow cytometry, the following formula was used to quantify cells: (# of cells acquired) x (volume of resuspended cells after staining and washing/volume of cells acquired) x (volume of cell suspension in blocking buffer prior to staining/volume of cells plated for staining) and divided by the weight of analyzed adult tissue where applicable. Flow data was analyzed by FlowJo and plots were generated using Graphpad Prism.

Statistical analysis

Two tailed unpaired t-test was used to estimate p-values for fly macrophage number and gene expression level, lymph gland cellularity, volume and number of PH3$^+$, Hml$^+$, Antp$^+$ cells. Flow cytometry data was quantified in Graphpad Prism using Tukey multiple comparisons test for time course analysis, One-way ANOVA for comparisons of multiple different populations within one sample and Mann-Whitney test for pairwise comparisons The number of animals used in each experiment and other experimental details are indicated in the figure legends.

Developmental Cell, Volume *59*

Supplemental information

Early-wave macrophages control late hematopoiesis

Sara Monticelli, Alina Sommer, Zeinab AlHajj Hassan, Clarisabel Garcia Rodriguez, Kémy Adé, Pierre Cattenoz, Claude Delaporte, Elisa Gomez Perdiguero, and Angela Giangrande

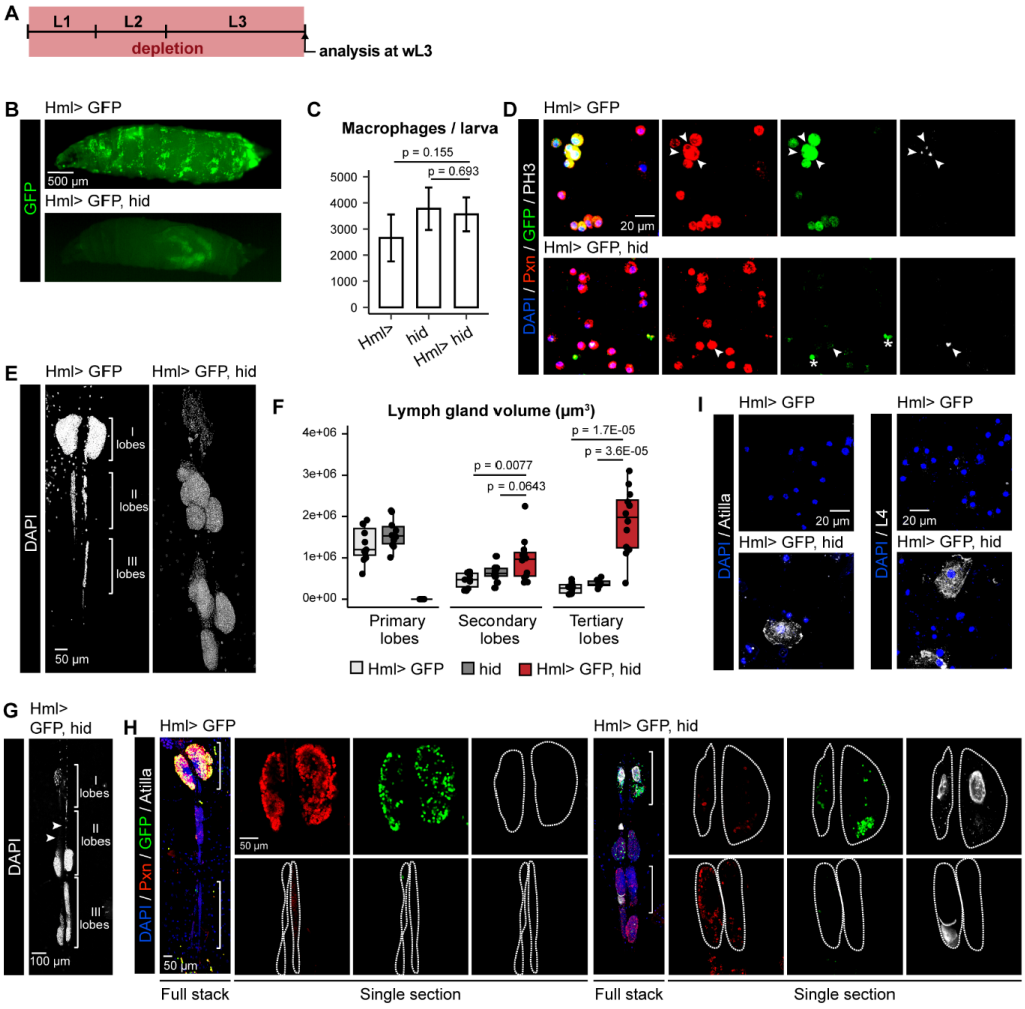

Supplementary Figure S1 – Constitutive macrophage depletion impacts the lymph gland development in the fly larva, related to Figure 2. (A) Experimental set up. The *HmlΔGal4* driver was used to express the cell death gene *hid* in macrophages throughout the larval life (constitutive depletion). Animals were raised at 25°C and analyzed at wandering L3 (wL3) ~120 h AEL (After Egg Laying). A reporter GFP was used to reveal *Hml* expression. **(B)** Side view of a control and a macrophage depleted larva (anterior on the left, posterior on the right). **(C)** Bar chart (mean ± standard deviation (SD)) representing the number of macrophages per larva assessed by brightfield counting. N ≥ 3. **(D)** Immunolabeling of macrophages bled from control and macrophage depleted larvae. The differentiated macrophage marker Pxn is in red, anti-GFP is in green, the anti-PH3 mitotic marker is in gray, nuclei are labeled with DAPI in blue. Proliferating cells are pointed by arrowheads. Asterisks indicate spurious GFP signal from bacteria/cellular debris. **(E)** Immunolabeling of lymph glands dissected from control and macrophage depleted larvae. Nuclei are labeled DAPI in gray. N ≥ 10. **(F)** Volume of the lymph gland lobes. N ≥ 10. **(G)** Example of partial histolysis of the lymph gland secondary lobes, sporadically observed in macrophage depleted larvae, that is in line with the bigger size of the tertiary lobes compared to the secondary ones. Nuclei are labeled DAPI in gray. Arrowheads indicate

histolyzed parts of the secondary lobes. **(H)** Immunolabeling of lymph glands dissected from control and macrophage depleted larvae. Anti-Pxn is in red, anti-GFP in green, the lamellocyte marker Atilla is in gray, nuclei are labeled with DAPI in blue. Brackets indicate the lobes represented in the blow-up. Dashed lines indicate the perimeter of the lymph gland lobes. N ≥ 10. **(I)** Immunolabeling of macrophages bled from control and macrophage depleted larvae. The lamellocyte markers Atilla and L4 are in gray, nuclei are labeled with DAPI in blue. Detailed genotypes: *w;HmlΔGal4,UAS-2XEGFP/+;+* (Hml> GFP), *w;UAS-hid/+;+* (hid), *w;HmlΔGal4,UAS-2XEGFP/UAS-hid;+* (Hml> GFP, hid), *w;HmlΔGal4/+;+* (Hml>), *w; HmlΔGal4/UAS-hid;+* (Hml> hid). Confocal images are shown as full stack projections for bled macrophages and representative single sections for lymph glands unless otherwise specified. Statistics: two tailed unpaired t-test.

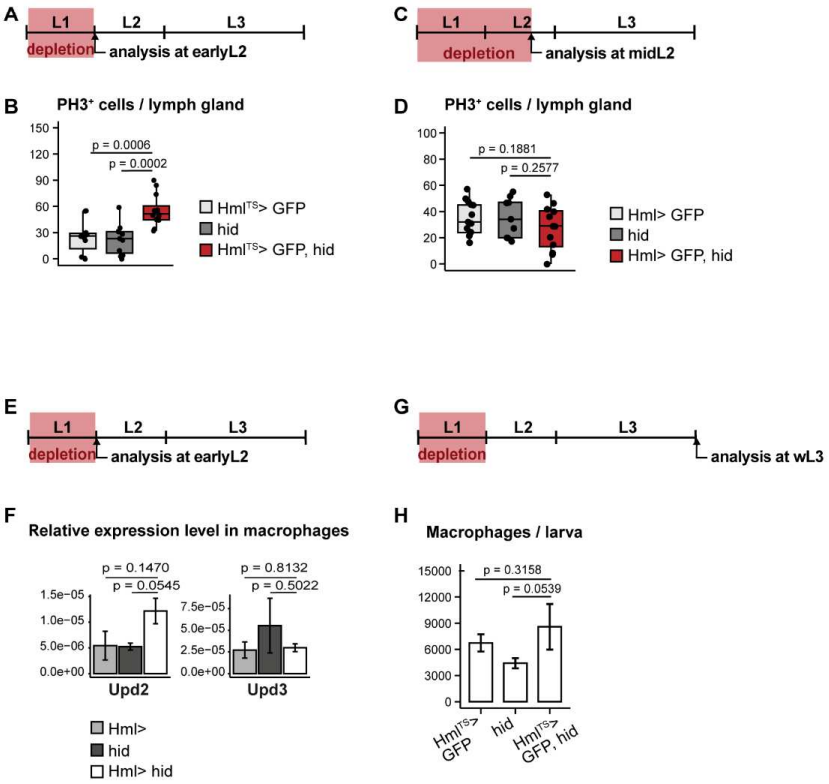

Supplementary Figure S2 – Early-wave macrophage depletion does not induce cytokine expression whereas impacts fly lymph gland cellularity, related to Figure 2 and Figure 3. (A) Experimental set up used in **(B)**. The cell death gene *hid* was expressed under the control of the *HmlΔGal4* driver in macrophages from the beginning of the larval life until earlyL2 (~48 h AEL) with animals raised at 25°C. No temperature shift was performed on these animals. **(B)** Number of PH3$^+$ cells in the lymph gland primary lobes in control and larvae depleted of early-wave macrophages (EMs). N ≥ 11. **(C)** Experimental set up used in **(D)**. EM depletion was carried out as in **(A)** but animals were analyzed at later stage namely midL2 (~65 h AEL). **(D)** Number of PH3$^+$ cells in the lymph gland primary lobes in control and EM depleted larvae. N ≥ 9. **(E)** Experimental set up in **(F)** (see **(A)**). **(F)** Bar chart (mean ± standard error (SE)) representing the relative expression level of the Upd2 and Upd3 cytokines assessed by RT-qPCR on macrophages bled from control or macrophage depleted larvae. N =3. **(G)** Experimental set up used in **(H)**. The genetic depletion was restricted to the first larval instar (L1) using a thermosensitive inhibitor of Gal4 (*tubulinGal80^{TS}*), which is active at low temperature (18°C) and inactive at higher temperature (≥25°C). Embryos and L1 larvae were raised at 25°C to trigger expression of *hid* under the control of *HmlΔGal4*, shifted at 18°C at earlyL2 (~48 h AEL) and analyzed at wL3. **(H)** Bar chart (mean ± SD) representing the number of macrophages per larva assessed by brightfield counting. N = 3. Detailed genotypes: *w;HmlΔGal4,UAS-2XEGFP/+;tubulinGal80^{TS}/+* (Hml^{TS}> GFP), *w;UAS-hid/+* (hid), *w;HmlΔGal4,UAS-2XEGFP/UAS-hid;tubulinGal80^{TS}/+* (Hml^{TS}> GFP, hid), *w;HmlΔGal4,UAS-2XEGFP/+;+* (Hml> GFP), *w;HmlΔGal4,UAS-2XEGFP/UAS-hid;+* (Hml> GFP, hid), *w;HmlΔGal4/+;+* (Hml>), *w; HmlΔGal4/UAS-hid;+* (Hml> hid). Statistics: two tailed unpaired t-test.

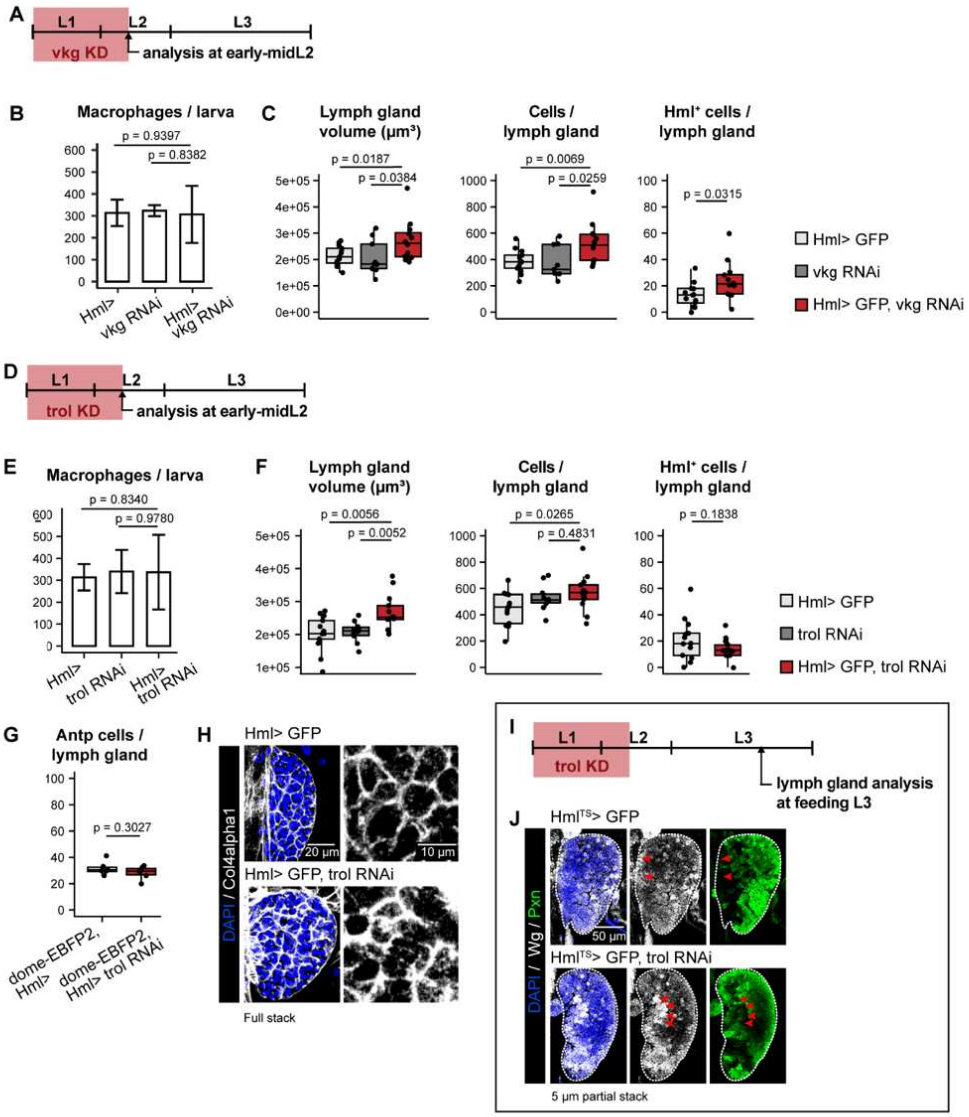

Supplementary Figure S3 - Knocking down extracellular matrix molecules in early-wave macrophages accelerates fly lymph gland development, related to Figure 7. (A) Experimental set up in **(B,C)**. The *HmlΔGal4* driver was used to knock down (KD) the extracellular matrix (ECM) component *vkg* (*vkg RNAi*) in EMs from the beginning of the larval life until early-midL2 (~45 h AEL) with animals raised at 29°C to increase the efficiency of the Gal4-UAS system. A reporter GFP was used to reveal *Hml* expression. **(B)** Bar chart (mean ± SD) representing the number of macrophages per larva assessed by brightfield counting. N ≥ 3. **(C)** Lymph gland primary lobes' volume, number of cells and number of Hml⁺ cells (N ≥ 9) in control and *vkg RNAi* larvae. **(D)** Experimental set up used in **(E-H).** The *HmlΔGal4* driver was used to knock down the ECM component *trol* (*trol RNAi*) in EMs from the beginning of the larval life until early-midL2 (~45 h AEL) with animals raised at 29°C. A reporter GFP was used to reveal *Hml* expression. **(E)** Bar chart (mean ± SD) representing the number of macrophages per larva assessed by brightfield counting. N ≥ 3. **(F)** Lymph gland primary lobes' volume, number of cells and number of Hml⁺ cells (N ≥ 11) in control and *trol RNAi* larvae. **(G)** Number of Antp⁺ cells per lymph gland in control and *trol RNAi* larvae. N = 6. **(H)** Immunolabeling of lymph glands dissected from control and *trol RNAi*

larvae. The ECM is labelled in gray with anti-Col4alpha1, nuclei are labeled with DAPI in blue. (N ≥ 6). **(I)** Experimental set up used in **(J).** *trol* knock down was restricted to L1 and beginning L2 using the thermosensitive inhibitor of Gal4 *tubulinGal80^{TS}*. Embryos and larvae were raised at 29°C (*tubulinGal80^{TS}* inactive) until early-midL2 (~45 h AEL) to trigger *trol* knock down and expression of a GFP reporter under the control of the Hml. Then animals were shifted at 18°C (*tubulinGal80^{TS}* active) and analyzed at fL3. **(J)** Immunolabeling of lymph glands dissected from control and *trol RNAi* larvae with anti-Pxn in green, the medullary zone marker wingless (Wg) in gray and nuclei labeled in blue with DAPI. N = 5. Detailed genotypes: *w;HmlΔGal4,UAS-2XEGFP/+;+* (Hml> GFP), *yv;+;vkg RNAi/+* (vkg RNAi), *w;HmlΔGal4,UAS-2XEGFP/+;vkg RNAi/+* (Hml> GFP, vkg RNAi), *w;HmlΔGal4/+;+* (Hml>), *w;HmlΔGal4/+; vkg RNAi/+* (Hml> vkg RNAi), *w;+;trol RNAi/+* (trol RNAi), *w;HmlΔGal4,UAS-2XEGFP/+;trol RNAi/+* (Hml> GFP, trol RNAi), *w;HmlΔGal4/+;trol RNAi/+* (Hml> trol RNAi), *w,domeMeso-EBFP2/+;HmlΔG4/+* (dome-EBFP2, Hml>), *w,domeMeso-EBFP2/+;HmlΔG4/+;trol RNAi/+* (dome-EBFP2, Hml> trol RNAi), *w;HmlΔGal4,UAS-2XEGFP/+;tubulinGal80TS/+* (HmlTS> GFP), *w;HmlΔGal4,UAS-2XEGFP/+;tubulinGal80TS/trol RNAi* (HmlTS> GFP, trol RNAi). Statistics: two tailed unpaired t-test.

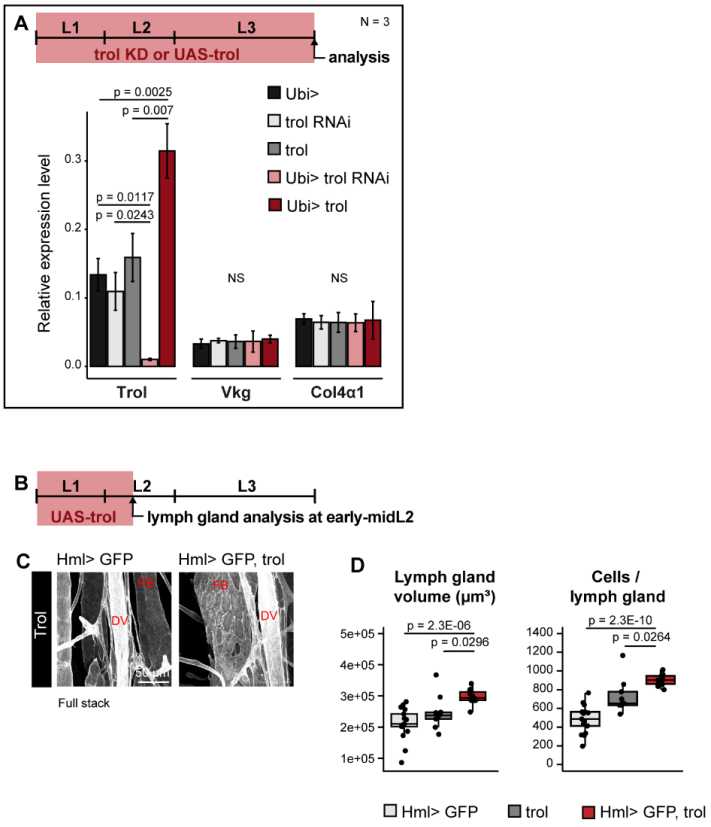

Supplementary Figure S4 - Increased expression of Trol in early-wave macrophages affects the fly fat body and lymph gland, related to Figure 7. (A) Bar chart (mean ± SE) representing the relative expression level of *trol*, *vkg* and *Col4alpha1* assessed by RT-qPCR on total RNA extracted from control, *trol RNAi* or *trol* overexpressing wL3 larvae. N =3. **(B)** Experimental set up in **(C,D)**. The *HmlΔGal4* driver was used to overexpress trol in EMs from the beginning of the larval life until early-midL2 (~45 h AEL) with animals being raised at 29°C to increase the UAS-Gal4 system efficiency. **(C)** Immunolabeling performed on fillet with an anti-Trol in gray. FB: dorsal fat body flanking the lymph gland, DV: dorsal vessel. N ≥ 8. **(D)** Lymph gland primary lobes' volume and number of cells in control and trol overexpressing larvae (N ≥ 9). Detailed genotypes: *w;UbiGal4/+;+* (Ubi>), *w;+;trol RNAi/+* (trol RNAi), *w;UbiGal4/+;trol RNAi/+* (Ubi> trol RNAi), *w;+;UAS-trol/+* (trol), *w;UbiGal4/+;UAS-trol/+* (Ubi> trol), *w;HmlΔGal4,UAS-2XEGFP/+;+* (Hml> GFP), *w;HmlΔGal4,UAS-2XEGFP/+; UAS-trol/+* (Hml> GFP, trol). Statistics: two tailed unpaired t-test.

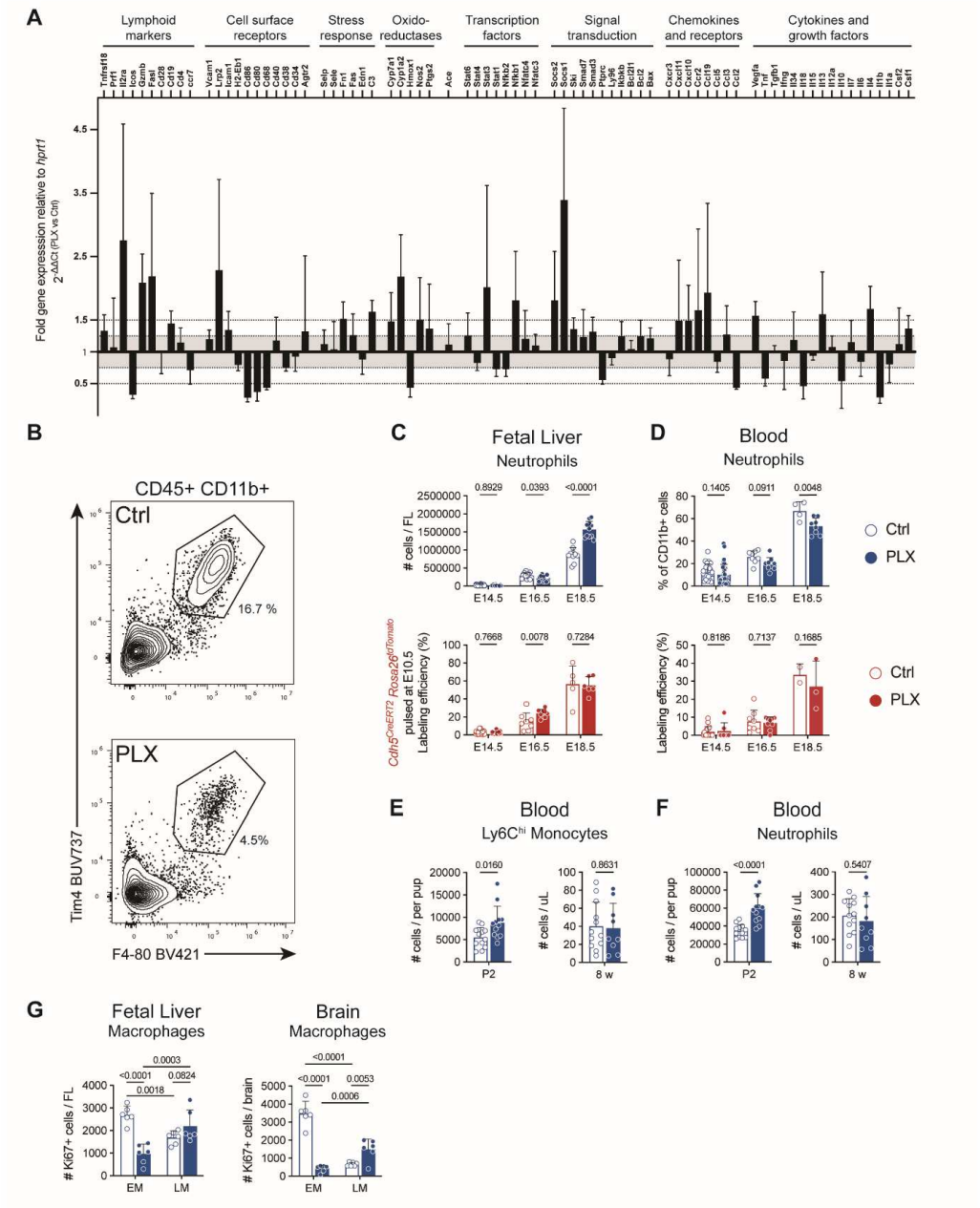

Supplementary Figure S5 - Murine EM depletion does not trigger inflammation and leads to an increased contribution of hematopoietic stem cells (HSCs) to myeloid cells, related to Figure 4. (A) Bar chart (mean ± SD) representing the fold gene expression relative to *hprt1* in E14.5 fetal livers upon macrophage depletion when compared to control livers. **(B)** Representative dotplot of F4/80+ Tim4+ macrophages among CD45+ CD11b+ cells in each one control and PLX treated embryo at E14.5. **(C)** Bar chart (mean ± SD) representing the number of CD45+ CD11b+ Ly6G+ neutrophils per fetal liver (top) and the frequency of cells expressing tdTomato among CD45+ CD11b+ Ly6Ghi neutrophils in the fetal liver (bottom) in control (Ctrl, blue border) and macrophage depleted (PLX, blue fill) embryos analyzed

at different timepoints after withdrawal of CSF1R inhibition. Symbols correspond to individual embryos from at least two independent litters per timepoint and per treatment group. Statistics of embryos: Tukey multiple comparisons test. **(D)** Bar chart (mean ± SD) representing the frequency of CD11b+ Ly6Ghi neutrophils among blood circulating CD11b+ cells (top) and the frequency of cells expressing tdTomato among CD11b+ Ly6Ghi neutrophils in the blood (bottom) at different timepoints. Symbols correspond to individual embryos from at least two independent litters. Statistics: Tukey multiple comparisons test. **(E)** Bar chart (mean ± SD) representing the number of circulating CD115+ Ly6Chi+ blood monocytes per pup (left) or per uL (right). Symbols correspond to individual pups from at least two independent litters per timepoint and per treatment group. Statistics: unpaired t-test. **(F)** Bar chart (mean ± SD) representing the number of circulating CD11b+ Ly6G+ blood neutrophils per pup (left) or per uL (right). Symbols correspond to individual pups from at least two independent litters per timepoint and per treatment group. Statistics: unpaired t-test. **(G)** Bar chart (mean ± SD) representing the number of Ki67+ CD45+ F4/80+ macrophages per fetal liver (left) or per brain (right) among tdTomato+ (EM) or tdTomato- (LM, HSC-derived) in control (Ctrl, blue border) or PLX-treated (PLX, blue fill) E16.5 *Cdh5*^{CreERT2} *Rosa26*^{tdTomato} embryos that were pulse-labeled with 4OHT at E7.5. Symbols correspond to individual pups from one litter per treatment group. Statistics: 2-way ANOVA.

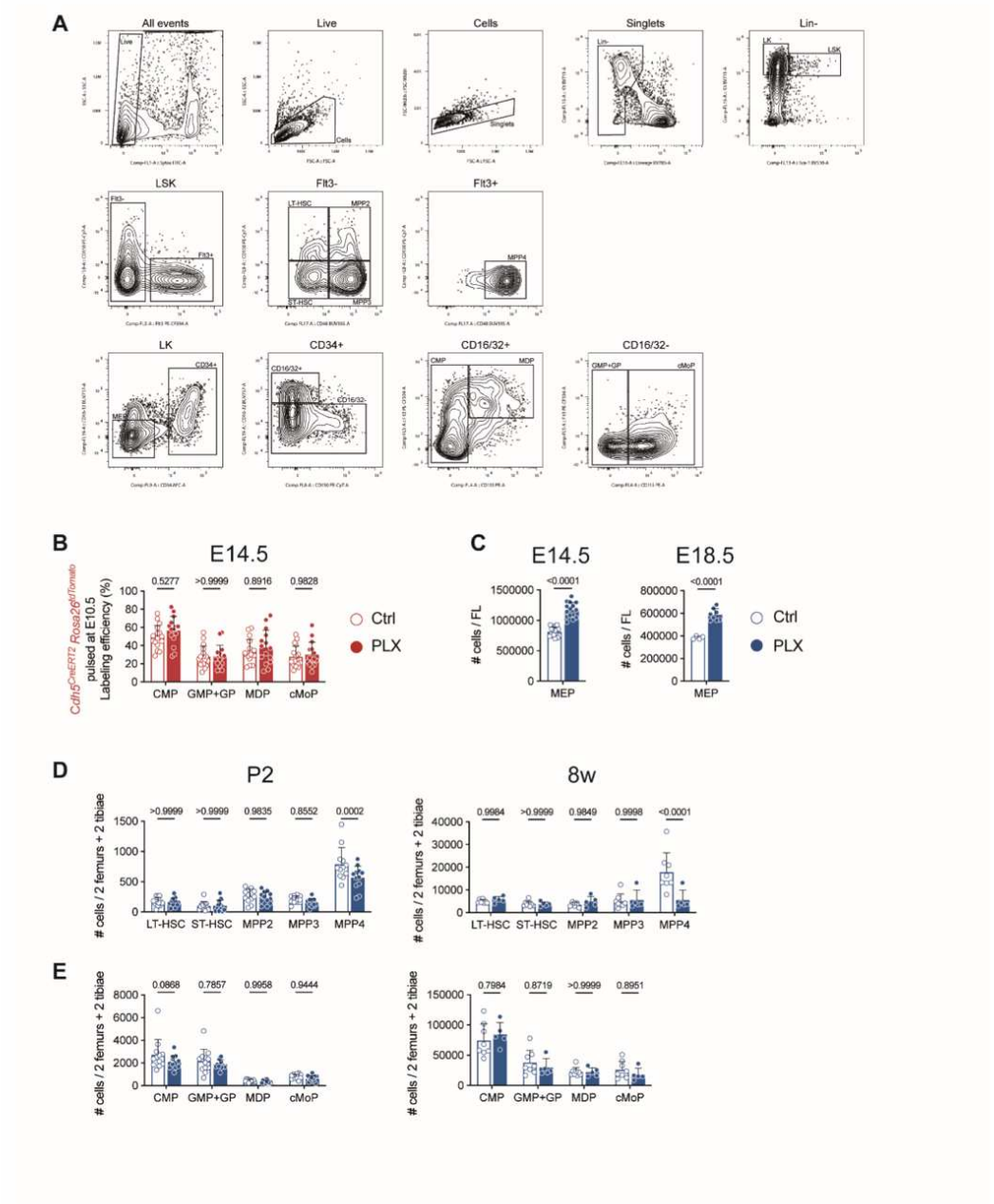

Supplementary Figure S6 - Murine EM depletion alters hematopoiesis in the fetal liver and postnatal bone marrow, related to Figure 5. (A) Gating strategy of hematopoietic progenitors in the fetal liver. **(B)** Bar chart (mean ± SD) representing the frequency of cells expressing tdTomato among fetal liver CMP, GMP+GP, MDP and cMoP in control (Ctrl, red border) and macrophage-depleted (PLX, red fill) embryos analyzed at different timepoints at E14.5. Symbols correspond to individual embryos from at least two independent litters per timepoint and per treatment group. Statistics: One-way ANOVA. **(C)** Bar chart (mean ± SD) representing the number of MEP per fetal liver in control (Ctrl, blue border) and Macrophage-depleted (PLX, blue fill) embryos analyzed at E14.5 (left) and E18.5 (right). Symbols

correspond to individual embryos from at least two independent litters per treatment group. Statistics: One-way ANOVA. **(D)** Bar chart (mean ± SD) representing the number of LT-HSC, ST-HSC and MPP2 (erythroid-biased), MPP3 (myeloid-biased), MMP4 (lymphoid-biased) per 2 tibia and 2 femurs in control (Ctrl, blue border) and Macrophage-depleted (PLX, blue fill) mice analyzed at P2 (left) and 8 weeks (right). Symbols correspond to individual embryos from at least two independent litters per timepoint and per treatment group. Statistics: One-way ANOVA. **(E)** Bar chart (mean ± SD) representing the number of CMP, GMP+GP, MDP and cMoP per 2 tibia and 2 femurs in control (Ctrl, blue border) and macrophage-depleted (PLX, blue fill) mice analyzed at P2 (left) and 8 weeks (right). Symbols correspond to individual embryos from at least two independent litters per timepoint and per treatment group. Statistics: One-way ANOVA.

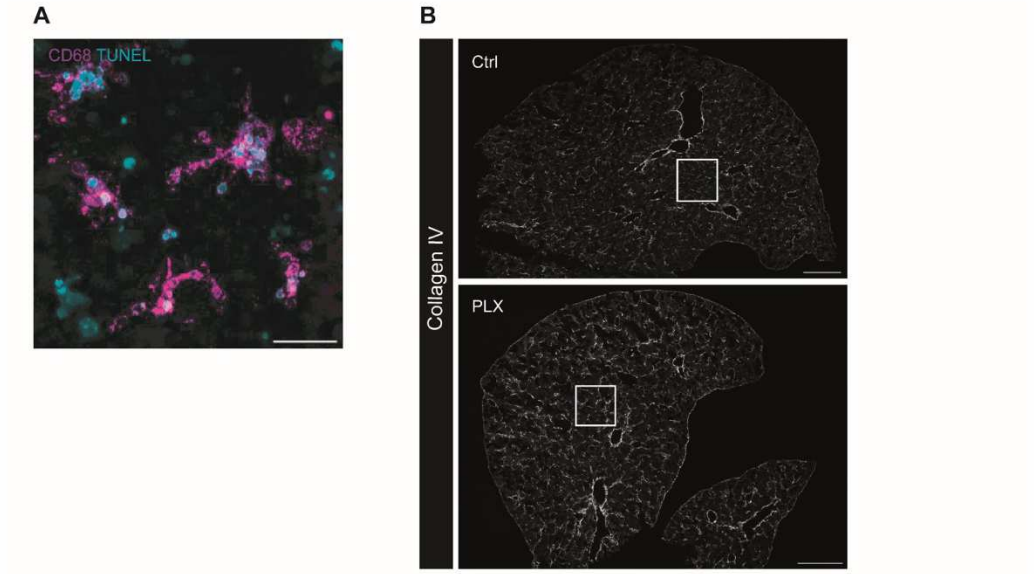

Supplementary Figure S7 - Murine EM depletion alters fetal liver extracellular matrix (ECM) organization, related to Figure 4 and Figure 5. (A) Surviving macrophages after EM depletion are filled with multiples vesicles containing TUNEL+ apoptotic materials. Representative Immunolabeling of fetal livers dissected from E14.5 control and PLX treated embryos. Anti-CD68 is in magenta. TUNEL staining is in cyan. Scale bar represents 25µm. **(B)** Representative immunolabeling of fetal livers dissected from E14.5 control and PLX treated embryos. Anti-Coll IV is in gray. White box represents region shown in Figure 5. Scale bar represents 250µm.

4 Discussion

4.1 Summary of the results

Both transient abnormal myelopoiesis in Down Syndrome (TAM or DS-TAM) and cutaneous mastocytosis are diseases that only occur in infants or children, respectively, and recede spontaneously (Zipursky, 2003; Valent et al., 2017). This dynamic is reminiscent of the kinetic of transient hematopoietic waves such as EMPs observed in mice (Gomez Perdiguero et al., 2015; Freyer et al., 2020; Iturri et al., 2021; Soares-da-Silva et al., 2021; Yokomizo et al., 2022). I, therefore, hypothesized that transient hematopoietic progenitors such as EMPs could be the cellular source of such diseases.

To elucidate whether progenitors and mature cells from distinct hematopoietic waves can be differently affected by a perturbation, I performed lineage tracing experiments. I tested how three different types of perturbations influence erythro-myeloid progenitors (EMPs), a transient hematopoietic wave, in comparison to hematopoietic stem (and progenitor) cells (HS(P)Cs) that sustain life-long hematopoiesis.

First, I investigated the effect of the knock-in fusion protein *Gata1*^{mCherry} on EMP- and HSPC-derived MEGAKARYOCYTES. *Gata1*^{mCherry} phenocopies *Gata1short* (*Gata1s*). The *Gata1s* mutation occurs in 10 % of all children with Down syndrome and causes an abnormal accumulation of immature megakaryocytes and blast cells. This preleukemic disorder is called transient abnormal myelopoiesis (TAM or DS-TAM), and spontaneously resolves around 3 months after birth in more than 80 % of all cases (reviewed in Zipursky, 2003). Only if additional mutations occur, TAM progresses to acute megakaryoblastic leukemia within the first 4 years of life (Labuhn et al., 2019; Wagenblast et al., 2021). Interestingly, my results suggest that *Gata1*^{mCherry} has an ontogeny-specific effect as yolk sac-derived megakaryopoiesis (primitive and EMP) is more severely impaired by *Gata1*^{mCherry} than megakaryocyte production from the HSPC wave. In addition to hyperproliferation, *Gata1*^{mCherry} also caused the development of CD244^{+} blast-like exclusively in yolk sac-derived waves (**Figure 13-1**).

Next, I induced the gain-of-function *Kit*^{D814V} point mutation in EMPs *in utero*. *Kit*^{D816V}, the human homolog to the murine *Kit*^{D814V}, causes mastocytosis – an abnormal accumulation and activation of mast cells – with different pathologies in children and adults (Valent et al., 2017). While in children mastocytosis is limited to the skin and remits by puberty (cutaneous mastocytosis), in adults *Kit*^{D816V} causes systemic mastocytosis, a chronic disease with the involvement of several organs, including for example the gut and the bone marrow. Indeed, I observed that *Kit*^{D814V} extends the survival and activity of EMP-derived MAST CELLS in the dermis several months into adulthood compared to control

littermates. However, the mouse model failed to recapitulate the human disease since I did not observe spontaneous remission. Further experiments will also have to elucidate whether the same mutation has a more systemic effect and later disease onset when induced in the HSPC compare to the EMP wave (**Figure 13-2**).

Finally, I depleted EMP-derived MACROPHAGES in the developmental period which caused precocious macrophage production by HSCs in development with long-term consequences for hematopoiesis. This revealed unique Csf1r-dependencies of EMP- and HSPC-derived macrophages as well as a distinct replenishing dynamic between the two waves (**Figure 13-3**).

Collectively, this demonstrates that the integrity of early hematopoietic waves such as EMPs is required to ensure the proper establishment of HSC hematopoiesis. In addition, my results show that perturbations such as mutations or the inhibition of signaling pathways can exert ontogeny-specific effects. Finally, my thesis provides proof of concept that perturbations in transient hematopoietic progenitor waves can have consequences beyond the developmental period. Importantly, these observations were not restricted to one but were consistent between three different cell types.

4.2 Extrinsic and intrinsic factors governing stage-specific phenotypes

The fate of a cell is determined by both intrinsic (genetic) and extrinsic (environmental) factors. Each hematopoietic wave has a distinct "biography" since they each emerge at different times, from different cell types (arterial- versus non-arterial endothelial cells), in distinct locations (discussed in Commonalities, differences, and interplay between EMPs and HSCs), and are thereby imprinted in a way that shapes their characteristic identity and function.

My work focused primarily on the role of the unique molecular (epi-/genetic) regulation and the lifespan of different hematopoietic waves, which are considered INTRINSIC factors. However, since the environment changes throughout development, EXTRINSIC factors could also be drivers of the stage-specific phenotypes that I observed. In the following, I will therefore discuss possible factors that I did not address in my experimental work, but that could play a role in influencing stage-specificity, particularly in disease.

Figure 13

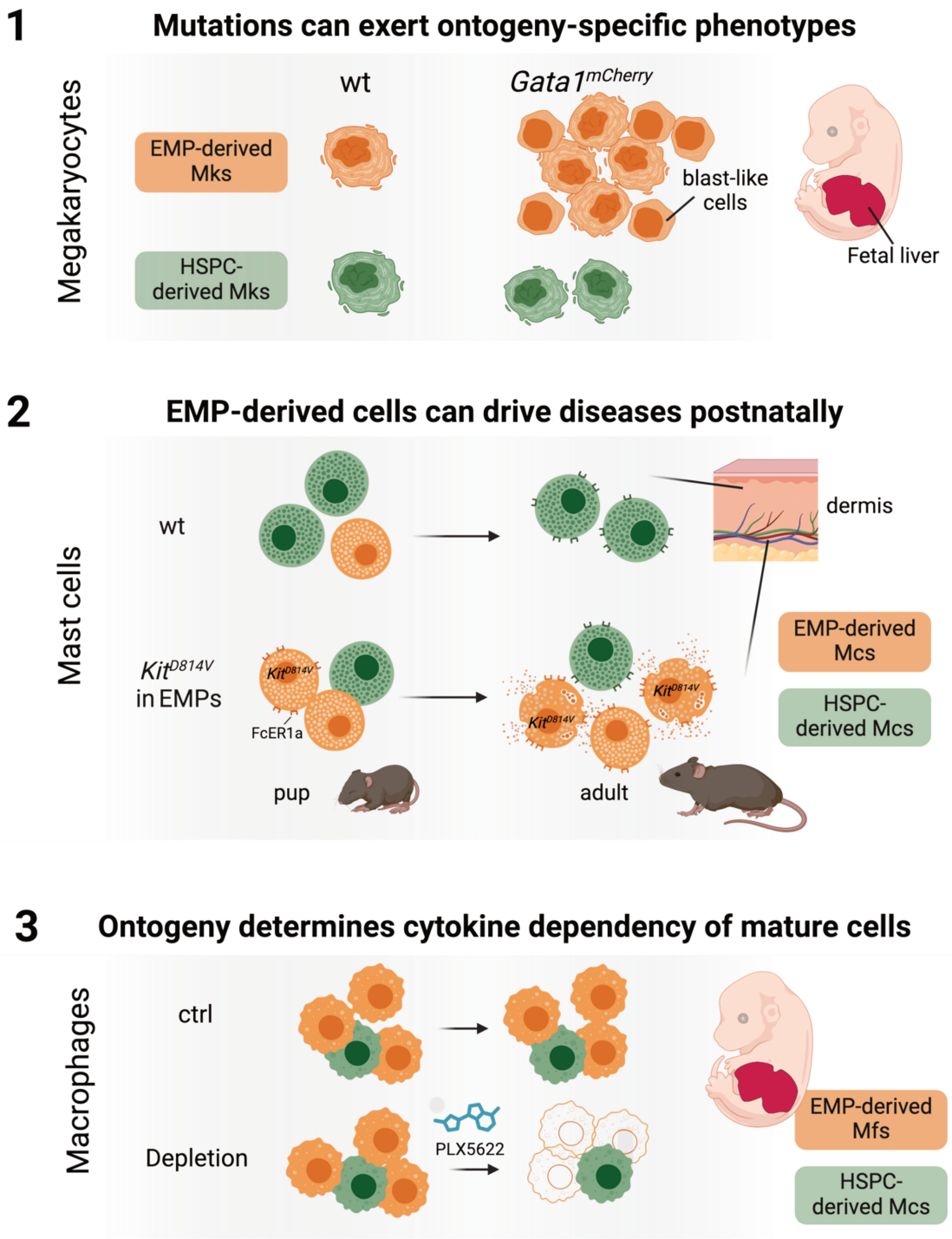

Figure 13. Perturbations cause ontogeny-specific effects in developmental hematopoiesis. (**1**) Lineage tracing of megakaryocytes in *Gata1*^{mCherry} embryos and fetuses revealed that mutant *Gata1* drives hyperproliferation and blast-like cell development specifically in yolk sac hematopoiesis (incl. primitive and EMP-derived megakaryocytes). (**2**) Inducing the mutation KitD814V specifically in EMPs provided proof of concept that EMPs can drive disease beyond the developmental period. (**3**) Treating embryos with the Csf1r inhibitor PLX5622 from E11.5 to E14.5 demonstrated that EMP but not HSPC-derived macrophages depend on Csf1r-signaling for their survival. Created with biorender.com.

4.2.1 Ontogeny-specific cytokine dependency of macrophages

CSF1 (Colony Stimulating Factor 1) – also termed Macrophage Colony-Stimulating Factor (M-CSF) – is a ligand of the CSF1 receptor (CSF1r). As its name says, it is essential for the induction and maintenance of myeloid fate as well as the proliferation and function of monocytes and macrophages (reviewed by Mun et al., 2020).

I discovered an ontogeny-specific dependency of Csf1r-signaling at the level of macrophage survival, as EMP- but not HSC-derived macrophages were depleted in the fetal liver at E14.5 after blocking Csf1r-signaling (Monticelli et al., 2024). This correlated with the different macrophage-differentiation pathways of EMPs and HSCs. EMP-derived macrophages directly differentiate *in situ* in the yolk sac, whereas HSC-derived macrophages differentiate through an intermediate monocyte stage in the fetal liver (Geissmann et al., 2010; Schulz et al., 2012; Gomez Perdiguero et al., 2015; Hoeffel et al., 2015). Indeed, the number of HSC-derived monocytes nearly doubled, concurrent with the increase in HSC-derived macrophages after PLX removal (Monticelli et al., 2024). This is consistent with previous studies showing that yolk sac-derived macrophages, but not monocytes, depend on Csf1r-signaling (Ginhoux et al., 2010; Hoeffel et al., 2015; Rojo et al., 2019). However, in the study of Hoeffel and colleagues, it was monocytes were ascribed an EMP origin, contrary to recent findings (Lazarov et al., 2024). Therefore they linked the discrepancy in Csf1r-dependency to the differentiation pathway but not to the progenitor origin (Hoeffel et al., 2015).

The yolk sac expresses no or only little *Csf1* but maternal CSF1 may be present (Regenstreif & Rossant, 1989; Gorivodsky et al., 1999). By contrast, endothelial cells, hepatoblasts, mesothelial, and mesenchymal cells in the fetal liver stroma express increasing levels of *Csf1* from E12.5 and E18.5 (Peixoto et al., 2024). Interestingly, the macrophages developing in the lower cytokine environment (EMP-derived macrophages in the yolk sac) are more Csf1r-dependent than the HSC-derived macrophages that differentiate in the fetal liver. This could indicate that HSC-derived macrophages and monocytes can resort to cytokines driving receptor-signaling pathways other than Csf1r. One candidate could be GM-CSF which binds to CSF2R but not to CSF1R and is particularly important for alveolar macrophages. However, at least at E12.5, I did not detect any GM-CSF expression in the fetal liver (preliminary data) when using the *Csf2*$^{flox\text{-}tdTomato}$ reporter (Gschwend et al., 2021).

Further investigation is therefore necessary to elucidate the differences in the molecular regulation of macrophage maintenance derived from the two hematopoietic waves (EMPs versus HSCs). Thanks to fate mapping, this could be done in unperturbed conditions. It would be interesting to not only understand which cytokines regulate HSC-derived macrophage survival in the fetal liver but also whether they depend on different cellular

sources and isoforms of cytokines compared to EMPs. For instance, CSF1 can either be presented on the cell surface or it can be secreted (Pixley & Stanley, 2004).

4.2.2 Extrinsic and intrinsic factors underlying cutaneous and systemic mastocytosis

The same mutation, *Kit*^{D816V}, can drive mastocytosis both in children and adults, but results in distinct pathology, namely cutaneous or systemic mastocytosis, respectively. These differ in two key aspects: (1) the kinetic of the disease and (2) the tissues involved. In children, mastocytosis primarily affects the skin and resolves spontaneously by adolescence. By contrast in adults, mastocytosis is systemic, and multiple organs can be infiltrated, including the gastrointestinal (GI) tract, bone marrow, and skin.
The turnover of mast cells has been extensively studied in both the skin and gut. In steady-state conditions, mast cells in the skin mostly self-maintain and they receive barely any input from circulation.

Studies in mice indicate that the first skin mast cells originate from an early progenitor wave, EMPs, and are replaced by HSPC during the first weeksafter birth (Gentek et al., 2018a). Indeed, the first mature mast cells in humans appear in the fetus around 10-12 weeks post-conception (Suo et al., 2022). As the human hematopoietic system develops in sequential waves reminiscent of mouse hematopoiesis, a similar ontogeny switch could be possible in the human skin. However, the exact stage when early-wave mast cells would disappear in humans is unknown.

In contrast, gut mast cells undergo continuous replacement by bone marrow-derived progenitors (Kitamura et al., 1979). Mouse fate-mapping studies showed that these gut mast cells are not derived from EMPs but only receive input from later hematopoietic waves (Li et al., 2018).

Several hypotheses may explain why pediatric mastocytosis is transient and confined to the skin: (1) The *Kit*^{D816V} mutation may occur specifically in mature mast cells within the dermis and not in circulating mast cell progenitors or precursors. (2) Mutated mast cells might derive from a transient progenitor wave (like EMPs). Due to the unique slow turnover of mast cells in the skin, these mutated cells persist longer, while in other tissues, they are replaced more quickly by later hematopoietic waves (Kitamura et al., 1979; Weitzmann et al., 2020). This would explain the absence of mutated cells in other tissues as well as the spontaneous resolution around adolescence. (3) There may be inherent transcriptional differences between mast cells derived from early and late progenitor waves (Gentek et al., 2018a), influencing how fast they are replaced by cells from circulation. (4) Shifts in the skin microenvironment between childhood and adulthood might contribute to the resolution of the disease as children grow older.

In addition, several hypotheses may explain why adults instead develop a systemic disease. Instead of the *Kit*^{D816V} mutation occurring locally in the skin, potentially, a

proliferative and self-renewing stem cell or mast cell precursor/progenitor that is located outside of the skin might be mutated. This mutated progenitor pool could reside in the bone marrow and continuously replenish different organs such as the gastrointestinal tract, thereby causing systemic effects leading to inflammation. In fact, during inflammation, a higher contribution from the circulation to dermal mast cells is observed compared to steady-state conditions (Weitzmann et al., 2020). This could explain why in systemic mastocytosis the skin is affected, even though skin mast cells usually do not receive contribution from the bone marrow.

Collectively, while the origin of cutaneous mastocytosis is not fully understood, the ontogeny or progenitor origin of mast cells appears to be a critical factor in the stage-specific nature of cutaneous mastocytosis, while extrinsic factors most likely play a minor role.

Mimicking cutaneous mastocytosis in the mouse model

Surprisingly, in the mouse model where I sought to induce cutaneous mastocytosis by inducing *Kit*^{D814V} in EMPs, mast cell accumulation, and activation did not spontaneously resolve, unlike cutaneous mastocytosis in humans. Several explanations could be conceivable:

(1) The mutation might have not only been induced in EMPs but also in life-long HSPCs. However, as there was no YFP labeling in progenitors in the bone marrow, this hypothesis can be excluded.

(2) Fetal mast cells in mice express lower levels of FcER1, higher levels of Itgb7, and have a distinct transcriptional profile compared to adult mast cells (Gentek et al., 2018a; Msallam et al., 2020). Inducing the Kit mutation in mice caused an upregulation of FcER1. This precocious maturation of EMP-derived mast cells might have extended their capacity to persist in tissues and prevented them from disappearing from the skin after birth.

(3) Finally, mature cells remain longer in the mouse than in humans in relation to the overall lifespan of the organism. For example, in mice, which can reach a maximum age of 2 years, a red blood cell has a lifespan of about 45 days (ratio of 1:16 in days). In comparison, in a human who can reach at least 90 years of age, a red blood cell circulates up to 120 days (ratio of 1:275 in days). While the lifespan of each cell type is different and this cannot be directly translated to mast cells, it exemplifies that in proportion to the speed of aging, a cell can potentially stay around 17 times longer in the mouse than in the human. Perhaps if the mice had been analyzed even later than 6 months the mutated EMP-derived mast cells would have disappeared.

4.2.3 Extrinsic and intrinsic factors driving the spontaneous remossion of DS-TAM

Compared to mastocytosis, where the same mutation drives a pediatric and adult disease, DS-TAM exclusively occurs in newborns and not in adults, even in people with Down syndrome. It is thus more likely, that extrinsic factors are involved in the stage-specificity of this disease compared to mastocytosis. Indeed, it has been postulated that the switch from the fetal liver environment to the bone marrow may be a key factor driving spontaneous remission in DS-TAM (Miyauchi, 2024).

In the human fetus, at least during the end of the first and during the second trimester, fetal liver and bone marrow hematopoiesis are active simultaneously (Fanni et al., 2018; Ranzoni et al., 2021; Marderstein et al., 2024). In mice, liver hematopoiesis ends during the first postnatal week which is linked to hemodynamic changes at the onset of adult circulation (Khan et al., 2016).

Even though it is unknown, when exactly fetal liver hematopoeisis ends in healthy development, intriguingly, abnormal megakaryocyte infiltration was detected only in the fetal liver and not in the bone marrow in neonates as well as in stillborn fetuses (20 cases reviewed in Miyauchi, 2024). This indicates that at least in pathological conditions, the fetal liver could be a site of hematopoiesis until birth in humans.

Indeed, the fetal liver stroma reinforces TAM-blast development and growth by providing cytokines and growth factors such as SCF, IL-3, and GM-CSF (Miyauchi et al., 2010; Miyauchi & Kawaguchi, 2014, 2021). In contrast to the fetal liver, the bone marrow has been proposed to inhibit the proliferation of megakaryocytes and blasts via interferon-α (Woo et al., 2013). This is in line with the finding that HSPCs in the healthy and pathological human fetal bone marrow express fewer cell cycle genes than in the fetal liver (Ranzoni et al., 2021; Marderstein et al., 2024). This implies that instead of providing particular enhancing cues, the fetal liver might simply be more permissive for proliferation than the bone marrow.

At least in mice, compared to the bone marrow, the fetal liver is a relatively low-cytokine environment (Peixoto et al., 2024) but is richer in cytokines than the yolk sac. Interestingly, this gradient of cytokine expression from the yolk sac to the fetal liver to the bone marrow niche is inversely correlated with cytokine dependency and the decreasing proliferative capacities of EMPs to adult HSC-derived progenitors (McGrath et al., 2015; Freyer et al., 2020). This illustrates that extrinsic (cytokine availability) and intrinsic factors (cytokine dependency) are not mutually exclusive, but intertwined.

For instance, EMP-derived erythropoiesis requires less erythropoietin (EPO) than HSCs (Soares-da-Silva et al., 2021). Similarly, the development of yolk sac-derived megakaryocytes is less dependent on thrombopoietin (TPO) than HSC-derived megakaryocytes (Xu et al., 2001) which correlates with my observation that EMP- in

contrast to HSPC-derived megakaryocytes hyperproliferate in the presence of *Gata1*^{mCherry}. Collectively, these examples indicate that EMPs respond very little to and are mostly independent of extrinsic factors such as cytokines compared to HSCs.

Potentially, the low cytokine levels in fetal hematopoietic niches are important to prevent differentiation of HSCs and to instead allow their proper expansion and maturation. Since the developing embryo, however, also requires mature blood and immune cells, the first hematopoietic waves have to be able to develop in a low-cytokine environment. This is in line with the observation that fewer signaling cues and transcription factors regulate the emergence of EMPs, and especially of primitive erythroblasts, compared to intraembryonic waves (elaborated in the introduction).

The low cytokine levels during development correlate with the high proliferative capacity of early hematopoietic waves. This indicates a level of autonomy, however, might also make them susceptible to abnormal hyperproliferation. Since most of the early blood cells are transient, it seems like an acceptable risk the organism takes that in the case of mutations, these cells might transform and drive transient diseases. By contrast, in the case of HSCs which sustain the organism throughout the entire life, proper establishment of the HSC pool is far more consequential and thus needs much tighter regulation. The *Gata1*^{mCherry} project of this thesis is a great example for this phenomenon. Even though *Gata1*^{mCherry} embryos and fetuses transiently develop a "disease", HSCs are barely affected and adults show no overt signs of sickness.

The notion that fetal hematopoietic progenitors are more autonomous regarding extrinsic cues is in line with the finding that the mutation threshold to develop infant acute lymphoblastic leukemia (ALL) with *MLL* rearrangements (*MLL*-R) in infants 1 year and younger is very low (1.3 mutation per case). This is in stark contrast not only to MLL-R leukemia in older children (7-19 years) in which more mutations occur per case (6.5 mutations per case) but also to most other human cancer types (Andersson et al., 2015).

4.3 Comparability of early transient hematopoietic waves in mice and humans

Two of my projects, involving megakaryocytes and mast cells, focused on mutations that drive human diseases.

I specifically investigated the contribution of yolk sac-derived EMPs (*Csf1r*^{MeriCreMer} pulsed with 4-OHT at E8.5) to disease and compared it to HSPCs that emerge in the intraembryonic AGM (*Cdh5*^{CreERT2} pulsed with 4-OHT at E10.5) (Gomez Perdiguero et al., 2015; Gentek et al., 2018a). As in mice, the first hematopoietic cells in human development arise in the yolk sac around Carnegie Stage 7 (CS7) which is primarily endowed with erythrocyte, megakaryocyte, and macrophage potential (Bloom &

Bartelmez, 1940; Tavian, Hallais & Peault, 1999; Tyser et al., 2021; Bian et al., 2021). Reminiscent, of transient lymphoid-primed multipotent progenitors (eMPPs, LMPs, drHSCs) in mice, a distinct lymphoid progenitor wave has been described in humans that emerges around CS14 (Böiers et al., 2013; Beaudin et al., 2016; Zhu et al., 2020; Patel et al., 2022; Calvanese et al., 2022).

As in mice, human transient EMPs and lymphoid progenitors sequentially seed the fetal liver, followed by HSCs that emerge in the AGM around CS14 to CS16 (4-5 weeks) (Tavian, Hallais & Peault, 1999). HSCs take over blood cell production around CS17 (6 weeks) when the first transient hematopoietic waves exhaust. Finally, HSCs seed the developing bone marrow around 12-14 weeks of gestation where they adapt a more quiescent phenotype (Charbord et al., 1996; Ranzoni et al., 2021; Zheng et al., 2022; Marderstein et al., 2024).

In contrast to mice, however, transient yolk sac-derived cells such as erythroblasts and megakaryocytes (except for macrophages) as well as transient lymphoid cells are only temporarily present during the first trimester in humans, due to the longer gestation period (Calvanese et al., 2022). In comparison, EMP-derived erythrocytes circulate through the bloodstream until around birth (Soares-da-Silva et al., 2021) and eMPP-derived cells are present even beyond birth (Patel et al., 2022; Yokomizo et al., 2022).

Therefore, the conclusions regarding EMPs from my studies in mice, especially in the assessment of postnatal effects, cannot be directly transferred to humans. Instead, rather the fact that the same mutation exerts different effects in distinct hematopoietic waves, particularly transient hematopoietic waves compared to adult *bona fide* HSCs, could be translated to humans.

In line with this notion, other studies in the mouse model suggested that pediatric acute lymphoid leukemias (ALLs) might originate from distinct cellular origins than adult ALL. For example, Sinha and colleagues demonstrated that MLL-ENL translocation causes a more aggressive disease when induced at E12.5 than in the adult bone marrow (Sinha et al., 2020). Furthermore, another study showed that the expression of the MLL-AF4 fusion gene causes a stronger effect between E12.5 and E14.5 than at later stages (Barrett et al., 2016). This effect was associated with lymphoid-primed multipotent progenitors (LMPPs) (Böiers et al., 2013) which correspond to eMPPs. In fact, there is increasing data that eMPPs may also be intrinsically regulated by different molecular mechanisms. For example, a currently unpublished study shows that the lack of *Smad7* impairs the maturation and repopulating potential of HSCs without affecting eMPP numbers (poster at ISEH 2024: Bennett et al., 2024). It is therefore plausible that a mutation might not only drive different phenotypes between EMPs and HSCs, but also between eMPPs and HSCs.

4.4 Conclusion

In summary, my PhD work provides evidence that even though embryonic hematopoietic waves such as EMPs are transient and only contribute little to mature cells after birth, perturbations in the developmental period can have long-lasting effects. The establishment of life-long hematopoiesis by HSCs relies on the integrity of previous transient waves. Additionally, if mutations occur in transient progenitor waves, this could significantly extend the lifespan of a cell derived from such a transient lineage and carry diseases to postnatal life. Furthermore, due to intrinsic differences between hematopoietic waves, mutations can drive ontogeny-specific effects causing stage-specific disease pathology.

For these reasons, it is important to gain an even further understanding of the complexity of developmental hematopoiesis and particularly the differences between hematopoietic waves as this has the potential to develop better treatments for diseases.

With technology evolving it will thus be exciting to further uncover the landscape of the developing hematopoietic system not only in mice but particularly in humans.

Bibliography

Abrams JM, White K, Fessler LI, Steller H. 1993. Programmed cell death during Drosophila embryogenesis. *Development (Cambridge, England)* 117:29–43. DOI: 10.1242/dev.117.1.29.

Adamo L, Naveiras O, Wenzel PL, McKinney-Freeman S, Mack PJ, Gracia-Sancho J, Suchy-Dicey A, Yoshimoto M, Lensch MW, Yoder MC, García-Cardeña G, Daley GQ. 2009. Biomechanical forces promote embryonic haematopoiesis. *Nature* 459:1131–1135. DOI: 10.1038/nature08073.

Adolfsson J, Månsson R, Buza-Vidas N, Hultquist A, Liuba K, Jensen CT, Bryder D, Yang L, Borge O-J, Thoren LAM, Anderson K, Sitnicka E, Sasaki Y, Sigvardsson M, Jacobsen SEW. 2005. Identification of Flt3+ Lympho-Myeloid Stem Cells Lacking Erythro-Megakaryocytic Potential: A Revised Road Map for Adult Blood Lineage Commitment. *Cell* 121:295–306. DOI: 10.1016/j.cell.2005.02.013.

Ahmed N, Kunz L, Hoppe PS, Loeffler D, Etzrodt M, Ortega GC, Hilsenbeck O, Anastassiadis K, Schroeder T. 2020. A Novel GATA2 Protein Reporter Mouse Reveals Hematopoietic Progenitor Cell Types. *Stem Cell Reports* 15:326–339. DOI: 10.1016/j.stemcr.2020.06.008.

Aibar S, González-Blas CB, Moerman T, Huynh-Thu VA, Imrichova H, Hulselmans G, Rambow F, Marine JC, Geurts P, Aerts J, Van Den Oord J, Atak ZK, Wouters J, Aerts S. 2017. SCENIC: Single-cell regulatory network inference and clustering. *Nature Methods* 14:1083–1086. DOI: 10.1038/nmeth.4463.

Ajami B, Bennett JL, Krieger C, Tetzlaff W, Rossi FMV. 2007. Local self-renewal can sustain CNS microglia maintenance and function throughout adult life. *Nature neuroscience* 10:1538–1543. DOI: 10.1038/NN2014.

Akashi K, Traver D, Miyamoto T, Weissman I. 2000. A clonogenic common myeloid progenitor that gives rise to all myeloid lineages. *Nature* 404:193–197.

Al-Adhami MA, Kunz YW. 1977. Ontogenesis of Haematopoietic Sites in Brachydanio Rerio (Hamilton-Buchanan) (Teleostei)*. *Development, Growth & Differentiation* 19:171–179. DOI: 10.1111/j.1440-169X.1977.00171.x.

Amemiya HM, Kundaje A, Boyle AP. 2019. The ENCODE Blacklist: Identification of Problematic Regions of the Genome. *Scientific Reports* 9:9354. DOI: 10.1038/s41598-019-45839-z.

Andersson AK, Ma J, Wang J, Chen X, Gedman AL, Dang J, Nakitandwe J, Holmfeldt L, Parker M, Easton J, Huether R, Kriwacki R, Rusch M, Wu G, Li Y, Mulder H, Raimondi S, Pounds S, Kang G, Shi L, Becksfort J, Gupta P, Payne-Turner D, Vadodaria B, Boggs K, Yergeau D, Manne J, Song G, Edmonson M, Nagahawatte P, Wei L, Cheng C, Pei D, Sutton R, Venn NC, Chetcuti A, Rush A, Catchpoole D, Heldrup J, Fioretos T, Lu C, Ding L, Pui C-H, Shurtleff S, Mullighan CG, Mardis ER, Wilson RK, Gruber TA, Zhang J, Downing JR. 2015. The landscape of somatic mutations in infant MLL-rearranged acute lymphoblastic leukemias. *Nature Genetics* 47:330–337. DOI: 10.1038/ng.3230.

de Andres B, Mueller AL, Verbeek S, Sandor M, Lynch RG. 1998. A Regulatory Role for Fc**γ** Receptors CD16 and CD32 in the Development of Murine B Cells. *Blood* 92:2823–2829. DOI: 10.1182/blood.V92.8.2823.

Ara T, Tokoyoda K, Sugiyama T, Egawa T, Kawabata K, Nagasawa T. 2003. Long-Term Hematopoietic Stem Cells Require Stromal Cell-Derived Factor-1 for Colonizing Bone Marrow during Ontogeny. *Immunity* 19:257–267. DOI: 10.1016/S1074-7613(03)00201-2.

Arinobu Y, Iwasaki H, Gurish MF, Mizuno S, Shigematsu H, Ozawa H, Tenen DG, Frank Austen K, Akashi K. 2005. Developmental checkpoints of the basophilmast cell lineages in adult murine hematopoiesis.

Arinobu Y, Mizuno S ichi, Chong Y, Shigematsu H, Iino T, Iwasaki H, Graf T, Mayfield R, Chan S, Kastner P, Akashi K. 2007. Reciprocal Activation of GATA-1 and PU.1 Marks Initial Specification of Hematopoietic Stem Cells into Myeloerythroid and Myelolymphoid Lineages. *Cell Stem Cell* 1:416–427. DOI: 10.1016/j.stem.2007.07.004.

Arnold SJ, Robertson EJ. 2009. Making a commitment: cell lineage allocation and axis patterning in the early mouse embryo. *Nature Reviews Molecular Cell Biology* 10:91–103. DOI: 10.1038/nrm2618.

Atkins MH, Scarfò R, McGrath KE, Yang D, Palis J, Ditadi A, Keller GM. 2021. Modeling human yolk sac hematopoiesis with pluripotent stem cells. *Journal of Experimental Medicine* 219. DOI: 10.1084/JEM.20211924/212927.

Auffray C, Fogg DK, Narni-Mancinelli E, Senechal B, Trouillet C, Saederup N, Leemput J, Bigot K, Campisi L, Abitbol M, Molina T, Charo I, Hume DA, Cumano A, Lauvau G, Geissmann F. 2009. CX3CR1+ CD115+ CD135+ common macrophage/DC precursors and the role of CX3CR1 in their response to inflammation. *Journal of Experimental Medicine* 206:595–606. DOI: 10.1084/jem.20081385.

Azzoni E, Frontera V, Anselmi G, Rode C, James C, Deltcheva EM, Demian AS, Brown J, Barone C, Patelli A, Harman JR, Nicholls M, Conway SJ, Morrissey E, Jacobsen SEW, Sparrow DB, Harris AL, Enver T, de Bruijn MFTR. 2021. The onset of circulation triggers a metabolic switch required for endothelial to hematopoietic transition. *Cell Reports* 37:110103. DOI: 10.1016/j.celrep.2021.110103.

Azzoni E, Frontera V, McGrath KE, Harman J, Carrelha J, Nerlov C, Palis J, Jacobsen SEW, Bruijn MF. 2018. Kit ligand has a critical role in mouse yolk sac and aorta–gonad–mesonephros hematopoiesis. *EMBO reports* 19:1–17. DOI: 10.15252/embr.201745477.

Bain CC, Bravo-Blas A, Scott CL, Gomez Perdiguero E, Geissmann F, Henri S, Malissen B, Osborne LC, Artis D, Mowat AM. 2014. Constant replenishment from circulating monocytes maintains the macrophage pool in the intestine of adult mice. *Nature Immunology* 15:929–937. DOI: 10.1038/ni.2967.

Banerjee U, Girard JR, Goins LM, Spratford CM. 2019. Drosophila as a Genetic Model for Hematopoiesis. *Genetics* 211:367–417. DOI: 10.1534/genetics.118.300223.

Barker JE. 1968. Development of the Mouse Hematopoietic System I. Types of Hemoglobin Produced in Embryonic Yolk Sac and Liver1j2. *DEVELOPMENTAL BIOLOGY* 18:14–29.

Barone C, Quattrini G, Orsenigo R, Timóteo-Ferreira F, Muratore A, Cazzola A, Patelli A, Soares-da-Silva F, Nicholls M, Mauri M, Bombelli S, Marco SD, D'Aliberti D, Spinelli S, Bonalume V, Domingues A, Sala G, Colonna A, D'Errico E, D'Orlando C, Bianchi C, Perego RA, Meneveri R, Bruijn MFTRD, Cumano A, Fantin A, Brunelli S, Piazza R, Azzoni E. 2024. Hemogenic endothelium of the vitelline and umbilical arteries is the major contributor to mouse fetal lympho-myelopoiesis. :2024.07.11.603050. DOI: 10.1101/2024.07.11.603050.

Barrett NA, Malouf C, Kapeni C, Bacon WA, Giotopoulos G, Jacobsen SEW, Huntly BJ, Ottersbach K. 2016. Mll-AF4 Confers Enhanced Self-Renewal and Lymphoid Potential during a Restricted Window in Development. *Cell Reports* 16:1039–1054. DOI: 10.1016/j.celrep.2016.06.046.

Bauer HC, Bauer H, Lametschwandtner A, Amberger A, Ruiz P, Steiner M. 1993. Neovascularization and the appearance of morphological characteristics of the blood-brain barrier in the embryonic mouse central nervous system. *Brain Research. Developmental Brain Research* 75:269–278. DOI: 10.1016/0165-3806(93)90031-5.

Beaudin AE, Boyer SW, Perez-Cunningham J, Hernandez GE, Derderian SC, Jujjavarapu C, Aaserude E, MacKenzie T, Forsberg EC. 2016. A Transient Developmental Hematopoietic Stem Cell Gives Rise to Innate-like B and T Cells. *Cell Stem Cell* 19:768–783. DOI: 10.1016/j.stem.2016.08.013.

Becker AJ, McCULLOCH EA, Till JE. 1963. Cytological Demonstration of the Clonal Nature of Spleen Colonies Derived from Transplanted Mouse Marrow Cells. *Nature* 197:452–454. DOI: 10.1038/197452a0.

Benjamini Y, Hochberg Y. 1995. Controlling the False Discovery Rate: A Practical and Powerful Approach to Multiple Testing. *Journal of the Royal Statistical Society: Series B (Methodological)* 57:289–300. DOI: 10.1111/j.2517-6161.1995.tb02031.x.

Bennett L, An HH, Speck N. 2024. 3024 – RESTRAINT OF TGF-B SIGNALING BY SMAD7 IS NECESSARY FOR HEMATOPOIETIC STEM CELL FORMATION IN THE MOUSE EMBRYO. *Experimental Hematology* 137:104346. DOI: 10.1016/j.exphem.2024.104346.

Bertrand JY, Chi NC, Santoso B, Teng S, Stainier DYR, Traver D. 2010a. Haematopoietic stem cells derive directly from aortic endothelium during development. *Nature* 464:108–111. DOI: 10.1038/nature08738.

Bertrand JY, Cisson JL, Stachura DL, Traver D. 2010b. Notch signaling distinguishes 2 waves of definitive hematopoiesis in the zebrafish embryo. *Blood* 115:2777–2783. DOI: 10.1182/blood-2009-09-244590.

Bertrand JY, Jalil A, Klaine M, Jung S, Cumano A, Godin I. 2005. Three pathways to mature macrophages in the early mouse yolk sac. *Blood* 106:3004–3011. DOI: 10.1182/blood-2005-02-0461.

Bertrand JY, Kim AD, Violette EP, Stachura DL, Cisson JL, Traver D. 2007. Definitive hematopoiesis initiates through a committed erythromyeloid progenitor in the zebrafish embryo. *Development* 134:4147–4156. DOI: 10.1242/DEV.012385.

Bian G, Gu Y, Xu C, Yang W, Pan X, Chen Y, Lai M, Zhou Y, Dong Y, Mao B, Zhou Q, Chen B, Nakathata T, Shi L, Wu M, Zhang Y, Ma F. 2021. Early development and functional properties of tryptase/chymase double-positive mast cells from human pluripotent stem cells. *Journal of Molecular Cell Biology* 13:104–115. DOI: 10.1093/jmcb/mjaa059.

Bizzozero G. 1868. Sulla funzione ematopoetica del midollo delle ossa. *Zentralbl Med Wissensch* 6:885.

Bizzozero G. 1869. *Sulla funzione ematopoetica del midollo delle ossa: seconda comunicazione preventiva*.

Bloom W, Bartelmez GW. 1940. Hematopoiesis in young human embryos. *American Journal of Anatomy* 67:21–53. DOI: 10.1002/AJA.1000670103.

Blume-Jensen P, Claesson-Welsh L, Siegbahn A, Zsebo KM, Westermark B, Heldin CH. 1991. Activation of the human c-kit product by ligand-induced dimerization mediates circular actin reorganization and chemotaxis. *The EMBO Journal* 10:4121–4128. DOI: 10.1002/j.1460-2075.1991.tb04989.x.

Böiers C, Carrelha J, Lutteropp M, Luc S, Green JCA, Azzoni E, Woll PS, Mead AJ, Hultquist A, Swiers G, Perdiguero EG, Macaulay IC, Melchiori L, Luis TC, Kharazi S, Bouriez-Jones T, Deng Q, Pontén A, Atkinson D, Jensen CT, Sitnicka E, Geissmann F, Godin I, Sandberg R, de Bruijn MFTR, Jacobsen SEW. 2013. Lymphomyeloid Contribution of an Immune-Restricted Progenitor Emerging Prior to Definitive Hematopoietic Stem Cells. *Cell Stem Cell* 13:535–548. DOI: 10.1016/j.stem.2013.08.012.

Boisset J-C, van Cappellen W, Andrieu-Soler C, Galjart N, Dzierzak E, Robin C. 2010. In vivo imaging of haematopoietic cells emerging from the mouse aortic endothelium. *Nature* 464:116–120. DOI: 10.1038/nature08764.

Bowie MB, Kent DG, Dykstra B, McKnight KD, McCaffrey L, Hoodless PA, Eaves CJ. 2007. Identification of a new intrinsically timed developmental checkpoint that reprograms key hematopoietic stem cell properties. *Proceedings of the National Academy of Sciences of the United States of America* 104:5878–5882. DOI: 10.1073/pnas.0700460104.

Bowie MB, McKnight KD, Kent DG, McCaffrey L, Hoodless PA, Eaves CJ. 2006. Hematopoietic stem cells proliferate until after birth and show a reversible phase-specific engraftment defect. *The Journal of Clinical Investigation* 116:2808–2816. DOI: 10.1172/JCI28310.

Bowling S, Sritharan D, Osorio FG, Nguyen M, Cheung P, Rodriguez-Fraticelli A, Patel S, Yuan W-C, Fujiwara Y, Li BE, Orkin SH, Hormoz S, Camargo FD. 2020. An Engineered CRISPR-Cas9 Mouse Line for Simultaneous Readout of Lineage Histories and Gene Expression Profiles in Single Cells. *Cell* 181:1410-1422.e27. DOI: 10.1016/j.cell.2020.04.048.

Boyer SW, Schroeder AV, Smith-Berdan S, Forsberg EC. 2011. All Hematopoietic Cells Develop from Hematopoietic Stem Cells through Flk2/Flt3-Positive Progenitor Cells. *Cell Stem Cell* 9:64–73. DOI: 10.1016/j.stem.2011.04.021.

Brownlie A, Hersey C, Oates AC, Paw BH, Falick AM, Witkowska HE, Flint J, Higgs D, Jessen J, Bahary N, Zhu H, Lin S, Zon L. 2003. Characterization of embryonic globin genes of the zebrafish. *Developmental Biology* 255:48–61. DOI: 10.1016/S0012-1606(02)00041-6.

de Bruijn MF, Speck NA, Peeters MC, Dzierzak E. 2000. Definitive hematopoietic stem cells first develop within the major arterial regions of the mouse embryo. *The EMBO journal* 19:2465–74. DOI: 10.1093/emboj/19.11.2465.

Buza-Vidas N, Woll P, Hultquist A, Duarte S, Lutteropp M, Bouriez-Jones T, Ferry H, Luc S, Jacobsen SEW. 2011. FLT3 expression initiates in fully multipotent mouse hematopoietic progenitor cells. *Blood* 118:1544–1548. DOI: 10.1182/blood-2010-10-316232.

Cabezas-Wallscheid N, Klimmeck D, Hansson J, Lipka DB, Reyes A, Wang Q, Weichenhan D, Lier A, Von Paleske L, Renders S, Wünsche P, Zeisberger P, Brocks D, Gu L, Herrmann C, Haas S, Essers MAG, Brors B, Eils R, Huber W, Milsom MD, Plass C, Krijgsveld J, Trumpp A. 2014. Identification of regulatory networks in HSCs and their immediate progeny via integrated proteome, transcriptome, and DNA methylome analysis. *Cell Stem Cell* 15:507–522. DOI: 10.1016/j.stem.2014.07.005.

Cai Z, Bruijn M de, Ma X, Dortland B, Luteijn T, Downing JR, Dzierzak E. 2000. Haploinsufficiency of AML1 Affects the Temporal and Spatial Generation of Hematopoietic Stem Cells in the Mouse Embryo. *Immunity* 13:423–431. DOI: 10.1016/S1074-7613(00)00042-X.

Calligaris R, Bottardi S, Cogoi S, Apezteguia I, Santoro C. 1995. Alternative Translation Initiation Site Usage Results in Two Functionally Distinct Forms of the GATA-1 Transcription Factor. *Proceedings of the National Academy of Sciences of the United States of America* 92:11598–11602.

Calvanese V, Capellera-Garcia S, Ma F, Fares I, Liebscher S, Ng ES, Ekstrand S, Aguadé-Gorgorió J, Vavilina A, Lefaudeux D, Nadel B, Li JY, Wang Y, Lee LK, Ardehali R, Iruela-Arispe ML, Pellegrini M, Stanley EG, Elefanty AG, Schenke-Layland K, Mikkola HKA. 2022. Mapping human haematopoietic stem cells from haemogenic endothelium to birth. *Nature* 604:534–540. DOI: 10.1038/s41586-022-04571-x.

Calvanese V, Mikkola HKA. 2023. The genesis of human hematopoietic stem cells. *Blood* 142:519–532. DOI: 10.1182/blood.2022017934.

Camiolo G, Mullen CG, Ottersbach K. 2024. Mechanistic insights into the developmental origin of pediatric hematologic disorders. *Experimental Hematology* 0. DOI: 10.1016/j.exphem.2024.104583.

Canu G, Ruhrberg C. 2021. First blood: the endothelial origins of hematopoietic progenitors. *Angiogenesis 2021 24:2* 24:199–211. DOI: 10.1007/S10456-021-09783-9.

Caplan RM. 1963. The Natural Course of Urticaria Pigmentosa: Analysis and Follow-Up of 112 Cases. *Archives of Dermatology* 87:146–157. DOI: 10.1001/archderm.1963.01590140008002.

Carrelha J, Mazzi S, Winroth A, Hagemann-Jensen M, Ziegenhain C, Högstrand K, Seki M, Brennan MS, Lehander M, Wu B, Meng Y, Markljung E, Norfo R, Ishida H, Belander Strålin K, Grasso F, Simoglou Karali C, Aliouat A, Hillen A, Chari E, Siletti K, Thongjuea S, Mead AJ, Linnarsson S, Nerlov C, Sandberg R, Yoshizato T, Woll PS, Jacobsen SEW. 2024. Alternative platelet differentiation pathways initiated by nonhierarchically related hematopoietic stem cells. *Nature Immunology* 25:1007–1019. DOI: 10.1038/s41590-024-01845-6.

Carrelha J, Meng Y, Kettyle LM, Luis TC, Norfo R, Alcolea V, Boukarabila H, Grasso F, Gambardella A, Grover A, Högstrand K, Lord AM, Sanjuan-Pla A, Woll PS, Nerlov C, Jacobsen SEW. 2018. Hierarchically related lineage-restricted fates of multipotent haematopoietic stem cells. *Nature* 554:106–111. DOI: 10.1038/nature25455.

Cattelino A, Liebner S, Gallini R, Zanetti A, Balconi G, Corsi A, Bianco P, Wolburg H, Moore R, Oreda B, Kemler R, Dejana E. 2003. The conditional inactivation of the β-catenin gene in endothelial cells causes a defective vascular pattern and increased vascular fragility. *Journal of Cell Biology* 162:1111–1122. DOI: 10.1083/jcb.200212157.

Cazzola A, Cazzaniga G, Biondi A, Meneveri R, Brunelli S, Azzoni E. 2021. Prenatal Origin of Pediatric Leukemia: Lessons From Hematopoietic Development. *Frontiers in Cell and Developmental Biology* 8. DOI: 10.3389/fcell.2020.618164.

Cecchini MG, Dominguez MG, Mocci S, Wetterwald A, Felix R, Fleisch H, Chisholm O, Hofstetter W, Pollard JW, Stanley ER. 1994. Role of colony stimulating factor-1 in the establishment and regulation of tissue macrophages during postnatal development of the mouse. *Development (Cambridge, England)* 120:1357–1372. DOI: 10.1242/dev.120.6.1357.

Challen GA, Pietras EM, Wallscheid NC, Signer RAJ. 2021. Simplified murine multipotent progenitor isolation scheme: Establishing a consensus approach for multipotent progenitor identification. *Experimental Hematology* 104:55–63. DOI: 10.1016/j.exphem.2021.09.007.

Chang AN, Cantor AB, Fujiwara Y, Lodish MB, Droho S, Crispino JD, Orkin SH. 2002. GATA-factor dependence of the multitype zinc-finger protein FOG-1 for its essential role in megakaryopoiesis. *Proceedings of the National Academy of Sciences* 99:9237–9242. DOI: 10.1073/pnas.142302099.

Charbord P, Tavian M, Humeau L, Peault B. 1996. Early Ontogeny of the Human Marrow From Long Bones: An Immunohistochemical Study of Hematopoiesis and Its Microenvironment. *Blood* 87:4109–4119. DOI: 10.1182/blood.V87.10.4109.bloodjournal87104109.

Chen MJ, Li Y, De Obaldia ME, Yang Q, Yzaguirre AD, Yamada-Inagawa T, Vink CS, Bhandoola A, Dzierzak E, Speck NA. 2011. Erythroid/myeloid progenitors and hematopoietic stem cells originate from distinct populations of endothelial cells. *Cell Stem Cell* 9:541–552. DOI: 10.1016/j.stem.2011.10.003.

Chen H, Ray-Gallet D, Zhang P, Hetherington CJ, Gonzalez DA, Zhang DE, Moreau-Gachelin F, Tenen DG. 1995. PU.1 (Spi-1) autoregulates its expression in myeloid cells. *Oncogene* 11:1549–1560.

Chen EY, Tan CM, Kou Y, Duan Q, Wang Z, Meirelles G, Clark NR, Ma'ayan A. 2013. Enrichr: interactive and collaborative HTML5 gene list enrichment analysis tool. *BMC Bioinformatics* 14:128. DOI: 10.1186/1471-2105-14-128.

Chen MJ, Yokomizo T, Zeigler BM, Dzierzak E, Speck NA. 2009. Runx1 is required for the endothelial to haematopoietic cell transition but not thereafter. *Nature* 457:887–891. DOI: 10.1038/nature07619.

Cheshier SH, Morrison SJ, Liao X, Weissman IL. 1999. In vivo proliferation and cell cycle kinetics of long-term self-renewing hematopoietic stem cells. *Proceedings of the National Academy of Sciences of the United States of America* 96:3120–3125.

Chia SL, Kapoor S, Carvalho C, Bajénoff M, Gentek R. 2023. Mast cell ontogeny: From fetal development to life-long health and disease. *Immunological Reviews* 315:31–53. DOI: 10.1111/imr.13191.

Chou ST, Khandros E, Bailey LC, Nichols KE, Vakoc CR, Yao Y, Huang Z, Crispino JD, Hardison RC, Blobel GA, Weiss MJ. 2009. Graded repression of PU.1/Sfpi1 gene transcription by GATA factors regulates hematopoietic cell fate. *Blood* 114:983–994. DOI: 10.1182/blood-2009-03-207944.

Chow A, Lucas D, Hidalgo A, Méndez-Ferrer S, Hashimoto D, Scheiermann C, Battista M, Leboeuf M, Prophete C, van Rooijen N, Tanaka M, Merad M, Frenette PS. 2011. Bone marrow CD169+ macrophages promote the retention of hematopoietic stem and progenitor cells in the mesenchymal stem cell niche. *Journal of Experimental Medicine* 208:261–271. DOI: 10.1084/jem.20101688.

Christensen JL, Weissman IL. 2001. Flk-2 is a marker in hematopoietic stem cell differentiation: A simple method to isolate long-term stem cells. *Proceedings of the National Academy of Sciences* 98:14541–14546. DOI: 10.1073/pnas.261562798.

Christensen JL, Wright DE, Wagers AJ, Weissman IL. 2004. Circulation and Chemotaxis of Fetal Hematopoietic Stem Cells. *PLOS Biology* 2:e75. DOI: 10.1371/JOURNAL.PBIO.0020075.

Cindrova-Davies T, Jauniaux E, Elliot MG, Gong S, Burton GJ, Charnock-Jones DS. 2017. RNA-seq reveals conservation of function among the yolk sacs of human, mouse, and chicken. *Proceedings of the National Academy of Sciences* 114:E4753–E4761. DOI: 10.1073/pnas.1702560114.

Cirovic B, Schönheit J, Kowenz-Leutz E, Ivanovska J, Klement C, Pronina N, Bégay V, Leutz A. 2017. C/EBP-Induced Transdifferentiation Reveals Granulocyte-Macrophage Precursor-like Plasticity of B Cells. *Stem Cell Reports* 8:346–359. DOI: 10.1016/j.stemcr.2016.12.015.

Clarke RL, Yzaguirre AD, Yashiro-Ohtani Y, Bondue A, Blanpain C, Pear WS, Speck NA, Keller G. 2013. The expression of Sox17 identifies and regulates haemogenic endothelium. *Nature Cell Biology* 15:502–510. DOI: 10.1038/ncb2724.

Coller BS. 2015. Blood at 70: its roots in the history of hematology and its birth. *Blood* 126:2548–2560. DOI: 10.1182/blood-2015-09-659581.

Coller BS, Peerschke EI, Scudder LE, Sullivan CA. 1983. Studies With a Murine Monoclonal Antibody That Abolishes Ristocetin-Induced Binding of von Willebrand Factor to Platelets: Additional Evidence in Support of GPIb as a Platelet Receptor for von Willebrand Factor. *Blood* 61:99–110. DOI: 10.1182/blood.V61.1.99.99.

Collins A, Swann JW, Proven MA, Patel CM, Mitchell CA, Kasbekar M, Dellorusso PV, Passegué E. 2024. Maternal inflammation regulates fetal emergency myelopoiesis. *Cell* 187:1402-1421.e21. DOI: 10.1016/j.cell.2024.02.002.

Corada M, Orsenigo F, Morini MF, Pitulescu ME, Bhat G, Nyqvist D, Breviario F, Conti V, Briot A, Iruela-Arispe ML, Adams RH, Dejana E. 2013. Sox17 is indispensable for acquisition and maintenance of arterial identity. *Nature Communications* 4:2609. DOI: 10.1038/ncomms3609.

Cortegano I, Serrano N, Ruiz C, Rodríguez M, Prado C, Alía M, Hidalgo A, Cano E, Andrés BD, Gaspar M, Gaspar M. 2019. CD45 expression discriminates waves of Correspondence : :1853–1865. DOI: 10.3324/haematol.2018.192559.

Coşkun S, Chao H, Vasavada H, Heydari K, Gonzales N, Zhou X, de Crombrugghe B, Hirschi KK. 2014. Development of the Fetal Bone Marrow Niche and Regulation of HSC Quiescence and Homing Ability by Emerging Osteolineage Cells. *Cell Reports* 9:581–590. DOI: 10.1016/j.celrep.2014.09.013.

Costa G, Mazan A, Gandillet A, Pearson S, Lacaud G, Kouskoff V. 2012. SOX7 regulates the expression of VE-cadherin in the haemogenic endothelium at the onset of haematopoietic development. *Development* 139:1587–1598. DOI: 10.1242/dev.071282.

Cova G, Taroni C, Deau M-C, Cai Q, Mittelheisser V, Philipps M, Jung M, Cerciat M, Le Gras S, Thibault-Carpentier C, Jost B, Carlsson L, Thornton AM, Shevach EM, Kirstetter P, Kastner P, Chan S. 2021. Helios represses megakaryocyte priming in hematopoietic stem and progenitor cells. *Journal of Experimental Medicine* 218:e20202317. DOI: 10.1084/jem.20202317.

Crozatier M, Meister M. 2007. Drosophila haematopoiesis. *Cellular Microbiology* 9:1117–1126. DOI: 10.1111/j.1462-5822.2007.00930.x.

Cumano A, Berthault C, Ramond C, Petit M, Golub R, Bandeira A, Pereira P. 2019. New Molecular Insights into Immune Cell Development. *Annual Review of Immunology* 37:497–519. DOI: 10.1146/annurev-immunol-042718-041319.

Cumano A, Dieterlen-Lievre F, Godin I. 1996. Lymphoid Potential, Probed before Circulation in Mouse, Is Restricted to Caudal Intraembryonic Splanchnopleura. *Cell* 86:907–916. DOI: 10.1016/S0092-8674(00)80166-X.

Cumano A, Ferraz JC, Klaine M, Di Santo JP, Godin I. 2001. Intraembryonic, but Not Yolk Sac Hematopoietic Precursors, Isolated before Circulation, Provide Long-Term Multilineage Reconstitution. *Immunity* 15:477–485. DOI: 10.1016/S1074-7613(01)00190-X.

Daga A, Karlovich CA, Dumstrei K, Banerjee U. 1996. Patterning of cells in the Drosophila eye by Lozenge, which shares homologous domains with AML1. *Genes & Development* 10:1194–1205. DOI: 10.1101/gad.10.10.1194.

Dahlin JS, Hamey FK, Pijuan-Sala B, Shepherd M, Lau WWY, Nestorowa S, Weinreb C, Wolock S, Hannah R, Diamanti E, Kent DG, Göttgens B, Wilson NK. 2018. A single-cell hematopoietic landscape resolves 8 lineage trajectories and defects in Kit mutant mice. *Blood* 131:e1–e11. DOI: 10.1182/blood-2017-12-821413.

D'Amico A, Wu L. 2003. The Early Progenitors of Mouse Dendritic Cells and Plasmacytoid Predendritic Cells Are within the Bone Marrow Hemopoietic Precursors Expressing Flt3. *The Journal of Experimental Medicine* 198:293–303. DOI: 10.1084/jem.20030107.

Dantschakoff W. 1908. Untersuchungen über die Entwickelung des Blutes und Bindegewebes bei den Vögeln. *Anatomische Hefte. I. Abteilung* 37. DOI: https://doi.org/10.1007/BF02284778.

De Biase D, Esposito F, De Martino M, Pirozzi C, Luciano A, Palma G, Raso GM, Iovane V, Marzocco S, Fusco A, Paciello O. 2019. Characterization of inflammatory infiltrate of ulcerative dermatitis in C57BL/6NCrl-Tg(HMGA1P6)1Pg mice. *Laboratory Animals* 53:447–458. DOI: 10.1177/0023677218815718.

De Bruijn MFTR, Ma X, Robin C, Ottersbach K, Sanchez MJ, Dzierzak E. 2002. Hematopoietic stem cells localize to the endothelial cell layer in the midgestation mouse aorta. *Immunity* 16:673–683. DOI: 10.1016/S1074-7613(02)00313-8.

Dege C, Fegan K, Creamer J, Berrien-Elliott M, Luff S, Kim D, Wagner J, Kingsley P, Mcgrath K, Fehniger T, Palis J, Sturgeon C. 2020. Potently Cytotoxic Natural Killer Cells Initially Emerge from Erythro-Myeloid Progenitors during Mammalian Development. *Developmental Cell* 53. DOI: 10.1016/j.devcel.2020.02.016.

Deng L, Zhou J-F, Sellers RS, Li J-F, Nguyen AV, Wang Y, Orlofsky A, Liu Q, Hume DA, Pollard JW, Augenlicht L, Lin EY. 2010. A Novel Mouse Model of Inflammatory Bowel Disease Links Mammalian Target of Rapamycin-Dependent Hyperproliferation of Colonic Epithelium to Inflammation-Associated Tumorigenesis. *The American Journal of Pathology* 176:952–967. DOI: 10.2353/ajpath.2010.090622.

Detrich HW, Kieran MW, Chan FY, Barone LM, Yee K, Rundstadler JA, Pratt S, Ransom D, Zon LI. 1995. Intraembryonic hematopoietic cell migration during vertebrate development. *Proceedings of the National Academy of Sciences* 92:10713–10717. DOI: 10.1073/pnas.92.23.10713.

Dieterlen-Lievre F. 1975. On the origin of haemopoietic stem cells in the avian embryo: an experimental approach. *Development* 33:607–619. DOI: 10.1242/dev.33.3.607.

Dignum T, Varnum-Finney B, Srivatsan SR, Dozono S, Waltner O, Heck AM, Ishida T, Nourigat-McKay C, Jackson DL, Rafii S, Trapnell C, Bernstein ID, Hadland B. 2021. Multipotent progenitors and hematopoietic stem cells arise independently from hemogenic endothelium in the mouse embryo. *Cell Reports* 36:109675. DOI: 10.1016/J.CELREP.2021.109675.

Doré LC, Crispino JD. 2011. Transcription factor networks in erythroid cell and megakaryocyte development. *Blood* 118:231–239. DOI: 10.1182/blood-2011-04-285981.

Drissen R, Buza-Vidas N, Woll P, Thongjuea S, Gambardella A, Giustacchini A, Mancini E, Zriwil A, Lutteropp M, Grover A, Mead A, Sitnicka E, Jacobsen SEW, Nerlov C. 2016. Distinct myeloid progenitor–differentiation pathways identified through single-cell RNA sequencing. *Nature Immunology* 17:666–676. DOI: 10.1038/ni.3412.

Drissen R, Thongjuea S, Theilgaard-Mönch K, Nerlov C. 2019. Identification of two distinct pathways of human myelopoiesis. *Science Immunology* 4:eaau7148. DOI: 10.1126/sciimmunol.aau7148.

Du T, Friend DS, Austen KF, Katz HR. 1996. Tissue-dependent differences in the asynchronous appearance of mast cells in normal mice and in congenic mast cell-deficient mice after infusion of normal bone marrow cells. *Clinical & Experimental Immunology* 103:316–321. DOI: 10.1046/j.1365-2249.1996.d01-610.x.

Duvic B, Hoffmann JA, Meister M, Royet J. 2002. Notch Signaling Controls Lineage Specification during *Drosophila* Larval Hematopoiesis. *Current Biology* 12:1923–1927. DOI: 10.1016/S0960-9822(02)01297-6.

Dwyer DF, Boyce JA. 2021. Neonatal mast cells and transplacental IgE transfer: A mechanism of disease inheritance or of passive infant barrier defense? *Journal of Allergy and Clinical Immunology* 148:76–77. DOI: 10.1016/j.jaci.2021.02.046.

Ehrlich P. 1878. *Beiträge zur Theorie und Praxis der histologischen Färbung*.

Eich C, Arlt J, Vink CS, Solaimani Kartalaei P, Kaimakis P, Mariani SA, van der Linden R, van Cappellen WA, Dzierzak E. 2017. In vivo single cell analysis reveals Gata2 dynamics in cells transitioning to hematopoietic fate. *Journal of Experimental Medicine* 215:233–248. DOI: 10.1084/jem.20170807.

Elsaid R, Meunier S, Burlen-Defranoux O, Soares-da-Silva F, Perchet T, Iturri L, Freyer L, Vieira P, Pereira P, Golub R, Bandeira A, Perdiguero EG, Cumano A. 2021. A wave of bipotent T/ILC-restricted progenitors shapes the embryonic thymus microenvironment in a time-dependent manner. *Blood* 137:1024–1036. DOI: 10.1182/blood.2020006779.

Elsaid R, Mikdache A, Castillo KQ, Salloum Y, Diabangouaya P, Gros G, Feijoo CG, Hernández PP. 2024. Definitive hematopoiesis is dispensable to sustain erythrocytes and macrophages during zebrafish ontogeny. *iScience* 27:108922. DOI: 10.1016/j.isci.2024.108922.

Epelman S, Lavine KJ, Beaudin AE, Sojka DK, Carrero JA, Calderon B, Brija T, Gautier EL, Ivanov S, Satpathy AT, Schilling JD, Schwendener R, Sergin I, Razani B, Forsberg EC, Yokoyama WM, Unanue ER, Colonna M, Randolph GJ, Mann DL. 2014. Embryonic and Adult-Derived Resident Cardiac Macrophages Are Maintained through Distinct Mechanisms at Steady State and during Inflammation. *Immunity* 40:91–104. DOI: 10.1016/j.immuni.2013.11.019.

Espín-Palazón R, Stachura DL, Campbell CA, García-Moreno D, Del Cid N, Kim AD, Candel S, Meseguer J, Mulero V, Traver D. 2014. Proinflammatory signaling regulates hematopoietic stem cell emergence. *Cell* 159:1070–1085. DOI: 10.1016/J.CELL.2014.10.031/ATTACHMENT/1AC4A3AF-EEDE-4F3E-8F4A-2531976CA050/MMC2.MP4.

Espín-Palazón R, Traver D. 2016. The NF-κB family: Key players during embryonic development and HSC emergence. *Experimental Hematology* 44:519–527. DOI: 10.1016/j.exphem.2016.03.010.

Ferkowicz MJ, Starr M, Xie X, Li W, Johnson SA, Shelley WC, Morrison PR, Yoder MC. 2003. CD41 expression defines the onset of primitive and definitive hematopoiesis in the murine embryo. *Development* 130:4393–4403. DOI: 10.1242/dev.00632.

Ferkowicz MJ, Yoder MC. 2005. Blood island formation: Longstanding observations and modern interpretations. *Experimental Hematology* 33:1041–1047. DOI: 10.1016/j.exphem.2005.06.006.

Ferrero G, Mahony CB, Dupuis E, Yvernogeau L, Di Ruggiero E, Miserocchi M, Caron M, Robin C, Traver D, Bertrand JY, Wittamer V. 2018. Embryonic Microglia Derive from Primitive Macrophages and Are Replaced by *cmyb*-Dependent Definitive Microglia in Zebrafish. *Cell Reports* 24:130–141. DOI: 10.1016/j.celrep.2018.05.066.

Finney BA, Schweighoffer E, Navarro-Núñez L, Bénézech C, Barone F, Hughes CE, Langan SA, Lowe KL, Pollitt AY, Mourao-Sa D, Sheardown S, Nash GB, Smithers N, Reis e Sousa C, Tybulewicz VLJ, Watson SP. 2012. CLEC-2 and Syk in the megakaryocytic/platelet lineage are essential for development. *Blood* 119:1747–1756. DOI: 10.1182/blood-2011-09-380709.

Fischer S, Gillis J. 2021. How many markers are needed to robustly determine a cell's type? *iScience* 24:103292. DOI: 10.1016/j.isci.2021.103292.

Fleck JS, Jansen SMJ, Wollny D, Zenk F, Seimiya M, Jain A, Okamoto R, Santel M, He Z, Camp JG, Treutlein B. 2023. Inferring and perturbing cell fate regulomes in human brain organoids. *Nature* 621:365–372. DOI: 10.1038/s41586-022-05279-8.

Fossett N, Tevosian SG, Gajewski K, Zhang Q, Orkin SH, Schulz RA. 2001. The Friend of GATA proteins U-shaped, FOG-1, and FOG-2 function as negative regulators of blood, heart, and eye development in Drosophila. *Proceedings of the National Academy of Sciences of the United States of America* 98:7342–7347. DOI: 10.1073/pnas.131215798.

Frame JM, Fegan KH, Conway SJ, McGrath KE, Palis J. 2016. Definitive Hematopoiesis in the Yolk Sac Emerges from Wnt-Responsive Hemogenic Endothelium Independently of Circulation and Arterial Identity. *STEM CELLS* 34:431–444. DOI: 10.1002/stem.2213.

Franc NC, Dimarcq J-L, Lagueux M, Hoffmann J, Ezekowitz RAB. 1996. Croquemort, A Novel Drosophila Hemocyte/Macrophage Receptor that Recognizes Apoptotic Cells. *Immunity* 4:431–443. DOI: 10.1016/S1074-7613(00)80410-0.

Francois M, Koopman P, Beltrame M. 2010. *SoxF* genes: Key players in the development of the cardio-vascular system. *The International Journal of Biochemistry & Cell Biology* 42:445–448. DOI: 10.1016/j.biocel.2009.08.017.

Freyer L, Iturri L, Biton A, Gomez Perdiguero E. 2020. Overlapping Definitive Progenitor Waves Divide and Conquer to Build a Layered Hematopoietic System. *bioRxiv*. DOI: 10.1101/2020.12.24.424302.

Freyer L, Iturri L, Biton A, Sommer A, Dardenne P, Cumano A, Gomez Perdiguero E. 2021. Fetal hematopoiesis is driven by privileged expansion and differentiation of yolk sac-derived erythro-myeloid progenitors. *Nature Immunology (in review)*. DOI: 10.21203/rs.3.rs-1002760/v1.

Frontelo P, Manwani D, Galdass M, Karsunky H, Lohmann F, Gallagher PG, Bieker JJ. 2007. Novel role for EKLF in megakaryocyte lineage commitment. *Blood* 110:3871–3880. DOI: 10.1182/blood-2007-03-082065.

Fujiwara Y, Browne CP, Cunniff K, Goff SC, Orkin SH. 1996. Arrested development of embryonic red cell precursors in mouse embryos lacking transcription factor GATA-1. *Proceedings of the National Academy of Sciences of the United States of America* 93:12355–12358. DOI: 10.1073/PNAS.93.22.12355.

Fujiwara Y, Chang AN, Williams AM, Orkin SH. 2004. Functional overlap of GATA-1 and GATA-2 in primitive hematopoietic development. *Blood* 103:583–585. DOI: 10.1182/blood-2003-08-2870.

Fujiwara T, O'Geen H, Keles S, Blahnik K, Linnemann AK, Kang Y-A, Choi K, Farnham PJ, Bresnick EH. 2009. Discovering Hematopoietic Mechanisms through Genome-wide Analysis of GATA Factor Chromatin Occupancy. *Molecular Cell* 36:667–681. DOI: 10.1016/j.molcel.2009.11.001.

van Furth R, Diesselhoff-den Dulk MM. 1984. Dual origin of mouse spleen macrophages. *Journal of Experimental Medicine* 160:1273–1283. DOI: 10.1084/jem.160.5.1273.

Gama-Norton L, Ferrando E, Ruiz-Herguido C, Liu Z, Guiu J, Islam ABMMK, Lee S-U, Yan M, Guidos CJ, López-Bigas N, Maeda T, Espinosa L, Kopan R, Bigas A. 2015. Notch signal strength controls cell fate in the haemogenic endothelium. *Nature Communications* 6:8510. DOI: 10.1038/ncomms9510.

Gandillet A, Serrano AG, Pearson S, Lie-A-Ling M, Lacaud G, Kouskoff V. 2009. Sox7-sustained expression alters the balance between proliferation and differentiation of hematopoietic progenitors at the onset of blood specification. *Blood* 114:4813–4822. DOI: 10.1182/blood-2009-06-226290.

Ganuza M, Hall T, Finkelstein D, Chabot A, Kang G, McKinney-Freeman S. 2017. Lifelong haematopoiesis is established by hundreds of precursors throughout mammalian ontogeny. *Nature Cell Biology 2017 19:10* 19:1153–1163. DOI: 10.1038/ncb3607.

Gao X, Johnson KD, Chang Y-I, Boyer ME, Dewey CN, Zhang J, Bresnick EH. 2013. Gata2 cis-element is required for hematopoietic stem cell generation in the mammalian embryo. *Journal of Experimental Medicine* 210:2833–2842. DOI: 10.1084/jem.20130733.

García-López JP, Grimaldi A, Chen Z, Meneses C, Bravo-Tello K, Bresciani E, Banderas A, Burgess SM, Hernández PP, Feijoo CG. 2023. Ontogenetically distinct neutrophils differ in function and transcriptional profile in zebrafish. *Nature Communications* 14:4942. DOI: 10.1038/s41467-023-40662-7.

Garni-Wagner BA, Purohit A, Mathew PA, Bennett M, Kumar V. 1993. A novel function-associated molecule related to non-MHC-restricted cytotoxicity mediated by activated natural killer cells and T cells. *Journal of Immunology (Baltimore, Md.: 1950)* 151:60–70.

Geissmann F, Manz MG, Jung S, Sieweke MH, Merad M, Ley K. 2010. Development of Monocytes, Macrophages, and Dendritic Cells. *Science* 327:656–661. DOI: 10.1126/science.1178331.

Gekas C, Dieterlen-Lièvre F, Orkin SH, Mikkola HKA. 2005. The Placenta Is a Niche for Hematopoietic Stem Cells. *Developmental Cell* 8:365–375. DOI: 10.1016/j.devcel.2004.12.016.

Gentek R, Ghigo C, Hoeffel G, Bulle MJ, Msallam R, Gautier G, Launay P, Chen J, Ginhoux F, Bajénoff M. 2018a. Hemogenic Endothelial Fate Mapping Reveals Dual Developmental Origin of Mast Cells. *Immunity* 48:1160-1171.e5. DOI: 10.1016/j.immuni.2018.04.025.

Gentek R, Ghigo C, Hoeffel G, Jorquera A, Msallam R, Wienert S, Klauschen F, Ginhoux F, Bajénoff M. 2018b. Epidermal **γδ** T cells originate from yolk sac hematopoiesis and clonally self-renew in the adult. *Journal of Experimental Medicine* 215:2994–3005. DOI: 10.1084/jem.20181206.

Gerbaulet A, Wickenhauser C, Scholten J, Peschke K, Drube S, Horny H-P, Kamradt T, Naumann R, Müller W, Krieg T, Waskow C, Hartmann K, Roers A. 2011. Mast cell hyperplasia, B-cell malignancy, and intestinal inflammation in mice with conditional expression of a constitutively active kit. *Blood* 117:2012–2021. DOI: 10.1182/blood-2008-11-189605.

Germain P-L, Lun A, Meixide CG, Macnair W, Robinson MD. 2022. Doublet identification in single-cell sequencing data using *scDblFinder*. DOI: 10.12688/f1000research.73600.2.

Ghosh S, Singh A, Mandal S, Mandal L. 2015. Active Hematopoietic Hubs in *Drosophila* Adults Generate Hemocytes and Contribute to Immune Response. *Developmental Cell* 33:478–488. DOI: 10.1016/j.devcel.2015.03.014.

Gialesaki S, Mahnken AK, Schmid L, Labuhn M, Bhayadia R, Heckl D, Klusmann JH. 2018. GATA1s exerts developmental stage-specific effects in human hematopoiesis. *Haematologica* 103:e336–e340. DOI: 10.3324/haematol.2018.191338.

Ginhoux F, Greter M, Leboeuf M, Nandi S, See P, Gokhan S, Mehler MF, Conway SJ, Ng LG, Stanley ER, Samokhvalov IM, Merad M. 2010. Fate Mapping Analysis Reveals That Adult Microglia Derive from Primitive Macrophages. *Science* 330:841–845. DOI: 10.1126/science.1194637.

Goh I, Botting RA, Rose A, Webb S, Engelbert J, Gitton Y, Stephenson E, Quiroga Londoño M, Mather M, Mende N, Imaz-Rosshandler I, Yang L, Horsfall D, Basurto-Lozada D, Chipampe N-J, Rook V, Lee JTH, Ton M-L, Keitley D, Mazin P, Vijayabaskar MS, Hannah R, Gambardella L, Green K, Ballereau S, Inoue M, Tuck E, Lorenzi V, Kwakwa K, Alsinet C, Olabi B, Miah M, Admane C, Popescu D-M, Acres M, Dixon D, Ness T, Coulthard R, Lisgo S, Henderson DJ, Dann E, Suo C, Kinston SJ, Park J, Polanski K, Marioni J, van Dongen S, Meyer KB, de Bruijn M, Palis J, Behjati S, Laurenti E, Wilson NK, Vento-Tormo R, Chédotal A, Bayraktar O, Roberts I, Jardine L, Göttgens B, Teichmann SA, Haniffa M. 2023. Yolk sac cell atlas reveals multiorgan functions during human early development. *Science* 381:eadd7564. DOI: 10.1126/science.add7564.

Gold KS, Brückner K. 2014. *Drosophila* as a model for the two myeloid blood cell systems in vertebrates. *Experimental Hematology* 42:717–727. DOI: 10.1016/j.exphem.2014.06.002.

Gomez Perdiguero E, Klapproth K, Schulz C, Busch K, Azzoni E, Crozet L, Garner H, Trouillet C, De Bruijn MF, Geissmann F, Rodewald HR. 2015. Tissue-resident macrophages originate from yolk-sac-derived erythro-myeloid progenitors. *Nature* 518:547–551. DOI: doi.org/10.1038/nature13989.

Gordon-Keylock S, Sobiesiak M, Rybtsov S, Moore K, Medvinsky A. 2013. Mouse extraembryonic arterial vessels harbor precursors capable of maturing into definitive HSCs. *Blood* 122:2338–2345. DOI: 10.1182/blood-2012-12-470971.

Gorivodsky M, Torchinsky A, Shepshelovich J, Savion S, Fein A, Carp H, Toder V. 1999. Colony-stimulating factor-1 (CSF-1) expression in the uteroplacental unit of mice with spontaneous and induced pregnancy loss. *Clinical and Experimental Immunology* 117:540–549. DOI: 10.1046/j.1365-2249.1999.00986.x.

Gouel-Chéron A, Dejoux A, Lamanna E, Bruhns P. 2023. Animal Models of IgE Anaphylaxis. *Biology* 12:931. DOI: 10.3390/biology12070931.

Gozalo AS, Zerfas PM, Qin J, Alves DA, Akkaya M, Peña MY, Elkins WR. 2023. Contributions of Diet and Age to Ulcerative Dermatitis in Female C57BL/6J Mice. *Comparative Medicine* 73:109–119. DOI: 10.30802/AALAS-CM-22-000096.

Grabert K, Sehgal A, Irvine KM, Wollscheid-Lengeling E, Ozdemir DD, Stables J, Luke GA, Ryan MD, Adamson A, Humphreys NE, Sandrock CJ, Rojo R, Verkasalo VA, Mueller W, Hohenstein P, Pettit AR, Pridans C, Hume DA. 2020. A Transgenic Line That Reports CSF1R Protein Expression Provides a Definitive Marker for the Mouse Mononuclear Phagocyte System. *The Journal of Immunology* 205:3154–3166. DOI: 10.4049/jimmunol.2000835.

Graf T, Enver T. 2009. Forcing cells to change lineages. *Nature* 462:587–594. DOI: 10.1038/nature08533.

Grass JA, Boyer ME, Pal S, Wu J, Weiss MJ, Bresnick EH. 2003. GATA-1-dependent transcriptional repression of GATA-2 via disruption of positive autoregulation and domain-wide chromatin remodeling. *Proceedings of the National Academy of Sciences* 100:8811–8816. DOI: 10.1073/pnas.1432147100.

Gregory GD, Miccio A, Bersenev A, Wang Y, Hong W, Zhang Z, Poncz M, Tong W, Blobel GA. 2010. FOG1 requires NuRD to promote hematopoiesis and maintain lineage fidelity within the megakaryocytic-erythroid compartment. *Blood* 115:2156–2166. DOI: 10.1182/blood-2009-10-251280.

Grigorian M, Mandal L, Hartenstein V. 2011. Hematopoiesis at the onset of metamorphosis: terminal differentiation and dissociation of the Drosophila lymph gland. *Development Genes and Evolution* 221:121–131. DOI: 10.1007/s00427-011-0364-6.

Grimbaldeston MA, Chen C-C, Piliponsky AM, Tsai M, Tam S-Y, Galli SJ. 2005. Mast Cell-Deficient W-sash c-kit Mutant KitW-sh/W-sh Mice as a Model for Investigating Mast Cell Biology in Vivo. *The American Journal of Pathology* 167:835–848.

Growney JD, Shigematsu H, Li Z, Lee BH, Adelsperger J, Rowan R, Curley DP, Kutok JL, Akashi K, Williams IR, Speck NA, Gilliland DG. 2005. Loss of Runx1 perturbs adult hematopoiesis and is associated with a myeloproliferative phenotype. *Blood* 106:494–504. DOI: 10.1182/blood-2004-08-3280.

Gschwend J, Sherman SPM, Ridder F, Feng X, Liang H-E, Locksley RM, Becher B, Schneider C. 2021. Alveolar macrophages rely on GM-CSF from alveolar epithelial type 2 cells before and after birth. *The Journal of Experimental Medicine* 218:e20210745. DOI: 10.1084/jem.20210745.

Guiu J, Shimizu R, D'Altri T, Fraser ST, Hatakeyama J, Bresnick EH, Kageyama R, Dzierzak E, Yamamoto M, Espinosa L, Bigas A. 2012. Hes repressors are essential regulators of hematopoietic stem cell development downstream of Notch signaling. *Journal of Experimental Medicine* 210:71–84. DOI: 10.1084/jem.20120993.

Gulliver G. 1875. Observations on the sizes and shapes of red corpuscles of the blood of vertebrates, with drawings of them to a uniform scale, and extended and revised tables of measurement. *Proc Zool Soc London*:474–495.

Haar JL, Ackerman GA. 1971. A phase and electron microscopic study of vasculogenesis and erythropoiesis in the yolk sac of the mouse. *The Anatomical Record* 170:199–223. DOI: 10.1002/ar.1091700206.

Haas JD, Ravens S, Düber S, Sandrock I, Oberdörfer L, Kashani E, Chennupati V, Föhse L, Naumann R, Weiss S, Krueger A, Förster R, Prinz I. 2012. Development of interleukin-17-producing **γδ** T cells is restricted to a functional embryonic wave. *Immunity* 37:48–59. DOI: 10.1016/j.immuni.2012.06.003.

Hadland BK, Huppert SS, Kanungo J, Xue Y, Jiang R, Gridley T, Conlon RA, Cheng AM, Kopan R, Longmore GD. 2004. A requirement for Notch1 distinguishes 2 phases of definitive hematopoiesis during development. *Blood* 104:3097–3105. DOI: 10.1182/blood-2004-03-1224.

Haematology reference ranges. 2024. *Available at https://www.gloshospitals.nhs.uk/our-services/services-we-offer/pathology/haematology/haematology-reference-ranges/* (accessed September 16, 2024).

Hahm K, Cobb BS, McCarty AS, Brown KE, Klug CA, Lee R, Akashi K, Weissman IL, Fisher AG, Smale ST. 1998. Helios, a T cell-restricted Ikaros family member that quantitatively associates with Ikaros at centromeric heterochromatin. *Genes & Development* 12:782–796.

Hall TD, Kim H, Dabbah M, Myers JA, Crawford JC, Morales-Hernandez A, Caprio CE, Sriram P, Kooienga E, Derecka M, Obeng EA, Thomas PG, McKinney-Freeman S. 2022. Murine fetal bone marrow does not support functional hematopoietic stem and progenitor cells until birth. *Nature Communications* 13:5403. DOI: 10.1038/s41467-022-33092-4.

Hao Y, Hao S, Andersen-Nissen E, Mauck WM, Zheng S, Butler A, Lee MJ, Wilk AJ, Darby C, Zager M, Hoffman P, Stoeckius M, Papalexi E, Mimitou EP, Jain J, Srivastava A, Stuart T, Fleming LM, Yeung B, Rogers AJ, McElrath JM, Blish CA, Gottardo R, Smibert P, Satija R. 2021. Integrated analysis of multimodal single-cell data. *Cell* 184:3573-3587.e29. DOI: 10.1016/j.cell.2021.04.048.

Hartmann K, Escribano L, Grattan C, Brockow K, Carter MC, Alvarez-Twose I, Matito A, Broesby-Olsen S, Siebenhaar F, Lange M, Niedoszytko M, Castells M, Oude Elberink JNG, Bonadonna P, Zanotti R, Hornick JL, Torrelo A, Grabbe J, Rabenhorst A, Nedoszytko B, Butterfield JH, Gotlib J, Reiter A, Radia D, Hermine O, Sotlar K, George TI, Kristensen TK, Kluin-Nelemans HC, Yavuz S, Hägglund H, Sperr WR, Schwartz LB, Triggiani M, Maurer M, Nilsson G, Horny H-P, Arock M, Orfao A, Metcalfe DD, Akin C, Valent P. 2016. Cutaneous manifestations in patients with mastocytosis: Consensus report of the European Competence Network on Mastocytosis; the American Academy of Allergy, Asthma & Immunology; and the European Academy of Allergology and Clinical Immunology. *Journal of Allergy and Clinical Immunology* 137:35–45. DOI: 10.1016/j.jaci.2015.08.034.

Hashimoto D, Chow A, Noizat C, Teo P, Beasley MB, Leboeuf M, Becker CD, See P, Price J, Lucas D, Greter M, Mortha A, Boyer SW, Forsberg EC, Tanaka M, van Rooijen N, García-Sastre A, Stanley ER, Ginhoux F, Frenette PS, Merad M. 2013. Tissue-resident macrophages self-maintain locally throughout adult life with minimal contribution from circulating monocytes. *Immunity* 38:792–804. DOI: 10.1016/J.IMMUNI.2013.04.004/ATTACHMENT/270941C3-B2EB-47A4-812D-CEBE26B3401B/MMC1.PDF.

Hatanaka K, Kitamura Y, Nishimune Y. 1979. Local Development of Mast Cells From Bone Marrow-Derived Precursors in the Skin of Mice. *Blood* 53:142–147. DOI: 10.1182/blood.V53.1.142.142.

Havran WL, Allison JP. 1990. Origin of Thy-1+ dendritic epidermal cells of adult mice from fetal thymic precursors. *Nature* 344:68–70. DOI: 10.1038/344068a0.

He S, Kim I, Lim MS, Morrison SJ. 2011. Sox17 expression confers self-renewal potential and fetal stem cell characteristics upon adult hematopoietic progenitors. *Genes & Development* 25:1613–1627. DOI: 10.1101/gad.2052911.

Herbomel P, Thisse B, Thisse C. 1999. Ontogeny and behaviour of early macrophages in the zebrafish embryo. *Development (Cambridge, England)* 126:3735–3745. DOI: 10.1242/DEV.126.17.3735.

Herbomel P, Thisse B, Thisse C. 2001. Zebrafish Early Macrophages Colonize Cephalic Mesenchyme and Developing Brain, Retina, and Epidermis through a M-CSF Receptor-Dependent Invasive Process. *Developmental Biology* 238:274–288. DOI: 10.1006/dbio.2001.0393.

Hettinger J, Richards DM, Hansson J, Barra MM, Joschko AC, Krijgsveld J, Feuerer M. 2013. Origin of monocytes and macrophages in a committed progenitor. *Nature Immunology* 14:821–830. DOI: 10.1038/ni.2638.

His W. 1868. *Untersuchungen über die erste Anlage des Wirbelthierleibes : die erste Entwickelung des Hühnchens im Ei*.

Hock H, Hamblen MJ, Rooke HM, Schindler JW, Saleque S, Fujiwara Y, Orkin SH. 2004. Gfi-1 restricts proliferation and preserves functional integrity of haematopoietic stem cells. *Nature* 431:1002–1007. DOI: 10.1038/nature02994.

Hoeffel G, Chen J, Lavin Y, Low D, Almeida FF, See P, Beaudin AE, Lum J, Low I, Forsberg EC, Poidinger M, Zolezzi F, Larbi A, Ng LG, Chan JKY, Greter M, Becher B, Samokhvalov IM, Merad M, Ginhoux F. 2015. C-Myb+ Erythro-Myeloid Progenitor-Derived Fetal Monocytes Give Rise to Adult Tissue-Resident Macrophages. *Immunity* 42:665–678. DOI: 10.1016/j.immuni.2015.03.011.

Hoffmann JA, Kafatos FC, Janeway CA, Ezekowitz RAB. 1999. Phylogenetic Perspectives in Innate Immunity. *Science* 284:1313–1318. DOI: 10.1126/science.284.5418.1313.

Holz A, Bossinger B, Strasser T, Janning W, Klapper R. 2003. The two origins of hemocytes in Drosophila. *Development* 130:4955–4962. DOI: 10.1242/dev.00702.

Hong W, Nakazawa M, Chen Y-Y, Kori R, Vakoc CR, Rakowski C, Blobel GA. 2005. FOG-1 recruits the NuRD repressor complex to mediate transcriptional repression by GATA-1. *The EMBO journal* 24:2367–2378. DOI: 10.1038/sj.emboj.7600703.

Honti V, Csordás G, Kurucz É, Márkus R, Andó I. 2014. The cell-mediated immunity of *Drosophila melanogaster*: Hemocyte lineages, immune compartments, microanatomy and regulation. *Developmental & Comparative Immunology* 42:47–56. DOI: 10.1016/j.dci.2013.06.005.

Hoover C, Kondo Y, Shao B, McDaniel MJ, Lee R, McGee S, Whiteheart S, Bergmeier W, McEver RP, Xia L. 2021. Heightened activation of embryonic megakaryocytes causes aneurysms in the developing brain of mice lacking podoplanin. *Blood* 137:2756–2769. DOI: 10.1182/blood.2020010310.

Hoppe PS, Schwarzfischer M, Loeffler D, Kokkaliaris KD, Hilsenbeck O, Moritz N, Endele M, Filipczyk A, Gambardella A, Ahmed N, Etzrodt M, Coutu DL, Rieger MA, Marr C, Strasser MK, Schauberger B, Burtscher I, Ermakova O, Bürger A, Lickert H, Nerlov C, Theis FJ, Schroeder T. 2016. Early myeloid lineage choice is not initiated by random PU.1 to GATA1 protein ratios. *Nature* 535:299–302. DOI: 10.1038/nature18320.

Huang Z, Dore LC, Li Z, Orkin SH, Feng G, Lin S, Crispino JD. 2009. GATA-2 Reinforces Megakaryocyte Development in the Absence of GATA-1. *Molecular and Cellular Biology* 29:5168–5180. DOI: 10.1128/MCB.00482-09.

Huling J, Bates D, Eddelbuettel D, Francois R, Qiu Y. 2022. fastglm: Fast and Stable Fitting of Generalized Linear Models using "RcppEigen."

Ikonomi P, Rivera CE, Riordan M, Washington G, Schechter AN, Noguchi CT. 2000. Overexpression of GATA-2 inhibits erythroid and promotes megakaryocyte differentiation. *Experimental Hematology* 28:1423–1431. DOI: 10.1016/S0301-472X(00)00553-1.

Iturri L, Freyer L, Biton A, Dardenne P, Lallemand Y, Gomez Perdiguero E. 2021. Megakaryocyte production is sustained by direct differentiation from erythromyeloid progenitors in the yolk sac until midgestation. *Immunity* 54:1433-1446.e5. DOI: 10.1016/j.immuni.2021.04.026.

Ivanovs A, Rybtsov S, Welch L, Anderson RA, Turner ML, Medvinsky A. 2011. Highly potent human hematopoietic stem cells first emerge in the intraembryonic aorta-gonad-mesonephros region. *Journal of Experimental Medicine* 208:2417–2427. DOI: 10.1084/jem.20111688.

Iwasaki H, Mizuno S, Wells RA, Cantor AB, Watanabe S, Akashi K. 2003. GATA-1 converts lymphoid and myelomonocytic progenitors into the megakaryocyte/erythrocyte lineages. *Immunity* 19:451–462. DOI: 10.1016/s1074-7613(03)00242-5.

Jaffredo T, Nottingham W, Liddiard K, Bollerot K, Pouget C, de Bruijn M. 2005. From hemangioblast to hematopoietic stem cell: An endothelial connection? *Experimental Hematology* 33:1029–1040. DOI: 10.1016/j.exphem.2005.06.005.

Jin H, Xu J, Wen Z. 2007. Migratory path of definitive hematopoietic stem/progenitor cells during zebrafish development. *Blood* 109:5208–5214. DOI: 10.1182/blood-2007-01-069005.

Jing H, Vakoc CR, Ying L, Mandat S, Wang H, Zheng X, Blobel GA. 2008. Exchange of GATA Factors Mediates Transitions in Looped Chromatin Organization at a Developmentally Regulated Gene Locus. *Molecular Cell* 29:232–242. DOI: 10.1016/j.molcel.2007.11.020.

Johnson KD, Hsu AP, Ryu M-J, Wang J, Gao X, Boyer ME, Liu Y, Lee Y, Calvo KR, Keles S, Zhang J, Holland SM, Bresnick EH. 2012. *Cis*-element mutated in *GATA2*-dependent immunodeficiency governs hematopoiesis and vascular integrity. *The Journal of Clinical Investigation* 122:3692–3704. DOI: 10.1172/JCI61623.

Jolly J. 1905. Sur l'évolution des globules rouges dans le sang des embryons des mammifères. Compt. rend. soc. biol.:T. 57.

Juban G, Sakakini N, Chagraoui H, Hernandez DC, Cheng Q, Soady K, Stoilova B, Garnett C, Waithe D, Otto G, Doondeea J, Usukhbayar B, Karkoulia E, Alexiou M, Strouboulis J, Morrissey E, Roberts I, Porcher C, Vyas P. 2021. Oncogenic Gata1 causes stage-specific megakaryocyte differentiation delay. *Haematologica* 106:1106–1119. DOI: 10.3324/haematol.2019.244541.

Jung S-H, Evans CJ, Uemura C, Banerjee U. 2005. The Drosophila lymph gland as a developmental model of hematopoiesis. *Development* 132:2521–2533. DOI: 10.1242/dev.01837.

Karsunky H, Inlay MA, Serwold T, Bhattacharya D, Weissman IL. 2008. Flk2+ common lymphoid progenitors possess equivalent differentiation potential for the B and T lineages. *Blood* 111:5562–5570. DOI: 10.1182/blood-2007-11-126219.

Kasaai B, Caolo V, Peacock HM, Lehoux S, Gomez-Perdiguero E, Luttun A, Jones EAV. 2017. Erythro-myeloid progenitors can differentiate from endothelial cells and modulate embryonic vascular remodeling. *Scientific Reports* 7:43817. DOI: 10.1038/srep43817.

Kaufman DP, Khattar J, Lappin SL. 2024. Physiology, Fetal Hemoglobin. In: *StatPearls*. Treasure Island (FL): StatPearls Publishing,.

Kawada H, Ito T, Pharr PN, Spyropoulos DD, Watson DK, Ogawa M. 2001. Defective megakaryopoiesis and abnormal erythroid development in Fli-1 gene-targeted mice. *International Journal of Hematology* 73:463–468. DOI: 10.1007/BF02994008.

Khan JA, Mendelson A, Kunisaki Y, Birbrair A, Kou Y, Arnal-Estapé A, Pinho S, Ciero P, Nakahara F, Ma'ayan A, Bergman A, Merad M, Frenette PS. 2016. Fetal liver hematopoietic stem cell niches associate with portal vessels. *Science* 351:176–180. DOI: 10.1126/science.aad0084.

Khandanpour C, Sharif-Askari E, Vassen L, Gaudreau M-C, Zhu J, Paul WE, Okayama T, Kosan C, Möröy T. 2010. Evidence that Growth factor independence 1b regulates dormancy and peripheral blood mobilization of hematopoietic stem cells. *Blood* 116:5149–5161. DOI: 10.1182/blood-2010-04-280305.

Kiel MJ, Yilmaz ÖH, Iwashita T, Yilmaz OH, Terhorst C, Morrison SJ. 2005. SLAM family receptors distinguish hematopoietic stem and progenitor cells and reveal endothelial niches for stem cells. *Cell* 121:1109–1121. DOI: 10.1016/J.CELL.2005.05.026.

Kieusseian A, de la Grange PB, Burlen-Defranoux O, Godin I, Cumano A. 2012. Immature hematopoietic stem cells undergo maturation in the fetal liver. *Development (Cambridge)* 139:3521–3530. DOI: 10.1242/dev.079210.

Kim I, He S, Yilmaz ÖH, Kiel MJ, Morrison SJ. 2006. Enhanced purification of fetal liver hematopoietic stem cells using SLAM family receptors. *Blood* 108:737–744. DOI: 10.1182/blood-2005-10-4135.

Kim I, Saunders TL, Morrison SJ. 2007. Sox17 Dependence Distinguishes the Transcriptional Regulation of Fetal from Adult Hematopoietic Stem Cells. *Cell* 130:470–483. DOI: 10.1016/j.cell.2007.06.011.

Kingsley PD, Malik J, Fantauzzo KA, Palis J. 2004. Yolk sac–derived primitive erythroblasts enucleate during mammalian embryogenesis. *Blood* 104:19–25. DOI: 10.1182/blood-2003-12-4162.

Kissa K, Herbomel P. 2010. Blood stem cells emerge from aortic endothelium by a novel type of cell transition. *Nature* 464:112–115. DOI: 10.1038/nature08761.

Kitamura Y, Hatanaka K, Murakami M, Shibata H. 1979. Presence of Mast Cell Precursors in Peripheral Blood of Mice Demonstrated by Parabiosis. *Blood* 53:1085–1088. DOI: 10.1182/blood.V53.6.1085.1085.

Kitchen H, Brett I. 1974. Embryonic and Fetal Hemoglobin in Animals. *Annals of the New York Academy of Sciences* 241:653–671. DOI: 10.1111/j.1749-6632.1974.tb21921.x.

Klempnauer K-H. 2022. C/EBP**β** sustains the oncogenic program of AML cells by cooperating with MYB and co-activator p300 in a transcriptional module. *Experimental Hematology* 108:8–15. DOI: 10.1016/j.exphem.2022.01.003.

Klusmann J, Godinho FJ, Heitmann K, Maroz A, Koch ML, Reinhardt D, Orkin SH, Li Z. 2010. Developmental stage-specific interplay of GATA1 and IGF signaling in fetal megakaryopoiesis and leukemogenesis. :1659–1672. DOI: 10.1101/gad.1903410.and.

Knudsen KJ, Rehn M, Hasemann MS, Rapin N, Bagger FO, Ohlsson E, Willer A, Frank A-K, Søndergaard E, Jendholm J, Thorén L, Lee J, Rak J, Theilgaard-Mönch K, Porse BT. 2015. ERG promotes the maintenance of hematopoietic stem cells by restricting their differentiation. *Genes & Development* 29:1915–1929. DOI: 10.1101/gad.268409.115.

Kocabas F, Zheng J, Thet S, Copeland NG, Jenkins NA, DeBerardinis RJ, Zhang C, Sadek HA. 2012. Meis1 regulates the metabolic phenotype and oxidant defense of hematopoietic stem cells. *Blood* 120:4963–4972. DOI: 10.1182/blood-2012-05-432260.

Kondo M, Weissman IL, Akashi K. 1997. Identification of Clonogenic Common Lymphoid Progenitors in Mouse Bone Marrow. *Cell* 91:661–672. DOI: 10.1016/S0092-8674(00)80453-5.

Korsunsky I, Millard N, Fan J, Slowikowski K, Zhang F, Wei K, Baglaenko Y, Brenner M, Loh P, Raychaudhuri S. 2019. Fast, sensitive and accurate integration of single-cell data with Harmony. *Nature Methods* 16:1289–1296. DOI: 10.1038/s41592-019-0619-0.

Koyunlar C, Gioacchino E, Vadgama D, de Looper H, Zink J, ter Borg MND, Hoogenboezem R, Havermans M, Sanders MA, Bindels E, Dzierzak E, Touw IP, de Pater E. 2023. Gata2-regulated Gfi1b expression controls endothelial programming during endothelial-to-hematopoietic transition. *Blood Advances* 7:2082–2093. DOI: 10.1182/bloodadvances.2022008019.

Krebs LT, Xue Y, Norton CR, Shutter JR, Maguire M, Sundberg JP, Gallahan D, Closson V, Kitajewski J, Callahan R, Smith GH, Stark KL, Gridley T. 2000. Notch signaling is essential for vascular morphogenesis in mice. *Genes & Development* 14:1343–1352. DOI: 10.1101/gad.14.11.1343.

Kruse EA, Loughran SJ, Baldwin TM, Josefsson EC, Ellis S, Watson DK, Nurden P, Metcalf D, Hilton DJ, Alexander WS, Kile BT. 2009. Dual requirement for the ETS transcription factors Fli-1 and Erg in hematopoietic stem cells and the

megakaryocyte lineage. *Proceedings of the National Academy of Sciences* 106:13814–13819. DOI: 10.1073/pnas.0906556106.

Kuhl C, Atzberger A, Iborra F, Nieswandt B, Porcher C, Vyas P. 2005. GATA1-mediated megakaryocyte differentiation and growth control can be uncoupled and mapped to different domains in GATA1. *Molecular and Cellular Biology* 25:8592–8606. DOI: 10.1128/MCB.25.19.8592-8606.2005.

Kuleshov MV, Jones MR, Rouillard AD, Fernandez NF, Duan Q, Wang Z, Koplev S, Jenkins SL, Jagodnik KM, Lachmann A, McDermott MG, Monteiro CD, Gundersen GW, Ma'ayan A. 2016. Enrichr: a comprehensive gene set enrichment analysis web server 2016 update. *Nucleic acids research* 44:W90–W97. DOI: 10.1093/nar/gkw377.

Kumano K, Chiba S, Kunisato A, Sata M, Saito T, Nakagami-Yamaguchi E, Yamaguchi T, Masuda S, Shimizu K, Takahashi T, Ogawa S, Hamada Y, Hirai H. 2003. Notch1 but Not Notch2 Is Essential for Generating Hematopoietic Stem Cells from Endothelial Cells. *Immunity* 18:699–711. DOI: 10.1016/S1074-7613(03)00117-1.

Kumaravelu P, Hook L, Morrison AM, Ure J, Zhao S, Zuyev S, Ansell J, Medvinsky A. 2002. Quantitative developmental anatomy of definitive haematopoietic stem cells/long-term repopulating units (HSC/RUs): role of the aorta-gonad-mesonephros (AGM) region and the yolk sac in colonisation of the mouse embryonic liver. *Development* 129:4891–4899. DOI: 10.1242/dev.129.21.4891.

Labuhn M, Perkins K, Matzk S, Varghese L, Garnett C, Papaemmanuil E, Metzner M, Kennedy A, Amstislavskiy V, Risch T, Bhayadia R, Samulowski D, Hernandez DC, Stoilova B, Iotchkova V, Oppermann U, Scheer C, Yoshida K, Schwarzer A, Taub JW, Crispino JD, Weiss MJ, Hayashi Y, Taga T, Ito E, Ogawa S, Reinhardt D, Yaspo M-L, Campbell PJ, Roberts I, Constantinescu SN, Vyas P, Heckl D, Klusmann J-H. 2019. Mechanisms of Progression of Myeloid Preleukemia to Transformed Myeloid Leukemia in Children with Down Syndrome. *Cancer Cell* 36:123-138.e10. DOI: 10.1016/j.ccell.2019.06.007.

Lacaud G, Gore L, Kennedy M, Kouskoff V, Kingsley P, Hogan C, Carlsson L, Speck N, Palis J, Keller G. 2002. Runx1 is essential for hematopoietic commitment at the hemangioblast stage of development in vitro. *Blood* 100:458–466. DOI: 10.1182/blood-2001-12-0321.

Lacombe J, Herblot S, Rojas-Sutterlin S, Haman A, Barakat S, Iscove NN, Sauvageau G, Hoang T. 2010. Scl regulates the quiescence and the long-term competence of hematopoietic stem cells. *Blood* 115:792–803. DOI: 10.1182/blood-2009-01-201384.

Lallemand Y, Luria V, Haffner-Krausz R, Lonai P. 1998. Maternally expressed PGK-Cre transgene as a tool for early and uniform activation of the Cre site-specific recombinase. *Transgenic Research* 7:105–112. DOI: 10.1023/a:1008868325009.

Lancrin C, Mazan M, Stefanska M, Patel R, Lichtinger M, Costa G, Vargel Ö, Wilson NK, Möröy T, Bonifer C, Göttgens B, Kouskoff V, Lacaud G. 2012. GFI1 and GFI1B control the loss of endothelial identity of hemogenic endothelium during hematopoietic commitment. *Blood* 120:314–322. DOI: 10.1182/blood-2011-10-386094.

Langfelder P, Zhang B, Horvath S. 2008. Defining clusters from a hierarchical cluster tree: the Dynamic Tree Cut package for R. *Bioinformatics* 24:719–720. DOI: 10.1093/bioinformatics/btm563.

Lanot R, Zachary D, Holder F, Meister M. 2001. Postembryonic Hematopoiesis in *Drosophila*. *Developmental Biology* 230:243–257. DOI: 10.1006/dbio.2000.0123.

Laurenti E, Doulatov S, Zandi S, Plumb I, Chen J, April C, Fan J-B, Dick JE. 2013. The transcriptional architecture of early human hematopoiesis identifies multilevel control of lymphoid commitment. *Nature Immunology* 14:756–763. DOI: 10.1038/ni.2615.

Laurenti E, Göttgens B. 2018. From haematopoietic stem cells to complex differentiation landscapes. *Nature* 553:418–426. DOI: 10.1038/nature25022.

Lawson ND, Scheer N, Pham VN, Kim C-H, Chitnis AB, Campos-Ortega JA, Weinstein BM. 2001. Notch signaling is required for arterial-venous differentiation during embryonic vascular development. *Development* 128:3675–3683. DOI: 10.1242/dev.128.19.3675.

Lazarov T, Loyher P-L, Yang H, Choo Z-N, Deng Z, Nowotschin S, Kuo Y-Y, Zhou T, Alberdi-Gonzalez A, Stumm R, Mass E, Perdiguero EG, Hadjantonakis A-K, Geissmann F. 2024. Identification of a mesodermal progenitor for the pro-definitive angio-hematopoietic lineage. :2024.08.24.609533. DOI: 10.1101/2024.08.24.609533.

Le Guyader D, Redd MJ, Colucci-Guyon E, Murayama E, Kissa K, Briolat V, Mordelet E, Zapata A, Shinomiya H, Herbomel P. 2008. Origins and unconventional behavior of neutrophils in developing zebrafish. *Blood* 111:132–141. DOI: 10.1182/blood-2007-06-095398.

Lebestky T, Chang T, Hartenstein V, Banerjee U. 2000. Specification of Drosophila hematopoietic lineage by conserved transcription factors. *Science (New York, N.Y.)* 288:146–149. DOI: 10.1126/science.288.5463.146.

Lecine P, Italiano JE, Kim S-W, Villeval J-L, Shivdasani RA. 2000. Hematopoietic-specific β1 tubulin participates in a pathway of platelet biogenesis dependent on the transcription factor NF-E2. *Blood* 96:1366–1373. DOI: 10.1182/blood.V96.4.1366.

Lee S-H, Lee S, Yang H, Song S, Kim K, Saunders TL, Yoon JK, Koh GY, Kim I. 2014. Notch Pathway Targets Proangiogenic Regulator Sox17 to Restrict Angiogenesis. *Circulation Research* 115:215–226. DOI: 10.1161/CIRCRESAHA.115.303142.

Li L, Bowling S, McGeary SE, Yu Q, Lemke B, Alcedo K, Jia Y, Liu X, Ferreira M, Klein AM, Wang S-W, Camargo FD. 2023a. A mouse model with high clonal barcode diversity for joint lineage, transcriptomic, and epigenomic profiling in single cells. *Cell* 186:5183-5199.e22. DOI: 10.1016/j.cell.2023.09.019.

Li Y, Esain V, Teng L, Xu J, Kwan W, Frost IM, Yzaguirre AD, Cai X, Cortes M, Maijenburg MW, Tober J, Dzierzak E, Orkin SH, Tan K, North TE, Speck NA. 2014. Inflammatory signaling regulates embryonic hematopoietic stem and progenitor cell production. *Genes & Development* 28:2597–2612. DOI: 10.1101/gad.253302.114.

Li Z, Godinho FJ, Klusmann JH, Garriga-Canut M, Yu C, Orkin SH. 2005. Developmental stage-selective effect of somatically mutated leukemogenic transcription factor GATA1. *Nature Genetics* 37:613–619. DOI: 10.1038/ng1566.

Li X, Li C, Zhang W, Wang Y, Qian P, Huang H. 2023b. Inflammation and aging: signaling pathways and intervention therapies. *Signal Transduction and Targeted Therapy* 8:1–29. DOI: 10.1038/s41392-023-01502-8.

Li Z, Liu S, Xu J, Zhang X, Han D, Liu J, Xia M, Yi L, Shen Q, Xu S, Lu L, Cao X. 2018. Adult Connective Tissue-Resident Mast Cells Originate from Late Erythro-Myeloid Progenitors. *Immunity* 49:640-653.e5. DOI: 10.1016/j.immuni.2018.09.023.

Lieschke GJ, Oates AC, Crowhurst MO, Ward AC, Layton JE. 2001. Morphologic and functional characterization of granulocytes and macrophages in embryonic and adult zebrafish. *Blood* 98:3087–3096. DOI: 10.1182/blood.V98.10.3087.

Lilly AJ, Costa G, Largeot A, Fadlullah MZH, Lie-A-Ling M, Lacaud G, Kouskoff V. 2016. Interplay between SOX7 and RUNX1 regulates hemogenic endothelial fate in the yolk sac. *Development* 143:4341–4351. DOI: 10.1242/dev.140970.

Lin H-F, Traver D, Zhu H, Dooley K, Paw BH, Zon LI, Handin RI. 2005. Analysis of thrombocyte development in CD41-GFP transgenic zebrafish. *Blood* 106:3803–3810. DOI: 10.1182/blood-2005-01-0179.

Ling T, Birger Y, Stankiewicz MJ, Ben-Haim N, Kalisky T, Rein A, Kugler E, Chen W, Fu C, Zhang K, Patel H, Sikora JW, Goo YA, Kelleher N, Zou L, Izraeli S, Crispino JD. 2019. Chromatin occupancy and epigenetic analysis reveal new insights into the function of the GATA1 N terminus in erythropoiesis. *Blood* 134:1619–1631. DOI: 10.1182/blood.2019001234.

Ling K-W, Ottersbach K, van Hamburg JP, Oziemlak A, Tsai F-Y, Orkin SH, Ploemacher R, Hendriks RW, Dzierzak E. 2004. GATA-2 Plays Two Functionally Distinct Roles during the Ontogeny of Hematopoietic Stem Cells. *Journal of Experimental Medicine* 200:871–882. DOI: 10.1084/jem.20031556.

Ling T, Zhang K, Yang J, Gurbuxani S, Crispino JD. 2023. Gata1s mutant mice display persistent defects in the erythroid lineage. *Blood Advances* 7:3253–3264. DOI: 10.1182/bloodadvances.2022008124.

Liu Z, Gu Y, Chakarov S, Bleriot C, Kwok I, Chen X, Shin A, Huang W, Dress RJ, Dutertre C-A, Schlitzer A, Chen J, Ng LG, Wang H, Liu Z, Su B, Ginhoux F. 2019. Fate Mapping via Ms4a3-Expression History Traces Monocyte-Derived Cells. *Cell* 178:1509-1525.e19. DOI: 10.1016/j.cell.2019.08.009.

Lizama CO, Hawkins JS, Schmitt CE, Bos FL, Zape JP, Cautivo KM, Borges Pinto H, Rhyner AM, Yu H, Donohoe ME, Wythe JD, Zovein AC. 2015. Repression of arterial genes in hemogenic endothelium is sufficient for haematopoietic fate acquisition. *Nature Communications* 6:7739. DOI: 10.1038/ncomms8739.

Lokka E, Lintukorpi L, Cisneros-Montalvo S, Mäkelä JA, Tyystjärvi S, Ojasalo V, Gerke H, Toppari J, Rantakari P, Salmi M. 2020. Generation, localization and functions of macrophages during the development of testis. *Nature Communications 2020 11:1* 11:1–16. DOI: 10.1038/s41467-020-18206-0.

Lösslein AK, Lohrmann F, Scheuermann L, Gharun K, Neuber J, Kolter J, Forde AJ, Kleimeyer C, Poh YY, Mack M, Triantafyllopoulou A, Dunlap MD, Khader SA, Seidl M, Hölscher A, Hölscher C, Guan XL, Dorhoi A, Henneke P. 2021. Monocyte progenitors give rise to multinucleated giant cells. *Nature Communications* 12:2027. DOI: 10.1038/s41467-021-22103-5.

Lu J, Guo S, Ebert BL, Zhang H, Peng X, Bosco J, Pretz J, Schlanger R, Wang JY, Mak RH, Dombkowski DM, Preffer FI, Scadden DT, Golub TR. 2008. MicroRNA-Mediated Control of Cell Fate in Megakaryocyte-Erythrocyte Progenitors. *Developmental Cell* 14:843–853. DOI: 10.1016/j.devcel.2008.03.012.

Luckett WP. 1978. Origin and differentiation of the yolk sac and extraembryonic mesoderm in presomite human and rhesus monkey embryos. *American Journal of Anatomy* 152:59–97. DOI: 10.1002/aja.1001520106.

Lurie LJ, Boyer ME, Grass JA, Bresnick EH. 2008. Differential GATA Factor Stabilities: Implications for Chromatin Occupancy by Structurally Similar Transcription Factors. *Biochemistry* 47:859–869. DOI: 10.1021/bi701692p.

Mancini E, Sanjuan-Pla A, Luciani L, Moore S, Grover A, Zay A, Rasmussen KD, Luc S, Bilbao D, O'Carroll D, Jacobsen SE, Nerlov C. 2012. FOG-1 and GATA-1 act sequentially to specify definitive megakaryocytic and erythroid progenitors. *The EMBO journal* 31:351–365. DOI: 10.1038/emboj.2011.390.

Manneken JD, Currie PD. 2023. Macrophage-stem cell crosstalk: regulation of the stem cell niche. *Development* 150:dev201510. DOI: 10.1242/dev.201510.

Manz MG, Traver D, Miyamoto T, Weissman IL, Akashi K. 2001. Dendritic cell potentials of early lymphoid and myeloid progenitors. *Blood* 97:3333–3341. DOI: 10.1182/BLOOD.V97.11.3333.

Marderstein AR, De Zuani M, Moeller R, Bezney J, Padhi EM, Wong S, Coorens THH, Xie Y, Xue H, Montgomery SB, Cvejic A. 2024. Single-cell multi-omics map of human fetal blood in Down syndrome. *Nature*:1–9. DOI: 10.1038/s41586-024-07946-4.

Margraf A, Nussbaum C, Rohwedder I, Klapproth S, Kurz ARM, Florian A, Wiebking V, Pircher J, Pruenster M, Immler R, Dietzel S, Kremer L, Kiefer F, Moser M, Flemmer AW, Quackenbush E, von Andrian UH, Sperandio M. 2017. Maturation of Platelet Function During Murine Fetal Development In Vivo. *Arteriosclerosis, Thrombosis, and Vascular Biology* 37:1076–1086. DOI: 10.1161/ATVBAHA.116.308464.

Mariani SA, Li Z, Rice S, Krieg C, Fragkogianni S, Robinson M, Vink CS, Pollard JW, Dzierzak E. 2019. Pro-inflammatory Aorta-Associated Macrophages Are Involved in Embryonic Development of Hematopoietic Stem Cells. *Immunity* 50:1439-1452.e5. DOI: 10.1016/j.immuni.2019.05.003.

Maroz A, Stachorski L, Emmrich S, Reinhardt K, Xu J, Shao Z, Käbler S, Dertmann T, Hitzler J, Roberts I, Vyas P, Juban G, Hennig C, Hansen G, Li Z, Orkin S, Reinhardt D, Klusmann JH. 2014. GATA1s induces hyperproliferation of eosinophil precursors in Down syndrome transient leukemia. *Leukemia* 28:1259–1270. DOI: 10.1038/leu.2013.373.

Martin DI, Orkin SH. 1990. Transcriptional activation and DNA binding by the erythroid factor GF-1/NF-E1/Eryf 1. *Genes & Development* 4:1886–1898. DOI: 10.1101/gad.4.11.1886.

Mass E, Ballesteros I, Farlik M, Halbritter F, Günther P, Crozet L, Jacome-Galarza CE, Händler K, Klughammer J, Kobayashi Y, Gomez-Perdiguero E, Schultze JL, Beyer M, Bock C, Geissmann F. 2016. Specification of tissue-resident macrophages during organogenesis. *Science* 353:aaf4238. DOI: 10.1126/science.aaf4238.

Mass E, Gentek R. 2021. Fetal-Derived Immune Cells at the Roots of Lifelong Pathophysiology. *Frontiers in Cell and Developmental Biology* 9:1–17. DOI: 10.3389/fcell.2021.648313.

Maximow AA. 1909. Untersuchungen über Blut und Bindegewebe. I. Die frühesten Entwicklungsstadien der Blut- und Bindegewebszellen beim Säugetierembryo, bis zum Anfang der Blutbildung in der Leber. *Archiv für Mikroskopische Anatomie* 73:444–561. DOI: https://doi.org/10.1007/BF02979896.

McGinnis CS, Murrow LM, Gartner ZJ. 2019. DoubletFinder: Doublet Detection in Single-Cell RNA Sequencing Data Using Artificial Nearest Neighbors. *Cell Systems* 8:329-337.e4. DOI: 10.1016/j.cels.2019.03.003.

McGrath KE, Frame JM, Fegan KH, Bowen JR, Conway SJ, Catherman SC, Kingsley PD, Koniski AD, Palis J. 2015. Distinct Sources of Hematopoietic Progenitors Emerge before HSCs and Provide Functional Blood Cells in the Mammalian Embryo. *Cell Reports* 11:1892–1904. DOI: 10.1016/j.celrep.2015.05.036.

Medvinsky A, Dzierzak E. 1996. Definitive Hematopoiesis Is Autonomously Initiated by the AGM Region. *Cell* 86:897–906. DOI: 10.1016/S0092-8674(00)80165-8.

Medvinsky AL, Samoylina NL, Müller AM, Dzierzak EA. 1993. An early pre-liver intraembryonic source of CFU-S in the developing mouse. *Nature* 364:64–67. DOI: 10.1038/364064a0.

Merad M, Manz MG, Karsunky H, Wagers A, Peters W, Charo I, Weissman IL, Cyster JG, Engleman EG. 2002. Langerhans cells renew in the skin throughout life under steady-state conditions. *Nature Immunology* 3:1135–1141. DOI: 10.1038/ni852.

Migliaccio AR, Rana RA, Sanchez M, Lorenzini R, Centurione L, Bianchi L, Vannucchi AM, Migliaccio G, Orkin SH. 2003. GATA-1 as a regulator of mast cell differentiation revealed by the phenotype of the GATA-1low mouse mutant. *Journal of Experimental Medicine* 197:281–296. DOI: 10.1084/jem.20021149.

Mikkola HKA, Fujiwara Y, Schlaeger TM, Traver D, Orkin SH. 2003. Expression of CD41 marks the initiation of definitive hematopoiesis in the mouse embryo. *Blood* 101:508–516. DOI: 10.1182/blood-2002-06-1699.

Miller IJ, Bieker JJ. 1993. A Novel, Erythroid Cell-Specific Murine Transcription Factor that Binds to the CACCC Element and is Related to the Krüppel Family of Nuclear Proteins†. *Molecular and Cellular Biology* 13:2776–2786. DOI: 10.1128/mcb.13.5.2776-2786.1993.

Miyauchi J. 2024. The hematopoietic microenvironment of the fetal liver and transient abnormal myelopoiesis associated with Down syndrome: A review. *Critical Reviews in Oncology/Hematology* 199:104382. DOI: 10.1016/j.critrevonc.2024.104382.

Miyauchi J, Ito Y, Tsukamoto K, Takahashi H, Ishikura K, Sugita K, Miyashita T. 2010. Blasts in transient leukaemia in neonates with Down syndrome differentiate into basophil/mast-cell and megakaryocyte lineages in vitro in association with down-regulation of truncated form of GATA1. *British Journal of Haematology* 148:898–909. DOI: 10.1111/j.1365-2141.2009.08038.x.

Miyauchi J, Kawaguchi H. 2014. Fetal Liver Stromal Cells Support Blast Growth in Transient Abnormal Myelopoiesis in Down Syndrome Through GM-CSF. *Journal of Cellular Biochemistry* 115:1176–1186. DOI: 10.1002/jcb.24764.

Miyauchi J, Kawaguchi H. 2021. The *in vitro* effects of hepatoblastoma cells on the growth and differentiation of blasts in transient abnormal myelopoiesis associated with Down syndrome. *Leukemia Research* 105:106570. DOI: 10.1016/j.leukres.2021.106570.

Monticelli S, Sommer A, AlHajj Hassan Z, Garcia Rodriguez C, Adé K, Cattenoz P, Delaporte C, Gomez Perdiguero E, Giangrande A. 2024. Early-wave macrophages control late hematopoiesis. *Developmental Cell*. DOI: 10.1016/j.devcel.2024.03.013.

Moore MAS, Metcalf D. 1970. Ontogeny of the Haemopoietic System: Yolk Sac Origin of In Vivo and In Vitro Colony Forming Cells in the Developing Mouse Embryo*. *British Journal of Haematology* 18:279–296. DOI: 10.1111/J.1365-2141.1970.TB01443.X.

Morcos MNF, Li C, Munz CM, Greco A, Dressel N, Reinhardt S, Sameith K, Dahl A, Becker NB, Roers A, Höfer T, Gerbaulet A. 2022. Fate mapping of hematopoietic stem cells reveals two pathways of native thrombopoiesis. *Nature Communications* 13:4504. DOI: 10.1038/s41467-022-31914-z.

Morris L, Graham CF, Gordon S. 1991. Macrophages in haemopoietic and other tissues of the developing mouse detected by the monoclonal antibody F4/80. *Development* 112:517–526. DOI: 10.1242/dev.112.2.517.

Morrison SJ, Hemmati HD, Wandycz AM, Weissman IL. 1995. The purification and characterization of fetal liver hematopoietic stem cells. *Proceedings of the National Academy of Sciences of the United States of America* 92:10302–10306. DOI: 10.1073/PNAS.92.22.10302.

Morrison SJ, Weissman IL. 1994. The long-term repopulating subset of hematopoietic stem cells is deterministic and isolatable by phenotype. *Immunity* 1:661–673. DOI: 10.1016/1074-7613(94)90037-X.

Mort RL, Ford MJ, Sakaue-Sawano A, Lindstrom NO, Casadio A, Douglas AT, Keighren MA, Hohenstein P, Miyawaki A, Jackson IJ. 2014. Fucci2a: a bicistronic cell cycle reporter that allows Cre mediated tissue specific expression in mice. *Cell cycle (Georgetown, Tex.)* 13:2681–2696. DOI: 10.4161/15384101.2015.945381.

Msallam R, Balla J, Rathore APS, Kared H, Malleret B, Saron WAA, Liu Z, Hang JW, Dutertre CA, Larbi A, Chan JKY, St. John AL, Ginhoux F. 2020. Fetal mast cells mediate postnatal allergic responses dependent on maternal IgE. *Science* 370:941–950. DOI: 10.1126/science.aba0864.

Mucenski ML, McLain K, Kier AB, Swerdlow SH, Schreiner CM, Miller TA, Pietryga DW, Scott WJ, Potter SS. 1991. A functional c-myb gene is required for normal murine fetal hepatic hematopoiesis. *Cell* 65:677–689. DOI: 10.1016/0092-8674(91)90099-K.

Müller AM, Medvinsky A, Strouboulis J, Grosveld F, Dzierzak E. 1994. Development of hematopoietic stem cell activity in the mouse embryo. *Immunity* 1:291–301. DOI: 10.1016/1074-7613(94)90081-7.

Mun SH, Park PSU, Park-Min K-H. 2020. The M-CSF receptor in osteoclasts and beyond. *Experimental & Molecular Medicine* 52:1239–1254. DOI: 10.1038/s12276-020-0484-z.

Mundschau G, Gurbuxani S, Gamis AS, Greene ME, Arceci RJ, Crispino JD. 2003. Mutagenesis of GATA1 is an initiating event in Down syndrome leukemogenesis. *Blood* 101:4298–4300. DOI: 10.1182/blood-2002-12-3904.

Muntean AG, Pang L, Poncz M, Dowdy SF, Blobel GA, Crispino JD. 2007. Cyclin D–Cdk4 is regulated by GATA-1 and required for megakaryocyte growth and polyploidization. *Blood* 109:5199–5207. DOI: 10.1182/blood-2006-11-059378.

Murayama E, Kissa K, Zapata A, Mordelet E, Briolat V, Lin H-F, Handin RI, Herbomel P. 2006. Tracing Hematopoietic Precursor Migration to Successive Hematopoietic Organs during Zebrafish Development. *Immunity* 25:963–975. DOI: 10.1016/j.immuni.2006.10.015.

Nagasawa T, Hirota S, Tachibana K, Takakura N, Nishikawa S, Kitamura Y, Yoshida N, Kikutani H, Kishimoto T. 1996. Defects of B-cell lymphopoiesis and bone-marrow myelopoiesis in mice lacking the CXC chemokine PBSF/SDF-1. *Nature* 382:635–638. DOI: 10.1038/382635a0.

Nagata H, Worobec AS, Oh CK, Chowdhury BA, Tannenbaum S, Suzuki Y, Metcalfe DD. 1995. Identification of a point mutation in the catalytic domain of the protooncogene c-kit in peripheral blood mononuclear cells of patients who have mastocytosis with an associated hematologic disorder. *Proceedings of the National Academy of Sciences* 92:10560–10564. DOI: 10.1073/pnas.92.23.10560.

Naik SH, Perié L, Swart E, Gerlach C, van Rooij N, de Boer RJ, Schumacher TN. 2013. Diverse and heritable lineage imprinting of early haematopoietic progenitors. *Nature* 496:229–232. DOI: 10.1038/nature12013.

Naito M, Yamamura F, Nishikawa S, Takahashi K. 1989. Development, Differentiation, and Maturation of Fetal Mouse Yolk Sac Macrophages in Cultures. *Journal of Leukocyte Biology* 46:1–10. DOI: 10.1002/JLB.46.1.1.

Nakagawa M, Ichikawa M, Kumano K, Goyama S, Kawazu M, Asai T, Ogawa S, Kurokawa M, Chiba S. 2006. AML1/Runx1 rescues Notch1-null mutation-induced deficiency of para-aortic splanchnopleural hematopoiesis. *Blood* 108:3329–3334. DOI: 10.1182/blood-2006-04-019570.

Nakagawa MM, Rathinam CV. 2018. Constitutive Activation of the Canonical NF-κB Pathway Leads to Bone Marrow Failure and Induction of Erythroid Signature in Hematopoietic Stem Cells. *Cell Reports* 25:2094-2109.e4. DOI: 10.1016/j.celrep.2018.10.071.

Nerlov C, Graf T. 1998. PU.1 induces myeloid lineage commitment in multipotent hematopoietic progenitors. *Genes & Development* 12:2403–2412. DOI: 10.1101/gad.12.15.2403.

Nerlov C, Querfurth E, Kulessa H, Graf T. 2000. GATA-1 interacts with the myeloid PU.1 transcription factor and represses PU.1-dependent transcription. *Blood* 95:2543–2551. DOI: 10.1182/blood.V95.8.2543.

Ness SA, Kowenz-Leutz E, Casini T, Graf T, Leutz A. 1993. Myb and NF-M: combinatorial activators of myeloid genes in heterologous cell types. *Genes & Development* 7:749–759. DOI: 10.1101/gad.7.5.749.

Nestorowa S, Hamey FK, Pijuan Sala B, Diamanti E, Shepherd M, Laurenti E, Wilson NK, Kent DG, Göttgens B. 2016. A single-cell resolution map of mouse hematopoietic stem and progenitor cell differentiation. *Blood* 128:e20–e31. DOI: 10.1182/blood-2016-05-716480.

Neumann E. 1868. Über die Bedeutung des Knochenmarks für die Blutbildung. *Zentralblatt für die medizinischen Wissenschaften* 44:122.

Neumann E. 1869. Du rôle de la moelle des os dansla formations du sang. *CR Acad Sci (Paris)* 68:1112–1113.

North TE, De Bruijn MFTR, Stacy T, Talebian L, Lind E, Robin C, Binder M, Dzierzak E, Speck NA. 2002. Runx1 expression marks long-term repopulating hematopoietic stem cells in the midgestation mouse embryo. *Immunity* 16:661–672. DOI: 10.1016/S1074-7613(02)00296-0.

North TE, Goessling W, Peeters M, Li P, Ceol C, Lord AM, Weber GJ, Harris J, Cutting CC, Huang P, Dzierzak E, Zon LI. 2009. Hematopoietic Stem Cell Development Is Dependent on Blood Flow. *Cell* 137:736–748. DOI: 10.1016/j.cell.2009.04.023.

North T, Gu TL, Stacy T, Wang Q, Howard L, Binder M, Marín-Padilla M, Speck NA. 1999. Cbfa2 is required for the formation of intra-aortic hematopoietic clusters. *Development* 126:2563–2575. DOI: 10.1242/dev.126.11.2563.

Nussbaum C, Gloning A, Pruenster M, Frommhold D, Bierschenk S, Genzel-Boroviczény O, von Andrian UH, Quackenbush E, Sperandio M. 2013. Neutrophil and endothelial adhesive function during human fetal ontogeny. *Journal of Leukocyte Biology* 93:175–184. DOI: 10.1189/jlb.0912468.

Nutt SL, Metcalf D, D'Amico A, Polli M, Wu L. 2005. Dynamic regulation of PU.1 expression in multipotent hematopoietic progenitors. *The Journal of Experimental Medicine* 201:221–231. DOI: 10.1084/jem.20041535.

Oeckinghaus A, Ghosh S. 2009. The NF-κB Family of Transcription Factors and Its Regulation. *Cold Spring Harbor Perspectives in Biology* 1:a000034. DOI: 10.1101/cshperspect.a000034.

Ohls RK, Li Y, Abdel-Mageed A, Buchanan G, Mandell L, Christensen RD. 1995. Neutrophil Pool Sizes and Granulocyte Colony-Stimulating Factor Production in Human Mid-Trimester Fetuses. *Pediatric Research* 37:806–811. DOI: 10.1203/00006450-199506000-00022.

Okada S, Nakauchi H, Nagayoshi K, Nishikawa S, Nishikawa S, Miura Y, Suda T. 1991. Enrichment and characterization of murine hematopoietic stem cells that express c-kit molecule. *Blood* 78:1706–1712.

Okuda T, van Deursen J, Hiebert SW, Grosveld G, Downing JR. 1996. AML1, the Target of Multiple Chromosomal Translocations in Human Leukemia, Is Essential for Normal Fetal Liver Hematopoiesis. *Cell* 84:321–330. DOI: 10.1016/S0092-8674(00)80986-1.

Olivera A, Beaven MA, Metcalfe DD. 2018. Mast cells signal their importance in health and disease. *Journal of Allergy and Clinical Immunology* 142:381–393. DOI: 10.1016/j.jaci.2018.01.034.

Orkin SH, Zon LI. 2008. Hematopoiesis: An Evolving Paradigm for Stem Cell Biology. *Cell* 132:631–644. DOI: 10.1016/j.cell.2008.01.025.

Ottersbach K. 2019. Endothelial-to-haematopoietic transition: an update on the process of making blood. *Biochemical Society Transactions* 47:591–601. DOI: 10.1042/BST20180320.

Pal S, Cantor AB, Johnson KD, Moran TB, Boyer ME, Orkin SH, Bresnick EH. 2004. Coregulator-dependent facilitation of chromatin occupancy by GATA-1. *Proceedings of the National Academy of Sciences* 101:980–985. DOI: 10.1073/pnas.0307612100.

Palis J. 2024. Erythropoiesis in the mammalian embryo. *Experimental Hematology* 136. DOI: 10.1016/j.exphem.2024.104283.

Palis J, Chan RJ, Koniski A, Patel R, Starr M, Yoder MC. 2001. Spatial and temporal emergence of high proliferative potential hematopoietic precursors during murine embryogenesis. *Proceedings of the National Academy of Sciences* 98:4528–4533. DOI: 10.1073/pnas.071002398.

Palis J, Robertson S, Kennedy M, Wall C, Keller G. 1999. Development of erythroid and myeloid progenitors in the yolk sac and embryo proper of the mouse. *Development* 126:5073–5084.

Pander C. 1817. *Dissertatio inauguralis sistens historiam metamorphoseos quam ovum incubatum prioribus quinque diebus subit.*

Park S-M, Cho H, Thornton AM, Barlowe TS, Chou T, Chhangawala S, Fairchild L, Taggart J, Chow A, Schurer A, Gruet A, Witkin MD, Kim JH, Shevach EM, Krivtsov A, Armstrong SA, Leslie C, Kharas MG. 2019. IKZF2 Drives Leukemia Stem Cell Self-Renewal and Inhibits Myeloid Differentiation. *Cell Stem Cell* 24:153-165.e7. DOI: 10.1016/j.stem.2018.10.016.

Patel SH, Christodoulou C, Weinreb C, Yu Q, da Rocha EL, Pepe-Mooney BJ, Bowling S, Li L, Osorio FG, Daley GQ, Camargo FD. 2022. Lifelong multilineage contribution by embryonic-born blood progenitors. *Nature* 606:747–753. DOI: 10.1038/s41586-022-04804-z.

Paul F, Arkin Y, Giladi A, Jaitin DA, Kenigsberg E, Keren-Shaul H, Winter D, Lara-Astiaso D, Gury M, Weiner A, David E, Cohen N, Lauridsen FKB, Haas S, Schlitzer A, Mildner A, Ginhoux F, Jung S, Trumpp A, Porse BT, Tanay A, Amit I. 2015. Transcriptional Heterogeneity and Lineage Commitment in Myeloid Progenitors. *Cell* 163:1663–1677. DOI: 10.1016/j.cell.2015.11.013.

Pei W, Feyerabend TB, Rössler J, Wang X, Postrach D, Busch K, Rode I, Klapproth K, Dietlein N, Quedenau C, Chen W, Sauer S, Wolf S, Höfer T, Rodewald H-R. 2017. Polylox barcoding reveals haematopoietic stem cell fates realized in vivo. *Nature* 548:456–460. DOI: 10.1038/nature23653.

Peixoto MM, Soares-da-Silva F, Bonnet V, Ronteix G, Santos RF, Mailhe M-P, Feng X, Pereira JP, Azzoni E, Anselmi G, Bruijn M de, Baroud CN, Pinto-do-Ó P, Cumano A. 2024. Spatiotemporal dynamics of cytokines expression dictate fetal liver hematopoiesis. :2023.08.24.554612. DOI: 10.1101/2023.08.24.554612.

Percin GI, Eitler J, Kranz A, Fu J, Pollard JW, Naumann R, Waskow C. 2018. CSF1R regulates the dendritic cell pool size in adult mice via embryo-derived tissue-resident macrophages. *Nature Communications* 9:5279. DOI: 10.1038/s41467-018-07685-x.

Percin G, Waskow claudia. 2023. 2001 – EMBRYONIC MACROPHAGES REGULATE THE SIZE OF THE DEFINITIVE HSC POOL. *Experimental Hematology* 124:S37. DOI: 10.1016/j.exphem.2023.06.038.

Perié L, Duffy KR, Kok L, de Boer RJ, Schumacher TN. 2015. The Branching Point in Erythro-Myeloid Differentiation. *Cell* 163:1655–1662. DOI: 10.1016/j.cell.2015.11.059.

Peschle C, Migliaccio AR, Migliaccio G, Petrini M, Calandrini M, Russo G, Mastroberardino G, Presta M, Gianni AM, Comi P. 1984. Embryonic----Fetal Hb switch in humans: studies on erythroid bursts generated by embryonic progenitors from yolk sac and liver. *Proceedings of the National Academy of Sciences* 81:2416–2420. DOI: 10.1073/pnas.81.8.2416.

Petrenko O, Beavis A, Klaine M, Kittappa R, Godin I, Lemischka IR. 1999. The Molecular Characterization of the Fetal Stem Cell Marker AA4. *Immunity* 10:691–700. DOI: 10.1016/S1074-7613(00)80068-0.

Pietras EM, Reynaud D, Kang Y-A, Carlin D, Calero-Nieto FJ, Leavitt AD, Stuart JM, Göttgens B, Passegué E. 2015. Functionally Distinct Subsets of Lineage-Biased Multipotent Progenitors Control Blood Production in Normal and Regenerative Conditions. *Cell Stem Cell* 17:35–46. DOI: 10.1016/j.stem.2015.05.003.

Pimanda JE, Donaldson IJ, de Bruijn MFTR, Kinston S, Knezevic K, Huckle L, Piltz S, Landry J-R, Green AR, Tannahill D, Göttgens B. 2007. The SCL transcriptional network and BMP signaling pathway interact to regulate RUNX1 activity. *Proceedings of the National Academy of Sciences* 104:840–845. DOI: 10.1073/pnas.0607196104.

Pixley FJ, Stanley ER. 2004. CSF-1 regulation of the wandering macrophage: complexity in action. *Trends in Cell Biology* 14:628–638. DOI: 10.1016/j.tcb.2004.09.016.

Popescu D-M, Botting RA, Stephenson E, Green K, Webb S, Jardine L, Calderbank EF, Polanski K, Goh I, Efremova M, Acres M, Maunder D, Vegh P, Gitton Y, Park J-E, Vento-Tormo R, Miao Z, Dixon D, Rowell R, McDonald D, Fletcher J, Poyner E, Reynolds G, Mather M, Moldovan C, Mamanova L, Greig F, Young MD, Meyer KB, Lisgo S, Bacardit J, Fuller A, Millar B, Innes B, Lindsay S, Stubbington MJT, Kowalczyk MS, Li B, Ashenberg O, Tabaka M, Dionne D, Tickle TL, Slyper M, Rozenblatt-Rosen O, Filby A, Carey P, Villani A-C, Roy A, Regev A, Chédotal A, Roberts I, Göttgens B, Behjati S, Laurenti E, Teichmann SA, Haniffa M. 2019. *Decoding human fetal liver haematopoiesis*. DOI: 10.1038/s41586-019-1652-y.

Poscablo DM, Worthington AK, Smith-Berdan S, Rommel MGE, Manso BA, Adili R, Mok L, Reggiardo RE, Cool T, Mogharrab R, Myers J, Dahmen S, Medina P, Beaudin AE, Boyer SW, Holinstat M, Jonsson VD, Forsberg EC. 2024. An age-progressive platelet differentiation path from hematopoietic stem cells causes exacerbated thrombosis. *Cell* 187:3090-3107.e21. DOI: 10.1016/j.cell.2024.04.018.

Potts KS, Sargeant TJ, Dawson CA, Josefsson EC, Hilton DJ, Alexander WS, Taoudi S. 2015. Mouse prenatal platelet-forming lineages share a core transcriptional program but divergent dependence on MPL. *Blood* 126:807–816. DOI: 10.1182/blood-2014-12-616607.

Potts KS, Sargeant TJ, Markham JF, Shi W, Biben C, Josefsson EC, Whitehead LW, Rogers KL, Liakhovitskaia A, Smyth GK, Kile BT, Medvinsky A, Alexander WS, Hilton DJ, Taoudi S. 2014. A lineage of diploid platelet-forming cells precedes polyploid megakaryocyte formation in the mouse embryo. *Blood* 124:2725–2729. DOI: 10.1182/blood-2014-02-559468.

Pronk CJH, Rossi DJ, Månsson R, Attema JL, Norddahl GL, Chan CKF, Sigvardsson M, Weissman IL, Bryder D. 2007. Elucidation of the phenotypic, functional, and molecular topography of a myeloerythroid progenitor cell hierarchy. *Cell stem cell* 1:428–442. DOI: 10.1016/J.STEM.2007.07.005.

Purton LE. 2022. Adult murine hematopoietic stem cells and progenitors: an update on their identities, functions, and assays. *Experimental Hematology* 116:1–14. DOI: 10.1016/j.exphem.2022.10.005.

Qi X, Hong J, Chaves L, Zhuang Y, Chen Y, Wang D, Chabon J, Graham B, Ohmori K, Li Y, Huang H. 2013. Antagonistic Regulation by the Transcription Factors C/EBP**α** and MITF Specifies Basophil and Mast Cell Fates. *Immunity* 39:97–110. DOI: 10.1016/j.immuni.2013.06.012.

Qian BZ, Li J, Zhang H, Kitamura T, Zhang J, Campion LR, Kaiser EA, Snyder LA, Pollard JW. 2011. CCL2 recruits inflammatory monocytes to facilitate breast-tumour metastasis. *Nature* 475:222–225. DOI: 10.1038/nature10138.

Rae F, Woods K, Sasmono T, Campanale N, Taylor D, Ovchinnikov DA, Grimmond SM, Hume DA, Ricardo SD, Little MH. 2007. Characterisation and trophic functions of murine embryonic macrophages based upon the use of a Csf1r-EGFP transgene reporter. *Developmental Biology* 308:232–246. DOI: 10.1016/J.YDBIO.2007.05.027.

Rainis L, Bercovich D, Strehl S, Teigler-Schlegel A, Stark B, Trka J, Amariglio N, Biondi A, Muler I, Rechavi G, Kempski H, Haas OA, Izraeli S. 2003. Mutations in exon 2 of GATA1 are early events in megakaryocytic malignancies associated with trisomy 21. *Blood* 102:981–986. DOI: 10.1182/blood-2002-11-3599.

Ramsay RG, Gonda TJ. 2008. MYB function in normal and cancer cells. *Nature Reviews Cancer* 8:523–534. DOI: 10.1038/nrc2439.

Ranzoni AM, Tangherloni A, Berest I, Riva SG, Myers B, Strzelecka PM, Xu J, Panada E, Mohorianu I, Zaugg JB, Cvejic A. 2021. Integrative Single-Cell RNA-Seq and ATAC-Seq Analysis of Human Developmental Hematopoiesis. *Cell Stem Cell* 28:472-487.e7. DOI: 10.1016/j.stem.2020.11.015.

Rauluseviciute I, Riudavets-Puig R, Blanc-Mathieu R, Castro-Mondragon JA, Ferenc K, Kumar V, Lemma RB, Lucas J, Chèneby J, Baranasic D, Khan A, Fornes O, Gundersen S, Johansen M, Hovig E, Lenhard B, Sandelin A, Wasserman WW, Parcy F, Mathelier A. 2024. JASPAR 2024: 20th anniversary of the open-access database of transcription factor binding profiles. *Nucleic Acids Research* 52:D174–D182. DOI: 10.1093/nar/gkad1059.

Regenstreif LJ, Rossant J. 1989. Expression of the c-*fms* proto-oncogene and of the cytokine, CSF-1, during mouse embryogenesis. *Developmental Biology* 133:284–294. DOI: 10.1016/0012-1606(89)90319-9.

Rehorn K-P, Thelen H, Michelson AM, Reuter R. 1996. A molecular aspect of hematopoiesis and endoderm development common to vertebrates and Drosophila. *Development* 122:4023–4031. DOI: 10.1242/dev.122.12.4023.

Risau W, Hallmann R, Albrecht U. 1986. Differentiation-dependent expression of proteins in brain endothelium during development of the blood-brain barrier. *Developmental Biology* 117:537–545. DOI: 10.1016/0012-1606(86)90321-0.

Rizki MTM. 1957. Alterations in the haemocyte population of Drosophila melanogaster. *Journal of Morphology* 100:437–458. DOI: 10.1002/jmor.1051000303.

Rizki TM, Rizki RM. 1992. Lamellocyte differentiation in *Drosophila* larvae parasitized by *Leptopilina*. *Developmental & Comparative Immunology* 16:103–110. DOI: 10.1016/0145-305X(92)90011-Z.

Rizki TM, Rizki RM. 1994. Parasitoid-induced cellular immune deficiency in Drosophila. *Annals of the New York Academy of Sciences* 712:178–194. DOI: 10.1111/j.1749-6632.1994.tb33572.x.

Robb L, Lyons I, Li R, Hartley L, Köntgen F, Harvey RP, Metcalf D, Begley CG. 1995. Absence of yolk sac hematopoiesis from mice with a targeted disruption of the scl gene. *Proceedings of the National Academy of Sciences of the United States of America* 92:7075–7079.

Robert-Moreno À, Espinosa L, de la Pompa JL, Bigas A. 2005. RBPjκ-dependent Notch function regulates Gata2 and is essential for the formation of intra-embryonic hematopoietic cells. *Development* 132:1117–1126. DOI: 10.1242/dev.01660.

Robert-Moreno À, Guiu J, Ruiz-Herguido C, López ME, Inglés-Esteve J, Riera L, Tipping A, Enver T, Dzierzak E, Gridley T, Espinosa L, Bigas A. 2008. Impaired embryonic haematopoiesis yet normal arterial development in the absence of the Notch ligand Jagged1. *The EMBO Journal* 27:1886–1895. DOI: 10.1038/emboj.2008.113.

Rodriguez-Fraticelli AE, Wolock SL, Weinreb CS, Panero R, Patel SH, Jankovic M, Sun J, Calogero RA, Klein AM, Camargo FD. 2018. Clonal analysis of lineage fate in native haematopoiesis. *Nature* 553:212–216. DOI: 10.1038/nature25168.

Rojo R, Raper A, Ozdemir DD, Lefevre L, Grabert K, Wollscheid-Lengeling E, Bradford B, Caruso M, Gazova I, Sánchez A, Lisowski ZM, Alves J, Molina-Gonzalez I, Davtyan H, Lodge RJ, Glover JD, Wallace R, Munro DAD, David E, Amit I, Miron VE, Priller J, Jenkins SJ, Hardingham GE, Blurton-Jones M, Mabbott NA, Summers KM, Hohenstein P, Hume DA, Pridans C. 2019. Deletion of a Csf1r enhancer selectively impacts CSF1R expression and development of tissue macrophage populations. *Nature Communications* 10:1–17. DOI: 10.1038/s41467-019-11053-8.

Ross C, Boroviak TE. 2020. Origin and function of the yolk sac in primate embryogenesis. *Nature Communications* 11:3760. DOI: 10.1038/s41467-020-17575-w.

Rugendorff A, Younossi-Hartenstein A, Hartenstein V. 1994. Embryonic origin and differentiation of the Drosophila heart. *Roux's archives of developmental biology* 203:266–280. DOI: 10.1007/BF00360522.

Ruiz-Herguido C, Guiu J, D'Altri T, Inglés-Esteve J, Dzierzak E, Espinosa L, Bigas A. 2012. Hematopoietic stem cell development requires transient Wnt/β-catenin activity. *Journal of Experimental Medicine* 209:1457–1468. DOI: 10.1084/jem.20120225.

Rybtsov S, Ivanovs A, Zhao S, Medvinsky A. 2016. Concealed expansion of immature precursors underpins acute burst of adult HSC activity in foetal liver. *Development* 143:1284–1289. DOI: 10.1242/dev.131193.

Sabin F. 1920. Studies on the origin of blood-vessels and of red blood-corpuscles as seen in the living blastoderm of chicks during the second day of incubation. *Contributions to embryology* 36.

Sanchez Bosch P, Makhijani K, Herboso L, Gold KS, Baginsky R, Woodcock KJ, Alexander B, Kukar K, Corcoran S, Jacobs T, Ouyang D, Wong C, Ramond EJV, Rhiner C, Moreno E, Lemaitre B, Geissmann F, Brückner K. 2019. Adult *Drosophila* Lack Hematopoiesis but Rely on a Blood Cell Reservoir at the Respiratory Epithelia to Relay Infection Signals to Surrounding Tissues. *Developmental Cell* 51:787-803.e5. DOI: 10.1016/j.devcel.2019.10.017.

Sánchez M-J, Holmes A, Miles C, Dzierzak E. 1996. Characterization of the First Definitive Hematopoietic Stem Cells in the AGM and Liver of the Mouse Embryo. *Immunity* 5:513–525. DOI: 10.1016/S1074-7613(00)80267-8.

Sánchez-Sánchez BJ, Urbano JM, Comber K, Dragu A, Wood W, Stramer B, Martín-Bermudo MD. 2017. *Drosophila* Embryonic Hemocytes Produce Laminins to Strengthen Migratory Response. *Cell Reports* 21:1461–1470. DOI: 10.1016/j.celrep.2017.10.047.

Sanjuan-Pla A, Macaulay IC, Jensen CT, Woll PS, Luis TC, Mead A, Moore S, Carella C, Matsuoka S, Jones TB, Chowdhury O, Stenson L, Lutteropp M, Green JCA, Facchini R, Boukarabila H, Grover A, Gambardella A, Thongjuea S, Carrelha J, Tarrant P, Atkinson D, Clark SA, Nerlov C, Jacobsen SEW. 2013. Platelet-biased stem cells reside at the apex of the haematopoietic stem-cell hierarchy. *Nature* 502:232–236. DOI: 10.1038/nature12495.

Sato T, Yoshida K, Toki T, Kanezaki R, Terui K, Saiki R, Ojima M, Ochi Y, Mizuno S, Yoshihara M, Uechi T, Kenmochi N, Tanaka S, Matsubayashi J, Kisai K, Kudo K, Yuzawa K, Takahashi Y, Tanaka T, Yamamoto Y, Kobayashi A, Kamio T, Sasaki S, Shiraishi Y, Chiba K, Tanaka H, Muramatsu H, Hama A, Hasegawa D, Sato A, Koh K, Karakawa S, Kobayashi M, Hara J, Taneyama Y, Imai C, Hasegawa D, Fujita N, Yoshitomi M, Iwamoto S, Yamato G, Saida S, Kiyokawa N, Deguchi T, Ito M, Matsuo H, Adachi S, Hayashi Y, Taga T, Saito AM, Horibe K, Watanabe K, Tomizawa D, Miyano S, Takahashi S, Ogawa S, Ito E. 2024. Landscape of driver mutations and their clinical effects on Down syndrome–related myeloid neoplasms. *Blood* 143:2627–2643. DOI: 10.1182/blood.2023022247.

Sawamiphak S, Kontarakis Z, Stainier DYR. 2014. Interferon Gamma Signaling Positively Regulates Hematopoietic Stem Cell Emergence. *Developmental Cell* 31:640–653. DOI: 10.1016/j.devcel.2014.11.007.

Saxer. 1896. Über die Entwickelung und den Bau normaler Lymphdrüsen. *Anat. Hefte* 6.

Schep AN, Wu B, Buenrostro JD, Greenleaf WJ. 2017. chromVAR: inferring transcription-factor-associated accessibility from single-cell epigenomic data. *Nature Methods* 14:975–978. DOI: 10.1038/nmeth.4401.

Schindelin J, Arganda-Carreras I, Frise E, Kaynig V, Longair M, Pietzsch T, Preibisch S, Rueden C, Saalfeld S, Schmid B, Tinevez JY, White DJ, Hartenstein V, Eliceiri K, Tomancak P, Cardona A. 2012. Fiji: An open-source platform for biological-image analysis. *Nature Methods* 9:676–682. DOI: 10.1038/nmeth.2019.

Schlitzer A, Sivakamasundari V, Chen J, Sumatoh HRB, Schreuder J, Lum J, Malleret B, Zhang S, Larbi A, Zolezzi F, Renia L, Poidinger M, Naik S, Newell EW, Robson P, Ginhoux F. 2015. Identification of cDC1- and cDC2-committed DC progenitors reveals early lineage priming at the common DC progenitor stage in the bone marrow. *Nature Immunology* 16:718–728. DOI: 10.1038/ni.3200.

Schulz C, Gomez Perdiguero E, Chorro L, Szabo-rogers H, Cagnard N, Kierdorf K, Prinz M, Wu B, Jacobsen SEW, Pollard JW, Frampton J, Liu KJ, Geissmann F. 2012. A Lineage of Myeloid Cells. *Science* 336:2–7. DOI: 10.1126/science.1219179.

Scott EW, Simon MC, Anastasi J, Singh H. 1994. Requirement of transcription factor PU.1 in the development of multiple hematopoietic lineages. *Science* 265:1573–1577. DOI: 10.1126/science.8079170.

Seita J, Weissman IL. 2010. Hematopoietic stem cell: Self-renewal versus differentiation. *Wiley Interdisciplinary Reviews: Systems Biology and Medicine* 2:640–653. DOI: 10.1002/WSBM.86.

Setty M, Kiseliovas V, Levine J, Gayoso A, Mazutis L, Pe'er D. 2019. Characterization of cell fate probabilities in single-cell data with Palantir. *Nature Biotechnology* 37:451–460. DOI: 10.1038/s41587-019-0068-4.

Sheng G, Foley AC. 2012. Diversification and conservation of the extraembryonic tissues in mediating nutrient uptake during amniote development. *Annals of the New York Academy of Sciences* 1271:97–103. DOI: 10.1111/j.1749-6632.2012.06726.x.

Shimizu R, Takahashi S, Ohneda K, Engel JD, Yamamoto M. 2001. In vivo requirements for GATA-1 functional domains during primitive and definitive erythropoiesis. *The EMBO Journal* 20:5250–5260. DOI: 10.1093/emboj/20.18.5250.

Shin M, Chang E, Lee D, Kim N, Cho B, Cha N, Koranteng F, Song J-J, Shim J. 2024. Drosophila immune cells transport oxygen through PPO2 protein phase transition. *Nature* 631:350–359. DOI: 10.1038/s41586-024-07583-x.

Shivdasani RA, Fujiwara Y, McDevitt MA, Orkin SH. 1997. A lineage-selective knockout establishes the critical role of transcription factor GATA-1 in megakaryocyte growth and platelet development. *The EMBO Journal* 16:3965–3973. DOI: 10.1093/emboj/16.13.3965.

Shivdasani RA, Mayer EL, Orkin SH. 1995. Absence of blood formation in mice lacking the T-cell leukaemia oncoprotein tal-1/SCL. *Nature* 373:432–434. DOI: 10.1038/373432a0.

Shivdasani RA, Rosenblatt MF, Zucker-Franklin D, Jackson CW, Hunt P, Saris CJM, Orkin SH. 1995. Transcription factor NF-E2 is required for platelet formation independent of the actions of thrombopoeitin/MGDF in megakaryocyte development. *Cell* 81:695–704. DOI: 10.1016/0092-8674(95)90531-6.

da Silva EZM, Jamur MC, Oliver C. 2014. Mast Cell Function: A New Vision of an Old Cell. *Journal of Histochemistry & Cytochemistry* 62:698–738. DOI: 10.1369/0022155414545334.

Silvério-Alves R, Kurochkin I, Rydström A, Vazquez Echegaray C, Haider J, Nicholls M, Rode C, Thelaus L, Lindgren AY, Ferreira AG, Brandão R, Larsson J, de Bruijn MFTR, Martin-Gonzalez J, Pereira C-F. 2023. GATA2 mitotic bookmarking is required for definitive haematopoiesis. *Nature Communications* 14:4645. DOI: 10.1038/s41467-023-40391-x.

Sinha R, Porcheri C, d'Altri T, González J, Ruiz-Herguido C, Rabbitts T, Espinosa L, Bigas A. 2020. Development of embryonic and adult leukemia mouse models driven by MLL-ENL translocation. *Experimental Hematology* 85:13–19. DOI: 10.1016/j.exphem.2020.04.008.

Slayton WB, Wainman DA, Li XM, Hu Z, Jotwani A, Cogle CR, Walker D, Fisher RC, Wingard JR, Scott EW, Sola MC. 2005. Developmental differences in megakaryocyte maturation are determined by the microenvironment. *Stem Cells (Dayton, Ohio)* 23:1400–1408. DOI: 10.1634/stemcells.2004-0373.

Smrcek JM, Baschat AA, Germer U, Gloeckner-Hofmann K, Gembruch U. 2001. Fetal hydrops and hepatosplenomegaly in the second half of pregnancy: a sign of myeloproliferative disorder in fetuses with trisomy 21. *Ultrasound in Obstetrics & Gynecology* 17:403–409. DOI: 10.1046/j.1469-0705.2001.00384.x.

Soares-da-Silva F, Burlen-Defranoux O, Elsaid R, Iturri L, Freyer L, Sismeiro O, Pinto-do-Ó P, Gomez-Perdiguero E, Cumano A. 2021. Yolk sac, but not hematopoietic stem cell-derived progenitors, sustain erythropoiesis throughout murine embryonic life. *Journal of Experimental Medicine*. DOI: https://doi.org/10.1084/jem.20201729.

Soares-da-Silva F, Elsaid R, Peixoto MM, Nogueira G, Pereira P, Bandeira A, Cumano A. 2023. Assembling the layers of the hematopoietic system: A window of opportunity for thymopoiesis in the embryo. *Immunological Reviews* 315:54–70. DOI: 10.1111/imr.13187.

Söderhäll K, Cerenius L. 1998. Role of the prophenoloxidase-activating system in invertebrate immunity. *Current Opinion in Immunology* 10:23–28. DOI: 10.1016/S0952-7915(98)80026-5.

Sommer A, Gomez Perdiguero E. 2024. Extraembryonic hematopoietic lineages—to macrophages and beyond. *Experimental Hematology* 136:104285. DOI: 10.1016/j.exphem.2024.104285.

Sommerkamp P, Romero-Mulero MC, Narr A, Ladel L, Hustin L, Schönberger K, Renders S, Altamura S, Zeisberger P, Jäcklein K, Klimmeck D, Rodriguez-Fraticelli A, Camargo FD, Perié L, Trumpp A, Cabezas-Wallscheid N. 2021. Mouse multipotent progenitor 5 cells are located at the interphase between hematopoietic stem and progenitor cells. *Blood* 137:3218–3224. DOI: 10.1182/blood.2020007876.

Sonoda T, Hayashi C, Kitamura Y. 1983. Presence of mast cell precursors in the yolk sac of mice. *Developmental Biology* 97:89–94. DOI: 10.1016/0012-1606(83)90066-0.

Sörensen I, Adams RH, Gossler A. 2009. DLL1-mediated Notch activation regulates endothelial identity in mouse fetal arteries. *Blood* 113:5680–5688. DOI: 10.1182/blood-2008-08-174508.

Souilhol C, Lendinez JG, Rybtsov S, Murphy F, Wilson H, Hills D, Batsivari A, Binagui-Casas A, McGarvey AC, MacDonald HR, Kageyama R, Siebel C, Zhao S, Medvinsky A. 2016. Developing HSCs become Notch independent by the end of maturation in the AGM region. *Blood* 128:1567–1577. DOI: 10.1182/blood-2016-03-708164.

Spangenberg E, Severson PL, Hohsfield LA, Crapser J, Zhang J, Burton EA, Zhang Y, Spevak W, Lin J, Phan NY, Habets G, Rymar A, Tsang G, Walters J, Nespi M, Singh P, Broome S, Ibrahim P, Zhang C, Bollag G, West BL, Green KN. 2019. Sustained microglial depletion with CSF1R inhibitor impairs parenchymal plaque development in an Alzheimer's disease model. *Nature Communications* 10:3758. DOI: 10.1038/s41467-019-11674-z.

Spangrude GJ, Heimfeld S, Weissman IL. 1988. Purification and Characterization of Mouse Hematopoietic Stem Cells. *Science* 241:58–62. DOI: 10.1126/science.2898810.

Sperandio M, Quackenbush EJ, Sushkova N, Altstätter J, Nussbaum C, Schmid S, Pruenster M, Kurz A, Margraf A, Steppner A, Schweiger N, Borsig L, Boros I, Krajewski N, Genzel-Boroviczeny O, Jeschke U, Frommhold D, von Andrian UH. 2013. Ontogenetic regulation of leukocyte recruitment in mouse yolk sac vessels. *Blood* 121:e118–e128. DOI: 10.1182/blood-2012-07-447144.

Spinelli SL, Casey AE, Pollock SJ, Gertz JM, McMillan DH, Narasipura SD, Mody NA, King MR, Maggirwar SB, Francis CW, Taubman MB, Blumberg N, Phipps RP. 2010. Platelets and Megakaryocytes Contain Functional Nuclear Factor-κB. *Arteriosclerosis, Thrombosis, and Vascular Biology* 30:591–598. DOI: 10.1161/ATVBAHA.109.197343.

Srinivas S, Watanabe T, Lin CS, William CM, Tanabe Y, Jessell TM, Costantini F. 2001. Cre reporter strains produced by targeted insertion of EYFP and ECFP into the ROSA26 locus. *BMC Developmental Biology* 1:1–8. DOI: 10.1186/1471-213X-1-4.

Staber PB, Zhang P, Ye M, Welner RS, Nombela-Arrieta C, Bach C, Kerenyi M, Bartholdy BA, Zhang H, Alberich-Jordà M, Lee S, Yang H, Ng F, Zhang J, Leddin M, Silberstein LE, Hoefler G, Orkin SH, Göttgens B, Rosenbauer F, Huang G, Tenen DG. 2013. Sustained PU.1 Levels Balance Cell-Cycle Regulators to Prevent Exhaustion of Adult Hematopoietic Stem Cells. *Molecular Cell* 49:934–946. DOI: 10.1016/j.molcel.2013.01.007.

Stonehouse OJ, Biben C, Weber TS, Garnham A, Fennell KA, Farley A, Terreaux AF, Alexander WS, Dawson MA, Naik SH, Taoudi S. 2024. Clonal analysis of fetal hematopoietic stem/progenitor cell subsets reveals how post-transplantation capabilities are distributed. :2024.02.19.579920. DOI: 10.1101/2024.02.19.579920.

Stremmel C, Schuchert R, Wagner F, Thaler R, Weinberger T, Pick R, Mass E, Ishikawa-Ankerhold HC, Margraf A, Hutter S, Vagnozzi R, Klapproth S, Frampton J, Yona S, Scheiermann C, Molkentin JD, Jeschke U, Moser M, Sperandio M, Massberg S, Geissmann F, Schulz C. 2018. Yolk sac macrophage progenitors traffic to the embryo during defined stages of development. *Nature Communications* 9:75. DOI: 10.1038/s41467-017-02492-2.

Stuart T, Srivastava A, Madad S, Lareau CA, Satija R. 2021. Single-cell chromatin state analysis with Signac. *Nature Methods* 18:1333–1341. DOI: 10.1038/s41592-021-01282-5.

Sun W, Downing JR. 2004. Haploinsufficiency of *AML1* results in a decrease in the number of LTR-HSCs while simultaneously inducing an increase in more mature progenitors. *Blood* 104:3565–3572. DOI: 10.1182/blood-2003-12-4349.

Sun J, Ramos A, Chapman B, Johnnidis JB, Le L, Ho Y-J, Klein A, Hofmann O, Camargo FD. 2014. Clonal dynamics of native haematopoiesis. *Nature* 514:322–327. DOI: 10.1038/nature13824.

Suo C, Dann E, Goh I, Jardine L, Kleshchevnikov V, Park J-E, Botting RA, Stephenson E, Engelbert J, Tuong ZK, Polanski K, Yayon N, Xu C, Suchanek O, Elmentaite R, Domínguez Conde C, He P, Pritchard S, Miah M, Moldovan C, Steemers AS, Mazin P, Prete M, Horsfall D, Marioni JC, Clatworthy MR, Haniffa M, Teichmann SA. 2022. Mapping the developing human immune system across organs. *Science* 376:eabo0510. DOI: 10.1126/science.abo0510.

Suzuki M, Kobayashi-Osaki M, Tsutsumi S, Pan X, Ohmori S, Takai J, Moriguchi T, Ohneda O, Ohneda K, Shimizu R, Kanki Y, Kodama T, Aburatani H, Yamamoto M. 2013. GATA factor switching from GATA2 to GATA1 contributes to erythroid differentiation. *Genes to Cells* 18:921–933. DOI: 10.1111/gtc.12086.

Takahashi K, Yamamurma F, Naito M. 1989. Differentiation , Maturation , and Proliferation Macrophages in the Mouse Yolk Sac: A light-microscopic, enzyme-cytochemical, Immunohistochemical and Ultrastructural Study. *Journal of Leukocyte Biology* 45:87–96. DOI: 10.1002/jlb.45.2.87.

Tallack MR, Perkins AC. 2010. Megakaryocyte-erythroid lineage promiscuity in EKLF null mouse blood. *Haematologica* 95:144–147. DOI: 10.3324/haematol.2009.010017.

Taoudi S, Bee T, Hilton A, Knezevic K, Scott J, Willson TA, Collin C, Thomas T, Voss AK, Kile BT, Alexander WS, Pimanda JE, Hilton DJ. 2011. ERG dependence distinguishes developmental control of hematopoietic stem cell maintenance from hematopoietic specification. *Genes & Development* 25:251–262. DOI: 10.1101/gad.2009211.

Tauber M, Basso L, Martin J, Bostan L, Pinto MM, Thierry GR, Houmadi R, Serhan N, Loste A, Blériot C, Kamphuis JBJ, Grujic M, Kjellén L, Pejler G, Paul C, Dong X, Galli SJ, Reber LL, Ginhoux F, Bajenoff M, Gentek R, Gaudenzio N. 2023. Landscape of mast cell populations across organs in mice and humans. *Journal of Experimental Medicine* 220:e20230570. DOI: 10.1084/jem.20230570.

Tavian M, Coulombel L, Luton D, Clemente H, Dieterlen-Lievre F, Peault B. 1996. Aorta-associated CD34+ hematopoietic cells in the early human embryo. *Blood* 87:67–72. DOI: 10.1182/blood.V87.1.67.67.

Tavian M, Hallais MF, Peault B. 1999. Emergence of intraembryonic hematopoietic precursors in the pre-liver human embryo. *Development* 126:793–803. DOI: 10.1242/dev.126.4.793.

Tepass U, Fessler LI, Aziz A, Hartenstein V. 1994. Embryonic origin of hemocytes and their relationship to cell death in Drosophila. *Development* 120:1829–1837. DOI: 10.1242/dev.120.7.1829.

Theodore LN, Hagedorn EJ, Cortes M, Natsuhara K, Liu SY, Perlin JR, Yang S, Daily ML, Zon LI, North TE. 2017. Distinct Roles for Matrix Metalloproteinases 2 and 9 in Embryonic Hematopoietic Stem Cell Emergence, Migration, and Niche Colonization. *Stem Cell Reports* 8:1226–1241. DOI: 10.1016/J.STEMCR.2017.03.016.

Thomas JR, Appios A, Calderbank EF, Yoshida N, Zhao X, Hamilton RS, Moffett A, Sharkey A, Laurenti E, Hanna CW, McGovern N. 2023. Primitive haematopoiesis in the human placenta gives rise to macrophages with epigenetically silenced HLA-DR. *Nature Communications* 14:1764. DOI: 10.1038/s41467-023-37383-2.

Thoms JAI, Truong P, Subramanian S, Knezevic K, Harvey G, Huang Y, Seneviratne JA, Carter DR, Joshi S, Skhinas J, Chacon D, Shah A, de Jong I, Beck D, Göttgens B, Larsson J, Wong JWH, Zanini F, Pimanda JE. 2021. Disruption

of a GATA2-TAL1-ERG regulatory circuit promotes erythroid transition in healthy and leukemic stem cells. *Blood* 138:1441–1455. DOI: 10.1182/blood.2020009707.

Thornton AM, Korty PE, Tran DQ, Wohlfert EA, Murray PE, Belkaid Y, Shevach EM. 2010. Expression of Helios, an Ikaros transcription factor family member, differentiates thymic-derived from peripherally induced Foxp3+ T regulatory cells. *Journal of Immunology (Baltimore, Md.: 1950)* 184:3433–3441. DOI: 10.4049/jimmunol.0904028.

Tian Y, Xu J, Feng S, He S, Zhao S, Zhu L, Jin W, Dai Y, Luo L, Qu JY, Wen Z. 2017. The first wave of T lymphopoiesis in zebrafish arises from aorta endothelium independent of hematopoietic stem cells. *The Journal of Experimental Medicine* 214:3347–3360. DOI: 10.1084/jem.20170488.

Till JE, McCulloch EA. 1961. A direct measurement of the radiation sensitivity of normal mouse bone marrow cells. *Radiation Research* 14:213–222.

Tiwari S, Italiano JE, Barral DC, Mules EH, Novak EK, Swank RT, Seabra MC, Shivdasani RA. 2003. A role for Rab27b in NF-E2-dependent pathways of platelet formation. *Blood* 102:3970–3979. DOI: 10.1182/blood-2003-03-0977.

Tober J, Koniski A, McGrath KE, Vemishetti R, Emerson R, de Mesy-Bentley KKL, Waugh R, Palis J. 2007. The megakaryocyte lineage originates from hemangioblast precursors and is an integral component both of primitive and of definitive hematopoiesis. *Blood* 109:1433–1441. DOI: 10.1182/blood-2006-06-031898.

Tober J, McGrath KE, Palis J. 2008. Primitive erythropoiesis and megakaryopoiesis in the yolk sac are independent of c-myb. *Blood* 111:2636–2639. DOI: 10.1182/blood-2007-11-124685.

Traver D, Akashi K, Manz M, Merad M, Miyamoto T, Engleman EG, Weissman IL. 2000. Development of CD8alpha-positive dendritic cells from a common myeloid progenitor. *Science (New York, N.Y.)* 290:2152–2154. DOI: 10.1126/SCIENCE.290.5499.2152.

Traver D, Zon LI. 2002. Walking the Walk: Migration and Other Common Themes in Blood and Vascular Development. *Cell* 108:731–734. DOI: 10.1016/S0092-8674(02)00686-4.

Travnickova J, Chau VT, Julien E, Mateos-Langerak J, Gonzalez C, Lelièvre E, Lutfalla G, Tavian M, Kissa K. 2015. Primitive macrophages control HSPC mobilization and definitive haematopoiesis. *Nature Communications* 6:1–9. DOI: 10.1038/ncomms7227.

Tripic T, Deng W, Cheng Y, Zhang Y, Vakoc CR, Gregory GD, Hardison RC, Blobel GA. 2009. SCL and associated proteins distinguish active from repressive GATA transcription factor complexes. *Blood* 113:2191–2201. DOI: 10.1182/blood-2008-07-169417.

Tsai F-Y, Keller G, Kuo FC, Weiss M, Chen J, Rosenblatt M, Alt FW, Orkin SH. 1994. An early haematopoietic defect in mice lacking the transcription factor GATA-2. *Nature* 371:221–226. DOI: 10.1038/371221a0.

Tsai F-Y, Orkin SH. 1997. Transcription Factor GATA-2 Is Required for Proliferation/Survival of Early Hematopoietic Cells and Mast Cell Formation, But Not for Erythroid and Myeloid Terminal Differentiation. *Blood* 89:3636–3643. DOI: 10.1182/blood.V89.10.3636.

Tsai SF, Strauss E, Orkin SH. 1991. Functional analysis and in vivo footprinting implicate the erythroid transcription factor GATA-1 as a positive regulator of its own promoter. *Genes & Development* 5:919–931. DOI: 10.1101/gad.5.6.919.

Tsai M, Valent P, Galli SJ. 2022. KIT as a master regulator of the mast cell lineage. *Journal of Allergy and Clinical Immunology* 149:1845–1854. DOI: 10.1016/j.jaci.2022.04.012.

Tsang AP, Fujiwara Y, Hom DB, Orkin SH. 1998. Failure of megakaryopoiesis and arrested erythropoiesis in mice lacking the GATA-1 transcriptional cofactor FOG. *Genes & Development* 12:1176–1188.

Tsunoda T, Doi K, Ishikura S, Luo H, Nishi K, Matsuzaki H, Koyanagi M, Tanaka Y, Okamura T, Shirasawa S. 2018. Zfat expression in ZsGreen reporter gene knock-in mice: Implications for a novel function of Zfat in definitive erythropoiesis. *International Journal of Molecular Medicine* 42:2595–2603. DOI: 10.3892/ijmm.2018.3806.

Tsunoda T, Takashima Y, Tanaka Y, Fujimoto T, Doi K, Hirose Y, Koyanagi M, Yoshida Y, Okamura T, Kuroki M, Sasazuki T, Shirasawa S. 2010. Immune-related zinc finger gene ZFAT is an essential transcriptional regulator for hematopoietic differentiation in blood islands. *Proceedings of the National Academy of Sciences* 107:14199–14204. DOI: 10.1073/pnas.1002494107.

Tusi BK, Wolock SL, Weinreb C, Hwang Y, Hidalgo D, Zilionis R, Waisman A, Huh JR, Klein AM, Socolovsky M. 2018. Population snapshots predict early haematopoietic and erythroid hierarchies. *Nature* 555:54–60. DOI: 10.1038/nature25741.

Tyser RCV, Mahammadov E, Nakanoh S, Vallier L, Scialdone A, Srinivas S. 2021. Single-cell transcriptomic characterization of a gastrulating human embryo. *Nature* 600:285–289. DOI: 10.1038/s41586-021-04158-y.

Uchida N, Weissman IL. 1992. Searching for hematopoietic stem cells: evidence that Thy-1.1lo Lin- Sca-1+ cells are the only stem cells in C57BL/Ka-Thy-1.1 bone marrow. *Journal of Experimental Medicine* 175:175–184. DOI: 10.1084/jem.175.1.175.

Ueno H, Weissman IL. 2006. Clonal Analysis of Mouse Development Reveals a Polyclonal Origin for Yolk Sac Blood Islands. *Developmental Cell* 11:519–533. DOI: 10.1016/J.DEVCEL.2006.08.001.

Ulloa Bianca A, Habbsa SS, Potts KS, Lewis A, McKinstry M, Payne SG, Flores J, Nizhnik A, Norberto MF, Mosimann C, Bowman TV. 2021. Definitive Hematopoietic Stem Cells Minimally Contribute to Embryonic Hematopoiesis.

Unnisa Z, Clark JP, Roychoudhury J, Thomas E, Tessarollo L, Copeland NG, Jenkins NA, Grimes HL, Kumar AR. 2012. Meis1 preserves hematopoietic stem cells in mice by limiting oxidative stress. *Blood* 120:4973–4981. DOI: 10.1182/blood-2012-06-435800.

Valent P, Akin C, Hartmann K, Nilsson G, Reiter A, Hermine O, Sotlar K, Sperr WR, Escribano L, George TI, Kluin-Nelemans HC, Ustun C, Triggiani M, Brockow K, Gotlib J, Orfao A, Schwartz LB, Broesby-Olsen S, Bindslev-Jensen C, Kovanen PT, Galli SJ, Austen KF, Arber DA, Horny H-P, Arock M, Metcalfe DD. 2017. Advances in the Classification and Treatment of Mastocytosis: Current Status and Outlook toward the Future. *Cancer Research* 77:1261–1270. DOI: 10.1158/0008-5472.CAN-16-2234.

Van Handel B, Prashad SL, Hassanzadeh-Kiabi N, Huang A, Magnusson M, Atanassova B, Chen A, Hamalainen EI, Mikkola HKA. 2010. The first trimester human placenta is a site for terminal maturation of primitive erythroid cells. *Blood* 116:3321–30. DOI: 10.1182/blood-2010-04-279489.

Vanuytsel K, Villacorta-Martin C, Lindstrom-Vautrin J, Wang Z, Garcia-Beltran WF, Vrbanac V, Parsons D, Lam EC, Matte TM, Dowrey TW, Kumar SS, Li M, Wang F, Yeung AK, Mostoslavsky G, Dries R, Campbell JD, Belkina AC, Balazs AB, Murphy GJ. 2022. Multi-modal profiling of human fetal liver hematopoietic stem cells reveals the molecular signature of engraftment. *Nature Communications* 13:1103. DOI: 10.1038/s41467-022-28616-x.

Vitrat N, Cohen-Solal K, Pique C, LeCouedic JP, Norol F, Larsen AK, Katz A, Vainchenker W, Debili N. 1998. Endomitosis of Human Megakaryocytes Are Due to Abortive Mitosis. *Blood* 91:3711–3723. DOI: 10.1182/blood.V91.10.3711.

Wagenblast E, Araújo J, Gan OI, Cutting SK, Murison A, Krivdova G, Azkanaz M, McLeod JL, Smith SA, Gratton BA, Marhon SA, Gabra M, Medeiros JJF, Manteghi S, Chen J, Chan-Seng-Yue M, Garcia-Prat L, Salmena L, De Carvalho DD, Abelson S, Abdelhaleem M, Chong K, Roifman M, Shannon P, Wang JCY, Hitzler JK, Chitayat D, Dick JE, Lechman ER. 2021. Mapping the cellular origin and early evolution of leukemia in Down syndrome. *Science* 373:eabf6202. DOI: 10.1126/science.abf6202.

Walsh JC, DeKoter RP, Lee HJ, Smith ED, Lancki DW, Gurish MF, Friend DS, Stevens RL, Anastasi J, Singh H. 2002. Cooperative and antagonistic interplay between PU.1 and GATA-2 in the specification of myeloid cell fates. *Immunity* 17:665–676. DOI: 10.1016/s1074-7613(02)00452-1.

Wanet A, Bassal MA, Patel SB, Marchi F, Mariani SA, Ahmed N, Zhang H, Borchiellini M, Chen S, Zhang J, Di Ruscio A, Miyake K, Tsai M, Paranjape A, Park SY, Karasuyama H, Schroeder T, Dzierzak E, Galli SJ, Tenen DG, Welner RS. 2021. E-cadherin is regulated by GATA-2 and marks the early commitment of mouse hematopoietic progenitors to the basophil and mast cell fates. *Science Immunology* 6. DOI: 10.1126/SCIIMMUNOL.ABA0178.

Wang X, Crispino JD, Letting DL, Nakazawa M, Poncz M, Blobel GA. 2002. Control of megakaryocyte-specific gene expression by GATA-1 and FOG-1: role of Ets transcription factors. *The EMBO Journal* 21:5225–5234. DOI: 10.1093/emboj/cdf527.

Wang Q, Stacy T, Binder M, Marín-Padilla M, Sharpe AH, Speck NA. 1996a. Disruption of the Cbfa2 gene causes necrosis and hemorrhaging in the central nervous system and blocks definitive hematopoiesis. *Proceedings of the National Academy of Sciences of the United States of America* 93:3444–3449. DOI: 10.1073/pnas.93.8.3444.

Wang J, Walker H, Lin Q, Jenkins N, Copeland NG, Watanabe T, Burrows PD, Cooper MD. 1996b. The mouse BP-1 gene: structure, chromosomal localization, and regulation of expression by type I interferons and interleukin-7. *Genomics* 33:167–176. DOI: 10.1006/geno.1996.0180.

Wechsler J, Greene M, McDevitt MA, Anastasi J, Karp JE, Le Beau MM, Crispino JD. 2002. Acquired mutations in GATA1 in the megakaryoblastic leukemia of Down syndrome. *Nature Genetics* 32:148–152. DOI: 10.1038/ng955.

Weinreb C, Rodriguez-Fraticelli A, Camargo FD, Klein AM. 2020. Lineage tracing on transcriptional landscapes links state to fate during differentiation. *Science* 367:eaaw3381. DOI: 10.1126/science.aaw3381.

Weitzmann A, Naumann R, Dudeck A, Zerjatke T, Gerbaulet A, Roers A. 2020. Mast Cells Occupy Stable Clonal Territories in Adult Steady-State Skin. *Journal of Investigative Dermatology* 140:2433-2441.e5. DOI: 10.1016/j.jid.2020.03.963.

Welch JJ, Watts JA, Vakoc CR, Yao Y, Wang H, Hardison RC, Blobel GA, Chodosh LA, Weiss MJ. 2004. Global regulation of erythroid gene expression by transcription factor GATA-1. *Blood* 104:3136–3147. DOI: 10.1182/blood-2004-04-1603.

Wheat JC, Sella Y, Willcockson M, Skoultchi AI, Bergman A, Singer RH, Steidl U. 2020. Single-molecule imaging of transcription dynamics in somatic stem cells. *Nature* 583:431–436. DOI: 10.1038/s41586-020-2432-4.

Wilkinson AC, Igarashi KJ, Nakauchi H. 2020. Haematopoietic stem cell self-renewal in vivo and ex vivo. *Nature Reviews Genetics* 21:541–554. DOI: 10.1038/s41576-020-0241-0.

Willett CE, Cortes A, Zuasti A, Zapata AG. 1999. Early hematopoiesis and developing lymphoid organs in the zebrafish. *Developmental Dynamics* 214:323–336. DOI: 10.1002/(SICI)1097-0177(199904)214:4<323::AID-AJA5>3.0.CO;2-3.

Wilson NK, Foster SD, Wang X, Knezevic K, Schütte J, Kaimakis P, Chilarska PM, Kinston S, Ouwehand WH, Dzierzak E, Pimanda JE, de Bruijn MFTR, Göttgens B. 2010. Combinatorial Transcriptional Control In Blood Stem/Progenitor Cells: Genome-wide Analysis of Ten Major Transcriptional Regulators. *Cell Stem Cell* 7:532–544. DOI: 10.1016/j.stem.2010.07.016.

Wilson A, Laurenti E, Oser G, van der Wath RC, Blanco-Bose W, Jaworski M, Offner S, Dunant CF, Eshkind L, Bockamp E, Lió P, MacDonald HR, Trumpp A. 2008. Hematopoietic Stem Cells Reversibly Switch from Dormancy to Self-Renewal during Homeostasis and Repair. *Cell* 135:1118–1129. DOI: 10.1016/j.cell.2008.10.048.

Winkler IG, Sims NA, Pettit AR, Barbier V, Nowlan B, Helwani F, Poulton IJ, van Rooijen N, Alexander KA, Raggatt LJ, Lévesque J-P. 2010. Bone marrow macrophages maintain hematopoietic stem cell (HSC) niches and their depletion mobilizes HSCs. *Blood* 116:4815–4828. DOI: 10.1182/blood-2009-11-253534.

Wolber FM, Leonard E, Michael S, Orschell-Traycoff CM, Yoder MC, Srour EF. 2002. Roles of spleen and liver in development of the murine hematopoietic system. *Experimental Hematology* 30:1010–1019. DOI: 10.1016/S0301-472X(02)00881-0.

Wolff CF. 1764. *Theorie von der Generation*.

Woo AJ, Wieland K, Huang H, Akie TE, Piers T, Kim J, Cantor AB. 2013. Developmental differences in IFN signaling affect GATA1s-induced megakaryocyte hyperproliferation. *Journal of Clinical Investigation* 123:3292–3304. DOI: 10.1172/JCI40609.

Xie Z, Bailey A, Kuleshov MV, Clarke DJB, Evangelista JE, Jenkins SL, Lachmann A, Wojciechowicz ML, Kropiwnicki E, Jagodnik KM, Jeon M, Ma'ayan A. 2021. Gene Set Knowledge Discovery with Enrichr. *Current Protocols* 1:e90. DOI: 10.1002/cpz1.90.

Xu MJ, Matsuoka S, Yang FC, Ebihara Y, Manabe A, Tanaka R, Eguchi M, Asano S, Nakahata T, Tsuji K. 2001. Evidence for the presence of murine primitive megakarycytopoiesis in the early yolk sac. *Blood* 97:2016–2022. DOI: 10.1182/BLOOD.V97.7.2016.

Xu J, Zhu L, He S, Wu Y, Jin W, Yu T, Qu JY, Wen Z. 2015. Temporal-Spatial Resolution Fate Mapping Reveals Distinct Origins for Embryonic and Adult Microglia in Zebrafish. *Developmental Cell* 34:632–641. DOI: 10.1016/j.devcel.2015.08.018.

Xue Y, Gao X, Lindsell CE, Norton CR, Chang B, Hicks C, Gendron-Maguire M, Rand EB, Weinmaster G, Gridley T. 1999. Embryonic lethality and vascular defects in mice lacking the Notch ligand Jagged1. *Human Molecular Genetics* 8:723–730. DOI: 10.1093/hmg/8.5.723.

Yamamizu K, Matsunaga T, Uosaki H, Fukushima H, Katayama S, Hiraoka-Kanie M, Mitani K, Yamashita JK. 2010. Convergence of Notch and β-catenin signaling induces arterial fate in vascular progenitors. *Journal of Cell Biology* 189:325–338. DOI: 10.1083/jcb.200904114.

Yáñez A, Coetzee SG, Olsson A, Muench DE, Berman BP, Hazelett DJ, Salomonis N, Grimes HL, Goodridge HS. 2017. Granulocyte-Monocyte Progenitors and Monocyte-Dendritic Cell Progenitors Independently Produce Functionally Distinct Monocytes. *Immunity* 47:890-902.e4. DOI: 10.1016/j.immuni.2017.10.021.

Yáñez A, Ng MY, Hassanzadeh-Kiabi N, Goodridge HS. 2015. IRF8 acts in lineage-committed rather than oligopotent progenitors to control neutrophil vs monocyte production. *Blood* 125:1452–1459. DOI: 10.1182/blood-2014-09-600833.

Yokomizo T, Ideue T, Morino-Koga S, Tham CY, Sato T, Takeda N, Kubota Y, Kurokawa M, Komatsu N, Ogawa M, Araki K, Osato M, Suda T. 2022. Independent origins of fetal liver haematopoietic stem and progenitor cells. *Nature* 609:779–784. DOI: 10.1038/s41586-022-05203-0.

Yona S, Kim K-W, Wolf Y, Mildner A, Varol D, Breker M, Strauss-Ayali D, Viukov S, Guilliams M, Misharin A, Hume DA, Perlman H, Malissen B, Zelzer E, Jung S. 2013. Fate Mapping Reveals Origins and Dynamics of Monocytes and Tissue Macrophages under Homeostasis. *Immunity* 38:79–91. DOI: 10.1016/j.immuni.2012.12.001.

Yoshimoto M, Porayette P, Glosson NL, Conway SJ, Carlesso N, Cardoso AA, Kaplan MH, Yoder MC. 2012. Autonomous murine T-cell progenitor production in the extra-embryonic yolk sac before HSC emergence. *Blood* 119:5706–5714. DOI: 10.1182/blood-2011-12-397489.

Yusenko MV, Biyanee A, Andersson MK, Radetzki S, von Kries JP, Stenman G, Klempnauer K-H. 2021. Proteasome inhibitors suppress MYB oncogenic activity in a p300-dependent manner. *Cancer Letters* 520:132–142. DOI: 10.1016/j.canlet.2021.07.010.

Yzaguirre AD, Howell ED, Li Y, Liu Z, Speck NA. 2018. Runx1 is sufficient for blood cell formation from non-hemogenic endothelial cells in vivo only during early embryogenesis. *Development* 145:dev158162. DOI: 10.1242/dev.158162.

Zeng H, Yücel R, Kosan C, Klein-Hitpass L, Möröy T. 2004. Transcription factor Gfi1 regulates self-renewal and engraftment of hematopoietic stem cells. *The EMBO Journal* 23:4116–4125. DOI: 10.1038/sj.emboj.7600419.

Zhang Y, McGrath KE, Ayoub E, Kingsley PD, Yu H, Fegan K, McGlynn KA, Rudzinskas S, Palis J, Perkins AS. 2021. *Mds1*CreERT2, an inducible Cre allele specific to adult-repopulating hematopoietic stem cells. *Cell Reports* 36:109562. DOI: 10.1016/j.celrep.2021.109562.

Zhang P, Zhang X, Iwama A, Yu C, Smith KA, Mueller BU, Narravula S, Torbett BE, Orkin SH, Tenen DG. 2000. PU.1 inhibits GATA-1 function and erythroid differentiation by blocking GATA-1 DNA binding. *Blood* 96:2641–2648. DOI: 10.1182/blood.V96.8.2641.h8002641_2641_2648.

Zhao YX, Song JY, Bao XW, Zhang JL, Wu JC, Wang LY, He C, Shao W, Bai XL, Liang TB, Sheng JP. 2023. Single-cell RNA sequencing-guided fate-mapping toolkit delineates the contribution of yolk sac erythro-myeloid progenitors. *Cell Reports* 42:113364. DOI: 10.1016/j.celrep.2023.113364.

Zheng Z, He H, Tang XT, Zhang H, Gou F, Yang H, Cao J, Shi S, Yang Z, Sun G, Xie X, Zeng Y, Wen A, Lan Y, Zhou J, Liu B, Zhou BO, Cheng T, Cheng H. 2022. Uncovering the emergence of HSCs in the human fetal bone marrow by single-cell RNA-seq analysis. *Cell Stem Cell* 29:1562-1579.e7. DOI: 10.1016/j.stem.2022.10.005.

Zhu Q, Gao P, Tober J, Bennett L, Chen C, Uzun Y, Li Y, Howell ED, Mumau M, Yu W, He B, Speck NA, Tan K. 2020. Developmental trajectory of prehematopoietic stem cell formation from endothelium. *Blood* 136:845–856. DOI: 10.1182/blood.2020004801.

Zipursky A. 2003. Transient leukaemia--a benign form of leukaemia in newborn infants with trisomy 21. *British Journal of Haematology* 120:930–938. DOI: 10.1046/j.1365-2141.2003.04229.x.

Zon LI, Tsai SF, Burgess S, Matsudaira P, Bruns GA, Orkin SH. 1990. The major human erythroid DNA-binding protein (GF-1): primary sequence and localization of the gene to the X chromosome. *Proceedings of the National Academy of Sciences of the United States of America* 87:668–672.

List of Figures & Tables

4.5 Figures

Figures of the general manuscript

Figures of the megakaryocyte paper

4.6 Tables

Abbreviations

(4-)OHT	4-hydroxytamoxifen
AGM	Aorta-gonad mesonephros
BM	Bone marrow
BSD	Back skin dermis
CDP	Common dendritic cell progenitor
CHT	Caudal hematopoietic tissue (zebrafish)
CLP	Common lymphoid progenitor
cMoP	Common monocyte progenitor
CMP	Common myeloid progenitor
CreERT2	Cre recombinase fused to an estrogen receptor T2
CS	Carnegie stage
Csf1(r)	Colony-stimulating factor-1 (receptor)
Dc	Dendritic cell
DS-TAM	Transient abnormal myelopoiesis (TAM) of Down syndrome (DS)
ECM	extracellular matrix
EHT	Endothelial-to-hematopoietic transition
EHT	endothelial-to-hematopoietic transition
EMP	Erythro-myeloid progenitor
eMPP	Embryonic multipotent progenitor
EPO	Erythropoietin
ESD	Ear skin dermis
FL	Fetal liver
Gata1s	Gata1short
GM-CSF	Granulocyte-macrophage colony-stimulating factor
GMP	Granulocyte-monocyte progenitor
HSC	Hematopoietic stem cell
HSPC	Hematopoietic stem and progenitor cell
IAHC	Intra-aortic hematopoietic clusters
iCre	Codon-improved Cre recombinase
IL-3	Interleukin 3
ILC	Innate lymphoid cell
LSK	$Lineage^{neg}$ Sca-1^{+} Kit^{high} cells
LT	Long term
M-CSF	Macrophage colony-stimulating factor
Mc	Mast cell
MDP	Monocyte-dendritic cell progenitor
MEP	Megakaryocyte-erythrocyte progenitor
MeriCreMer	2 mutated estrogen receptor sites flanking a codon-improved Cre recombinase
Mf	Macrophage(s)
Mk	Megakaryocyte(s)
Mo	Monocyte (s)
MPP	Multipotent progenitor
NK	Natural killer cell(s)
Nt	Neutrophil(s)
P-Sp	Para-aortic splanchnopleura (P-Sp)
PBI	Posterior blood island (zebrafish)
pcw	Post conception weeks
plt	Platelet
PLX	Plexxikon 5622
RBC	Red blood cell(s)
RBI	Rostral blood islands (zebrafish)
SCF	Stem cell factor
ST	Short term
Tom	Tomato
TPO	Thrombopoietin
VDA	Ventral wall of the dorsal aorta (zebrafish)
wt	Wild-type
YS	Yolk sac

Abstract

4.7 English

The layered blood and immune system is built by the sequential emergence of hematopoietic waves. Initially, transient progenitors, such as erythro-myeloid progenitors (EMPs), supply all blood and immune cells of the fetus. Before birth, however, these are superseded by cells derived from hematopoietic stem and progenitor cells (HSPCs). The short-lived nature of the first blood and immune cells is reminiscent of the spontaneous resolution of some childhood blood disorders. This raises the question, of whether transient hematopoietic progenitors could be the cellular origin of pediatric diseases. Thus, the objective of my PhD thesis was to decipher how perturbations in different hematopoietic waves impact perinatal disease development.

First, I discovered that the integrity of early hematopoietic waves is essential to ensure proper development of life-long hematopoiesis. Further, I showed that mutations can significantly prolong the persistence of EMP-derived cells in the organism. Finally, lineage tracing experiments revealed that each hematopoietic wave is governed by unique molecular mechanisms resulting in ontogeny-specific effects of mutations. Consequently, the variations between pediatric and adult blood disorders could indeed stem from distinct progenitor origins as initially hypothesized.

This illustrates that despite being transient, early hematopoietic waves can potentially cause disease after birth. A deeper understanding of developmental hematopoiesis is thus key to unraveling the unique features of childhood blood disorders and developing tailored therapies.

4.8 Français

Le système sanguin et immunitaire est construit par l'émergence successive de vagues hématopoïétiques. Au départ, des progéniteurs transitoires, tels que les progéniteurs érythro-myéloïdes (EMP), fournissent toutes les cellules sanguines et immunitaires du fœtus. Toutefois, avant la naissance, ces cellules sont remplacés par des cellules dérivées des cellules souches et progénitrices hématopoïétiques (HSPCs). La nature transitoire des premières cellules sanguines et immunitaires pourrait être liée à la guérison spontanée de certains troubles sanguins de l'enfance ; ceci soulève la question de savoir si les progéniteurs hématopoïétiques transitoires pourraient être l'origine cellulaire de certaines maladies pédiatriques. L'objectif de ma thèse de doctorat a donc été de comprendre comment les perturbations des différentes vagues hématopoïétiques influent sur le développement des maladies périnatales.

Tout d'abord, j'ai découvert que l'intégrité des premières vagues hématopoïétiques est essentielle pour assurer le bon développement de l'hématopoïèse tout au long de la vie. En outre, j'ai montré que certaines mutations peuvent prolonger significativement la persistance des cellules dérivées des EMP dans l'organisme. Enfin, des expériences de traçage génétique ont révélé que chaque vague hématopoïétique est régie par des mécanismes moléculaires uniques qui entraînent, pour chaque mutation, des effets spécifiques liés à l'ontogénèse. Par conséquent, les variations entre les troubles sanguins de l'enfant et de l'adulte pourraient effectivement provenir des origines distinctes des progéniteurs hématopoïétiques, comme on l'avait initialement supposé.

Cela montre qu'en dépit de leur caractère transitoire, les premières vagues hématopoïétiques peuvent potentiellement être à l'origine de maladies après la naissance. Une compréhension plus approfondie de l'hématopoïèse développementale est donc essentielle pour démêler les caractéristiques uniques des troubles sanguins infantiles et développer des thérapies adaptées.

List of Publications

Research articles

Sommer, A., Fischer, S., Freyer, L., Dardenne, P., Lallemand, Y., Gomez Perdiguero, E. Ontogeny drives stage-specific effects of a Gata1 mutation. *Submitted*.

Monticelli, S., **Sommer, A.,** AlHajj Hassan, Z., Garcia Rodriguez, C., Adé, K., Cattenoz, P., Delaporte, C., Gomez Perdiguero, E., & Giangrande, A. (2024). Early-wave macrophages control late hematopoiesis. *Developmental Cell*. https://doi.org/10.1016/j.devcel.2024.03.013

Freyer, L., Lallemand, Y., Dardenne, P., **Sommer, A.**, Biton, A., & Gomez Perdiguero, E. (2022). Erythro-myeloid progenitor origin of Hofbauer cells in the early mouse placenta. *Development*, *149*(8). https://doi.org/10.1242/dev.200104

Freyer, L., Iturri, L., Biton, A., **Sommer, A**., Dardenne, P., Cumano, A., & Gomez Perdiguero, E. (2021). Fetal hematopoiesis is driven by privileged expansion and differentiation of yolk sac-derived erythro-myeloid progenitors. *Preprint*. https://doi.org/10.21203/rs.3.rs-1002760/v1

Review and book chapter

Sommer, A., & Perdiguero, E. G. (2024). Extraembryonic hematopoietic lineages—To macrophages and beyond. *Experimental Hematology*, *136*, 104285. https://doi.org/10.1016/j.exphem.2024.104285

Sommer, A., Ade, K., Freyer, L., & Gomez Perdiguero, E. (2022). Development and Function of Macrophages. In *Reference Module in Life Sciences*. Elsevier. https://doi.org/10.1016/B978-0-12-821618-7.00259-5